NASA Technical Memorandum 101503

4th Annual NASA MDLT* Workshop

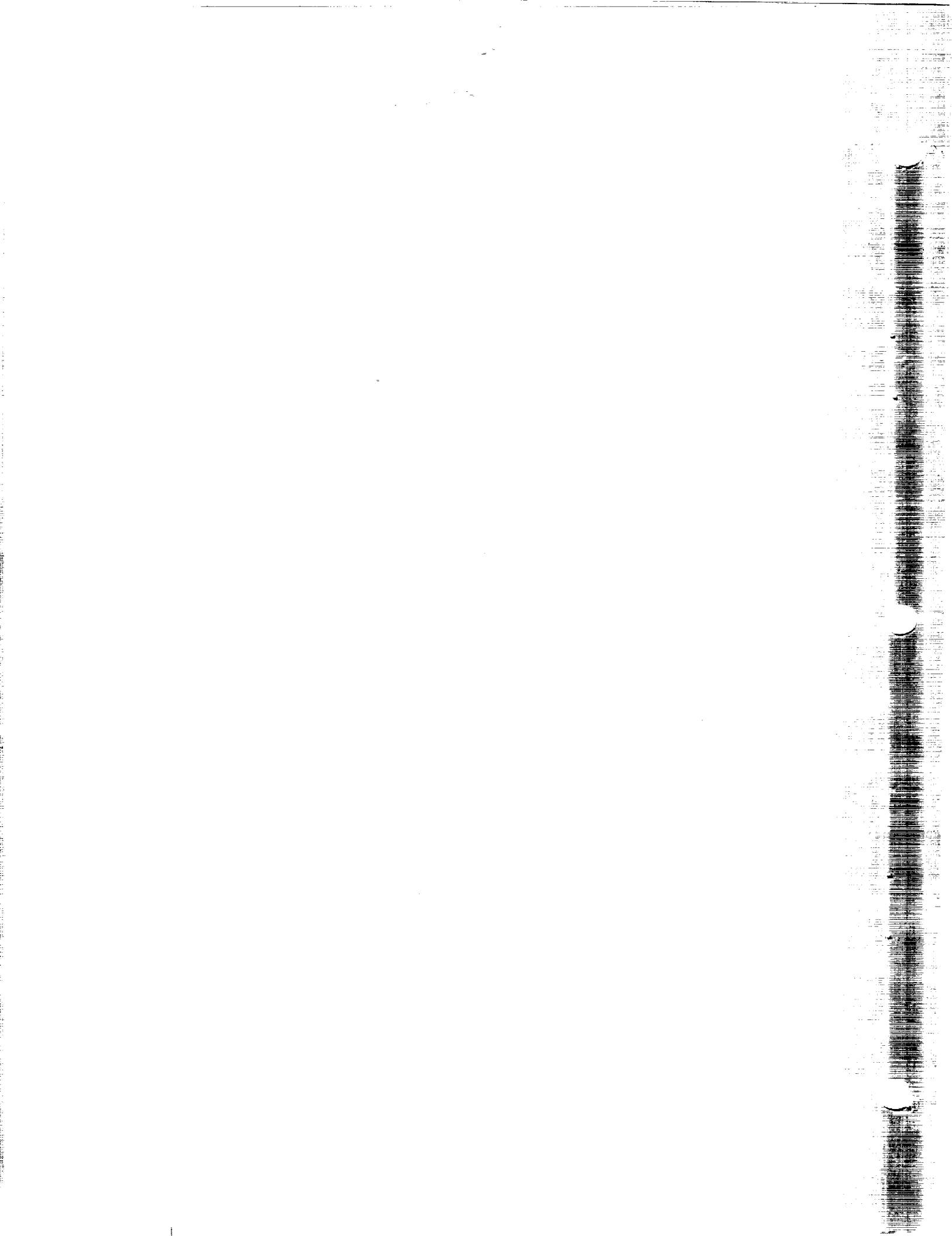

Introduction

SCOLE stands for "Spacecraft Control Laboratory Experiment". The objective of the SCOLE Program is to provide an example configuration and control objectives which enables direct comparison of different techniques in modeling, systems identification and control. The "SCOLE Design Challenge" was formulated in 1983 by L. W. Taylor and A. V. Balakrishnan. The details of this challenge are reprinted at the end of this document.

Annual SCOLE Workshops have been held for specialists to share and compare their research results. This proceedings is a compilation of the material presented at the 4th Workshop held at the USAF Academy on November 16, 1987.

Table of Contents

Table of Contents, Continued

PARAMETER IDENTIFICATION USING MODAL DATA

L. Meirovitch & M. A. Norris
Department of Engineering Science and Mechanics
Virginia Polytechnic Institute and State University
Blacksburg, VA 24061

PARAMETER IDENTIFICATION USING EXPERIMENTAL MODAL DATA

Introduction: Parameter Identification

(1) Direct Approach - using actual sensor measurements to obtain parameters (e.g., ERA, ITD)

(2) Indirect Approach - identifies parameters using measured modal data*

* in this work, only the natural frequencies are used to identify physical parameters

Equations of Motion

The motion of a distributed structure with zero damping is governed by a PDE of the form

$$\mathcal{L}\, u(P,t) + m(P)\ddot{u}(P,t) = f(P,t), \quad P \in D$$

$$B_i u(P,t) = 0, \quad P \in S \quad i = 1,2,\ldots,p$$

u = displacement at position P at time t

m = mass distribution

$\mathcal{L}$ = stiffness differential operator of order 2p

f = external force density

B_i = homogeneous differential operators of order ranging from zero to 2p-1

Discretization

Rayleigh-Ritz method: $u(P,t) = \underset{\sim}{\psi}^T(P)\underset{\sim}{q}(t)$

$\underset{\sim}{\psi}(P)$ - n-vector of admissible functions

$\underset{\sim}{q}(t)$ - n-vector of generalized coordinates

$$M\ddot{\underset{\sim}{q}}(t) + K\underset{\sim}{q}(t) = \underset{\sim}{0}$$

$$M = \int_D m(P)\underset{\sim}{\psi}(P)\underset{\sim}{\psi}^T(P)\, dD, \quad K = \int_D \underset{\sim}{\psi}(P)\underset{\sim}{\psi}^T(P)\, dD$$

Discretization (cont'd)

Rayleigh-Ritz Type Parameter Expansion: $m(P) = \sum_{r=1}^{g} \alpha_r m_r(P)$

$$\lambda = \sum_{r=1}^{h} \beta_r \lambda_r$$

$$M = \sum_{r=1}^{g} \alpha_r M_r, \quad K = \sum_{r=1}^{h} \beta_r K_r$$

$$M_r = \int_D \underset{\sim}{\psi}(P) m_r(P) \underset{\sim}{\psi}^T(P)\, dD = \text{rth mass matrix}$$

$$K_r = \int_D \underset{\sim}{\psi}(P) \lambda_r \underset{\sim}{\psi}^T(P)\, dD = \text{rth stiffness matrix}$$

Iterative Approach Using Measured Natural Frequencies

$$\underset{\sim}{q}(t) = \sum_{r=1}^{n} \underset{\sim}{x}_r e^{i\omega_r t}$$

$$\omega_r^2 M \underset{\sim}{x}_r = K \underset{\sim}{x}_r \quad \text{(Actual Model)}$$

$$\omega_{0r}^2 M_0 \underset{\sim}{x}_{0r} = K_0 \underset{\sim}{x}_{0r} \quad \text{(Postulated Model)}$$

To refine the parameters α_{0r}, β_{0r}, we update them such that the theoretical natural frequencies converge to the measured natural frequencies of the actual structure.

Postulated Parameters: $\underset{\sim}{p}_0 = [\alpha_{01}\ \alpha_{02} \cdots \alpha_{0g}\ \beta_{01} \cdots \beta_{0h}]^T$

Measured Natural Frequencies: $\underset{\sim}{\omega} = [\omega_1\ \omega_2 \cdots \omega_f]^T$

Postulated Natural Frequencies: $\underset{\sim}{\omega}_0(\underset{\sim}{p}_0) = [\omega_{01}\ \omega_{02} \cdots \omega_{0f}]^T$

Iterative Approach (cont'd)

Sensitivity Analysis: $\Delta\underset{\sim}{\omega} = \frac{\partial\underset{\sim}{\omega}}{\partial\underset{\sim}{p}} \Delta\underset{\sim}{p}$, $[\frac{\partial\underset{\sim}{\omega}}{\partial\underset{\sim}{p}}] = [\frac{\partial\omega_i}{\partial p_j}]$

$$\Delta\underset{\sim}{\omega} = \underset{\sim}{\omega} - \underset{\sim}{\omega}(\underset{\sim}{p}_0), \quad \Delta\underset{\sim}{p} = \underset{\sim}{p} - \underset{\sim}{p}_0$$

$\underset{\sim}{p}$ = updated parameters

Least-Squares Solution:

$$\Delta\underset{\sim}{p} = \left([\frac{\partial\underset{\sim}{\omega}}{\partial\underset{\sim}{p}}]^T [\frac{\partial\underset{\sim}{\omega}}{\partial\underset{\sim}{p}}]\right)^{-1} [\frac{\partial\underset{\sim}{\omega}}{\partial\underset{\sim}{p}}]^T \Delta\underset{\sim}{\omega}$$

7

Iterative Approach (cont'd)

Jacobian $\left(\frac{\partial \omega}{\partial p}\right)$: $\frac{\partial \omega_r}{\partial p_i} = \frac{1}{2\omega_r} [\ldots \frac{\partial K}{\partial p_i} \ldots - x_r^T \frac{\partial M}{\partial p_i} x_r]$

$$\frac{\partial M}{\partial p_i} = M_i, \quad \frac{\partial K}{\partial p_i} = 0 \quad (i = 1,2,\ldots,g)$$

$$\frac{\partial M}{\partial p_i} = 0, \quad \frac{\partial K}{\partial p_i} = K_{i-g} \quad (i = g+1, g+2, \ldots, g+h)$$

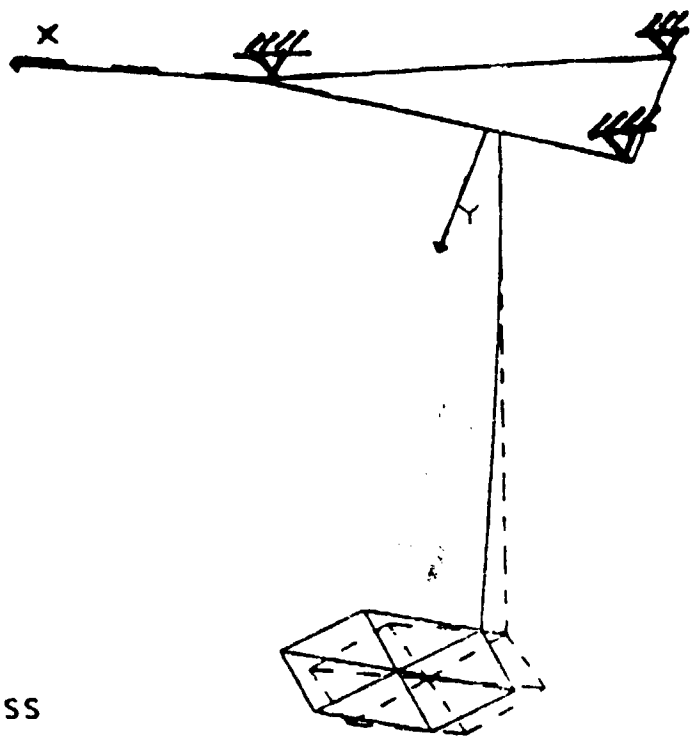

Numerical Example

SCOLE MODEL:

Parameters:

m_A = antenna mass

I_{XA} = antenna moment of inertia with respect to roll axis

m = mast mass density

EI = mast bending rigidity

m_i = sensors and actuators at z = -41.0, -87.8 (i = 1,2)

I_{x_i} = additional mass moment of inertia (i = 1,2)

Numerical Example

SCALE MODEL

Kinetic Energy:

$$T(t) = \frac{1}{2}\int_0^L m\dot{w}^2(z,t)\,dz + \frac{1}{2}\sum_{i=1}^{2}\{[m_i\dot{w}^2(z_i,t) + I_{xi}[\dot{w}'(z_i,t)]^2\}$$

$$+ \frac{1}{2}m_A\dot{w}^2(L,t) + \frac{1}{2}I_{xA}[\dot{w}'(L,t)]^2$$

Potential Energy:

$$V(t) = \frac{1}{2}\int_0^L \{EI[w''(z,t)]^2 + P(z)[w'(z,t)]^2\}\,dz$$

$w(z,t)$ - transverse displacement from equilibrium position

$P(z)$ = axial load

Numerical Example

- We used an n = 4 degree of freedom model:

$$M\ddot{q} + Kq = F$$

- Natural frequencies agree well with those obtained experimentally (data provided by Lee, Williams and Sparks)

- We used the first 2 natural frequencies to update the bending rigidity EI and the mass moment of inertia of the antenna.

se I: Zero Error in Natural Frequencies

- I_{x_A} Antenna Mass Moment of Inertia
- EI - Root Bending Stiffness

Normalized Root-Mean-Square Error in Natural Frequencies (RMS) = $\left(\sum_{i=1}^{3} \left(\frac{\omega_i - \omega_{0i}}{\omega_i} \right)^2 \right)^{1/2}$

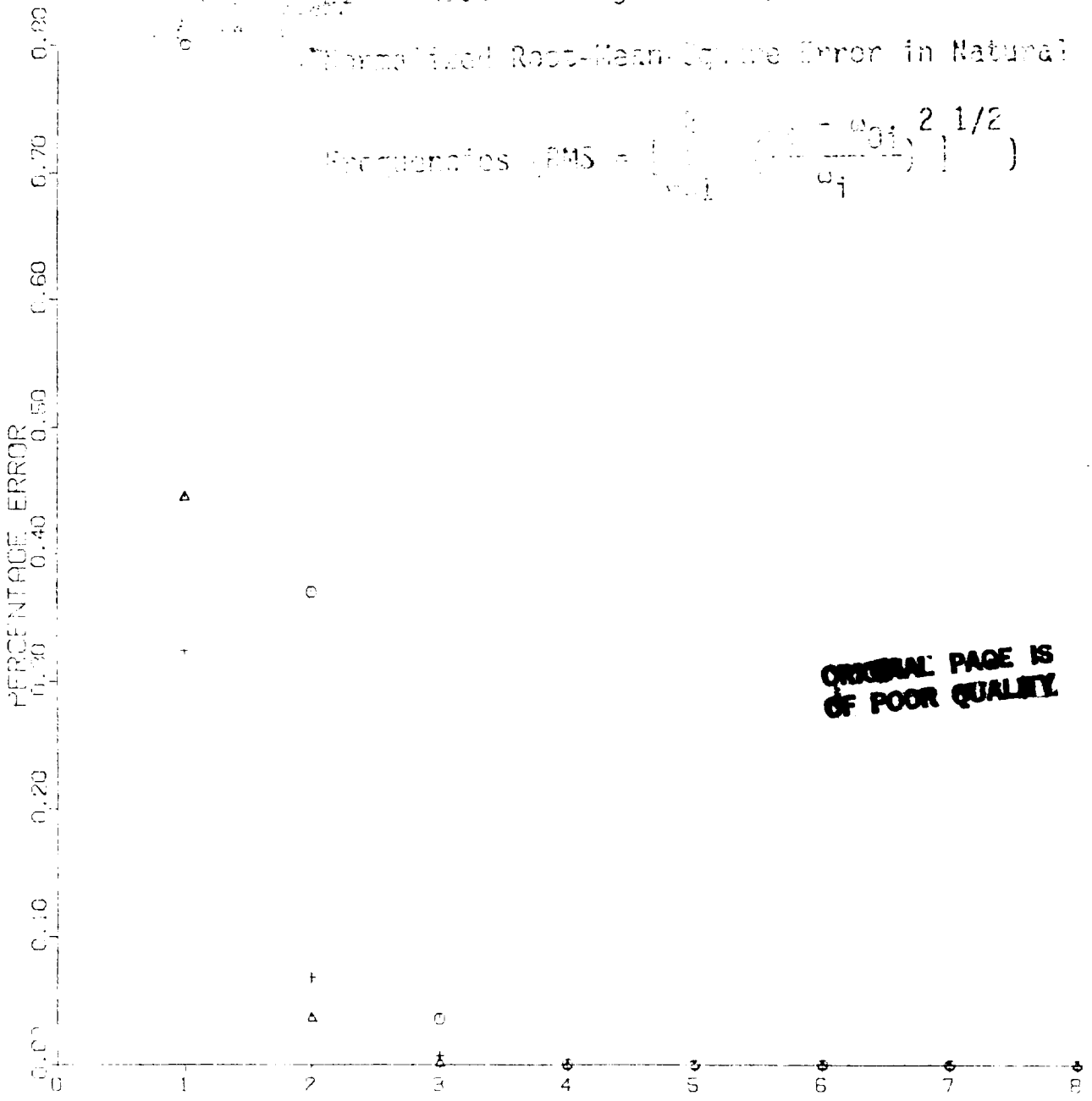

Case II: 1% Error in ω_1

5% Error in ω_2

- I_{y_A} = Antenna Mass Moment of Inertia
- EI = Mast Bending Rigidity
- Normalized Root-Mean-Square Error in Natural Frequencies (RMS) = $\left[\frac{1}{n}\sum_{i=1}^{n}\left(\frac{\omega_i - \omega_{0i}}{\omega_i}\right)^2\right]^{1/2}$

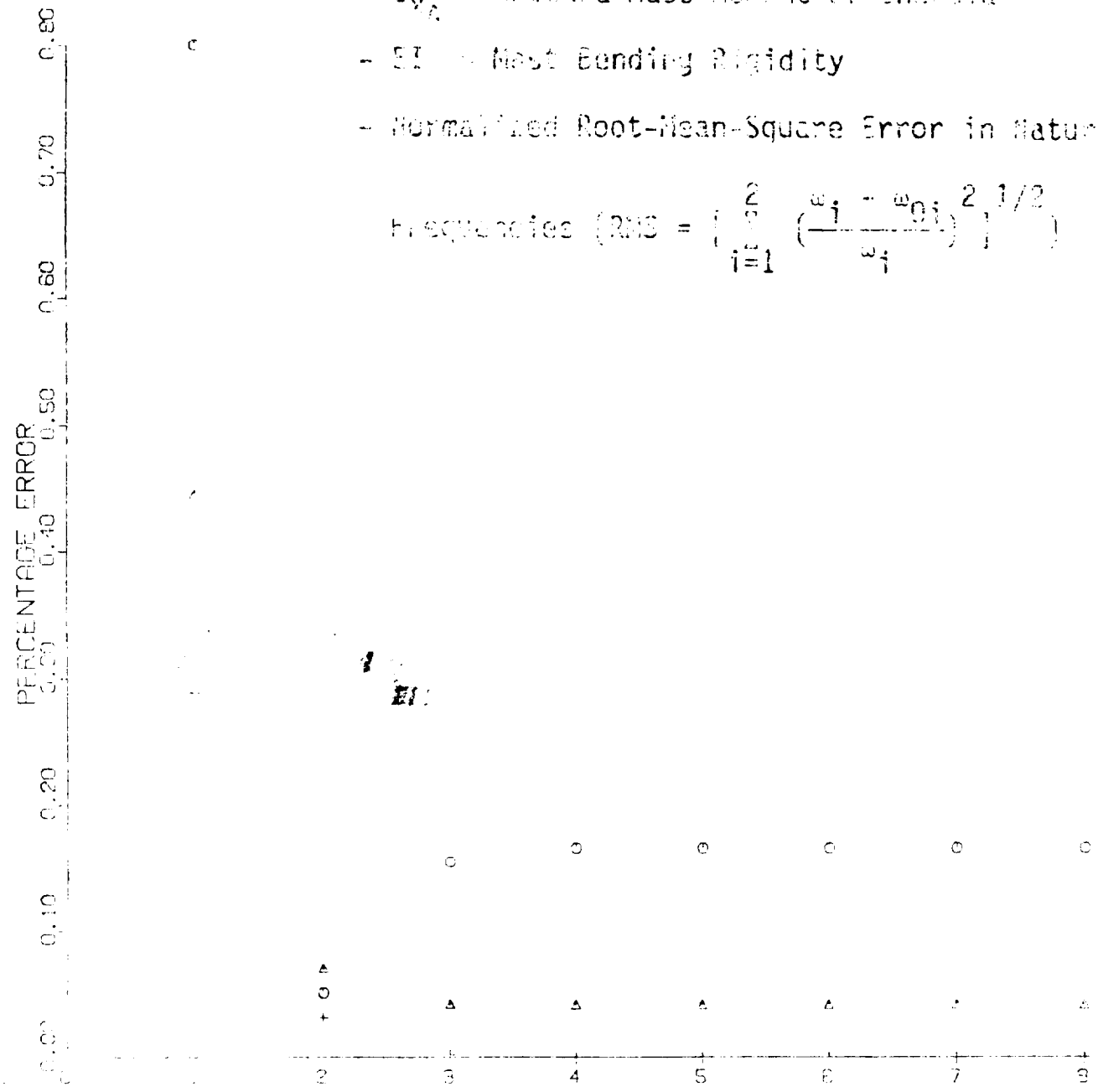

Case III: 2% Error in ω_1

10% Error in ω_2

- I_{x_2} = Antenna Mass Moment of Inertia
- EI = Mast Bending Rigidity
- Normalized Root-Mean-Square Error in Natural

$$\text{Percentage Error} = \left(\sum_{i=1}^{n} \left(\frac{\omega_i - \omega_{0i}}{\omega_i} \right)^2 \right)^{1/2}$$

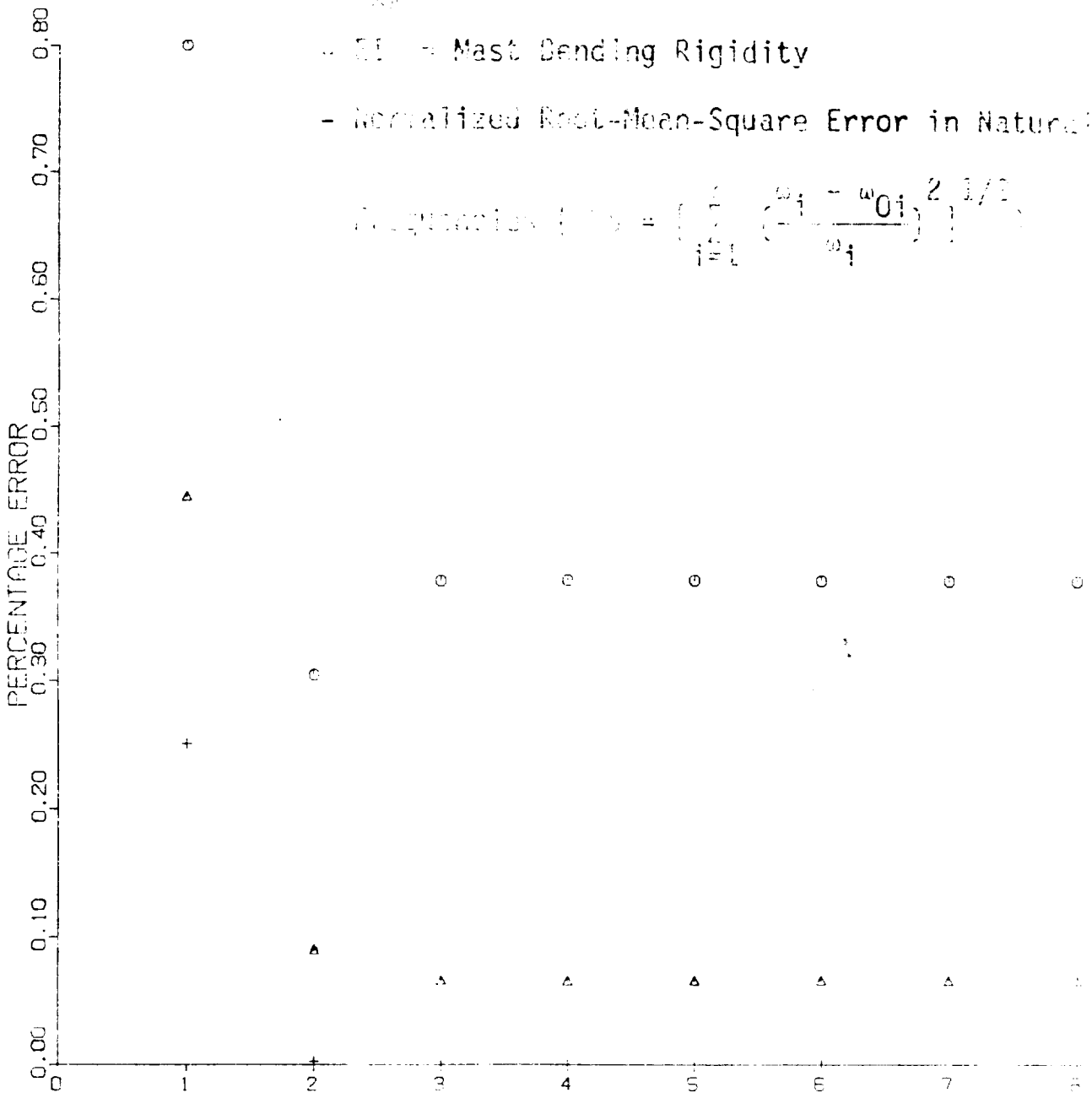

Conclusions

- Indirect approach is used to obtain physical parameters
- Results indicate that the parameters converge quickly
- The algorithm is relatively insensitive to noise

INFINITE-DIMENSIONAL APPROACH TO SYSTEM IDENTIFICATION OF SPACE CONTROL LABORATORY EXPERIMENT (SCOLE)

S. A. Hossain and K. Y. Lee

Department of Electrical Engineering
The Pennsylvania State University
University Park, Pennsylvania 16802

ABSTRACT

The identification of a unique set of system parameters in large space structures poses a significant new problem in control technology. This paper presents an infinite-dimensional identification scheme to determine system parameters in large flexible structures in space. The method retains the distributed nature of the structure throughout the development of the algorithm and a finite-element approximation is used only to implement the algorithm. This approach eliminates many problems associated with model truncation used in other methods of identification. The identification problem is formulated in Hilbert space and an optimal control technique is used to minimize weighted least squares of error between the actual and the model data. A variational approach is used to solve the problem. A costate equation, gradients of parameter variations and conditions for optimal estimates are obtained. Computer simulation studies are conducted using a shuttle-attached antenna configuration, more popularly known as the Space Control Laboratory Experiment (SCOLE) as an example. Numerical results show a close match between the estimated and true values of the parameters.

DISTRIBUTED PARAMETER IDENTIFICATION

TWO APPROACHES :

FINITE-DIMESIONAL METHOD

INFINITE-DIMENSIONAL METHOD

Table 1

Literature Surveyed on the Parameter Estimation of Large Space Structures.

Reference	Approach
Wells and Spalding (1977) [2] Tung (1981) [3] Balas and Lilly (1981) [4] Balas (1981) [5] Lee and Bitter (1981) [6] Banks (1982) [7] Hendricks et al (1982) [8] Hendricks et al (1984) [9] Banks and Rosen (1984) [10] Rajaram and Junkins (1985) [11] Lee, Walker and Hossain (1985) [12] Lee (1986) [13]	A finite-dimensional design approach where the structural model is truncated and the estimator is designed based on the reduced-order model.
Spalding (1976) [14] Burns and Cliff (1977)[15] Sun and Juang (1982) [16] Lee (1986) [13]	An infinite-dimensional design approach where the PDE model is retained as long as possible and truncation is carried out only after the estimation algorithm is developed.

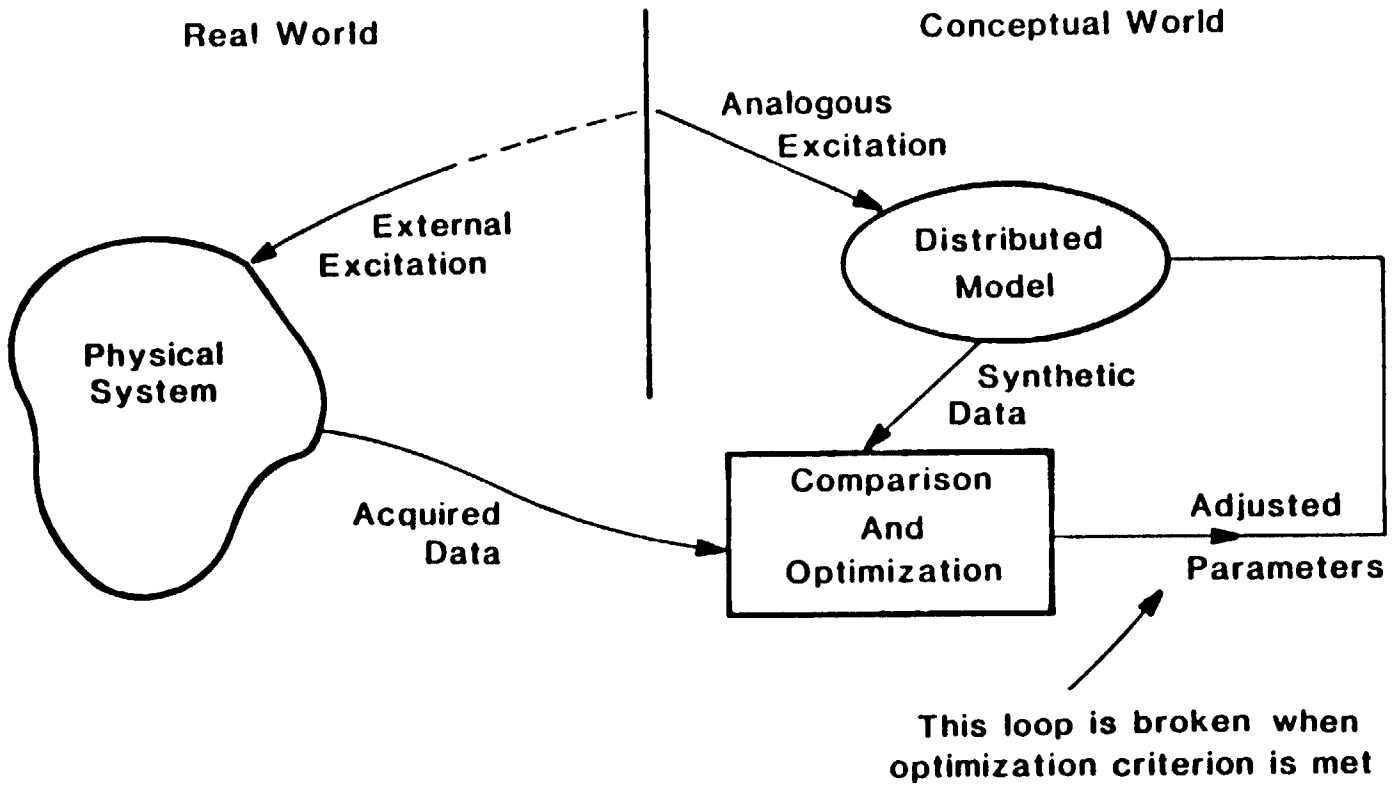

SYSTEM IDENTIFICATION SCHEME

A Distributed System Model

$$m(x)\frac{\partial^2 u}{\partial t^2}(x,t) + D_0\frac{\partial u}{\partial t}(x,t) + A_0 u(x,t) = F(x,t),$$

$$x \in \Omega, \qquad t \in (0,T],$$

$$F(x,t) = F_B(x,t) + F_C(x,t) + F_D(x,t),$$

$$F_C(x,t) = B_0 f = \sum_{i=1}^{M} b_i(x) f_i(t),$$

$$F_B(x,t) = B_b g = \sum_{i=1}^{N} b_i(x) g_i(t),$$

$$y = C_0 u + E_0 u_t,$$

Basic Problem Formulation

$$J(q) = \frac{1}{2T}\int_0^T (y-z)^T R(t)(y-z)\,dt,$$

where z is the measurement of output vector y given as

$$z(x,t) = y(x,t) + e(x,t)$$

with a measurement error $e(x,t)$. Also, it is defined that

$$(y-z)^T R(t)(y-z) = \int_\Omega [y(x,t)-z(x,t)]^T R(x,t)[y(x,t)-z(x,t)]\,dx,$$

Infinite-Dimensional Formulation

$$\frac{\partial^2}{\partial t^2}u(t) + D(q)\frac{\partial}{\partial t}u(t) + A(q)u(t) = B(q)f(t) \qquad \text{in}(0,T],$$

$$u \in L_2(0,T;V), \qquad \frac{\partial u}{\partial t} \in L_2(0,T;H),$$

where $f(t)$ is given in $L_2(0,T;V)$, and the initial conditions are

$$u(0) = u_0, \qquad u_0 \text{ given in } V,$$

and

$$\frac{\partial}{\partial t}u(0) = u_1, \qquad u_1 \text{ given in } H.$$

The output function is

$$y(t) = Cu(t),$$

The identification problem can now be formulated as an abstract problem of determining the parameter vector $q^*(x) \in Q$ that minimizes

$$J(q) = \frac{1}{2T}\int_0^T [y(t) - z(t)]^T R(t)[y(t) - z(t)]\,dt,$$

where $z(t)$ is the observed data belonging to Y

Development of Infinite-Dimensional Identfication Algorithm

THEOREM : Given a state equation (18) with initial conditions given by Eq. (19) and the cost function by Eq. (22) with y(t) satisfying Eq. (21), then the optimal parameter vector q^* satisfies the state equations (18)-(19) and the follwing system of equations :

$$\frac{d^2}{dt^2}p(t) - D^*\frac{d}{dt}p(t) + A^*p(t) = -\frac{1}{T}C^T R(Cu - z), \tag{23}$$

with the final conditions

$$p(T) = \frac{d}{dt}p(T) = 0, \tag{24}$$

and the first variation of an augmented cost functional is

$$\delta J_a = \int_0^T p^T \frac{\partial}{\partial q}\left[D\frac{du}{dt} + Au - Bf\right]\delta q\, dt = 0, \tag{25}$$

where $p(t)$ is a costate variable also belonging to the Hilbert space V.

PROOF : By combining Eqs. (18) and (22) an augmented cost functional can be defined as

$$\begin{aligned} J_a(q) = \frac{1}{2T}\int_0^T [y(t) - z(t)]^T R(t)[y(t) - z(t)]\, dt \\ + \int_0^T p(t)^T\left[\frac{d^2}{dt^2}u(t) + D\frac{du}{dt} + Au(t) - Bf(t)\right] dt. \end{aligned} \tag{26}$$

Parameter Identification of Vibrating Beams

Case I : A Simply-Supported Beam

$$\rho A \frac{\partial^2 u}{\partial t^2} + EI \frac{\partial^4 u}{\partial x^4} = b(x) f(t), \qquad x \in [0, L], t > 0,$$

$$u(x,t) = \frac{\partial^2}{\partial x^2} u(x,t) = 0, \qquad x \in \partial[0, L], \quad t > 0,$$

$$u(x,0) = \frac{\partial}{\partial t} u(x,t)\Big|_{t=0} = 0, \qquad x \in [0, L].$$

$$y(t) = u(\frac{L}{2}, t).$$

$$z(t) = y(t) + e(t).$$

$$J = \frac{1}{2T} \int_0^T [y - z]^T R[y - z]\, dt.$$

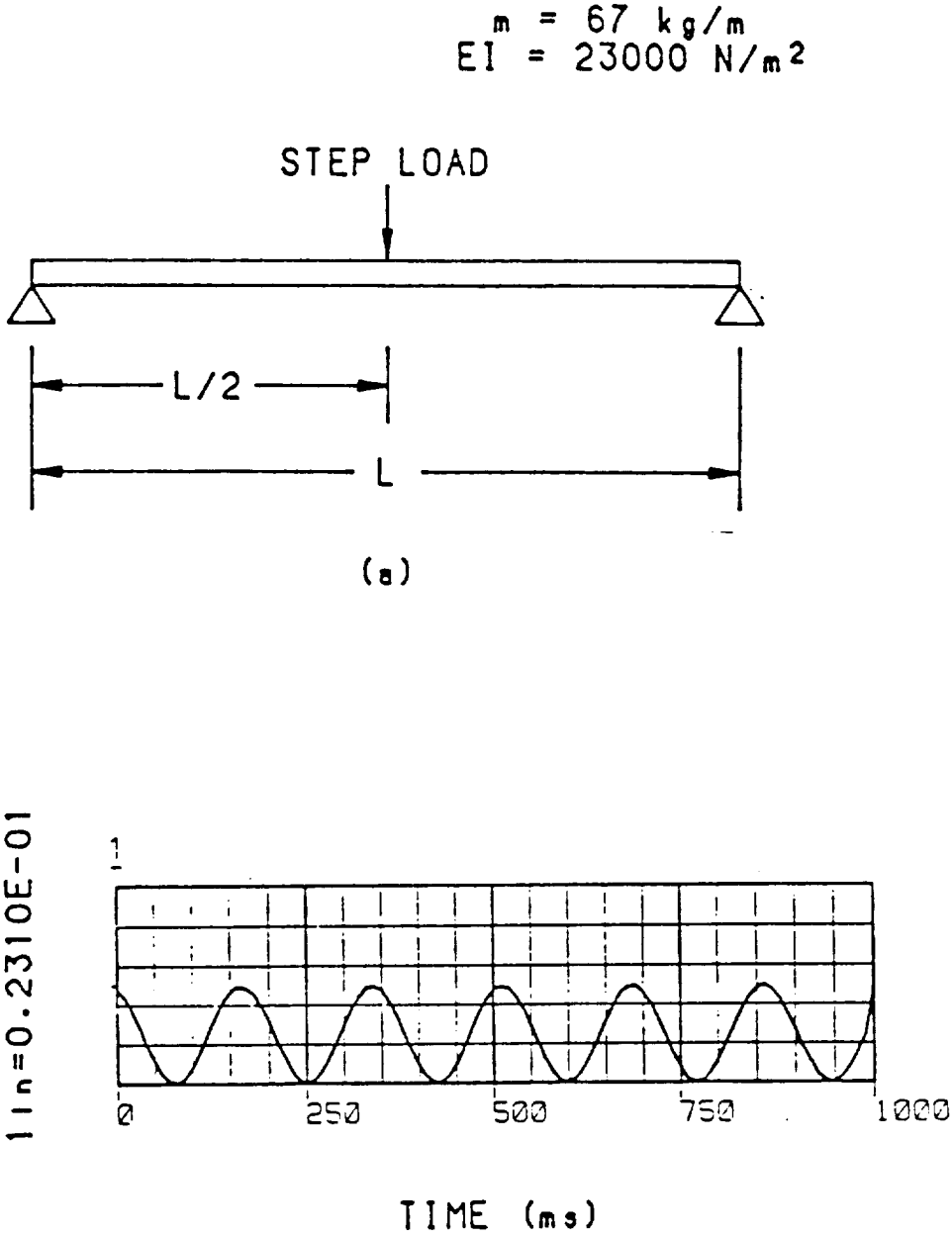

Fig. 2 (a) Simply-supprted beam with step load,
(b) resultant displacements.

$$\frac{\partial^2 u}{\partial t^2} = -\frac{EI}{m}\frac{\partial^4 u}{\partial x^4} + \frac{1}{m}\delta(x - \frac{L}{2})f(t),$$

or

$$\frac{\partial^2 u}{\partial t^2} = -q_1\frac{\partial^4 u}{\partial x^4} + q_2\delta(x - \frac{L}{2})f(t),$$

where

$$q_1 = \frac{EI}{m},$$

$$q_2 = \frac{1.}{m},$$

and the parameter vector is defined by $q = [q_1, q_2]^T$.

$$\frac{\partial^2 p}{\partial t^2} = -q_1\frac{\partial^4 p}{\partial x^4} + \frac{R}{T}|u - z|\delta(x - \frac{L}{2}), \qquad x \in [0, L], t \in [0, T),$$

$$p(x, T) = \frac{\partial}{\partial t}p(x, t)\Big|_{t=T} = 0, \qquad x \in [0, L].$$

$$p(x, t) = \frac{\partial^2}{\partial x^2}p(x, t) = 0, \qquad x \in \partial[0, L], t \in [0, T).$$

$$\frac{\delta J_a}{\delta q_1} = \int_0^T \frac{\partial^2 p}{\partial x^2}\frac{\partial^2 u}{\partial x^2}\, dt,$$

and

$$\frac{\delta J_a}{\delta q_2} = -\int_0^T p\,\delta(x - \frac{L}{2})f(t)\, dt.$$

Thus, parameters can be updated by the steepest descent algorithm

$$q_i^{k+1} = q_i^k - w_i\left(\frac{\delta J_a}{\delta q_i}\right)^k, \qquad i = 1, 2.$$

Table 2

Performance Data for Case I

Iteration	q_1	q_2	m	EI	$\int_0^T \text{error}^2\, dt$
1	301.58	0.0158	63.00	19000.00	0.20178E-01
2	311.68	0.0154	64.84	20207.72	0.16640E-01
3	325.65	0.0151	66.27	21582.87	0.71528E-02
4	338.48	0.0149	66.91	22647.68	0.57208E-03
5	342.11	0.0149	66.98	22913.64	0.34507E-04
6	342.96	0.0149	66.99	22973.13	0.26524E-04
7	343.19	0.0149	66.99	22989.35	0.24364E-04
True values	343.28	0.0149	67.00	23000.00	

Case II : A Cantileverd Beam

$$m\frac{\partial^2 u}{\partial t^2} - 2\xi\sqrt{mEI}\frac{\partial^3 u}{\partial x^2 \partial t} + EI\frac{\partial^4 u}{\partial x^4} = b(x)f(t),$$
$$x \in [0, L],\ t > 0,$$

where ξ is a damping coefficient.

$$y(t) = u(L, t).$$

The boundary conditions for a cantilevered beam are :

$$u(0,t) = \frac{\partial^2}{\partial x^2}u(x,t)\Big|_{x=0} = 0, \qquad t > 0,$$
$$\frac{\partial^2}{\partial x^2}u(x,t)\Big|_{x=L} = \frac{\partial^3}{\partial x^3}u(x,t)\Big|_{x=L} = 0, \qquad t > 0.$$

The beam is initially at rest and hence the initial conditions are

$$u(x,0) = \frac{\partial}{\partial t}u(x,t)\Big|_{t=0} = 0, \qquad x \in [0, L].$$
$$\frac{\partial u(x,t)}{\partial x}\Big|_{t=0} = \frac{\partial^2}{\partial x^2}u(x,t)\Big|_{t=0} = 0, \qquad x \in [0, L].$$

$$\frac{\partial^2 u}{\partial t^2} = q_3\frac{\partial^3 u}{\partial x^2 \partial t} - q_1\frac{\partial^4 u}{\partial x^4} + q_2\delta(x - L)f(t),$$

where

$$q_1 = \frac{EI}{m},$$
$$q_2 = \frac{1}{m},$$
$$q_3 = 2\xi\sqrt{\frac{EI}{m}},$$

and the parameter vector is defined by $q = [q_1, q_2, q_3]^T$

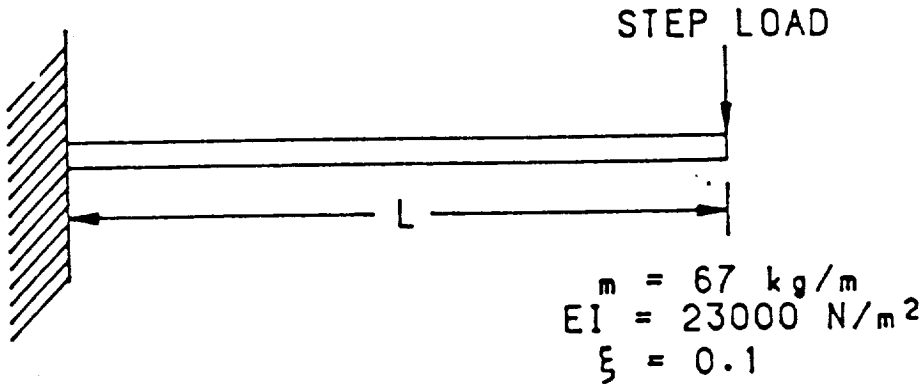

(a)

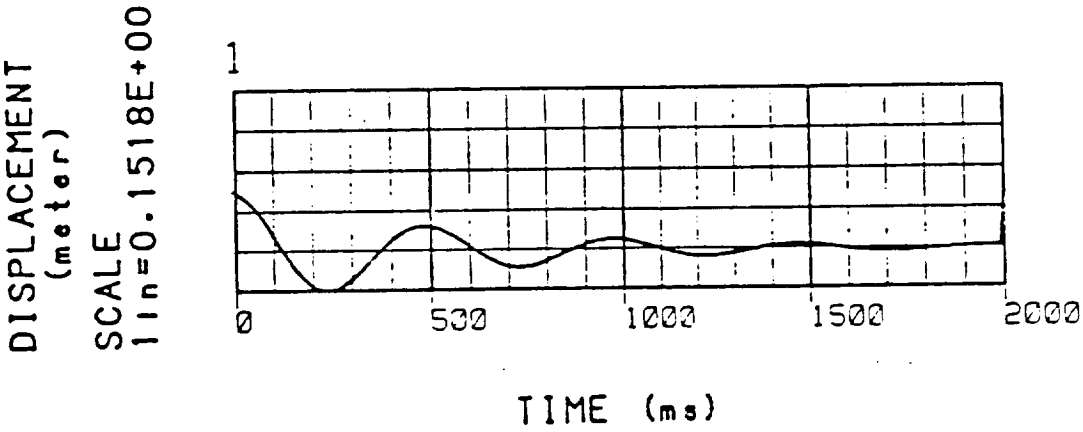

(b)

Fig. 3 (a) Cantilevered beam with a step load,
(b) resultant displacements.

Table 3

Performance Data for Case II

Iteration	q_1	q_2	q_3	m	EI	ξ	$\int_0^T \text{error}^2\, dt$
1	301.59	0.0159	2.08	63.00	19000.00	0.060	0.7843E-01
2	318.01	0.0155	2.76	64.50	20512.92	0.077	0.1664E-01
3	326.20	0.0153	3.06	65.26	21286.34	0.085	0.9432E-02
4	331.30	0.0152	3.23	65.73	21775.47	0.089	0.4498E-02
5	334.72	0.0151	3.34	66.05	22107.25	0.091	0.2284E-02
6	337.10	0.0151	3.43	66.27	22339.85	0.093	0.1238E-02
7	338.83	0.0151	3.49	66.43	22510.09	0.095	0.6649E-03
8	340.07	0.0150	3.53	66.55	22632.61	0.096	0.3796E-03
9	340.96	0.0150	3.55	66.65	22721.78	0.096	0.2199E-03
10	341.56	0.0150	3.56	66.71	22783.93	0.096	0.1519E-03
11	342.06	0.0150	3.59	66.76	22835.96	0.097	0.8667E-04
12	342.44	0.01497	3.62	66.80	22874.19	0.098	0.4961E-04
13	342.73	0.01496	3.64	66.83	22903.95	0.098	0.1165E-04
True values	343.28	0.0149	3.70	67.00	23000.00	0.1	

Case III : A Simply-Supported Beam with Spatially Variable Parameter

$$\frac{\partial^2 u}{\partial t^2} + \frac{\partial^2}{\partial x^2}\left(q(x)\frac{\partial^2 u}{\partial x^2}\right) = b(x)f(t), \qquad x \in [0, L],\, t > 0,$$

where $q = EI(x)$.

$$\frac{\partial^2 p}{\partial t^2} = -\frac{\partial^2}{\partial x^2}\left(q(x)\frac{\partial^2 p}{\partial x^2}\right) - \frac{R}{T}[u - z], \qquad x \in [0, L],\, t \in [0, T),$$

$$\frac{\delta J_a(x)}{\delta q} = \int_0^T \frac{\partial^2 p}{\partial x^2}\frac{\partial^2 u}{\partial x^2}\, dt.$$

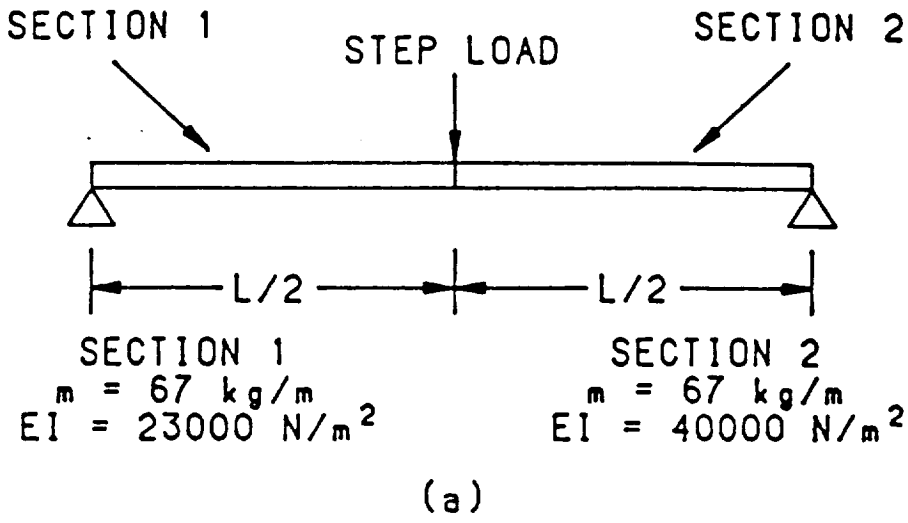

(a)

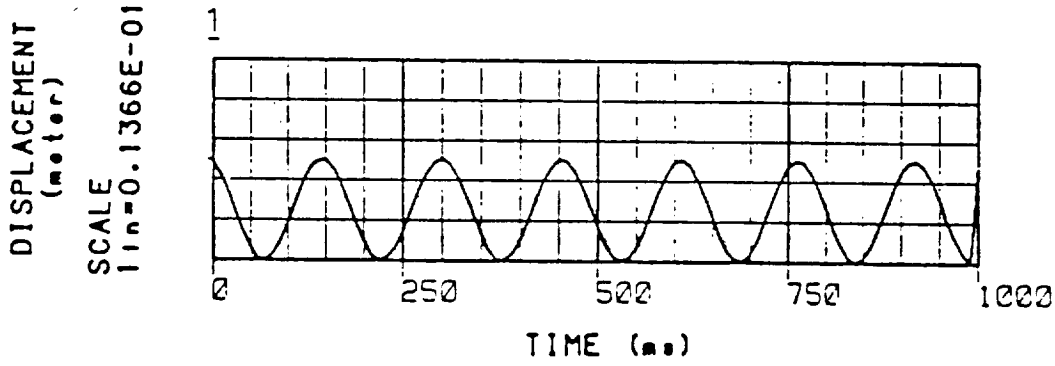

(b)

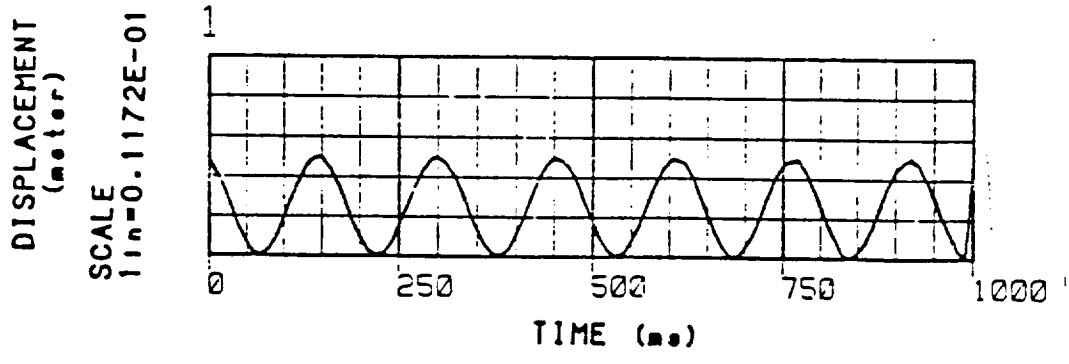

(c)

Fig. 4 (a) Simply-supported beam with spatially variable flexible rigidity,
(b) resultant displacements at L/4,
(c) resultant displcements at 3L/4.

Table 4

Performance Data for Case III

Iteration	q(sec. 1)	q(sec. 2)	$\int_0^T \text{error}^2\, dt$
1	21000.00	39000.00	0.76863E-02
2	21686.15	39286.47	0.40601E-02
3	22261.30	39521.45	0.14636E-02
4	22630.66	39688.41	0.41442E-03
5	22814.49	39759.51	0.13629E-03
6	22911.04	39793.95	0.51151E-04
7	22968.10	39815.07	0.11209E-04
True values	23000.00	40000.00	

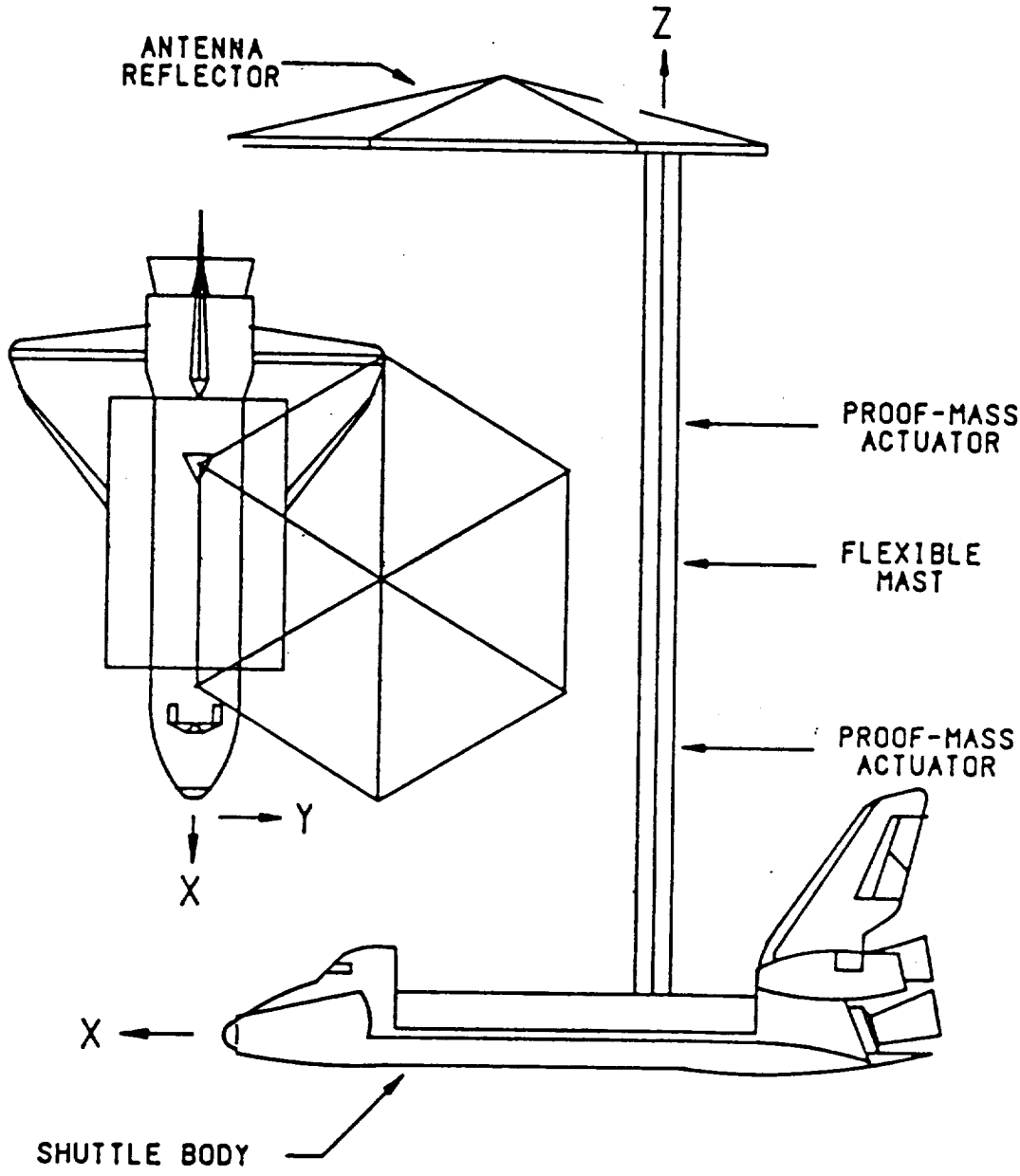

Fig. 1 The shuttle / antenna configuration of the spacecraft control laboratory experiment (SCOLE).

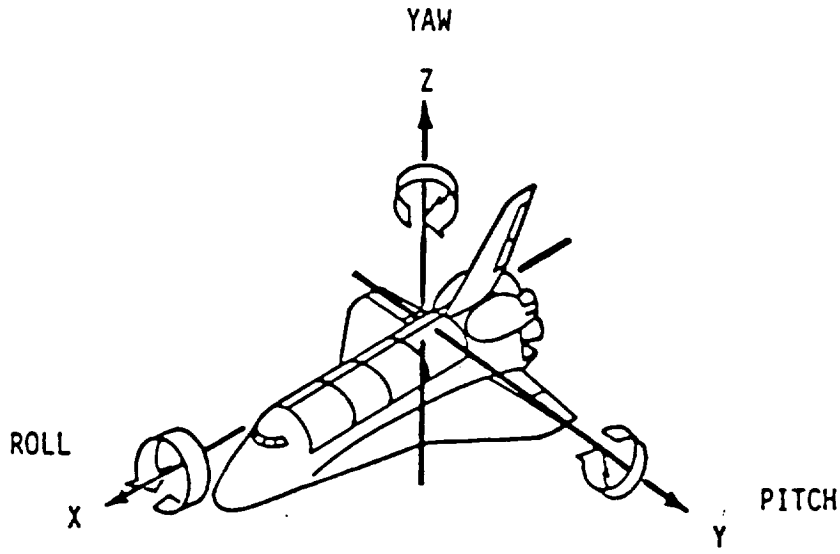

Fig. 2 Drawing showing the direction of "roll" bending, "pitch" bending and "yaw" twisting.

The SCOLE Mathematical Model

A. Dynamic Equations

Roll Beam Bending Equation in y-z Plane

$$\rho A\frac{\partial^2 u_\phi}{\partial t^2} - 2\xi_\phi\sqrt{\rho A E I_\phi}\frac{\partial^3 u_\phi}{\partial s^2\partial t} + EI_\phi\frac{\partial^4 u_\phi}{\partial s^4}$$
$$= \sum_{n=1}^{4}\left(f_{\phi,n}(t)\delta(s-s_n) + g_{\phi,n}(t)\frac{\partial}{\partial s}\delta(s-s_n)\right),$$
$$t \geq 0, \quad -\infty < s < \infty, \quad 0 \leq s_n \leq L.$$

Pitch Beam Bending Equation in x-z Plane

$$\rho A\frac{\partial^2 u_\theta}{\partial t^2} - 2\xi_\theta\sqrt{\rho A E I_\theta}\frac{\partial^3 u_\theta}{\partial s^2\partial t} + EI_\theta\frac{\partial^4 u_\theta}{\partial s^4}$$
$$= \sum_{n=1}^{4}\left(f_{\theta,n}(t)\delta(s-s_n) + g_{\theta,n}(t)\frac{\partial}{\partial s}\delta(s-s_n)\right),$$
$$t \geq 0, \quad -\infty < s < \infty, \quad 0 \leq s_n \leq L.$$

Yaw Beam Torsion Equation for z-Axis

$$\rho I_\psi\frac{\partial^2 u_\psi}{\partial t^2} - 2\xi_\psi I_\psi\sqrt{G\rho}\frac{\partial^3 u_\psi}{\partial s^2\partial t} - GI_\psi\frac{\partial^2 u_\psi}{\partial s^2}$$
$$= \sum_{n=1}^{4} g_{\psi,n}(t)\delta(s-s_n),$$
$$t \geq 0, \quad -\infty < s < \infty, \quad 0 \leq s_n \leq L.$$

B. Forcing Functions

The forcing functions on the right side of each equation are dependent on boundary conditions and proof-mass actuators.

Forces at $s = s_1 = 0$ (shuttle body forces)

The forces at $s_1 = 0$ involves the shears at that point which are equal to the shuttle mass m_1 times the corresponding component of acceleration.

$$f_{\phi,1}(t) = -m_1 \frac{\partial^2}{\partial t^2} u_\phi(0,t),$$
$$f_{\theta,1}(t) = -m_1 \frac{\partial^2}{\partial t^2} u_\theta(0,t).$$

Forces at $s = s_4 = L$ (reflector body forces)

$$f_{\phi,4}(t) = -m_4 \frac{\partial^2}{\partial t^2} u_\phi(L,t) - m_4 r_x \frac{\partial^2}{\partial t^2} u_\psi(L,t) - F_y,$$
$$f_{\theta,4}(t) = -m_4 \frac{\partial^2}{\partial t^2} u_\theta(L,t) + m_4 r_y \frac{\partial^2}{\partial t^2} u_\psi(L,t) + F_x,$$

where m_4 is the reflector mass, (r_x, r_y) is center of reflector mass from the beam tip at $s = L$, and F_x and F_y are the applied forces at the center of the reflector mass.

Forces at $s = s_2$ (proof-mass actuator forces)

$$f_{\phi,2}(t) = -m_2 \frac{\partial^2}{\partial t^2} u_\phi(s_2,t) + m_2 \frac{\partial^2}{\partial t^2} \Delta_{\phi,2},$$
$$f_{\theta,2}(t) = -m_2 \frac{\partial^2}{\partial t^2} u_\theta(s_2,t) + m_2 \frac{\partial^2}{\partial t^2} \Delta_{\theta,2},$$

where Δ and m denote displacement and mass of the proof-mass actuator.

Forces at $s = s_3$ (proof-mass actuator force)

$$f_{\phi,3}(t) = -m_3 \frac{\partial^2}{\partial t^2} u_\phi(s_3,t) + m_3 \frac{\partial^2}{\partial t^2} \Delta_{\phi 3},$$
$$f_{\theta,3}(t) = -m_3 \frac{\partial^2}{\partial t^2} u_\theta(s_3,t) + m_3 \frac{\partial^2}{\partial t^2} \Delta_{\theta,3}.$$

C. Moments

Moments at $s = 0$ (shuttle body moments)

$$\begin{pmatrix} g_{\phi,1} \\ g_{\theta,1} \\ g_{\psi,1} \end{pmatrix} = -[I_1\dot{w}_1 + w_1 \otimes I_1 w_1] + M_1(t) + M_D(t),$$

where I_1 is the moment of inertia of the shuttle body, $M_1(t)$ and $M_D(t)$ are control and disturbance moments, respectively, applied to the shuttle body, and $\otimes$ denotes the vector product.

Moments at $s = L$ (reflector body moments)

$$\begin{pmatrix} g_{\phi,4} \\ g_{\theta,4} \\ g_{\psi,4} \end{pmatrix} = -\left(\hat{I}_4\dot{w}_4 + w_4 \otimes \hat{I}_4 w_4 - M_4(t) + r \otimes F_4(t)\right) - m_4 r \otimes \frac{\partial^2 \xi_4}{\partial t^2},$$

where M_4 and F_4 are the control moment and force applied at the reflector center of the mass and ξ_4 is the coordinates of the beam tip.

Also, I_4 is the moment of inertia of the reflector, and $\hat{I}_4$ is that with respect to the beam tip given by

$$\hat{I}_4 = I_4 + m_4 \begin{pmatrix} r_y^2 & -r_x r_y & 0 \\ -r_x r_y & r_x^2 & 0 \\ 0 & 0 & r_x^2 + r_y^2 \end{pmatrix}$$

$$M_0\ddot{r}(t) + A_0 r(t) + B_0 F(t) + K_0(\dot{r}(t)^2) = 0 \ ,$$

where M_0 is the 17×17 matrix specified by

	x_1	x_2	x_3	x_4	x_5	x_6	x_7	x_8	x_9	x_{10}	x_{11}	x_{12}	x_{13}	x_{14}	x_{15}	x_{16}	x_{17}
x_1	ρA	0	0														
x_2	0	ρA	0														
x_3	0	0	ρA														
x_4				m_1	0												
x_5				0	m_1												
x_6						m_4	0	0	0	0	0	0	$m_4 r_z$				
x_7						0	m_4	0	0	0	0	0	$-m_4 r_y$				
x_8						0	0				0	0	0				
x_9						0	0		I_1		0	0	0				
x_{10}						0	0				0	0	0				
x_{11}						0	0	0	0	0							
x_{12}						0	0	0	0	0		I_4					
x_{13}						$m_4 r_z$	$-m_4 r_y$	0	0	0							
x_{14}														m_2	0		
x_{15}														0	m_2		
x_{16}																m_3	0
x_{17}																0	m_3

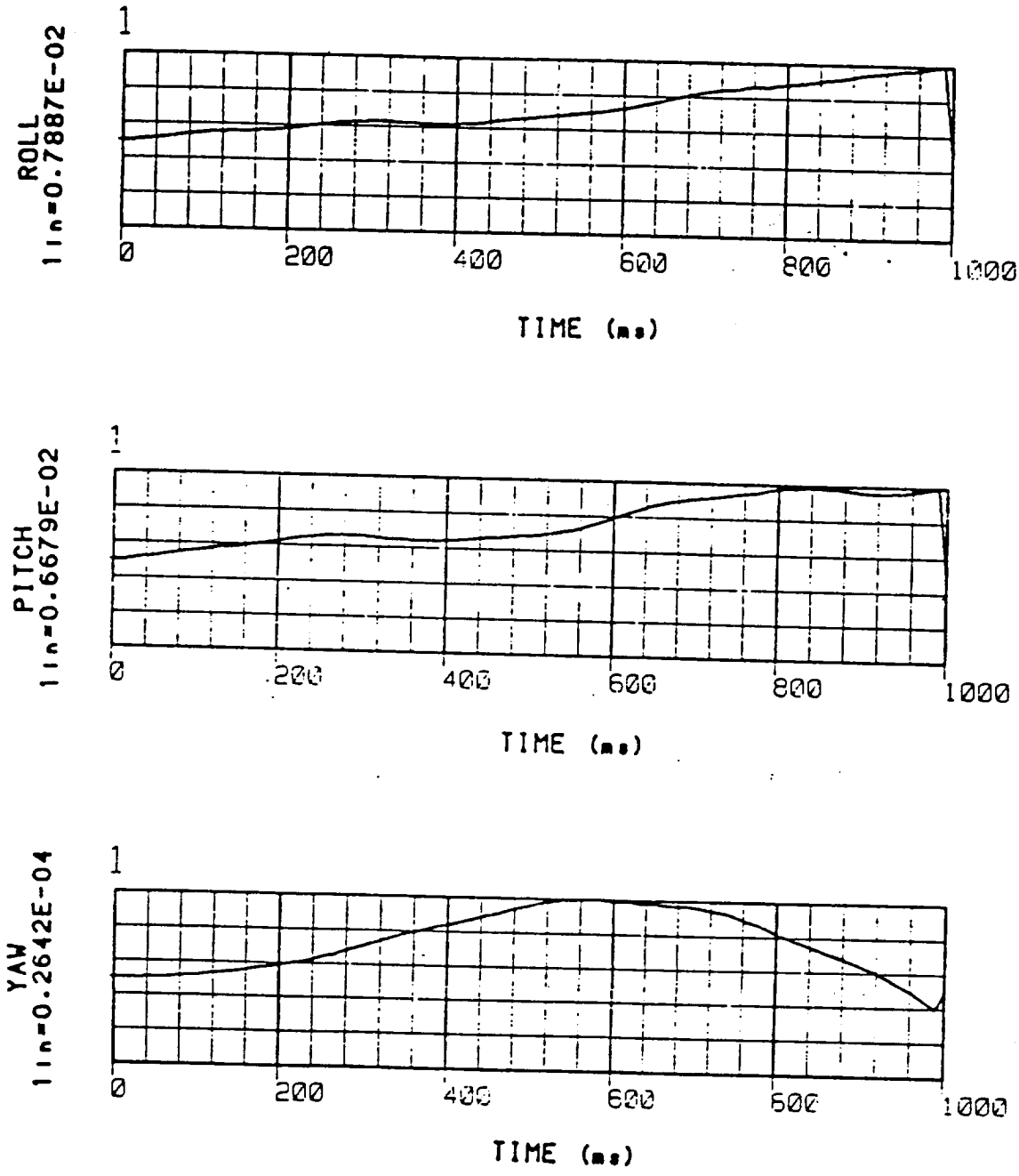

Fig. 3 Roll, pitch and yaw displacements with no damping.

Table 2

Performance Data for Case I : Nonlinear SCOLE Model

Iteration	q_1	q_2	m	EI	$\int_0^T \text{error}^2\, dt$
1	4.2353E+08	11.765	0.0850	3.6000E+07	0.1341E-04
2	4.2531E+08	11.067	0.0904	3.8427E+07	0.1896E-05
3	4.2612E+08	10.809	0.0925	3.9422E+07	0.3038E-06
4	4.2743E+08	10.705	0.0934	3.9929E+07	0.9131E-07
5	4.2704E+08	10.665	0.0938	4.0041E+07	0.8031E-07
6	4.2617E+08	10.637	0.0940	4.0064E+07	0.6646E-07
7	4.2508E+08	10.611	0.0942	4.0059E+07	0.4938E-07
8	4.2390E+08	10.589	0.0944	4.0029E+07	0.3237E-07
9	4.2277E+08	10.574	0.0945	3.9982E+07	0.2032E-07
10	4.2174E+08	10.561	0.0947	3.9934E+07	0.1465E-07
11	4.2072E+08	10.546	0.0948	3.9894E+07	0.1332E-07
12	4.1959E+08	10.525	0.0950	3.9867E+07	0.1365E-07
13	4.1819E+08	10.495	0.0953	3.9845E+07	0.1676E-07
14	4.1783E+08	10.471	0.0955	3.9903E+07	0.7113E-08
True values	4.1858E+08	10.465	0.0956	4.0000E+07.00	

Table 3

Performance Data for Case I : Linearized SCOLE Model

Iteration	q_1	q_2	m	EI	$\int_0^T \text{error}^2\, dt$
1	4.2353E+08	11.765	0.0850	3.6000E+07	0.1341E-04
2	4.2531E+08	11.068	0.0904	3.8427E+07	0.1894E-05
3	4.2613E+08	10.809	0.0925	3.9422E+07	0.3051E-06
4	4.2744E+08	10.704	0.0934	3.9929E+07	0.9142E-07
5	4.2705E+08	10.665	0.0938	4.0041E+07	0.8040E-07
6	4.2618E+08	10.637	0.0940	4.0064E+07	0.6660E-07
7	4.2509E+08	10.611	0.0942	4.0060E+07	0.4955E-07
8	4.2392E+08	10.590	0.0944	4.0030E+07	0.3255E-07
9	4.2277E+08	10.574	0.0945	3.9982E+07	0.2032E-07
10	4.2175E+08	10.561	0.0947	3.9933E+07	0.1478E-07
11	4.2066E+08	10.546	0.0948	3.9888E+07	0.1378E-07
12	4.1957E+08	10.524	0.0950	3.9867E+07	0.1361E-07
13	4.1816E+08	10.495	0.0953	3.9846E+07	0.1667E-07
14	4.1773E+08	10.471	0.0955	3.9893E+07	0.8371E-08
True values	4.1858E+08	10.465	0.0956	4.0000E+07.00	

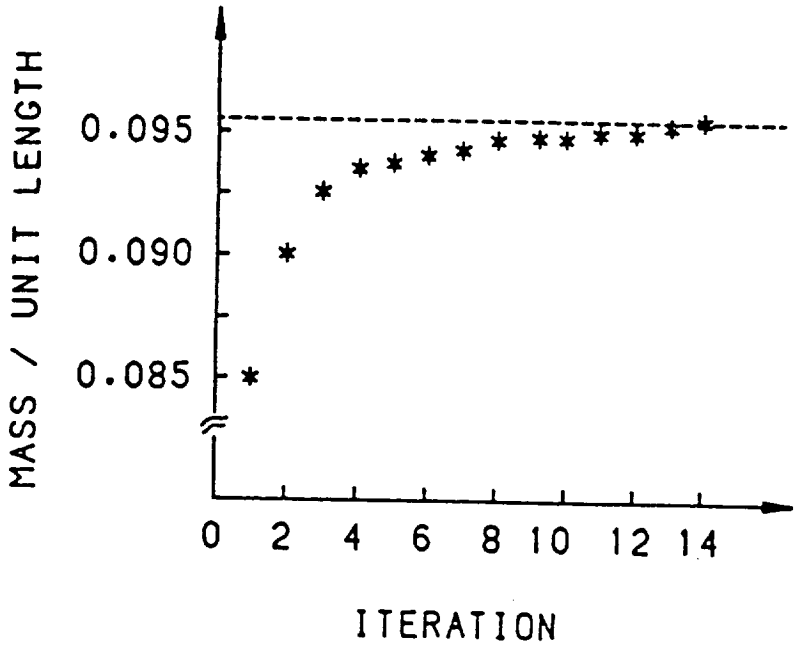

(a)

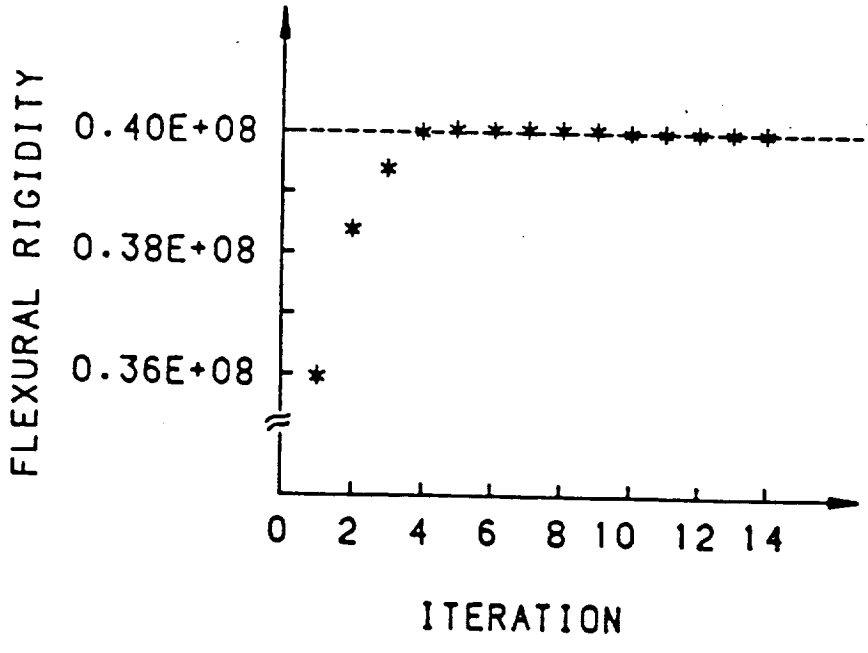

(b)

Fig. 5 Convergence of parameters for the SCOLE problem in Case I using nonlinear model.

(a) For ρA / unit length.

(b) For flexural rigidity, EI.

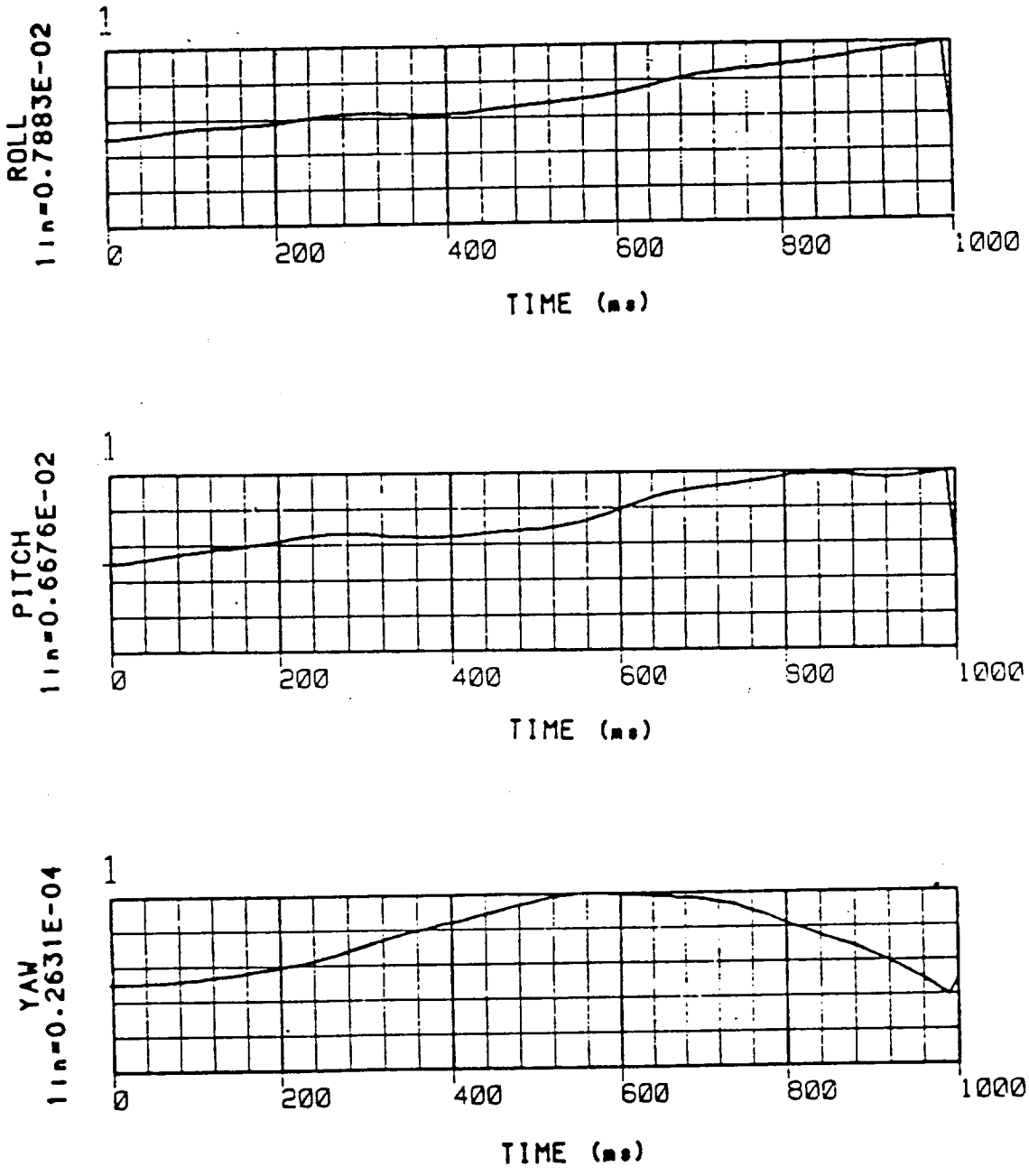

Fig. 4 Roll, pitch and yaw displacements when a damping factor of 0.003 is added to the system.

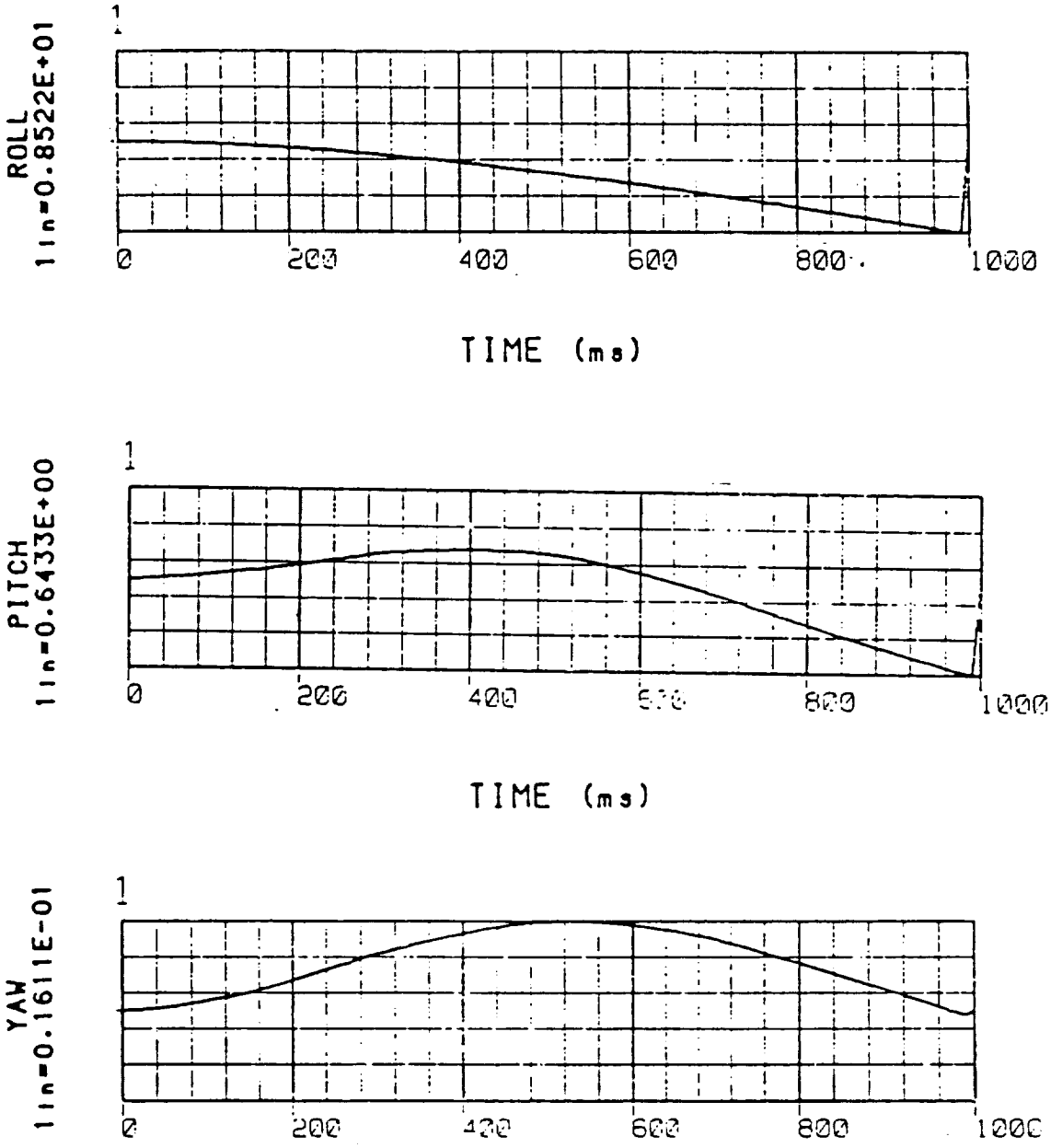

Fig. 6 Roll, pitch and yaw displacements when a force and a moment are applied at the antenna-end of the beam.

Table 4

Performance Data for Case II

Iteration	EI	ρA	ρI_ψ	ξ
1	32000000.00	0.0750	1.1000	0.00250
2	37582208.00	0.0881	0.9690	0.00250
3	39607652.00	0.0928	0.9428	0.00250
4	40157244.00	0.0941	0.9362	0.00250
5	40372424.00	0.0946	0.9247	0.00280
6	40338068.00	0.0945	0.9183	0.00288
7	40309128.00	0.0945	0.9127	0.00293
8	40282296.00	0.0943	0.9088	0.00289
9	40260868.00	0.0943	0.9047	0.00287
10	40243016.00	0.0942	0.9008	0.00285
11	40226244.00	0.0942	0.8983	0.00281
12	40202376.00	0.0942	0.8979	0.00286
13	40181576.00	0.0942	0.8977	0.00292
14	40162324.00	0.0941	0.8974	0.00299
15	40149520.00	0.0941	0.8973	0.00298
16	40140040.00	0.0941	0.8973	0.00295
True values	40000000.00	0.0956	0.9089	0.003

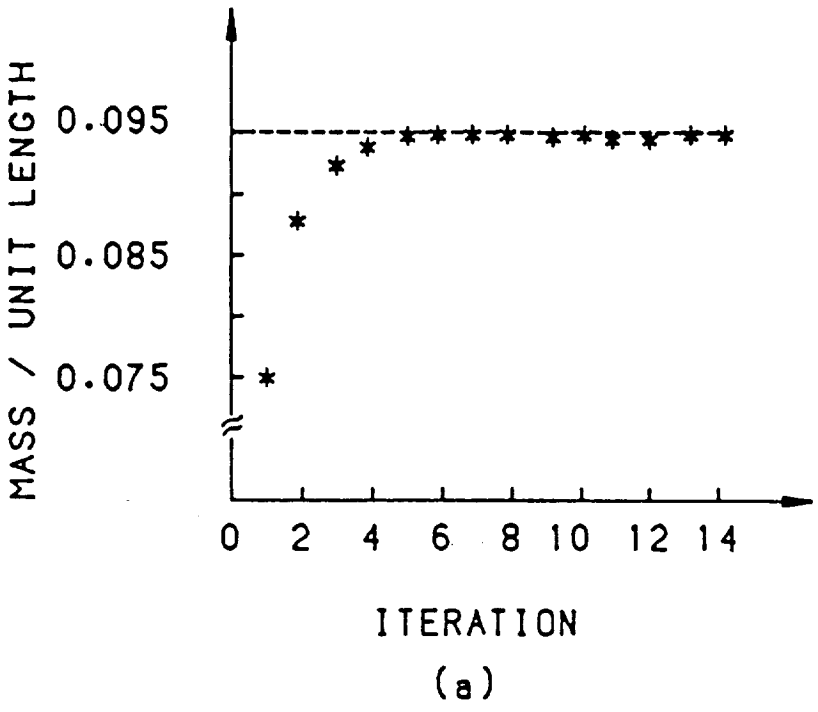

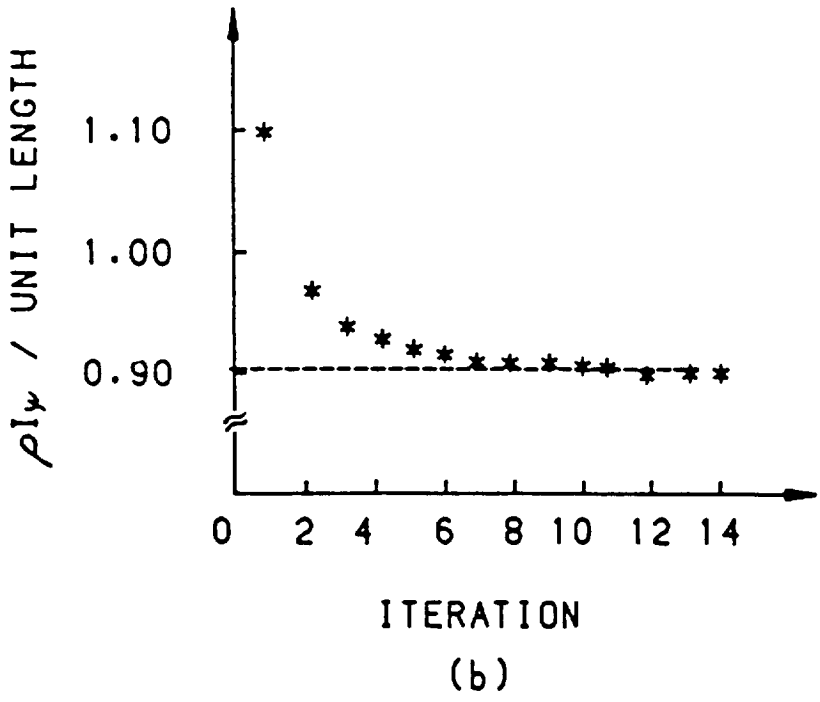

Fig. 7 Convergence of error criterion for Case II.

(a) For ρA / unit length.

(b) For ρI_ψ /unit length.

CONCLUSION

Infinite-dimensional identification method presented in this paper shows a significant promise in the parameter estimation of flexible structures with great potentials for applications to LSS's. The basic approach is the abstract formultion of the system dynamics in function spaces and then applying optimal control theory to adjust system parameters so that the error between actual and model data is minimized. The use of partial differential equation for the purpose of estimation elimainates many problems associated with model trunction in the finite dimensional approach. Based on partial differential equation models and a quadratic performance index an algorithm to estimate the optimal parameters has been developed. The numerical results show the effectiveness of the algorithm in estimating parameters of the flexible beam in the SCOLE problem. The results show fairly good match between the model and the estimated parameters. However, as the number of parameters to be identified increases it becomes increasingly time consuming and difficult to solve. Also, due to model mismatch, slightly less accuracies are expected if experimental measurement data from physical beam were used.

BIBLOGRAPHY

1. M. J. Balas, "Trends in Large Space Structure Control Theory : Fondest Hopes, Wildest Dreams," *IEEE Transaction on Automatic Control*, vol. 1, pp. 522-535, June 1982.

2. W. R. Wells and G. R. Spalding, "Parameter Estimation and Identification of Distributed Syatems," *Proceedings of the Symposium on Dynamics and Control of Large Flexible Spacecraft*, Blacksburg, VA, pp. 107-117, June 13-15, 1977.

3. F. C. Tung, "Finite Elements Models and System Identification of Large Space Structures," *Proceedings of the Symposium on Dynamics and Control of Large Flexible Spacecraft*, Blacksburg, VA, pp. 255-267, June 15-17, 1977.

4. M. J. Balas and J. H. Lilly, "Adaptive Parameter Estimation of Large-scale Systems by Reduced-order Modeling," *Proceedings of the 20th Conference on Decision and Control*, San Diego, CA, vol. 1, pp. 233-239, Dec. 1981.

5. M. J. Balas, "Parameter Estimation of Large Flexible Aerospace Structures with Application to the Control of the Maypole Deployable Reflector," Rensselaer Polytechnic Institute, Troy, NY, Nov. 1981.

6. K. Y. Lee and S. M. Bitter, "Identification of Distributed Parameter Systems using Finite Element Approximation," *Proceedings of the 1982 American Control Conference*, Arlington, VA, vol. 1, pp. 433-434, June 14-16, 1982.

7. H. T. Banks, "Algorithm for Estimation in Distributed Models with application to Large Space Structures," *Proceedings of the Workshop on Application of Distributed System Theory to the Control of Large Space Stuctures*, JPL, Pasadena, CA, pp. 505-

509, July 14-16, 1982.

8. S. L. Hendricks, S. Rajaram, M. P. Kamat, and J. L. Junkins, "Identification of Large Flexible Structures Mass/ Stiffnes and Damping from On-orbit Experiments", *Proceedings of the Workshop on Application of Distributed System Theory to the Control of Large Space Stuctures*, JPL, Pasadena, CA, pp. 511-520, July 14-16, 1982.

9. S. L. Hendricks, et al., "Identification of Large Flexible Structures Mass/ Stiffnes and Damping Matrices for Large Linear Vibratory Systems," *AIAA Journal of Guidance, Control, and Dynamics*, vol. 7, pp. 244-245, Mar.-Apr. 1984.

10. H. T. Bank and I. G. Rosen, "Approximation Techniques for Parameter Estimation and Feedback Control distributed Models of Large Flexible Structures," *Proceedings of NASA/ACC Workshop on Identification and Control of Flexible Space Stuctures*, San Diego, CA, June 4-6, 1984.

11. S. Rajaram and J. L. Junkins, "Identification of Vibrating Flexible Structures", *AIAA Journal of Guidance, Control, and Dynamics*, vol.87, pp. 463-470, July-Aug. 1985.

12. K. Y. Lee, D. Walker and S. A. Hossain, "Structural Parameter Identification of Distributed System Using Finite Element Approximation," *Proceedings of the 24th IEEE Conference on Decision and Control*, Fort Lauderdale, FL, pp. 1145-1150, Dec. 11-13, 1985.

13. K. Y. Lee, "Technique for the Identification of Distributed Systems using Finite Element Approximation," *Advances in Control and Dynamic Systems*, C. T. Leondes, (ed.), vol. 24, New York: Academic Press, 1986.

14. G. R. Spalding, "Distributed System Identification - A Green's Function Approach," *ASME, Transaction, Series G - Journal of Dynamic Systems, Measurement, and*

Control, vol. 98, pp.146-151, June 1976.

15. J. A. Burns and E. M. Cliff, "On the Formulation of Some Distributed System Parameter Identification Problems," *Proceedings of the Symposium on Dynamics and Control of Large Flexible Spacecraft*, Blacksburg, VA, pp. 87-105, June 13-15, 1977.

16. C. T. Sun and J. N. Juang, "Parameter Estimation in Beams using Timoshenko Beam Model with Damping," *Proceedings of the Workshop on Application of Distributed System Theory to the Control of Large Space Stuctures*, JPL, Pasadena, CA, pp. 531-545, July 14-16, 1982.

17. K. Y. Lee and J. W. Clary, "Optimal Control of Bilinear Distributed Parameter Systems," *Proceedings of the 17th IEEE Conference on Decision and Control*, pp. 886-891, 1979.

18. J. L. Lions, *Optimal Control of Systems Governed by Partial Differential Equation*, Berlin: Springer-Verlag, 1971.

19. G. Chavent, "Identification of Functional Parameters in Partial Differential Equation," *Identification of Parameters in Distributed System*, Goodson and Polis (ed.), ASME, New York, pp. 31-48, 1974.

20. G. Chavent, "Identification of Distributed Parameter System :About the output Least Square Method, Its Implementation, and Identifiability," *Proceedings of the 5th IFAC Symp. on Identification and System Parameter Estimation*, Darmstadt, FRG: Pergamon Presss, pp. 85-87, 1979.

21. K. Y. Lee and S. A. Hossain, "System Identification of Distributed Systems Applied to Seismic Inverse Problem," *Proceedings of the 24th IEEE Conference on Decision and Control*, Fort Lauderdale, FL, pp. 1139-1144, Dec. 11-13, 1985.

22. L. W. Taylor and A. V. Balakrishnan, "A Mathematical Problem and A Spacecraft Control Laboratory Experiment (SCOLE) used to Evaluate Control Laws for Flexible Spacecraft - NASA/IEEE Design Challenge," University of California at Los Angeles, Los Angeles, CA, June 1984.

23. A. V. Balakrishnan, "A Mathematical Formulation of the SCOLE Control Problem : Part 1," University of California at Los Angeles, Los Angeles, CA, May 1985.

24. S. A. Hossain "System Identification of Flexible Structures using Distributed Parameter Models," Ph.D. dissertation, Department of Electrical Engineering, University of Houston-University Park, Houston, Tx, May 1986.

25. K. Y. Lee and S. A. Hossain, "A Distributed System Approach to the identification of Flexible Structures", submitted for publication to *AIAA Journal of Guidance, Control, and Dynamics.*

Revised November 1987

SOME NONLINEAR DAMPING MODELS IN FLEXIBLE STRUCTURES

A.V. Balakrishnan†
Electrical Engineering Department
UCLA

September 1987

Abstract

We introduce a class of nonlinear damping models with application to flexible flight structures characterized by low damping. We are able to obtain approximate solutions of engineering interest for our model using the classical "averaging" technique of Krylov and Bogoliubov. The results should be considered preliminary pending further investigation.

---

† Paper presented at NASA SCOLE Workshop, November 1987, Colorado Springs, Colorado.

1. Introduction

The problem of characterizing the damping mechanism in flexible structures has received renewed attention in recent years in connection with the need to stabilize flexible flight structures such as antennas deployed in space. The damping models even when simplified to be linear appear to lead to rather complex mathematics if the structure is described by partial differential equations and much progress has been made (the analyticity of the generated semigroup has been shown to be essential). But experimental evidence as in SCOLE [1] seems to support the need for nonlinear models — the decrement is much smaller than predicted by linear models. Some of the difficulty inherent in handling nonlinear models is offset by the fact that damping, whatever its nature, is still small. This opens up in particular the feasibility of obtaining approximate solutions using the classical averaging method of Krylov-Bogoliubov [2].

In this paper we study a class of nonlinear models and approximate the response by the Krylov-Bogoliubov technique. We use a modal expansion and neglect off-diagonal terms. The emphasis is on useful engineering solutions rather than abstract mathematics.

We begin in Section 2 with the primary nonlinear damping model for the simplest system — the one-dimenisonal or single-mode case. We emphasize in particular one feature that emerges, viz., the potential lack of identifiability from response data. In Section 3 we generalize to the multi- (non-finite-) dimensional case. In Section 4 we show the relevance of the Krylov-Bogoliubov technique for approximating solutions to nonlinear boundary feedback. We may mention that there is much work — even classical in nature — on nonlinear oscillations such as the nonlinear pendulum where the spring constant is no longer linear; however, relatively little attention appears to have been paid to the small nonlinear damping term case.

2. Single-mode Example

To illustrate ideas, let us begin with a one-dimensional (single-mode) example:

$$\ddot{x}(t) + \varepsilon D(x, \dot{x}) + \omega^2 x(t) = 0 \tag{2.1}$$

where the dots indicate time-derivatives, as usual. We assume that:

$$D(x, \dot{x})\dot{x} \geq 0 \tag{2.2}$$

so that for $E(t)$, the energy

$$E(t) = \tfrac{1}{2}(\dot{x}(t)^2 + \omega^2 x(t)^2) \tag{2.3}$$

we have

$$\frac{d}{dt}E(t) = -\varepsilon D(x, \dot{x})\dot{x} \leq 0 \tag{2.4}$$

satisfying the energy nonincrease requirement. The particular choice for $D(x, \dot{x})$ we shall make is:

$$D(x, \dot{x}) = 2\omega\zeta\dot{x} + \gamma x^{2m}|x|^{\alpha}\, \dot{x}^{(2n+1)}|\dot{x}|^{\beta} \tag{2.5}$$

where m, n are nonnegative integers,

$$0 \leq \alpha, \beta \quad \text{and} \quad 0 \leq \alpha + \beta < 1; \quad 0 < \zeta < 1, \; 0 < \gamma < 1 .$$

For small enough ε we may apply the averaging method of Krylov-Bogoliubov [2, 5]. Thus, we write for the approximate solution:

$$x(t) = a(t) \sin(\omega t + \phi(t)) \tag{2.6}$$

where the amplitude function $a(t)$ and the phase function $\phi(t)$ are slowly varying over the period $T = 2\pi/\omega$. According to the K-B approximation [2]:

$$\frac{da}{dt} = -\frac{\varepsilon}{\omega} K_0(a) \tag{2.7}$$

where

$$K_0(a) = \frac{1}{2\pi}\int_0^{2\pi} D(a \sin\phi,\; a\omega\cos\phi)\cos\phi \; d\phi \tag{2.8}$$

and

$$\frac{d\phi}{dt} = \frac{\varepsilon}{\omega a} P_0(a) \tag{2.9}$$

$$P_0(a) = \frac{1}{2\pi} \int_0^{2\pi} D(a \sin\phi,\ a\omega \cos\phi) \sin\phi \ d\phi \ . \tag{2.10}$$

Now we can readily calculate that for our choice, because of (2.2),

$$P_0(a) = 0$$

$$\begin{aligned} K_0(a) &= 2\omega\zeta a \left(\frac{1}{2\pi} \int_0^{2\pi} \omega \cos^2\phi \ d\phi \right) \\ &\quad + \omega^{1+\beta} \gamma a^{2m+2n+1+\alpha+\beta} \left(\frac{1}{2\pi} \int_0^{2\pi} \sin^{2m}\phi \cos^{2n+2}\phi \ |\sin\phi|^{\alpha} \ |\cos\phi|^{\beta} \ d\phi \right) \\ &= \omega^2 \zeta a + a^{2m+2n+1+\alpha+\beta} \gamma \omega^{2n+1+\beta} \mu \end{aligned}$$

where

$$\mu = \frac{1}{2\pi} \int_0^{2\pi} \sin^{2m}\phi \cos^{2n}\phi \cos^2\phi \ |\sin\phi|^{\alpha} \ |\cos\phi|^{\beta} \ d\phi \tag{2.11}$$

and is a constant less than 1/2. Hence letting $p = 2m + 2n$, we have

$$\frac{da}{dt} = -\varepsilon(\omega\zeta a + a^{p+1+\alpha+\beta} \omega^{2n+\beta} \gamma\mu) \tag{2.12}$$

We may set $\varepsilon = 1$ without loss of generality since we may absorb it into ζ and γ. Then

$$t = -\int_{a(0)}^{a(t)} \frac{da}{\omega\zeta a + a^{p+1+\alpha+\beta} \omega^{2n+\beta} \gamma\mu} \tag{2.13}$$

yielding

$$a(t) = a(0) e^{-t\omega\zeta} \left[1 + a(0)^{p+\alpha+\beta} \omega^{2n-1+\beta} \frac{\gamma\mu}{\zeta} (1 - e^{-t\omega\zeta(p+\alpha+\beta)}) \right]^{-\frac{1}{p+\alpha+\beta}} \tag{2.14}$$

We can readily verify that for $\zeta = 0$, we have

$$a(t) = a(0)[1 + a(0)^{p+\alpha+\beta} \omega^{2n+\beta} \gamma\mu(p + \alpha + \beta)t]^{-\frac{1}{p+\alpha+\beta}} \tag{2.15}$$

The case $\gamma = 0$ is even more obvious. One salient fact that emerges immediately from (2.14) and (2.15) is that it would be difficult to resolve $p + \alpha + \beta$ into its components from response data, unless we can change ω.

Note also from (2.15) that the rate of decay is not exponential in t and further the decrement over any integral multiple of the period depends on the initial amplitude as well as the frequency of oscillation. Finally for inegral k and

$$t = \frac{2\pi k}{\omega}$$

we have, taking logarithms and setting $c = p + \alpha + \beta$

$$\log \frac{a\left(\frac{2\pi k}{\omega}\right)}{a(0)} = -2\pi k\zeta - \frac{1}{c}\log\left[1 + \frac{a(0)^c \omega^{2n-1+\beta}\gamma\mu}{\zeta}\left(1 - e^{-2\pi k\zeta c}\right)\right]. \qquad (2.16)$$

For small ζ this is well approximated by

$$-2\pi k\zeta - \frac{1}{c}\log\left(1 + 2\pi k\lambda a(0)^c\right),$$

where

$$\lambda = \omega^{2n+\beta-1}\gamma\mu.$$

The slope (as a function of k)

$$= -2\pi\zeta - \frac{2\pi\lambda a(0)^c}{c(1 + 2\pi k\lambda a(0)^c)} \qquad (2.17)$$

and hence the linear damping term is yielded by the asymptotic slope as $k \to \infty$, while for small k there is a marked curvature which depends also on the initial amplitude $a(0)$. The inital (at $k = 0$) slope

$$= -2\pi\zeta - \frac{2\pi\lambda a(0)^c}{c} \qquad (2.18)$$

is larger (in absolute value). The second derivative being positive, the curve is convex — CUP. This is in excellent qualitative agreement with SCOLE damping data: see Figure 1 where amplitude is plotted on logarithmic scale (period = 5 seconds).

SCOLE DAMPING

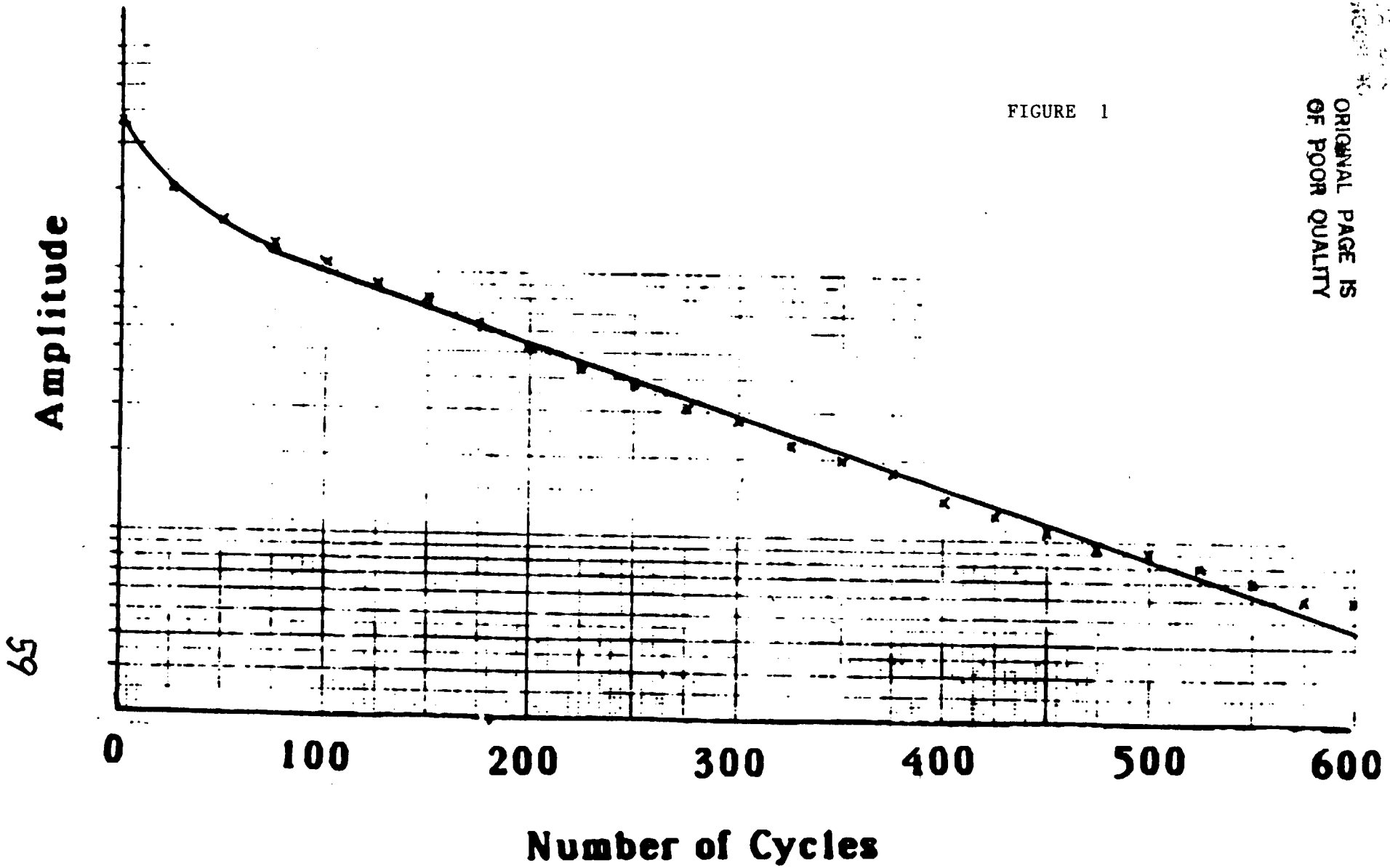

FIGURE 1

To get another version of (2.16) we may replace (2.7) by the more exact formula

$$\frac{a(t+T) - a(t)}{T} = -\frac{\varepsilon}{\omega} K_0(a(t)) \tag{2.19}$$

and hence using

$$a_k = a(kT) \tag{2.20}$$

we would have

$$a_{k+1} = a_k - \frac{\varepsilon T}{\omega} K_0(a_k) \tag{2.21}$$

so that

$$\log\left(\frac{a_k+1}{a_k}\right) = \left(1 - \frac{\varepsilon T}{\omega}\frac{K_0(a_k)}{a_k}\right)$$

which under our "small damping" assumption, may be replaced by

$$\log\frac{a_k+1}{a_k} = -\frac{\varepsilon T}{\omega}\frac{K_0(a_k)}{a_k}, \tag{2.22}$$

$$= -\varepsilon 2\pi(\zeta + a_k^c \gamma\mu\omega^{2n-1+\beta}). \tag{2.23}$$

3. Multidimensional Generalization

Analogous entirely to the one-dimensional case, we may write the general nonlinear dynamic equation for flexible structures [2] as

$$M\ddot{x}(t) + \mathfrak{D}(x(t), \dot{x}(t)) + Ax(t) = 0 \tag{3.1}$$

where the state $x(t)$ ranges in a separable (real) Hilbert space $\mathcal{H}$; M is a self-adjoint positive definite (with bounded inverse) operator on $\mathcal{H}$ onto $\mathcal{H}$; A is a self-adjoint nonnegative definite closed linear operator with domain dense in $\mathcal{H}$ and with compact resolvent; we shall (for simplicity) assume that zero is in the resolvent set of A. In the *linear* case

$$\mathfrak{D}(x(t), \dot{x}(t)) = D\dot{x}(t) \tag{3.2}$$

where D is also a self-adjoint nonnegative definite closed linear operator whose domain includes that of $\sqrt{A}$. In the most important case we further specify that

$$D\phi_k = 2\zeta_k \omega_k M\phi_k \tag{3.3}$$

where $\{\phi_k\}$ are the M-orthonormalized eigenfunctions of A with eigenvalues ω_k^2 such that

$$A\phi_k = \omega_k^2 M\phi_k . \tag{3.4}$$

Here ζ_k is the damping ratio. If $\zeta_k = \zeta$ and we have strict proportional damping — see [3] for more — D is then essentially the positive square root of A (except for M). More generally we require that $\lim_k \zeta_k \geq \zeta > 0$. In the nonlinear analogue of (2.5) we set

$$\mathfrak{D}(\phi_j, \phi_k) = 0 \qquad j \neq k \tag{3.5}$$

and more generally for x, y such that

$$\sum \omega_k^2 b_k^2 + \sum a_k^{4m+2\alpha} b_k^{2n+2+2\beta} \gamma_k^2 < \infty \tag{3.6}$$

where

$$a_k = [x, \phi_k] ; \qquad b_k = [y, \phi_k] \tag{3.7}$$

we define:

$$[\mathfrak{D}(x, y), \phi_k] = \gamma_k a_k^{2m} |a_k|^{\alpha} b_k^{2n+1} |b_k|^{\beta} + 2\zeta_k \omega_k b_k \tag{3.8}$$

where, as before, m and n are nonnegative integers and that

$$0 \leq a , \qquad \beta < 1 ; \qquad \alpha + \beta < 1 ; \qquad 0 \leq \gamma . \tag{3.9}$$

Note that

$$[\mathfrak{D}(x, y), y] \geq 0$$

for every x and y. Hence if

$$E(t) = \tfrac{1}{2} \{[Ax(t), x(t)] + [M\dot{x}(t), \dot{x}(t)]\}$$

we have that

$$\frac{d}{dt} E(t) = -[\mathfrak{D}(x(t), \dot{x}(t)), \dot{x}(t)] \leq 0 . \tag{3.10}$$

Or, the energy is nonincreasing. Using the modal expansion

$$x(t) = \sum a_k(t)\, \phi_k \tag{3.11}$$

we see that for each k

$$\ddot{a}_k(t) + \omega_k^2\, a_k(t) + a_k(t)^2\, |a_k(t)|^{\alpha}\, \dot{a}_k(t)\, |\dot{a}_k(t)|^{\beta} + 2\zeta_k \omega_k\, \dot{a}_k(t) = 0\,. \tag{3.12}$$

We can therefore invoke the K-B averaging procedure obtaining the approximate solution

$$a_k(t) = A_k(t) \sin(\omega_k t + \phi_k) \tag{3.13}$$

$$A_k(t) = A_k(0)\, e^{-t\zeta_k \omega_k} \left(1 + A_k(0)^c\, \omega_k^{2n+\beta-1}\, \frac{\gamma_k \mu}{\zeta} \left(1 - e^{-t\zeta_k \omega_k c}\right)\right)^{-\frac{1}{c}}\,. \tag{3.14}$$

And for $\zeta_k = 0$,

$$A_k(t) = A_k(0) \left(1 + A_k(0)^c\, \omega_k^{2n+\beta}\, \gamma_k\, \mu c t\right)^{-\frac{1}{c}}$$

where, as before,

$$\mu = \frac{1}{2\pi} \int_0^{2\pi} \sin^{2m}\phi \cos^{2n}\phi\, |\sin\phi|^{\alpha}\, |\cos\phi|^{\beta} \cos^2\phi\; d\phi\,. \tag{3.15}$$

For $\alpha + \beta = 0$, we can give a kernel representation. Thus

$$z = \mathfrak{D}(x, y) = \sum \gamma_i\, \phi_i [\phi_i, x]^{2m}\, [\phi_i, y]^{2n+1}$$

where

$$\sum \gamma_i^2 < \infty\,; \qquad \gamma_i \geq 0\,;$$

and for the concrete realization $\mathcal{H} = L_2(0, L)$, the corresponding "kernel" would be

$$W(s, \sigma_1, \ldots, \sigma_{2m}, s_1, \ldots, s_{2n+1}) = \sum_i \gamma_i\, \phi_i(s)\, \phi_i(\sigma_1) \cdots \phi_i(\sigma_{2m})\, \phi_i(s_1) \cdots \phi_i(s_{2n+1}) \tag{3.16}$$

and

$$\begin{aligned} z(s) = \int_0^L \cdots \int_0^L & W(s, \sigma_1, \ldots, \sigma_{2m}, s_1, \ldots, s_{2n+1})\, x(\sigma_1)\, x(\sigma_2) \cdots x(\sigma_{2m}) \\ & \times y(s_1) \cdots y(s_{2n+1})\; d\sigma_1\, d\sigma_2 \cdots d\sigma_{2m}\, ds_1 \cdots ds_{2n+1}\,. \end{aligned} \tag{3.17}$$

A plausible model in this case would be to rewrite (3.1) as

$$M\ddot{x}(t) + \mathfrak{D}(x(t), D\dot{x}(t)) + 2\zeta D\dot{x}(t) + Ax(t) = 0\,. \tag{3.18}$$

which will satisfy (3.10), since the γ_i in (3.16) are nonnegative. In the notation of (3), the "roll" equations for example will have the form:

$$\rho A \ddot{u}_\phi(t, s) + EI_\phi u_\phi''''(t, s) - 2\zeta\sqrt{\rho A E I_\phi}\,\frac{\partial^3 u_\phi(t, s)}{\partial t\,\partial^2 s}$$

$$- \int_0^L \cdots \int_0^L W(s, \sigma_1, \ldots, \sigma_{2m}, s_1, \ldots, s_{2n+1}) \times u_\phi(t, \sigma_1) \cdots u_\phi(t, \sigma_{2m})$$

$$\times \frac{\partial^3 u_\phi(t, s_1)}{\partial t\,\partial^2 s} \cdots \frac{\partial^3 u_\phi(t, s_{2n+1})}{\partial t\,\partial^2 s}\, d\sigma_1 \cdots d\sigma_{2m}\, ds_1 \cdots ds_{2n+1}$$

$$= 0 .$$

It is clear that we may generalize (3.17) without recourse to modes. The "nonlocal" nature of the operator should hardly be surprising, since this is already so in the linear case if we want strict proportionality ($\zeta_k = \zeta$) for example.

4. Application to Nonlinear Boundary Feedback

In this section we shall apply the K-B averaging technique to obtain approximate solution to the response of a flexible structure to nonlinear boundary feedback control. The control effort is small so that the K-B approximation is reasonable. We follow [4] for the model where the "boundary" is finite-dimensional. Thus we have in the same setting as Section 3, but omitting the natural damping term:

$$M\ddot{x}(t) + Bf(B^*\dot{x}(t)) + Ax(t) = 0 \tag{4.1}$$

where B means R^m onto $\mathcal{H}$ and $f(\cdot)$ maps R^m into R^m and is such that

$$[f(u), u] > 0 \qquad \text{for } u \neq 0 . \tag{4.2}$$

Using the modal expansion as in Section 3:

$$x(t) = \Sigma\, a_k(t)\, \phi_k$$

we obtain

$$\ddot{a}_k(t) + \omega_k^2 a_k(t) + [f(\Sigma\, \dot{a}_j(t) b_j),\ b_k] = 0 \tag{4.3}$$

where

$$B^*\phi_k = b_k .$$

Taking the approximation

$$[f(\Sigma\, \dot{a}_j(t)b_j),\ b_k] = [f(\dot{a}_k(t)b_k),\ b_k]$$

we see that setting

$$a_k(t) = A_k(t) \sin(\omega_k t + \phi_k(t))$$

that

$$\frac{d}{dt}\phi_k(t) = 0$$

$$\frac{d}{dt}A_k(t) = -\frac{K_0(A_k(t))}{\omega_k}$$

where

$$K_0(a) = \frac{1}{2\pi}\int_0^{2\pi} [f(a\omega_k \cos\phi\, b_k),\ b_k] \cos\phi\ d\phi .$$

To simplify matters further let us take

$$m = 1 .$$

Then

$$[f(a\omega_k b_k \cos\phi),\ b_k] = b_k\, f(a b_k \omega_k \cos\phi) .$$

We shall take:

$$f(u) = \lambda \tan^{-1} u$$

which is consistent with (4.2). Then (4.3) becomes

$$\ddot{a}_k(t) + \omega_k^2 a_k(t) + \lambda b_k^2 \tan^{-1} \dot{a}_k(t) = 0 \qquad (4.4)$$

$$K_0(a) = \frac{1}{2\pi}\int_0^{2\pi} \lambda b_k \tan^{-1}(a b_k \omega_k \cos\phi) \cos\phi\ d\phi$$

$$= \frac{\lambda}{2\omega_k}[\sqrt{1 + a^2 b_k^2 \omega_k^2} - 1]$$

Hence

$$\frac{A_k(t)\ dA_k(t)}{[\sqrt{1 + a^2 b_k^2 \omega_k^2} - 1} = -\frac{\lambda}{\omega_k^2}\, dt .$$

To solve this, let

$$z(t) = 1 + A_k(t)^2 b_k^2 \omega_k^2 \qquad (4.5)$$

so that

$$\frac{dz(t)}{2(\sqrt{z(t)} - 1)} = -b_k^2 \lambda \, dt . \tag{4.6}$$

Let

$$F(z) = e^{\sqrt{z}} (\sqrt{z} - 1) , \qquad z \geq 1 . \tag{4.7}$$

Then

$$F'(z) > 0 \qquad \text{for } z > 1$$

and hence we may define the inverse function

$$F(z) = y ; \qquad z = F^{-1}(y) .$$

Thus (4.6) has the solution:

$$z(t) = F^{-1}[F(z(0))e^{-b_k^2 \lambda t}] , \tag{4.8}$$

$$b_k \omega_k A_k(t) = \sqrt{F^{-1}(F(1 + A_k(0)^2 b_k^2 \omega_k^2)e^{-b_k^2 \lambda t}) - 1} \tag{4.9}$$

where

$$z(0) = 1 + A_k(0)^2 b_k^2 \omega_k^2 > 1$$

unless $A_k(0) = 0$. Note that

$$F^{-1}(y) \to 1 \qquad \text{as } y \to 0$$

and hence $z(t)$ decreases monotonically to 1 and hence the amplitude $A_k(t)$ decays to zero asymptotically.

Note that the decay rate depends on the control effort λb_k^2 as well as the initial amplitude. Of course we have in (4.4) yet another nonlinear damping model. Following (2.22) we have:

$$\log \frac{a_{j+1}}{a_j} = \frac{2\pi\lambda}{2\omega_k^2} \left(\frac{\sqrt{1 + a_j^2 b_k^2 \omega_k^2} - 1}{a_j} \right)$$

where

$$a_j = A_k(jT) ; \qquad T = \frac{2\pi}{\omega_k}$$

References

[1] *Proceedings of the 3rd Annual NASA SCOLE Workshop, November 1986.* NASA Technical Memorandum 89075. Edited by L.W. Taylor.

[2] N. Krylov and N. Bogoliubov. *Introduction to Non-Linear Mechanics*, Princeton: Princeton University Press, 1949.

[3] A.V. Balakrishnan. Control of Flexible Flight Structures. In: Volume dedicated to J.L. Lions. To be published by Gauthier-Villars, Paris, 1988.

[4] A.V. Balakrishnan. Stability Enhancement of Flexible Structures by Nonlinear Boundary Feedback. In: *Proceedings of IFIP Working Conference on Boundary Control and Boundary Variations, Nice, June 1986.*

[5] S.C. Hayashi. *Nonlinear Oscillations in Physical Systems.* New York: McGraw-Hill, 1964.

N89-13464

Nonlinearities in Spacecraft Structural Dynamics

Larry Taylor
NASA Langley Research Center
and
Kelly Latimer
U.S. Air Force and G.W.U.

4th Annual SCOLE Workshop
Colorado Springs, CO
November 16, 1987

OUTLINE

- SCOLE Configuration - Equations of Motion
- Modeling Error Sources
- Approximate Solutions
- Comparison of Model Accuracy
- Linear & Nonlinear Damping
- Experimental Results
- Future Work

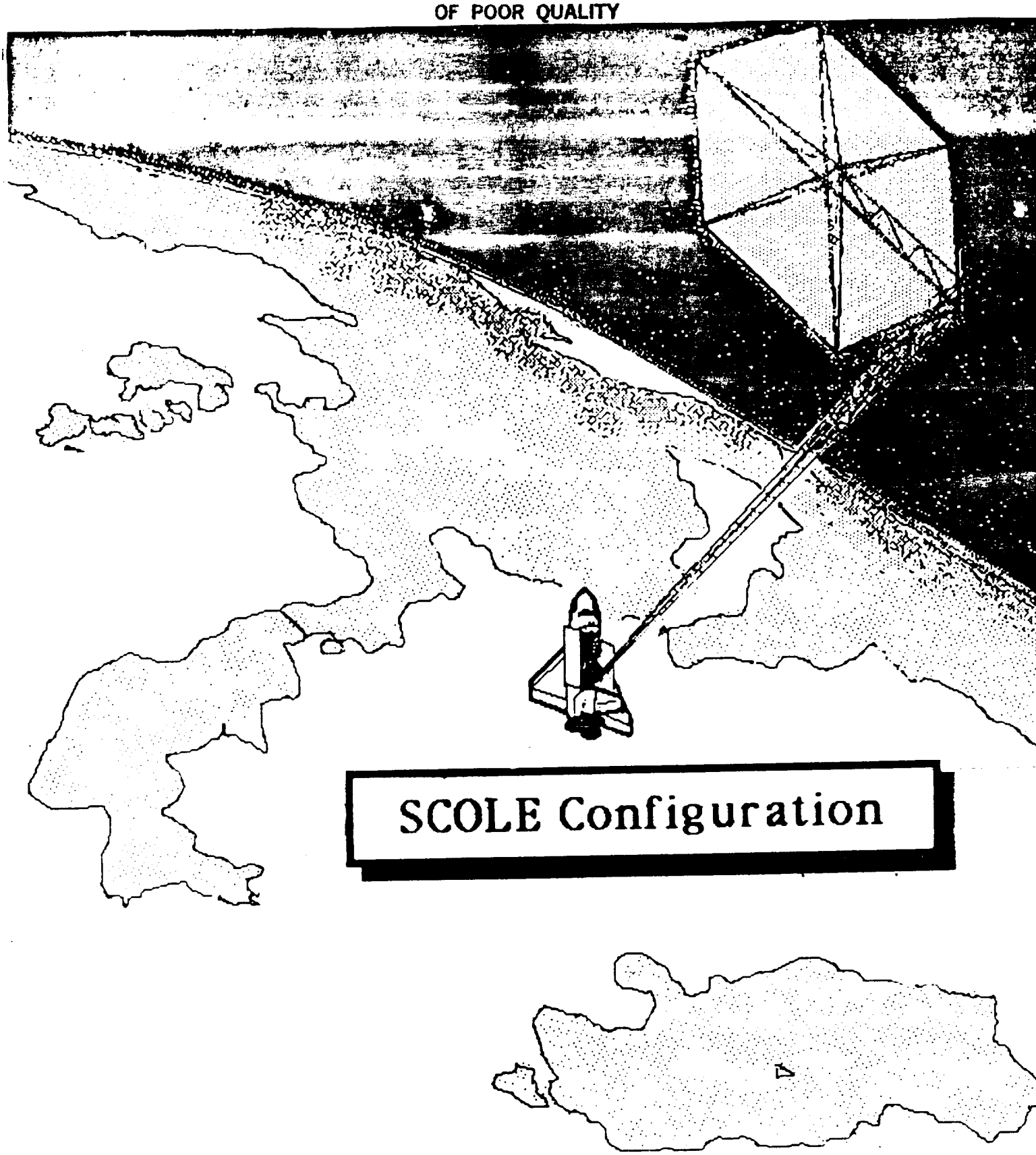

SCOLE Configuration

Equations of Motion

Shuttle (and Reflector) Body

$$\dot{\boldsymbol{\omega}}_1 = -\mathbf{I}_1^{-1}(\tilde{\boldsymbol{\omega}}_1 \mathbf{I}_1 \boldsymbol{\omega}_1 - \mathbf{M}_1 - \mathbf{M}_{1,Beam})$$

$$\dot{\mathbf{v}}_1 = (\mathbf{F}_1 + \mathbf{F}_{1,Beam})/m_1$$

$$\dot{\mathbf{T}}_1^T = -\tilde{\boldsymbol{\omega}}_1 \mathbf{T}_1^T$$

Roll (and Pitch) Beam Bending

$$\rho A_\phi \frac{d^2 u_\phi}{dt^2} - C I_\phi \frac{d^3 u_\phi}{ds^2 dt} + E I_\phi \frac{d^4 u_\phi}{ds^4} = \sum_{n=1}^{4} [f_{\phi,n}\,\delta(s-s_n) + g_{\phi,n}\frac{d\delta}{ds}(s-s_n)$$

Yaw Beam Torsion

$$\rho I_\psi \frac{d^2 u_\psi}{dt^2} + C I_\psi \frac{d^3 u_\psi}{ds^2 dt} - G I_\psi \frac{d^2 u_\psi}{ds^2} = \sum_{n=1}^{4} g_{\psi,n}\,\delta(s-s_n)$$

Beam Elongation

$$\rho A \frac{d^2 u_z}{dt^2} + C_z A \frac{d^2 u_z}{ds dt} - E A \frac{d^2 u_z}{ds^2} = \sum_{n=1}^{4} f_{z,n}\,\delta(s-s_n)$$

Static Deflection Error

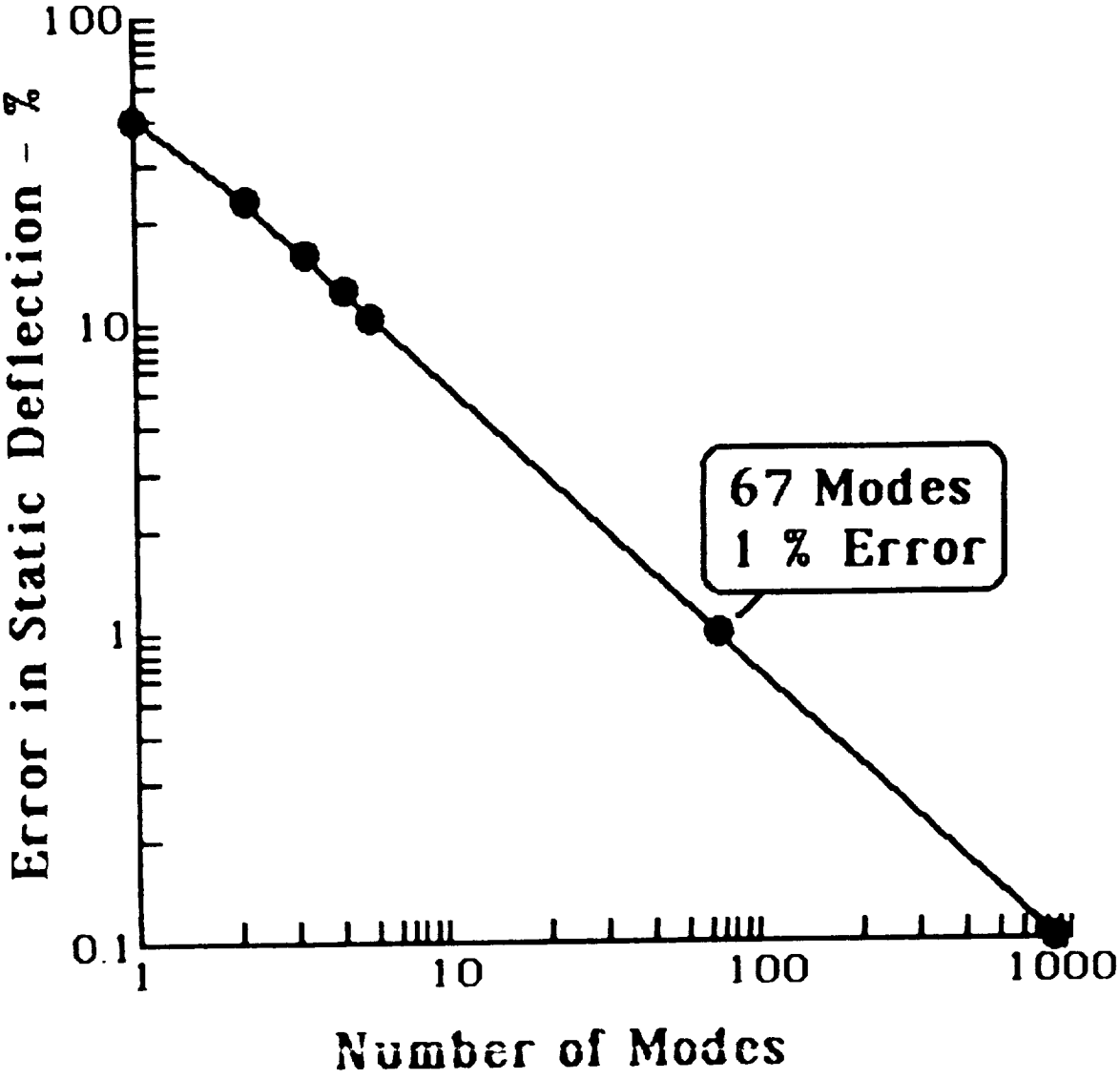

Large Amplitude Deflection Effects

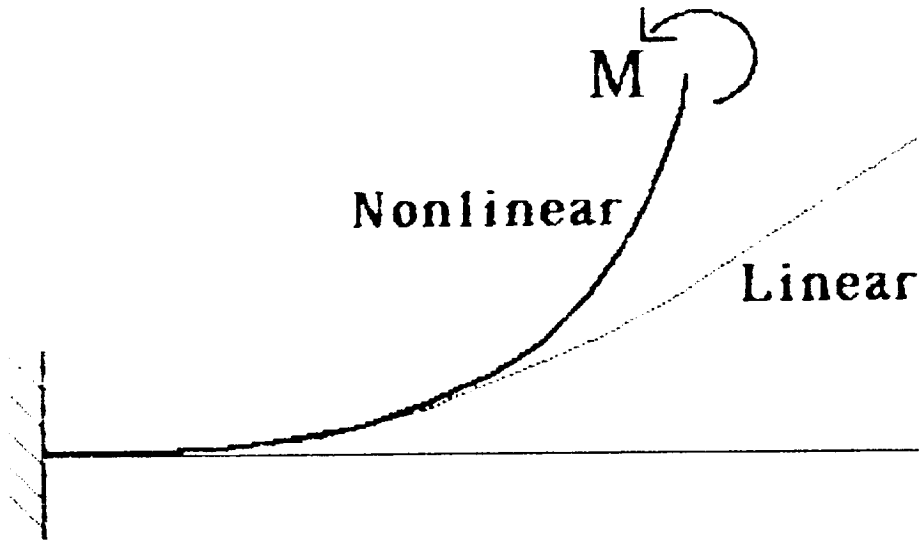

Deflection, y/L	Error, e/y
.05	.17 %
.10	.67 %
.20	2.7 %
.30	6.0 %
.40	10.6 %
.50	16.4 %

Lumped-Mass Model

- Exact Static Deflection
- Approximates Low-Frequency Modes
- Nonlinear Kinematics
- Linearized State Space, Modal Model
- Classical Damping(Working Proportional)
- Extended to n-Body Network

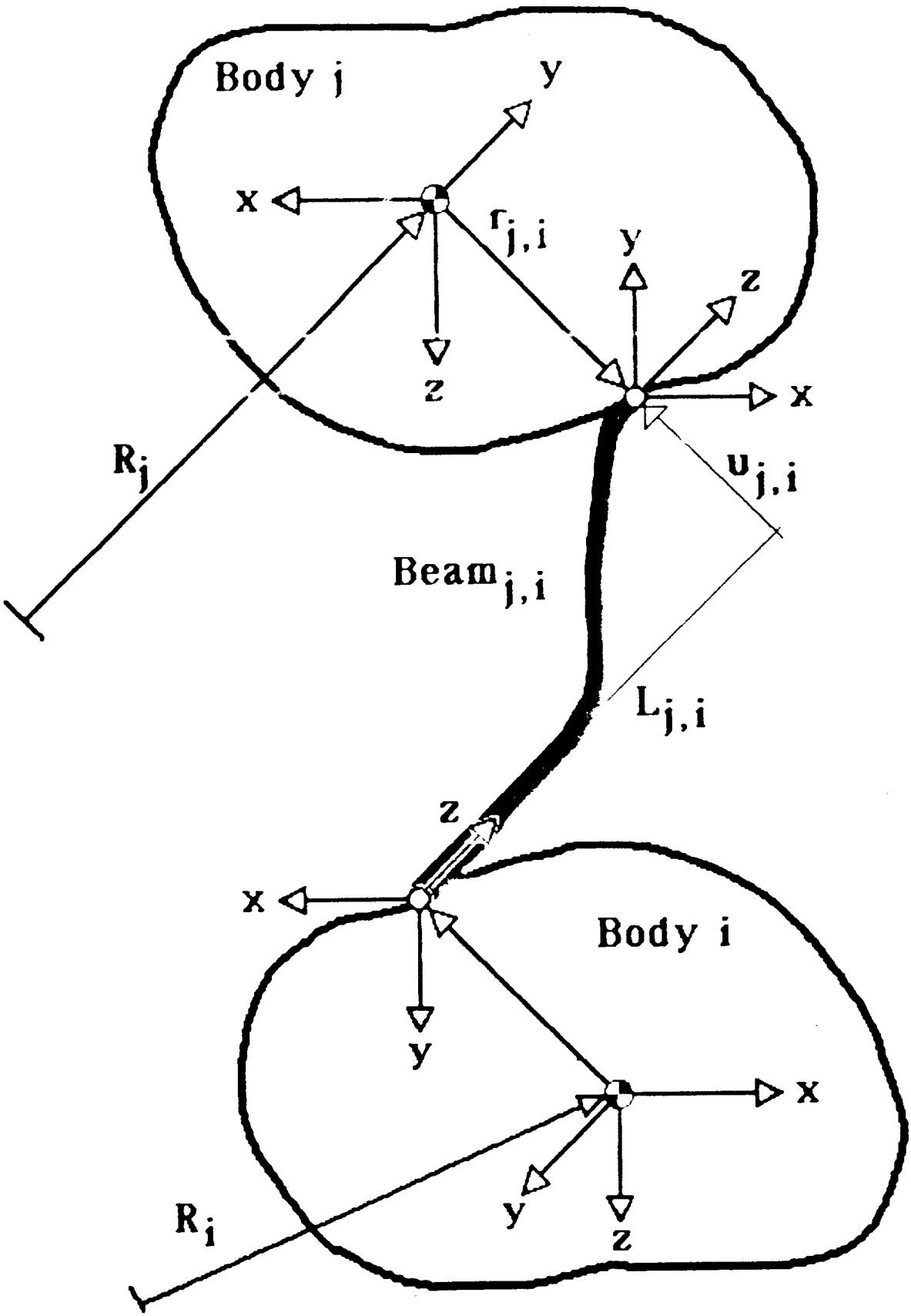
Body j
y
x
$r_{j,i}$
y
z
z
x
R_j
$u_{j,i}$
$Beam_{j,i}$
$L_{j,i}$
z
x
Body i
y
x
y
z
R_i

Stiffness Matrices

$$M_{u'} = \begin{bmatrix} -\frac{4EI}{L} - \frac{2WL}{15}^{*} & 0 & 0 \\ 0 & -\frac{4EI}{L} - \frac{2WL}{15}^{*} & 0 \\ 0 & 0 & -\frac{GJ}{L} \end{bmatrix}$$

$$M_{u} = \begin{bmatrix} 0 & \frac{6EI}{L^2} + \frac{W}{10}^{*} & 0 \\ \frac{6EI}{L^2} + \frac{W}{10}^{*} & 0 & 0 \\ 0 & 0 & 0 \end{bmatrix}$$

* Gravity Effect

Stiffness Matrices

$$F_u = \begin{bmatrix} -\frac{12EI}{L^3} - \frac{6W^*}{5L} & 0 & 0 \\ 0 & -\frac{12EI}{L^3} - \frac{6W^*}{5L} & 0 \\ 0 & 0 & -\frac{EA}{L} \end{bmatrix}$$

$$F_{u'} = \begin{bmatrix} 0 & \frac{6EI}{L^2} & 0 \\ \frac{6EI}{L^2} & 0 & 0 \\ 0 & 0 & 0 \end{bmatrix}$$

* Gravity Effect

Asymptotic Approximation

- Motion Approaches Clamp-Clamped System as Mode Number Increases
- Accuracy Increases with Increasing Mode Number
- Explicit Expressions for Modal Frequencies and Mode Shapes
- First Variation Approximation for Motion of End Bodies
- Singular Perturbation Technique can be used to Improve Approximate Solutions

Comparison of Modal Frequencies

MODE NO	EXACT REF.5&6	FINITE ELEMENT REF. 9	REF. 10	REF. 11
1	.278025624	.278	.277	.2740
2	.313776751	.317	.314	3279
3	.812326353	.726	.805	.7494
4	1.18366347	1.226	1.175	1.244
5	2.05047101	2.069	2.028	2.052
6	4.75561758	4.77	4.617	
7	5.51248431	5.52	5.388	
8	12.2598619	12.4	11.782	
9	12.8877037	13.0	12.513	
10	23.5359367	24.2	14.670	
11	24.2568205	24.7	22.968	
12	26.4794890	26.2	23.490	
13	38.9199260	45.4	37.568	
14	39.4643489	45.9	38.146	
15	45.1313668	56.3	44.653	
16	57.90		45.161	
17	57.92			
18	80.72			
19	80.72			

16% ERROR

Comparison of Modal Frequencies

MODE NO.	EXACT REF.5&6	Lumped Mass	Asymptotic
1	.278025624	.258	
2	.313776751	.370	
3	.812326353	.926	
4	1.18366347	1.79	
5	2.05047101	2.57	
6	4.75561758		4.23885
7	5.51248431		4.23885
8	12.2598619		11.88805
9	12.8877037		11.88805
10	23.5359367		23.313674
11	24.2568205		23.313674
12	26.4794890		
13	38.9199260		38.534998
14	39.4643489		38.534998
15	45.1313668		
16	57.90*		57.455629
17	57.92*		57.455629
18	80.72*		80.24802
19	80.72*		80.24802

51 % ERROR

30 % ERROR

.6 % ERROR

* - Uncoupled (Reference 3).

Comparison of Modal Frequencies

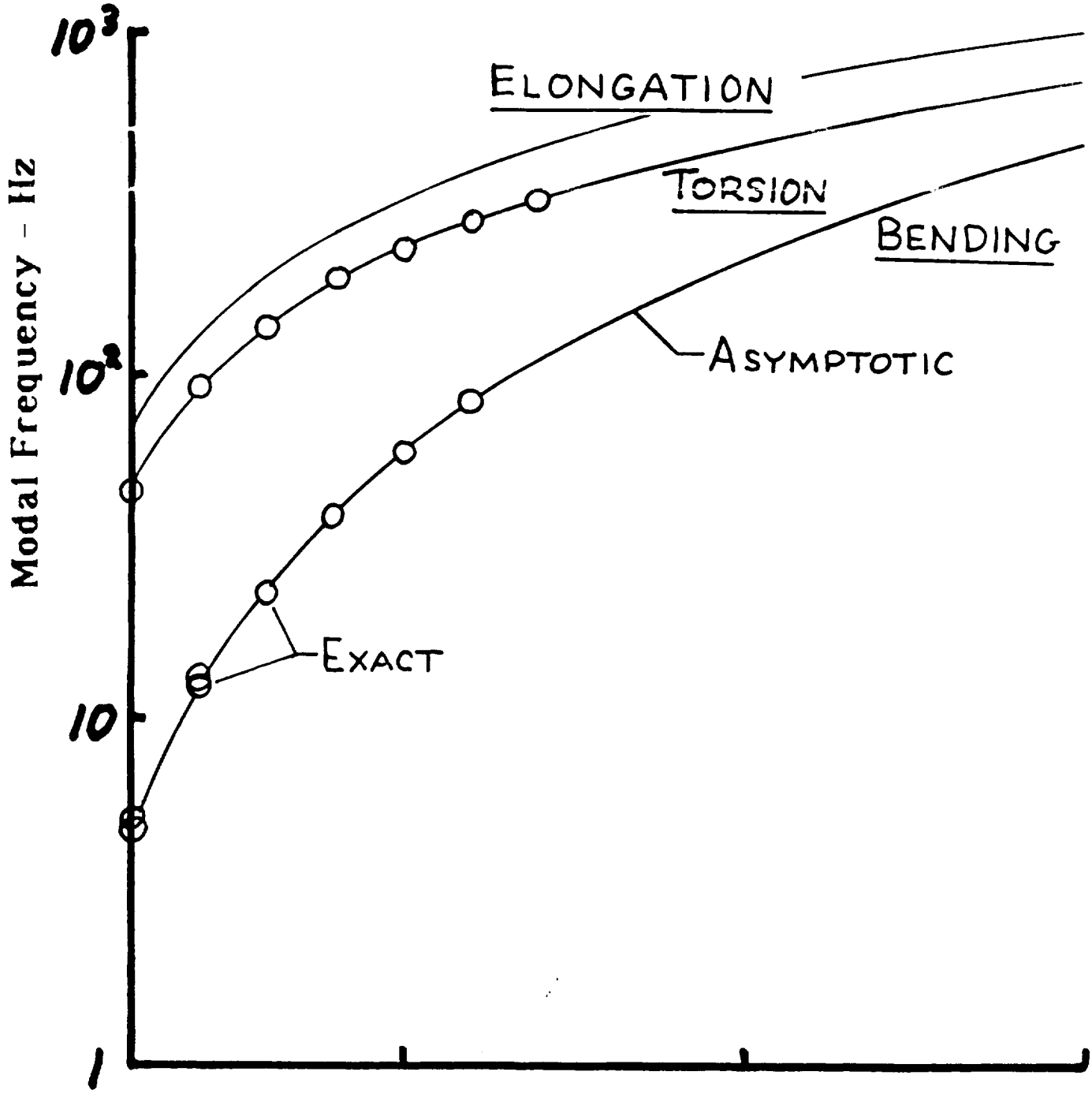

Comparison of Deflections

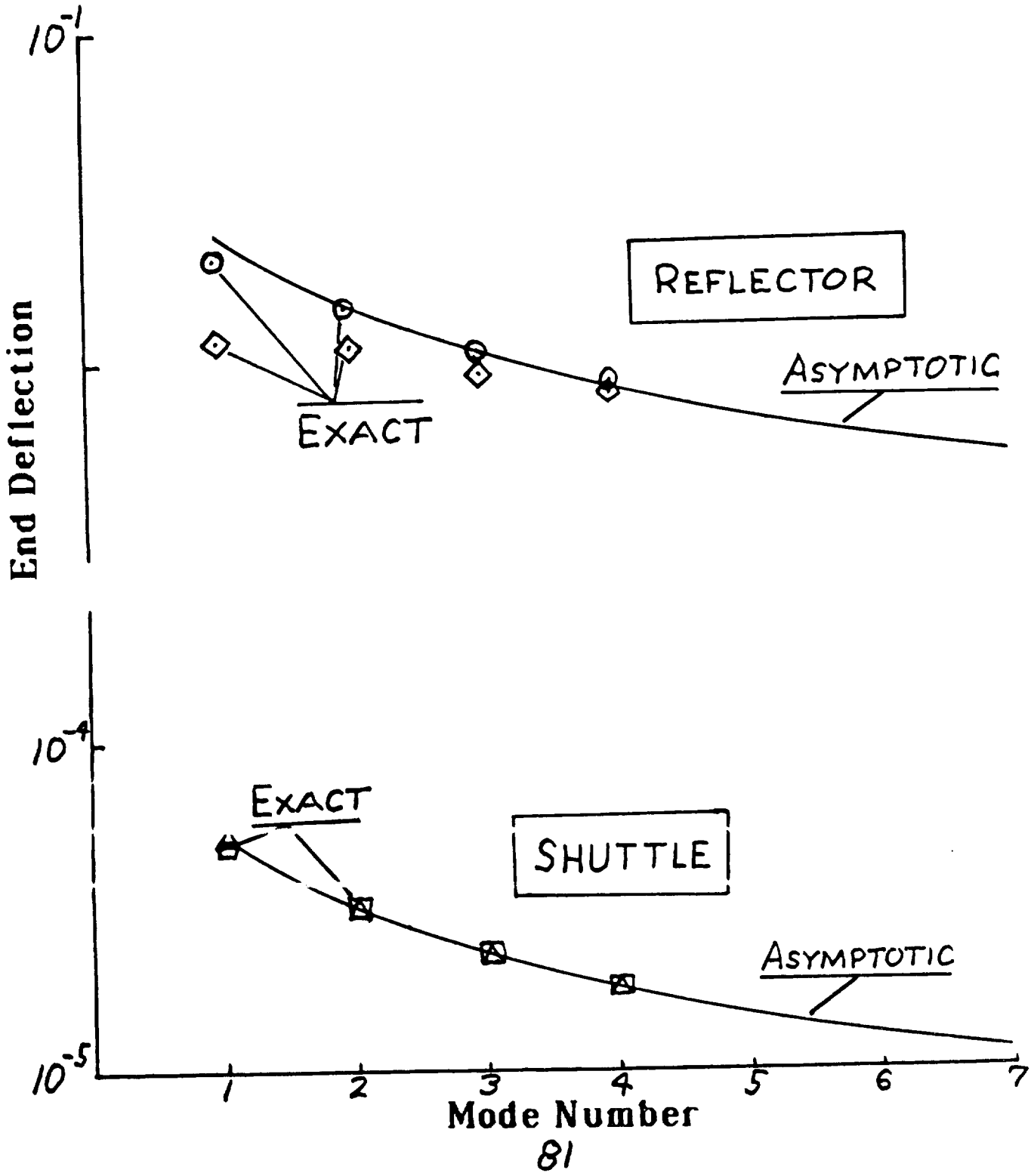

A 3-Dimensional Beam Equation

- Includes Nonlinear Kinematics
- Makes No Small Angle Approximation
- Bending(2 Directions), Torsion & Elongation

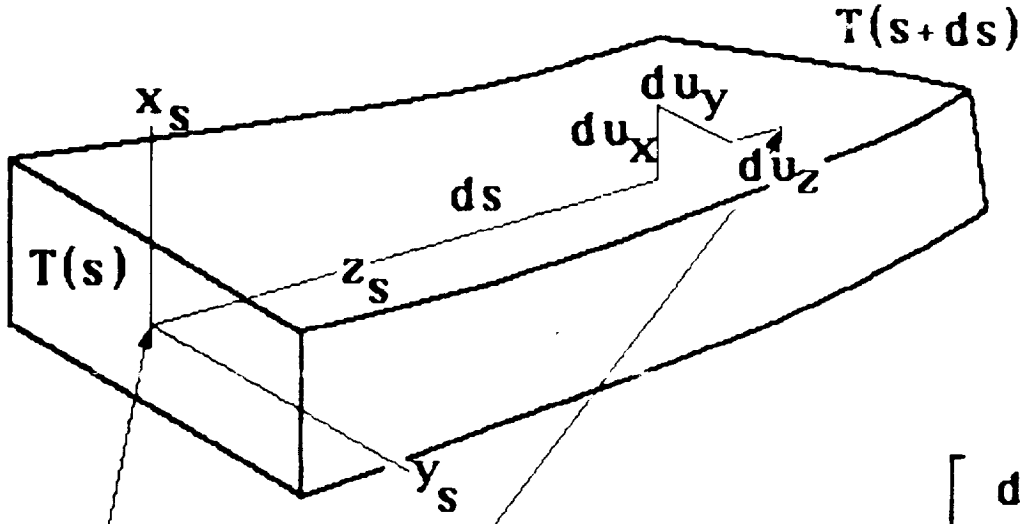

$$R(s+ds)=R(s)+T(s)\begin{bmatrix} du_x/ds \\ du_y/ds \\ 1+du_z/ds \end{bmatrix} ds$$

R(s)

$$T(s+ds)=T(s)\left[1+\begin{bmatrix} 0 & -d\psi/ds & d\theta/ds \\ d\psi/ds & 0 & -d\phi/ds \\ -d\theta/ds & d\phi/ds & 0 \end{bmatrix} ds\right]$$

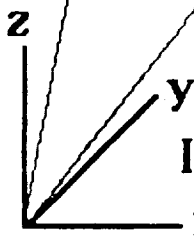

Inertial Axes

It follows that the deflection vector of the beam is:

$$R(s) = \int_0^s T(s') \begin{bmatrix} du_x/ds' \\ du_y/ds' \\ 1 + du_z/ds' \end{bmatrix} ds'$$

and the direction cosine of the cross section axes is given by:

$$\frac{dT(s)}{ds} = T(s) \begin{bmatrix} 0 & -d\psi/ds & d\theta/ds \\ d\psi/ds & 0 & -d\phi/ds \\ -d\theta/ds & d\phi/ds & 0 \end{bmatrix}$$

The forces and moments applied to the beam are related to the beam deformations by:

$$\begin{matrix} dFx \\ dFy \\ dFz \\ dMx \\ dMy \\ dMz \end{matrix} = \left[\begin{array}{ccc|ccc} -k'GA & & & & & \\ & -k'GA & & & & \\ & & -EA & & & \\ \hline & & & -EI_{xx} & & \\ & & & & -EIyy & \\ & & & & & -EI_{zz} \end{array}\right] \begin{bmatrix} du_x/ds \\ du_y/ds \\ du_z/ds \\ d\phi/ds \\ d\theta/ds \\ d\psi/ds \end{bmatrix} ds$$

$$dF = F_u du + F_e de$$
$$dM = M_u du + M_e de$$

Where

$$du = \begin{bmatrix} du_x/ds \\ du_y/ds \\ du_z/ds \end{bmatrix} ds \qquad de = \begin{bmatrix} d\phi/ds \\ d\theta/ds \\ d\psi/ds \end{bmatrix} ds$$

The incremental force can be related to deformation of the beam.

$$\frac{dR}{ds} = \frac{R(s+ds)-R(s)}{ds} = T\begin{bmatrix}0\\0\\1\end{bmatrix} + T\begin{bmatrix}du_x/ds\\du_y/ds\\du_z/ds\end{bmatrix}$$

$$\begin{bmatrix}du_x/ds\\du_y/ds\\du_z/ds\end{bmatrix} = T^T\frac{dR}{ds} - \begin{bmatrix}0\\0\\1\end{bmatrix}$$

$$\frac{dF}{ds} = \frac{F(s+ds) - F(s)}{ds} = F_u T^T\frac{dR}{ds} - F_u\begin{bmatrix}0\\0\\1\end{bmatrix} + F_e\frac{de}{ds}$$

Similarly, for the incremental moment..

$$\frac{dM}{ds} = M_u T^T\frac{dR}{ds} - M_u\begin{bmatrix}0\\0\\1\end{bmatrix} + M_e\frac{de}{eds} + \frac{dF}{ds}$$

The equations of motion for the beam element are:

$$m\frac{d^2R}{dt^2} = T\frac{d}{ds}\left[\frac{dF}{ds}\right] + TF$$

and

$$I_o\frac{d^2e}{dt^2} = -\frac{\widetilde{de}}{dt}I_o\frac{de}{dt} + \frac{d}{ds}\left[\frac{dM}{ds}\right] + M$$

The equations of motion for the beam element become:

$$m\frac{d^2R}{dt^2} = T\frac{d}{ds}\left[F_U\left(T^T\frac{dR}{ds} - \begin{vmatrix}0\\0\\1\end{vmatrix}\right) + F_e\frac{de}{ds}\right] + T\,F$$

$$I_o\frac{d^2e}{dt^2} = -\frac{\tilde{de}}{dt}I_o\frac{de}{dt} + \frac{d}{ds}\left[M_U\left(T^T\frac{dR}{ds} - \begin{vmatrix}0\\0\\1\end{vmatrix}\right) + M_e\frac{de}{ds}\right]$$

$$+ F_U\left(T^T\frac{dR}{ds} - \begin{vmatrix}0\\0\\1\end{vmatrix}\right) + F_e\frac{de}{ds} + M$$

Where

e = the arc direction cosine$[T] = \begin{bmatrix}\phi\\ \theta\\ \psi\end{bmatrix}$

$$\frac{de}{dt} = \begin{bmatrix}d\phi/dt\\ d\theta/dt\\ d\psi/dt\end{bmatrix}$$

$$\frac{dT}{dt} = T\frac{\tilde{de}}{dt}$$

$$\frac{dT}{ds} = T\frac{\tilde{de}}{ds}$$

m = the mass per unit length

I_o = the moment of inertia per unit length

$$= \begin{bmatrix} I_{xx} & -I_{xy} & -I_{xz}\\ -I_{xy} & I_{yy} & -I_{yz}\\ -I_{xz} & -I_{yz} & I_{zz}\end{bmatrix}$$

For the case in which deflections are small and the end of the beam is aligned with the inertial axes:

$$T \approx I + \tilde{e} = \begin{bmatrix} 1 & -dU & d\theta \\ d\psi & 1 & -d\phi \\ -d\theta & d\phi & 1 \end{bmatrix}$$

$$\frac{dR}{ds} = T \begin{bmatrix} du_x/ds \\ du_y/ds \\ du_z/ds \end{bmatrix} + \begin{bmatrix} 0 \\ 0 \\ 1 \end{bmatrix} \approx \begin{bmatrix} du_x/ds \\ du_y/ds \\ du_z/ds \end{bmatrix} + \begin{bmatrix} \theta \\ -\phi \\ 1 \end{bmatrix}$$

$$R \approx R_o + u + \int_o^s \begin{bmatrix} \theta \\ -\phi \\ 1 \end{bmatrix} ds$$

The linearized equations become:

$$m\frac{d^2R}{dt^2} = \frac{d}{ds}\left[F_u\left(\frac{dR}{ds} - \begin{vmatrix} \theta \\ -\phi \\ 1 \end{vmatrix}\right) + F_e\frac{de}{ds}\right] + F + \tilde{e}F$$

$$I_o\frac{d^2e}{dt^2} = \frac{d}{ds}\left[M_u\left(\frac{dR}{ds} - \begin{vmatrix} \theta \\ -\phi \\ 1 \end{vmatrix}\right) + M_e\frac{de}{ds}\right] + F_u\left(\frac{dR}{ds} - \begin{vmatrix} \theta \\ -\phi \\ 1 \end{vmatrix}\right) + F_e\frac{de}{ds} + M$$

For bending only, in a single plane the equations of motion become those for the Timoshenko beam.

$$m\frac{d^2R_x}{dt^2} = \frac{d}{ds}\left[kGA\left(\frac{dR_x}{ds} - \theta\right)\right] + F_x$$

$$I_{xx}\frac{d^2\theta}{dt^2} = \frac{d}{ds}\left[EI_{xx}\frac{dR_x}{ds}\right] - kGA\left(\frac{dR_x}{ds} - \theta\right) + M_x$$

If rotary inertia effects are neglected the result is the Bernoulli-Euler beam.

$$m\frac{d^2R_x}{dt^2} = -\frac{d^2}{ds^2}\left[EI_{xx}\frac{d^2R_x}{ds^2}\right] + F_x$$

Kelvin-Voight Damping

Bernoulli-Euler Beam Equation with Kelvin-Voight Damping

$$EIu'''' + C\dot{u}'''' + m\ddot{u} = 0$$

Allows Separation of Variables

Theoretical Basis for Damping

Locus of Modal Characteristics

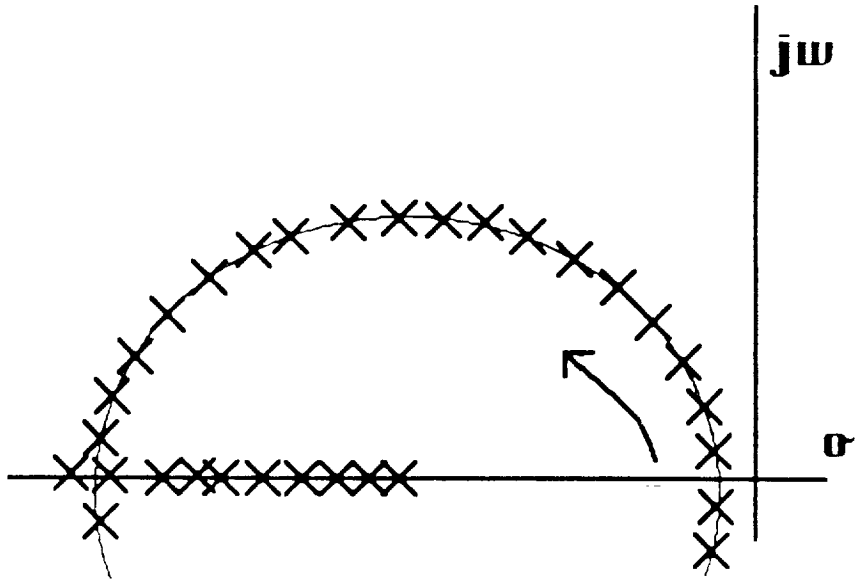

EXCESSIVE DAMPING AT HIGH MODE NUMBERS !!!!

Proportional Damping

Bernoulli-Euler Beam Equation with Proportional Damping

$$EIu'''' + C\dot{u}'' + m\ddot{u} = 0$$

Allows Separation of Variables for Pinned and Infinite End Conditions

Lacks Theoretical Basis for Damping

Locus of Modal Characteristics

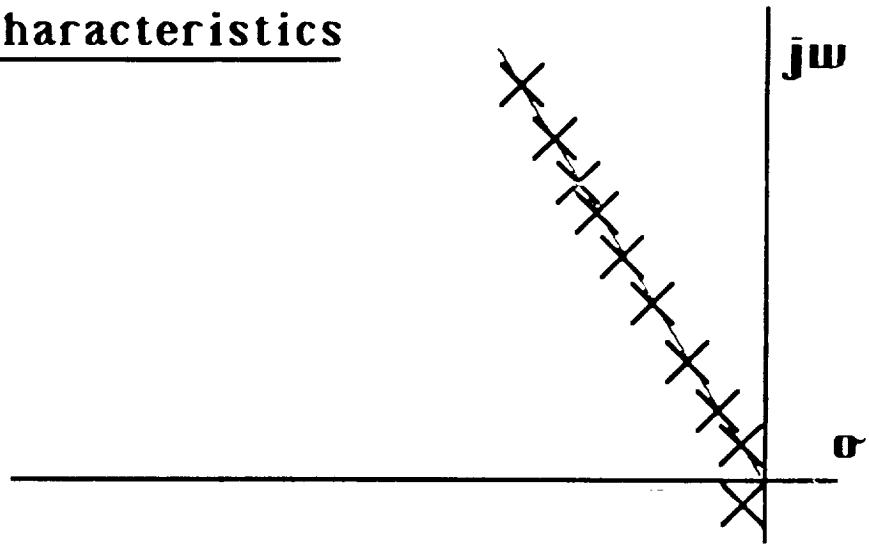

REASONABLE DAMPING AT HIGH MODE NUMBERS

Piano-Wire Damping

Viscous Damping Ratio

Smaller Mass $\zeta = .0015$

Larger Mass $\zeta = .0013$

General Mass $\zeta = .0015\sqrt{\frac{m_1}{m}}$

Nonlinear Damping

$$m\ddot{x} = -c_1\dot{x} - c_2|\dot{x}|\dot{x} - kx$$

$$A_{n+1} = A_n - A_n(.00138)2\pi - (.0012)A_n^2$$

Determined to be Air Damping

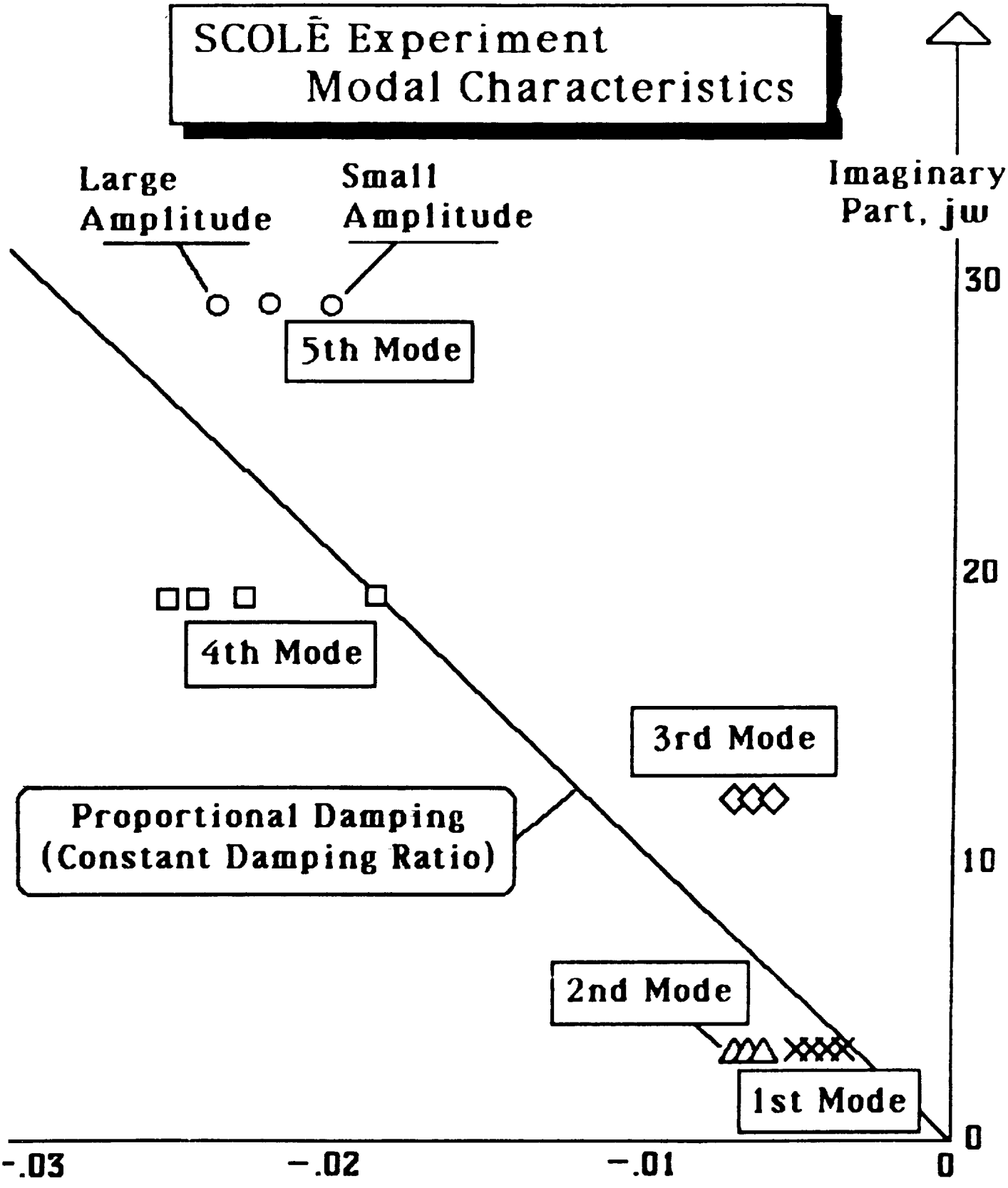
SCOLE Experiment
Modal Characteristics
Large Amplitude
Small Amplitude
Imaginary Part, jw
30
20
10
0
5th Mode
4th Mode
3rd Mode
Proportional Damping
(Constant Damping Ratio)
2nd Mode
1st Mode
-.03
-.02
-.01
0
Real Part, σ

91 C 2

SCOLE DAMPING

Viscous Damping Ratio

Mode	Configuration #1	Configuration #2
1	.0016	.0013
2	.0011	.0009
3	.00058	
4	.0011	
5	.00084	

Nonlinear Damping is Evident for Large Amplitude Motion. Analysis is Underway.

Nonlinear Damping

Mass, Spring, Nonlinear Damper

$$m\ddot{x} = -c|x|^a|\dot{x}|^b\dot{x} - kx$$

Considering Only Light Damping ...

$$\omega = \sqrt{k/m}$$

For Free Decay

$$x(t) = A(t)\sin(\omega t)$$

$$\dot{A} = -\frac{c}{m}|x|^a|\dot{x}|^b = -\frac{c}{m}\omega^b A^{a+b}$$

Solving

$$dt = \frac{m\,dA}{c\omega^b A^{a+b}}$$

$$t = t_0 - \frac{m}{c(a+b-1)\omega^b A^{a+b-1}}$$

$$A(t) = \left[\frac{m}{c(a+b-1)\omega^b(t+t_0)}\right]^{\frac{1}{a+b-1}}$$

Nonlinear Damping

$$A(n) = \left[\frac{m}{c(a+b-1)\omega^b n}\right]^{\frac{1}{a+b-1}}$$

Where $t+t_o = n\frac{2\pi}{\omega}$, $\omega = [k/m]^{1/2}$

$$A(n) = \left[\frac{m^{(b+1)/2}}{c(a+b-1)k^{(b-1)/2}2\pi n}\right]^{\frac{1}{a+b-1}}$$

For Example

- $\frac{c}{m}\dot{x}$ $\quad a=b=0$ $\quad \frac{dA}{A} = 2\pi\zeta = \frac{c\pi}{\sqrt{km}}$
- $\frac{c}{m}|\dot{x}|\dot{x}$ $\quad a=0,\ b=1$ $\quad \frac{dA}{A} = \frac{4cA\omega}{3m} = \frac{4cAk^{1/2}}{3m^{3/2}}$
- $\frac{c}{m}|x|\dot{x}$ $\quad a=1,\ b=0$ $\quad \frac{dA}{A} = \frac{2cA}{3m}$

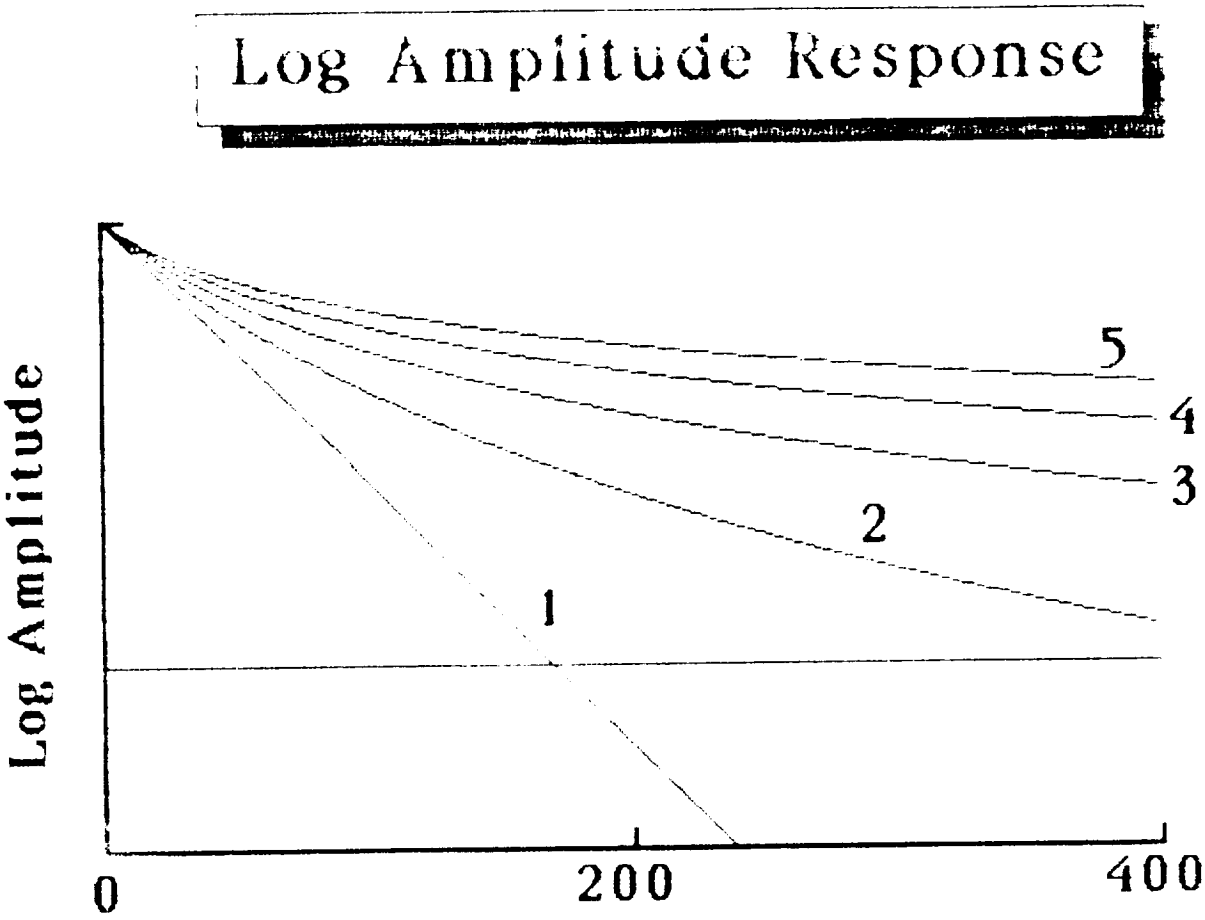

Log Amplitude Response

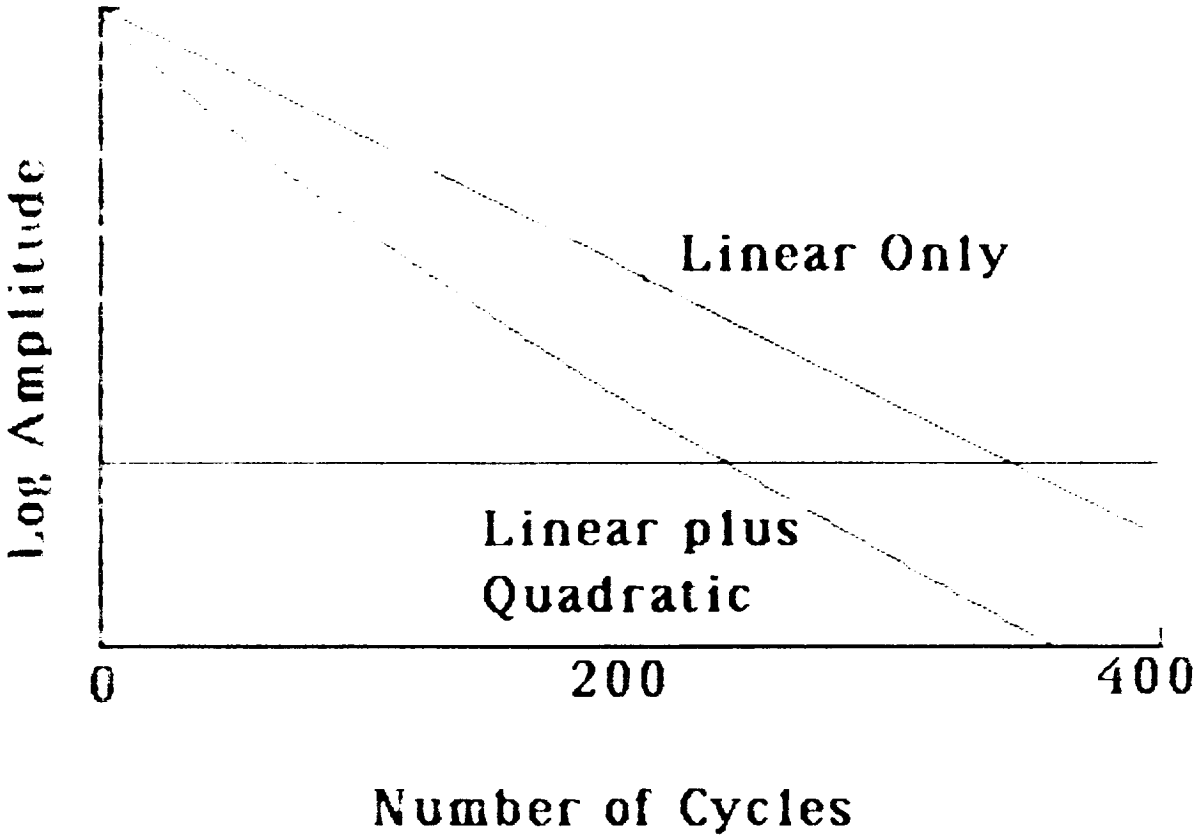

SCOLE DAMPING

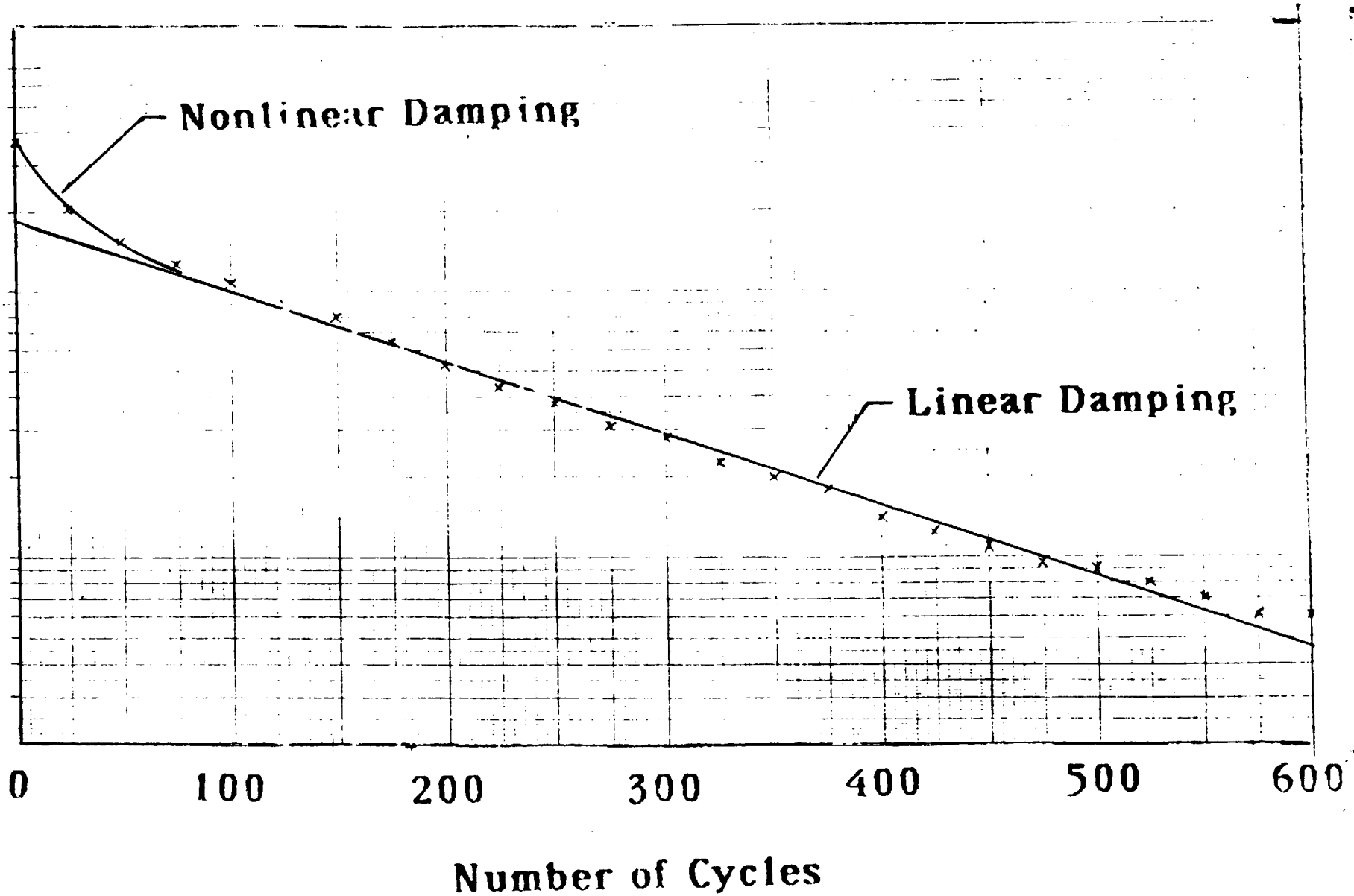

The Curse of Dimensionality

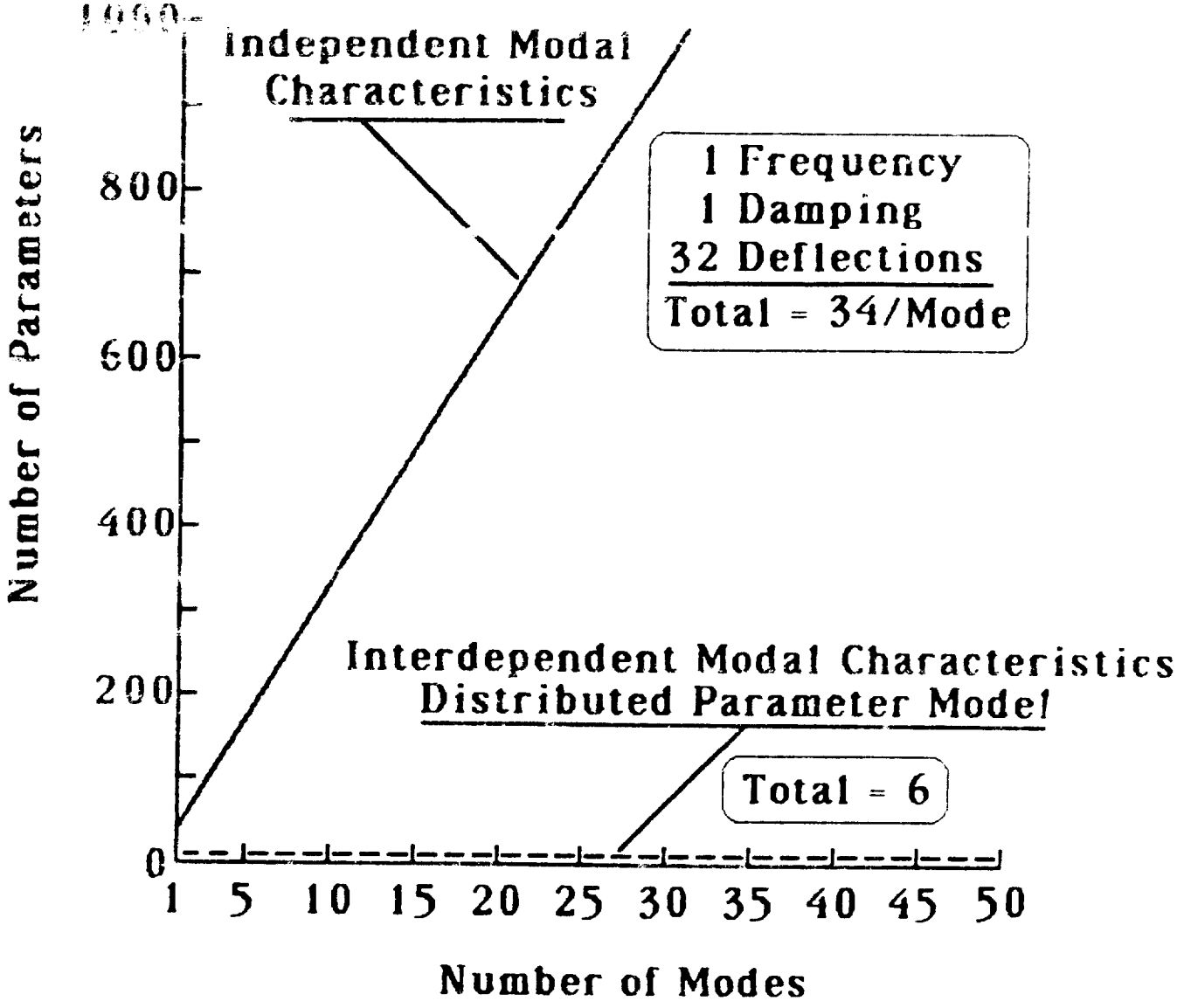

Concluding Remarks

- The Accuracy of the Modal Characteristics of the SCOLE Configuration were Examined Using Exact and Approximate Solutions.
- Sixty-Seven Modes are Required for a Static Deflection Error of less than 1 %. SCOLE Model Requires Hundreds of Modes.
- Exact Solutions Encounter Numerical Difficulties.
- Asymptotic Solutions in Combination with Limited Exact Solutions Enable Generation of a Proof Model with the Required Accuracy.
- Damping Must be Incorporated into the Model from the Start. Proportional Damping is Not Adequate.

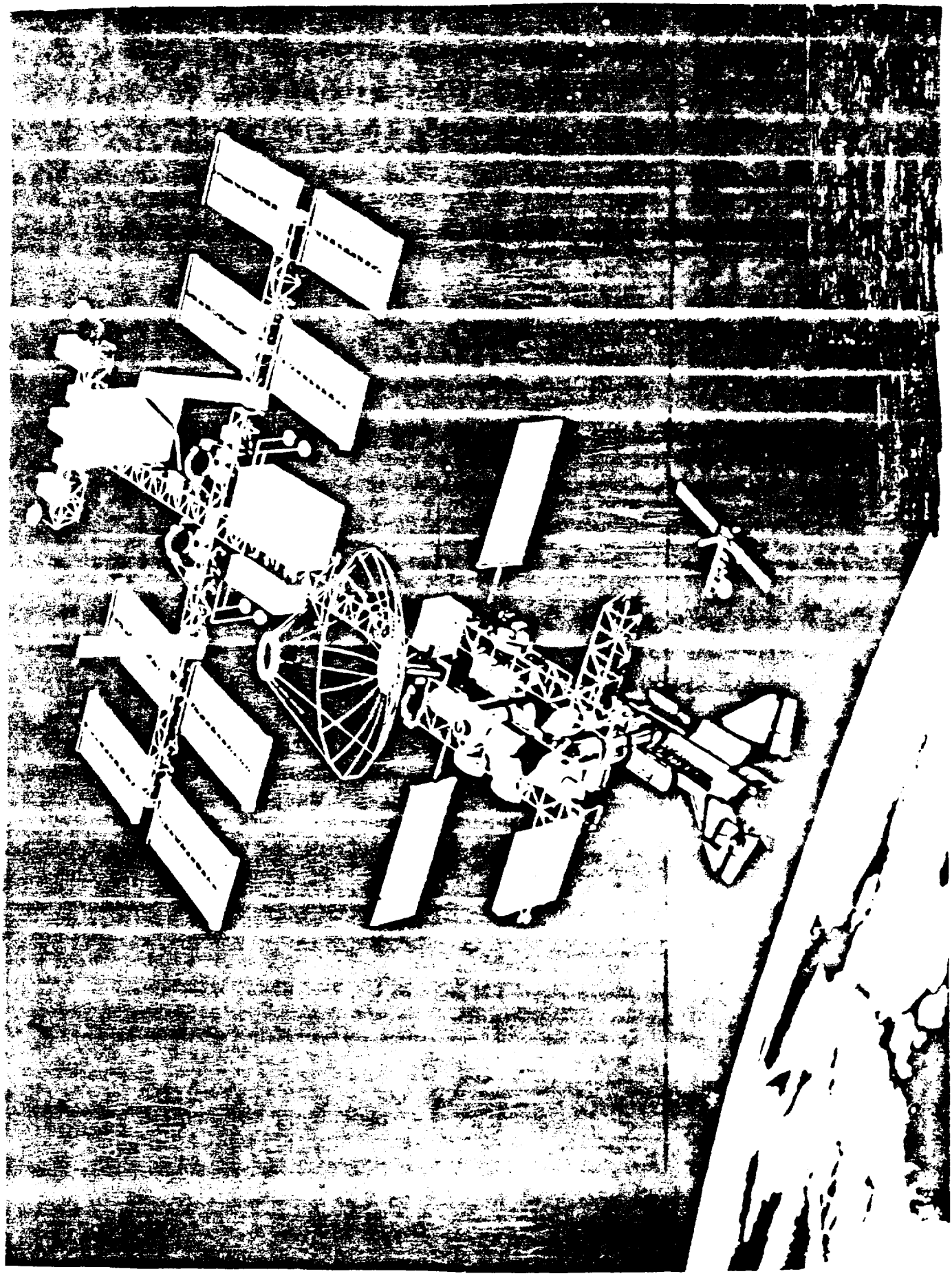

"It will never be possible to have the absolute conviction before flight that a valid mathematical model has been devised for a space vehicle.

....we surely must make every effort to ensure that failures do not come from inadequate analysis of the best models available."

Peter Likins
1971

Control Design Approaches for LaRC Experiments

Steve Yurkovich
Ümit Özgüner

The Ohio State University
Columbus, OH

The 4th Annual SCOLE Workshop

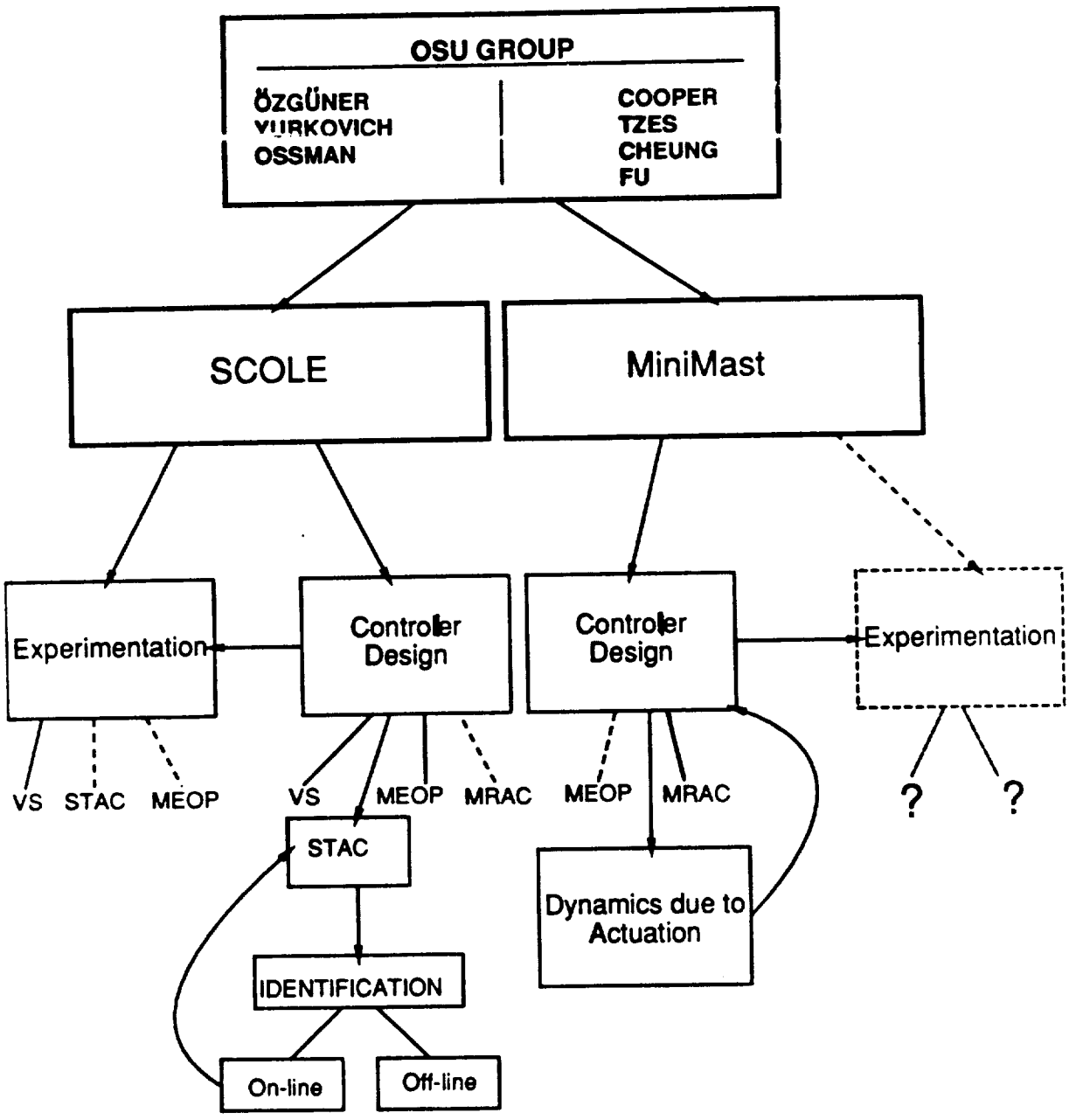
OSU GROUP
ÖZGÜNER
YURKOVICH
OSSMAN
COOPER
TZES
CHEUNG
FU
SCOLE
MiniMast
Experimentation
Controler Design
Controler Design
Experimentation
VS
STAC
MEOP
VS
MEOP
MRAC
MEOP
MRAC
?
?
STAC
Dynamics due to Actuation
IDENTIFICATION
On-line
Off-line

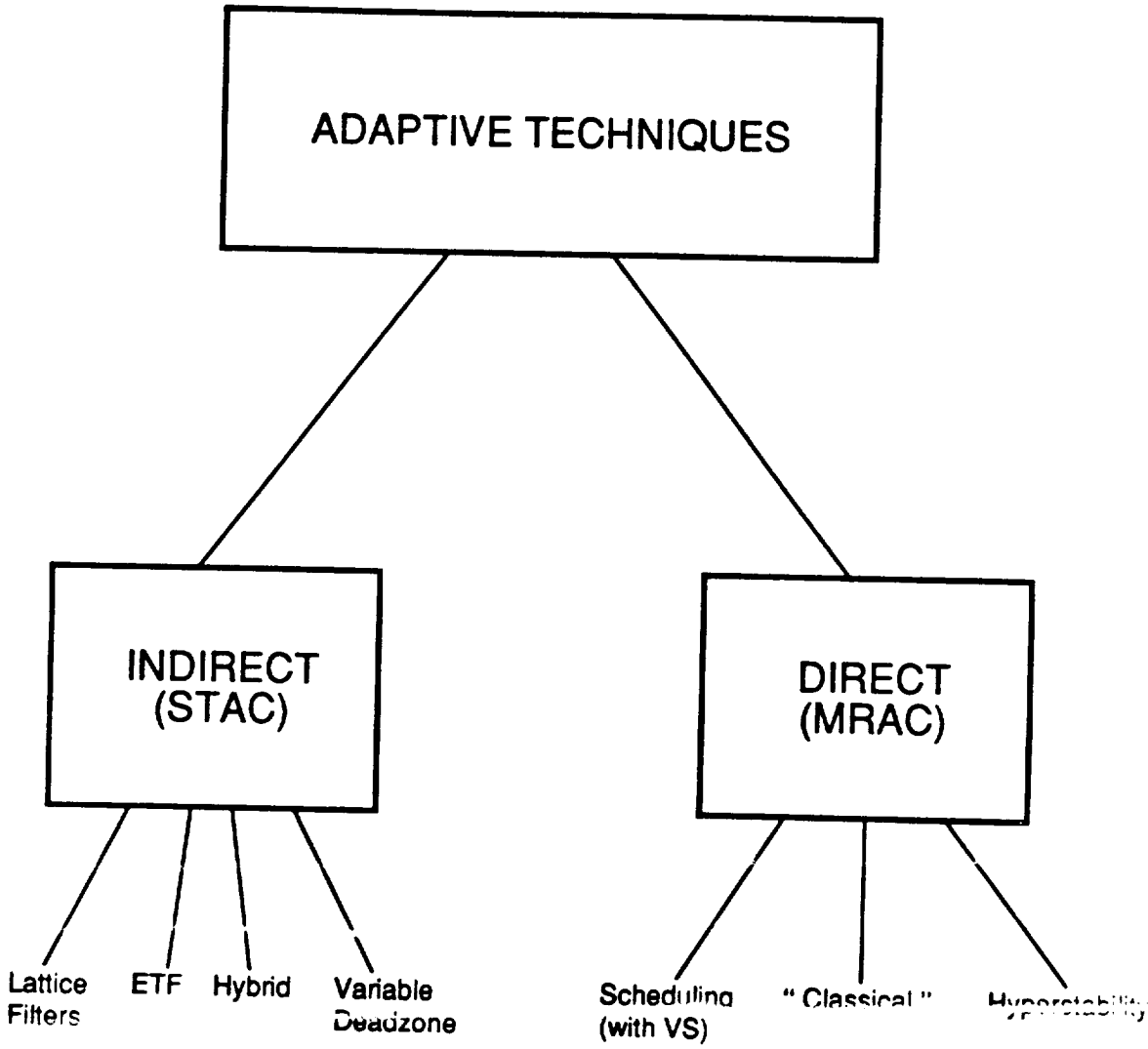
ADAPTIVE TECHNIQUES
INDIRECT (STAC)
DIRECT (MRAC)
Lattice Filters
ETF
Hybrid
Variable Deadzone
Scheduling (with VS)
" Classical "

Direct Fixed–Order Compensator Design

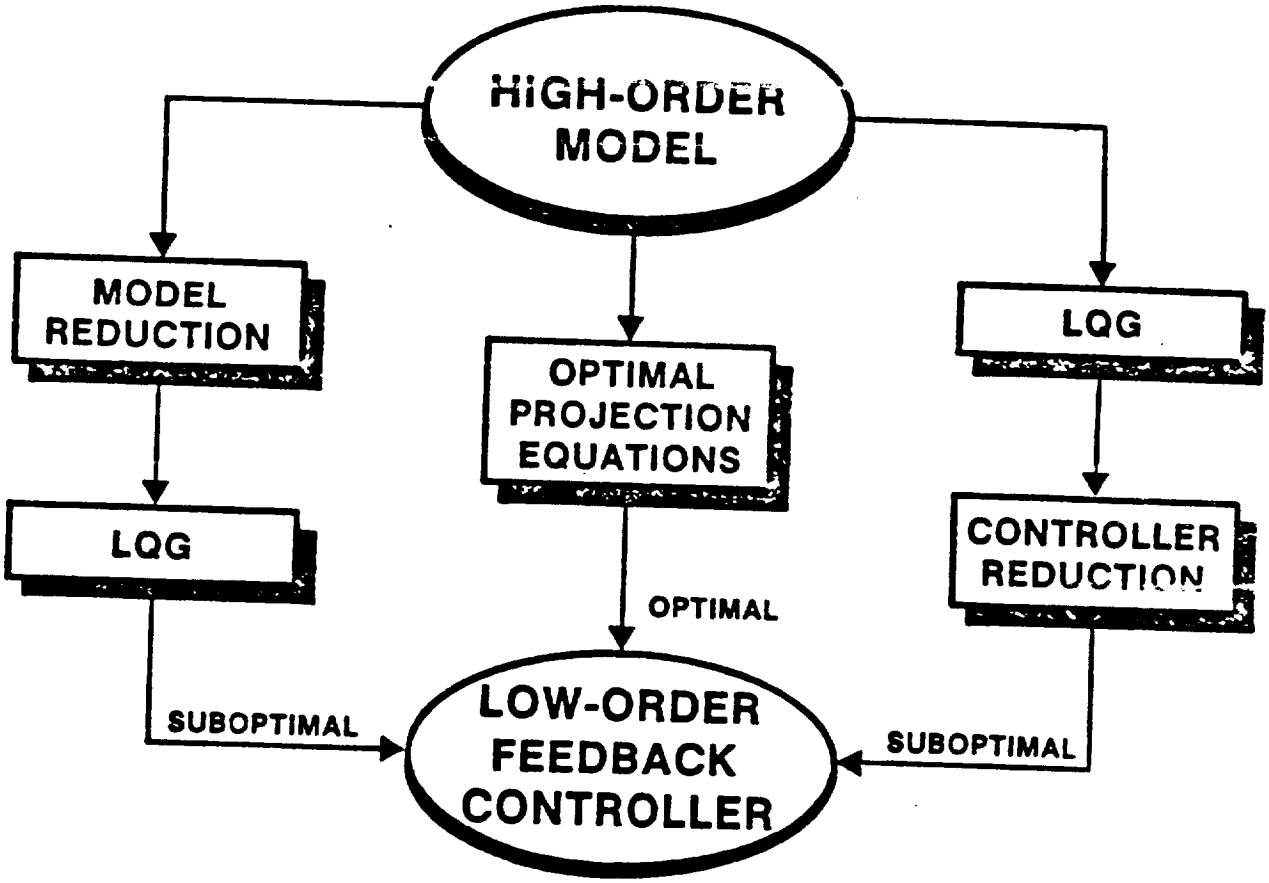

Given ...

$$\dot{x} = Ax + Bu + w_1$$

$$y = Cx + w_2 \quad ,$$

... design an n_c^{th} order *robust*, zero set-point compensator

$$\dot{x_c} = A_c x + Fy$$

$$u = -Kx_c$$

to minimize

$$J = \lim_{\tau \to \infty} \frac{1}{\tau} \int_0^\tau (x^T(t) R_1 x(t) + u^T(t) R_2 u(t)) dt \quad ,$$

LQG Solution

$$K = R_2^{-1} B^T P \quad ,$$

$$F = Q C^T V_2^{-1} \quad ,$$

$$A_c = A - BK - FC \quad ,$$

P and Q positive definite solutions to

$$PA + A^T P + R_1 - P B R_2^{-1} B^T P = 0 \quad ,$$

$$Q A^T + A Q + V_1 - Q C^T V_2^{-1} C Q = 0 \quad .$$

$$
\begin{aligned}
0 &= P A_s + A_s^T P + \sum_{i=1}^{\mu} A_i^T P A_i - P_s^T R_{2s}^{-1} P_s + R_1 \\
&\quad + \sum_{i=1}^{\mu} (A_i - Q_s V_{2s}^{-1} C_i)^T \hat{P} (A_i - Q_s V_{2s}^{-1} C_i) + \tau_\perp^T P B R_2^{-1} B^T P \tau_\perp \\
0 &= A_s Q + Q A_s^T + \sum_{i=1}^{\mu} A_i Q A_i^T - Q_s V_{2s}^{-1} Q_S^T + V_1 \\
&\quad + \sum_{i=1}^{\mu} (A_i - B_i R_{2s}^{-1} P_s) \hat{Q} (A_i - B_i R_{2s}^{-1} P_s)^T + \tau_\perp Q C^T V_2^{-1} C Q \tau_\perp^T \\
0 &= \hat{P} A_{QS} + A_{QS}^T \hat{P} + P_s^T R_{2s}^{-1} P_s - \tau_\perp^T P B R_2^{-1} B^T P \tau_\perp \\
0 &= A_{PS} \hat{Q} + \hat{Q} A_{PS}^T + Q_s V_{2s}^{-1} Q_s^T - \tau_\perp Q C^T V_2^{-1} C Q \tau_\perp^T
\end{aligned}
$$

Application to SCOLE

- Reflector Panel
- Objective: Vibration Damping
- 3 inputs (reaction wheels at hub)
- 5 outputs (gyros at hub, accelerometers at reflector center)
- 10 modes

MEOP procedure

- Robustification with respect to modal frequencies
- Robustness measure: ϵ
- Results:

Order	$\lvert\epsilon\rvert$	$\frac{d\omega}{\omega}$ (%)	Cost
20	0.0138	-20 to +4	0.229
12	0.0141	-30 to +20	0.231
10	0.0153	-45 to +30	0.231
8	0.0140	-9 to +30	0.235

Optimal Projection Design

Order	$\lvert\epsilon\rvert$	$\frac{d\omega}{\omega}$ (%)	Cost
20	0.0148	-25 to +40	0.407
12	0.0156	-50 to +50	0.311
10	0.0154	-50 to +50	0.319
8	0.0154	-40 to +40	0.322

MEOP Designs

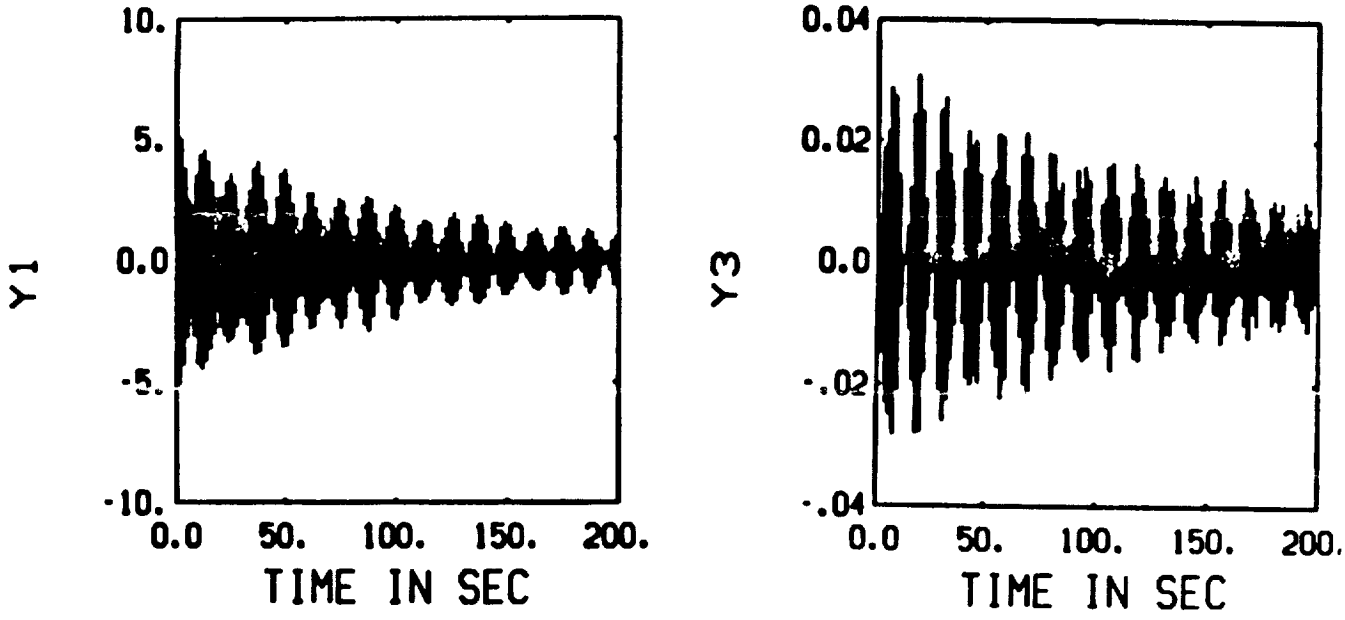

Open loop outputs.

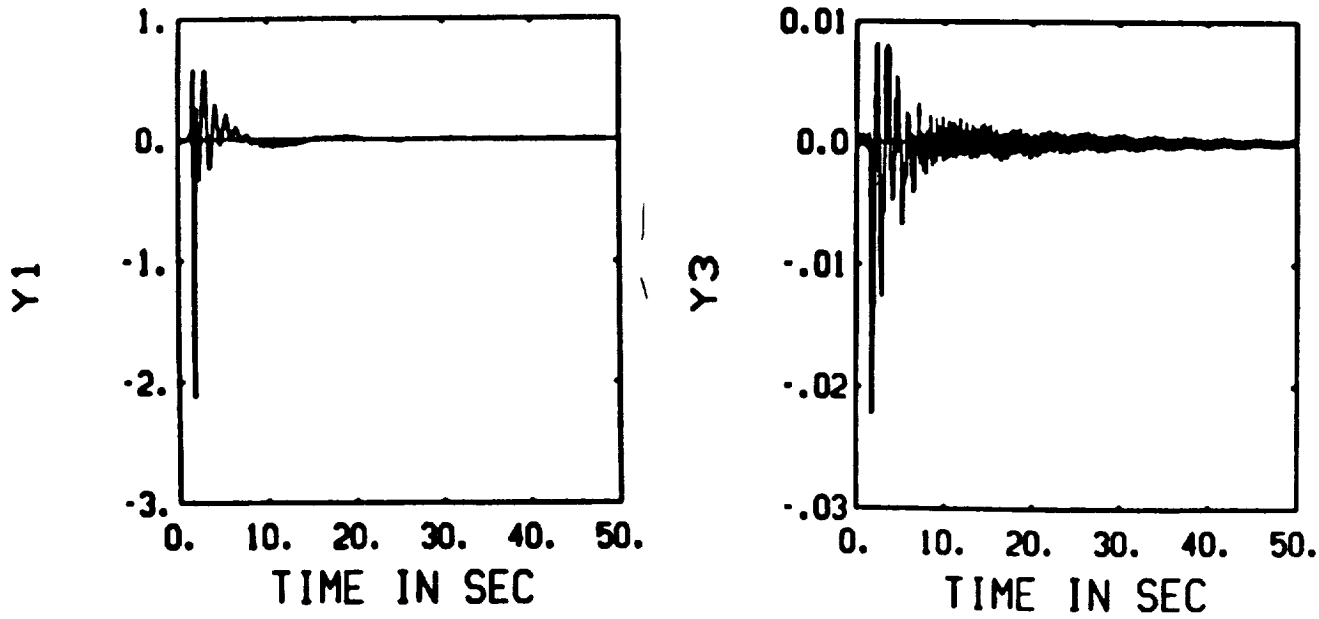

Closed loop outputs.

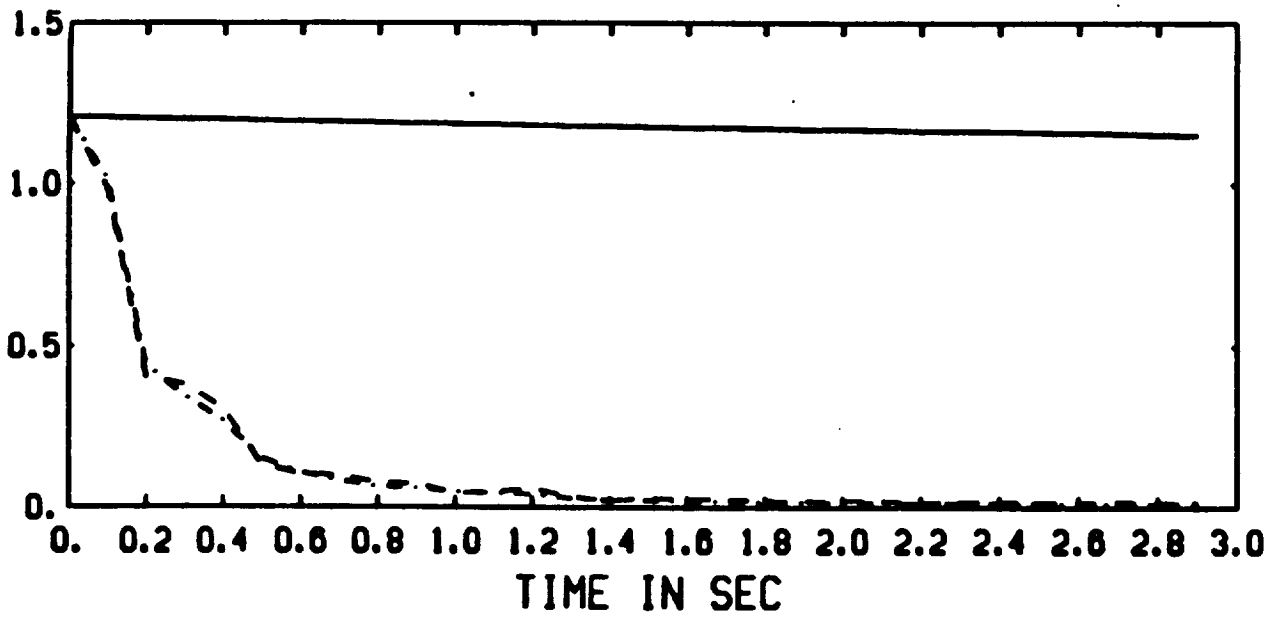

Vibrational energy profile
(full order designs)

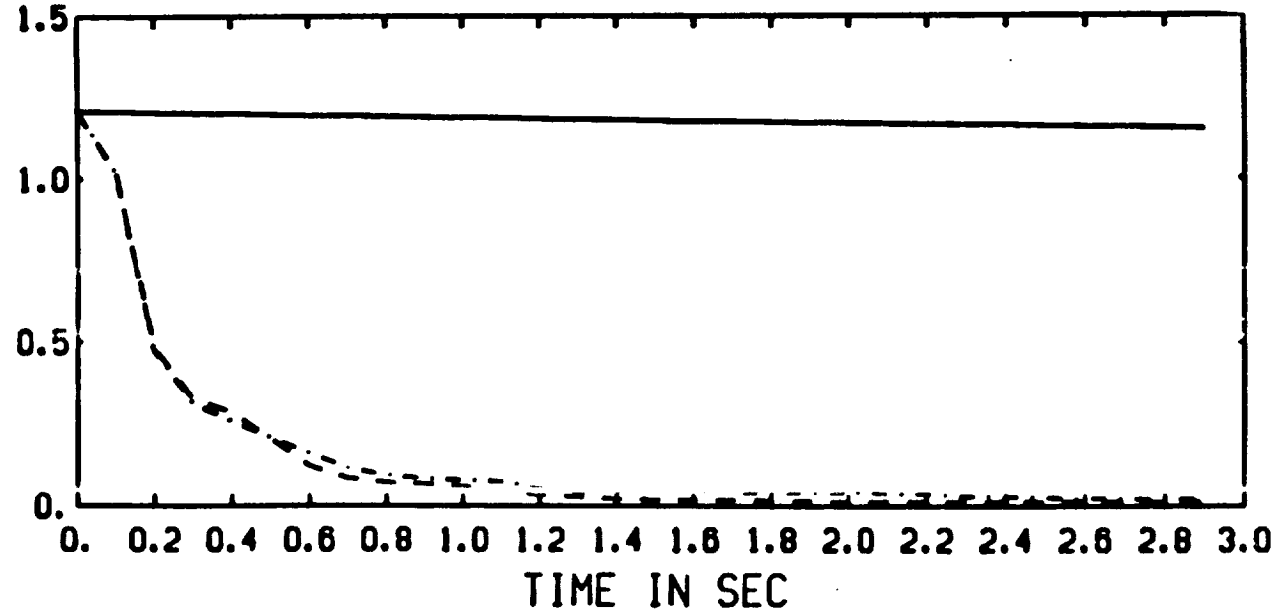

Vibrational energy profile
(reduced-order designs)

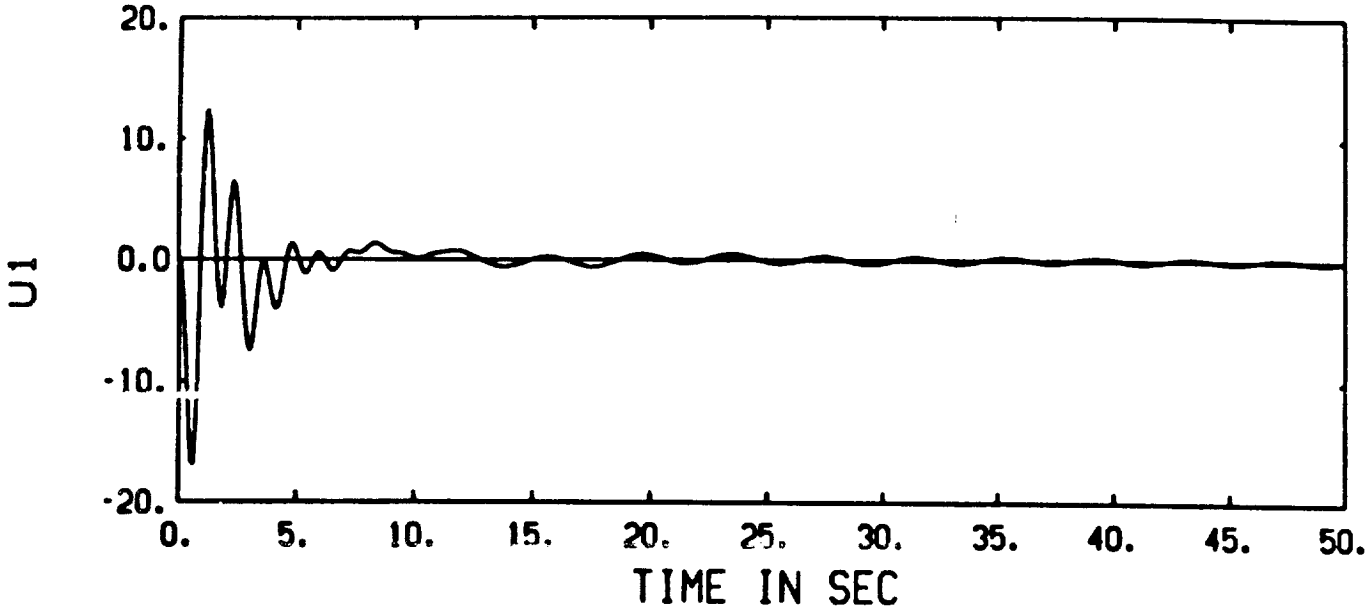

Torque input on x-axis at the hub.

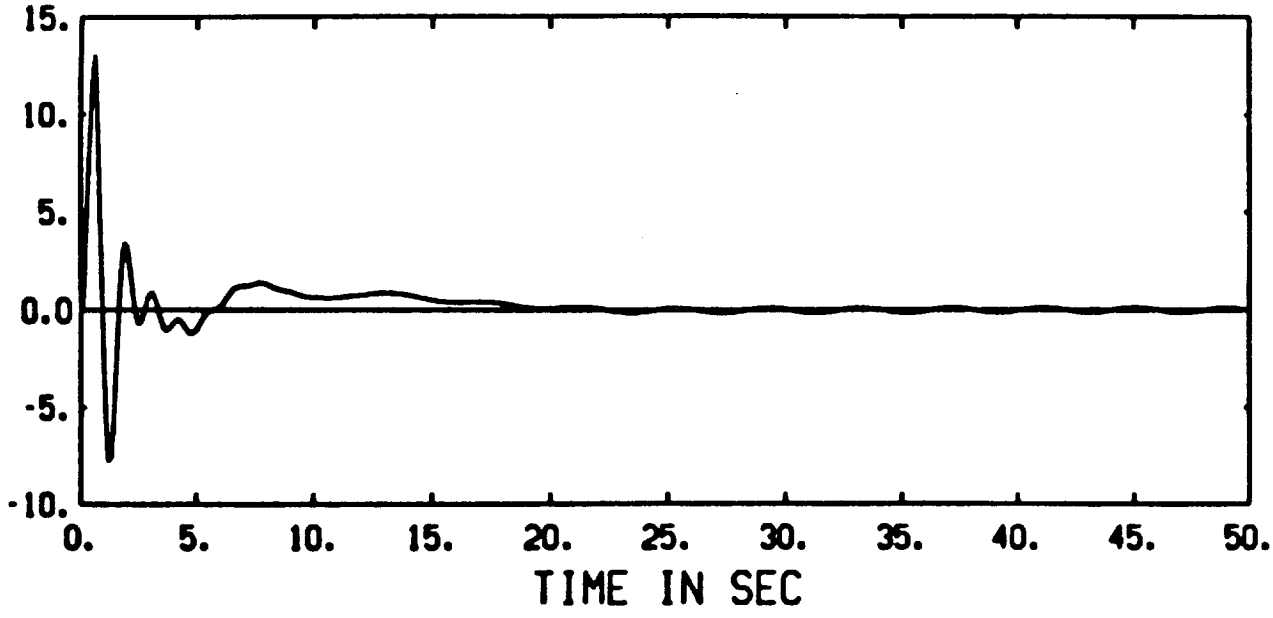

Torque input on y-axis at the hub.

Model Reference Adaptive Control (MRAC)

Procedure:

Find largest possible family of adaptation laws assuring stability, select specific adaptation law for particular application.

Methods:

Hyperstability and Positivity Concepts

Control Approach

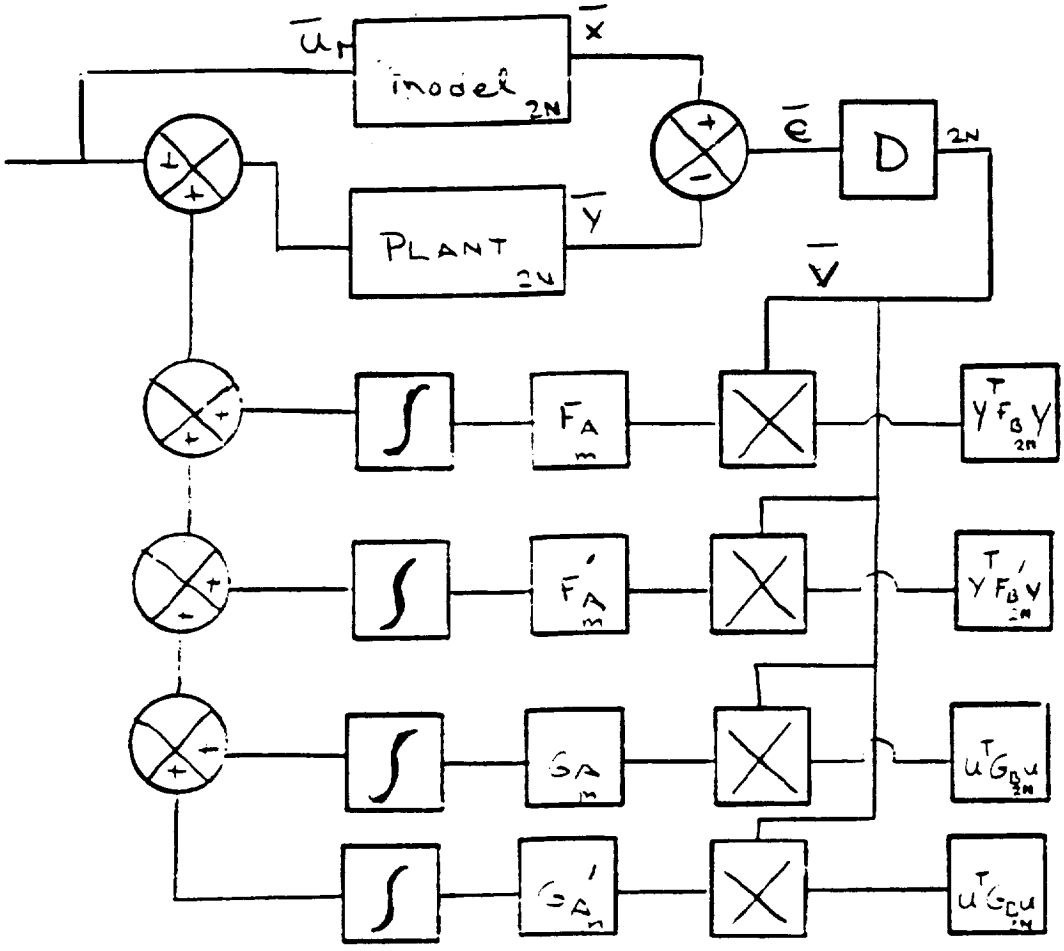

PI Adaptive Model Following Feedback

Control Objectives

- Control designed for first five modes
- 2–10% damping required

mode number	Frequency Hertz	Desired Damping
1	.964	10%
2	.964	10%
3	7.17	2%
4	7.51	2%
5	9.6	2%

- Effects of actuator dynamics not included

Application to MiniMast

Mini Mast Modal Frequencies		
mode number	Frequency Hertz	Mode Type
1	.964	x - y
2	.964	y - z
3	7.17	plate
4	7.51	torsion
5	9.6	y - z
6	9.8	x - z
7	10.2	y - z
8	12.1	mix
9	16.08	mix
10	16.8	mix

Mini Mast Model Actuators						
number	FEM Point	Actuator Type	Cordinate Frame X	Y	Z	Force Limitations
1	334	Linear Actuator	1	0	0	30 newtons
2	336	Linear Actuator	1	0	0	30 newtons
3	335	Linear Actuator	0	1	0	30 newtons
4	337	Linear Actuator	0	1	0	30 newtons
5	338	Reaction Wheel	0	0	1 Rot	50 Ft. - lb.

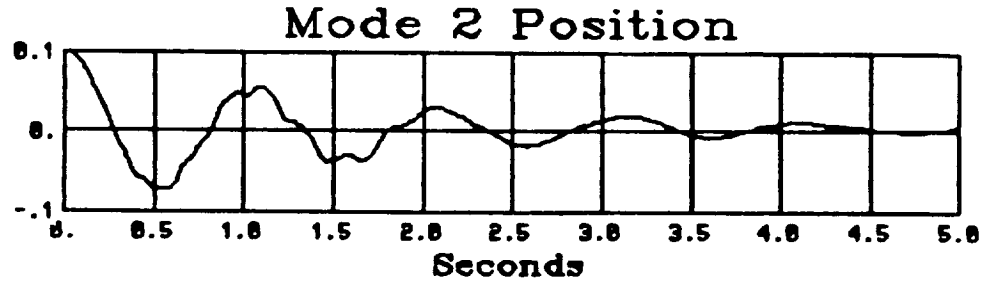
Mode 2 Position
0.1
0.
-.1
0.
0.5
1.0
1.5
2.0
2.5
3.0
3.5
4.0
4.5
5.0
Seconds

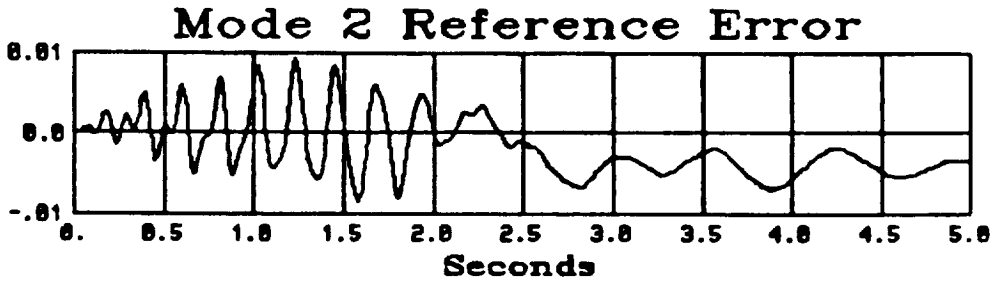
Mode 2 Reference Error
0.01
0.0
-.01
0.
0.5
1.0
1.5
2.0
2.5
3.0
3.5
4.0
4.5
5.0
Seconds

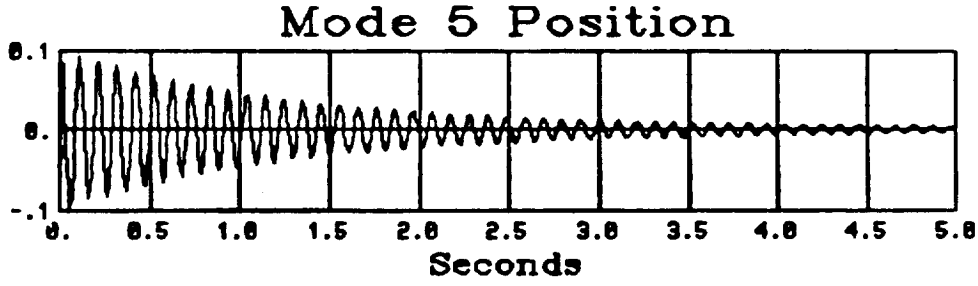
Mode 5 Position
0.1
0.
-.1
0.
0.5
1.0
1.5
2.0
2.5
3.0
3.5
4.0
4.5
5.0
Seconds

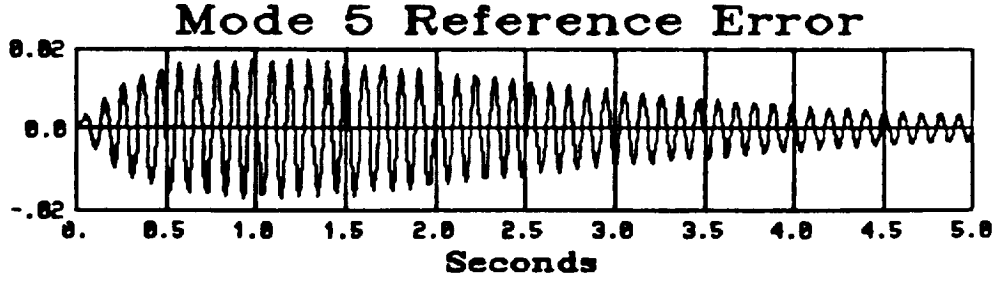
Mode 5 Reference Error
0.02
0.0
-.02
0.
0.5
1.0
1.5
2.0
2.5
3.0
3.5
4.0
4.5
5.0
Seconds

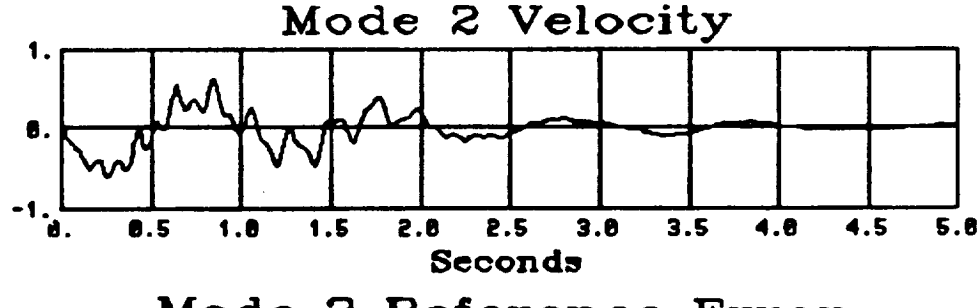
Mode 2 Velocity
1.
0.
-1.
0.
0.5
1.0
1.5
2.0
2.5
3.0
3.5
4.0
4.5
5.0
Seconds

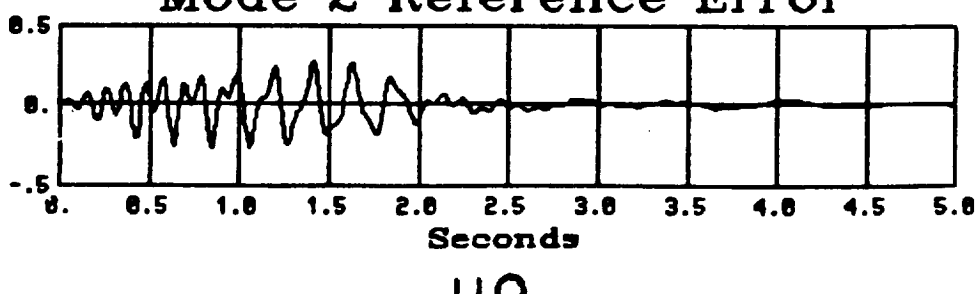
Mode 2 Reference Error
0.5
0.
-.5
0.
0.5
1.0
1.5
2.0
2.5
3.0
3.5
4.0
4.5
5.0
Seconds

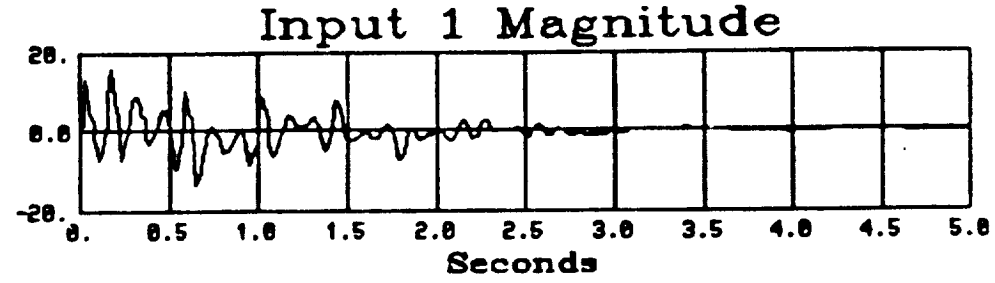
Input 1 Magnitude
20.
0.0
-20.
0. 0.5 1.0 1.5 2.0 2.5 3.0 3.5 4.0 4.5 5.0
Seconds

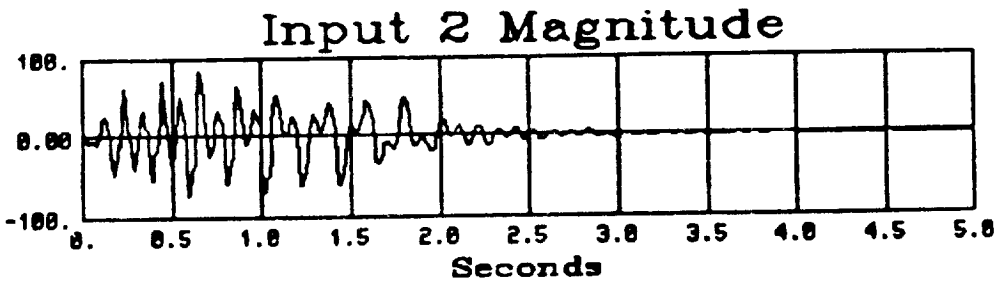
Input 2 Magnitude
100.
0.00
-100.
0. 0.5 1.0 1.5 2.0 2.5 3.0 3.5 4.0 4.5 5.0
Seconds

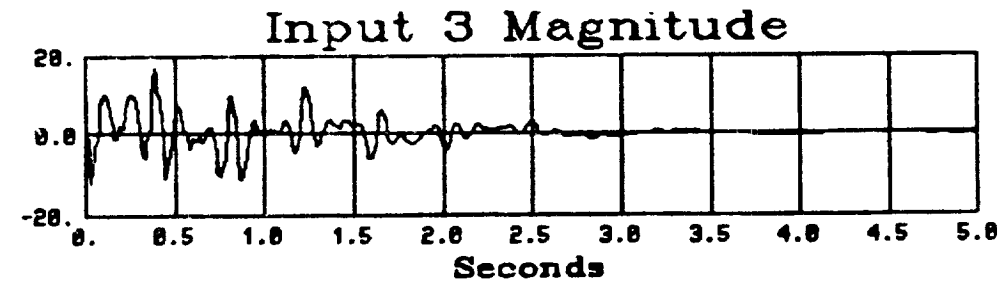
Input 3 Magnitude
20.
0.0
-20.
0. 0.5 1.0 1.5 2.0 2.5 3.0 3.5 4.0 4.5 5.0
Seconds

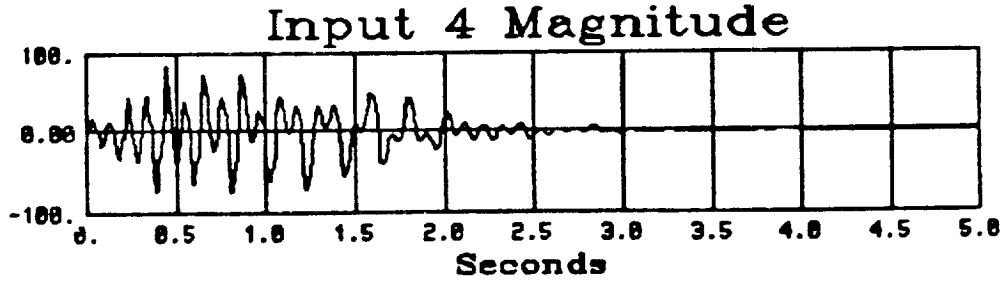
Input 4 Magnitude
100.
0.00
-100.
0. 0.5 1.0 1.5 2.0 2.5 3.0 3.5 4.0 4.5 5.0
Seconds

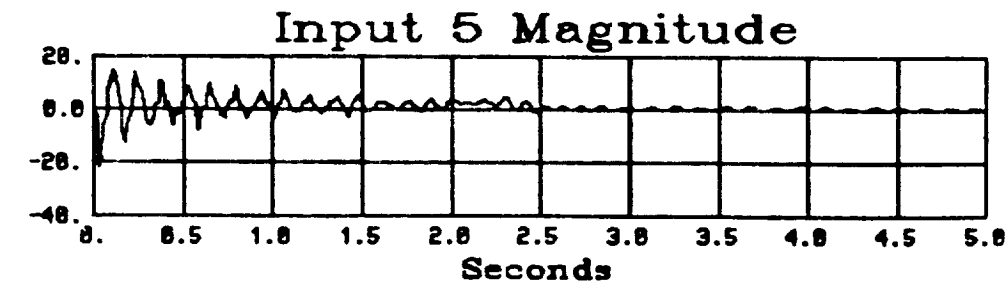
Input 5 Magnitude
20.
0.0
-20.
-40.
0. 0.5 1.0 1.5 2.0 2.5 3.0 3.5 4.0 4.5 5.0
Seconds

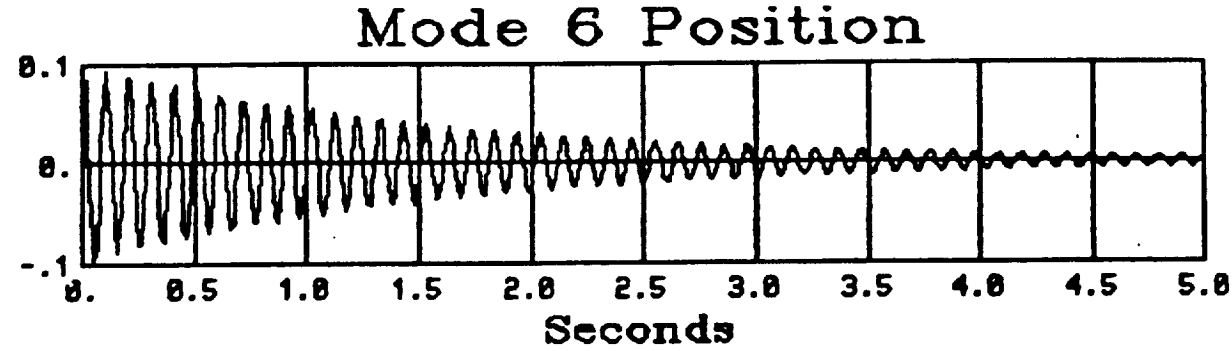
Mode 6 Position
0.1
0.
-.1
0.
0.5
1.0
1.5
2.0
2.5
3.0
3.5
4.0
4.5
5.0
Seconds

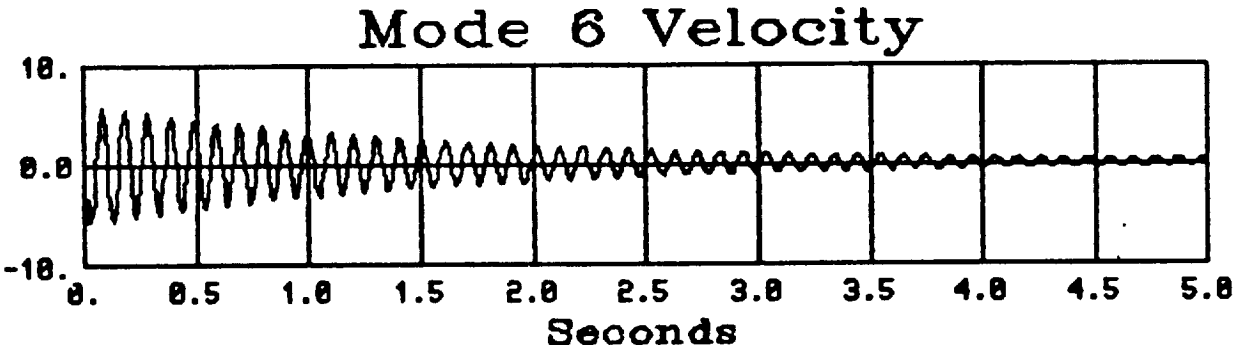
Mode 6 Velocity
10.
0.0
-10.
0.
0.5
1.0
1.5
2.0
2.5
3.0
3.5
4.0
4.5
5.0
Seconds

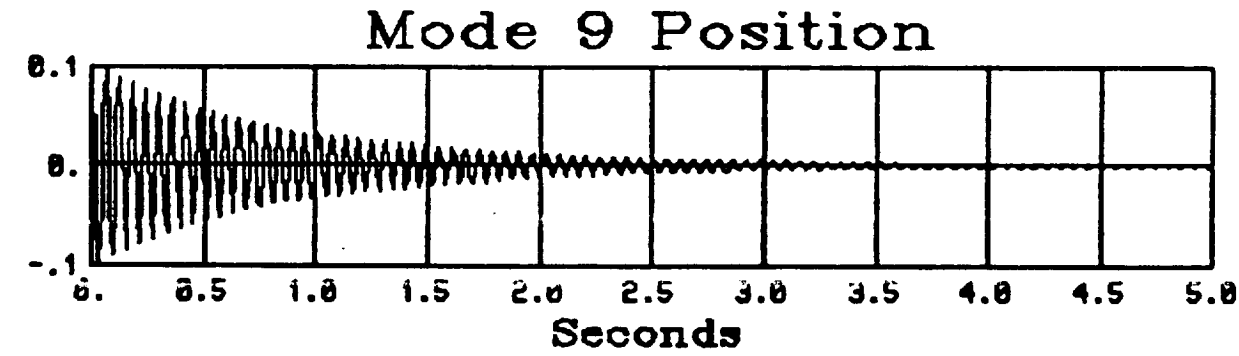
Mode 9 Position
0.1
0.
-.1
0.
0.5
1.0
1.5
2.0
2.5
3.0
3.5
4.0
4.5
5.0
Seconds

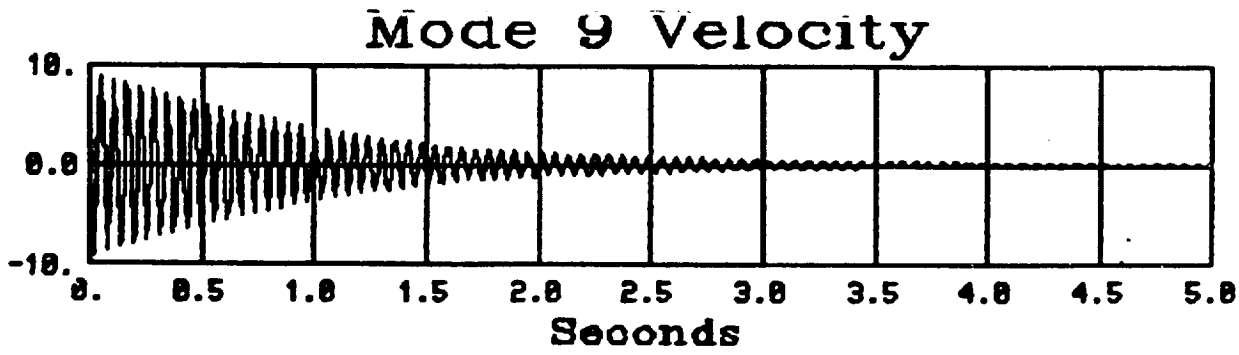
Mode 9 Velocity
10.
0.0
-10.
0.
0.5
1.0
1.5
2.0
2.5
3.0
3.5
4.0
4.5
5.0
Seconds

Outlook

- Effects of Actuator Dynamics
- Refinement of STAC
- System Identification
- Experimentation

STABILITY ANALYSIS OF LARGE SPACE STRUCTURE CONTROL SYSTEMS WITH DELAYED INPUT

by

A.S.S.R. Reddy
Assistant Professor

Peter M. Bainum
Graduate Professor

Department of Mechanical Engineering
Howard University
Washington, D.C. 20059

Presented at the

Sixth VPI&SU/AIAA Symposium on
Dynamics and Control of Large Structures

Abstract

Large space structural systems, due to their inherent flexibility and low mass to area ratio, are represented by large dimensional mathematical models. For implementation of the control laws for such systems a finite amount of time is required to evaluate the control signals; and this time delay may cause instability in the closed loop control system that was previously designed without taking the input delay into consideration. The stability analysis of a simple harmonic oscillator representing the equation of a single mode as a function of delay time is analyzed analytically and verified numerically. The effect of inherent damping on the delay is also analyzed. The control problem with delayed input is also formulated in the discrete time domain.

I. Introduction

Large flexible space structures have been proposed for possible use in communications, electronic orbital based mail systems, and solar energy collection.[1,2] The size and the low mass to area ratio of such systems warrant the consideration of the flexibility as the main contribution to the dynamics and control problem as compared to the inherently rigid nature of earlier spacecraft systems. For such large flexible systems, both orientation and surface shape control may often be required.

The equations of motion describing the shape of any large space structure are either represented by a few partial differential equations or a large number of ordinary differential equations. As the partial differential equations are difficult to solve for control system design purposes, the structural dynamics are commonly described using Finite Element Methods (FEM). Two typical large space structures namely the Hoop/Column antenna[3] and the Space Station initial operational configuration (IOC)[4] are both described using 672 degrees of freedom. Thus the dynamics of a large space structure can be written as[5]:

$$M \ddot{Z} + K Z = U_c \qquad (1)$$

where

M = NXN mass/inertia symmetric matrix

K = NXN stiffness symmetric matrix

Z = NXl generalize coordinates representing the degrees of freedom

U_C= influence of the external forces in each degree of freedom = B'U.

With the modal transformation

$$Z = \phi\, q$$

and the properties of the modal transformation such as

$$\phi^T M \phi = I$$

$$\phi^T K \phi = \text{diag}\ [\omega_1^2\ \omega_2^2\ \ldots.,\ \omega_n^2]$$

and neglecting the higher modes, equation (1) can be written in standard state space form as

$$\dot{X} = AX + BU \tag{2}$$

where

X = 2nxl state vector representing modal coordinates and their velocities $[q, \dot{q}]^T$

U = mxl control vector

$$A = \left[\begin{array}{c|c} O & I_{nxn} \\ \hline -\omega_1^2 & O \\ & -\omega_n^2 \end{array}\right]$$ system matrix

$$B = \left[\begin{array}{c} O_{nxm} \\ \hline \phi^T B'_{nxm} \end{array}\right]$$ control influence matrix

II. Control with Delayed Input

The proposed control systems for large space structures are based on state variable feedback of the form:

$$U = -FX \tag{3}$$

and the control gain matrix, F, is designed using techniques such as the linear quadratic regulator (LQR) theory[6], pole placement[7], and/or linear quadratic Gaussian/loop transfer recovery (LQG/LTR).[8]

For the case when the complete state is not available for feedback, an estimate of the state, $\hat{X}$, is obtained using an appropriate estimator from the measurements of the form

$$Y = CX \tag{4}$$

where

Y = ℓxl measurement vector

C = ℓxn sensor influence matrix

In general, it is assumed that the estimated state, $\hat{X}$, is instantaneously available. As the state estimator is implemented using a digital computer and the number of the status (2n) is of the order of hundreds for a large space structure, the computational time becomes appreciable. Thus, in the present paper, the stability of the closed loop control system, with the control as given in equation (2), is analyzed as a function of the delay time (h) using the modified control law of the form:

$$U(t) = -FX(t-h) \tag{5}$$

The characteristic equation of the closed loop system

$$\dot{X} = AX(t) - BFX(t-h) \tag{6}$$

is given by

$$G(s,h) = \det (sI-A+BFe^{-sh}) = 0 \tag{7}$$

which, in turn, can be written as

$$G(s,h) = \sum_{i=0}^{2n} P_i(s)e^{-shi} = 0. \tag{8}$$

The roots of the characteristic equation, (8), as a function of the delay, h, are obtained from the corresponding auxiliary equation[9]

$$G'(s,h) = \sum_{i=0}^{2n} P_i(s)(1-Ts)^{2i}\,(1+Ts)^{4n-2i} = 0 \tag{9}$$

where

$$e^{-sh} = \left[\frac{1-sT}{1+sT}\right]^2. \tag{10}$$

The value of T for which the roots of the equation (9) cross the imaginary axis in the s-plane is obtained and the corresponding h is evaluated using the relation, (10).

III. Example of a Harmonic Oscillator

The equation of motion representing the i^{th} structural mode is the familiar harmonic oscillator and is given by

$$\ddot{x}_i + \omega_i^2 x_i = f_i \tag{11}$$

Considering the delayed velocity feedback of the form

$$f_i = -2\zeta_i \omega_i \dot{x}_i \ (t-h) \tag{12}$$

with

$$\omega_i = 6, \quad \zeta_i = 0.5,$$

the characteristic equation is given by

$$G(s,h) = s^2+36+6se^{-sh} = 0 \tag{13}$$

$$= \sum_{i=0}^{1} P_i(s)e^{-shi} = 0$$

where

$$P_o(s) = s^2 + 36$$

$$P_1(s) = 6s$$

The corresponding auxilary equation is given by

$$\sum_{i=0}^{1} P_i(s) \ (1-Ts)^{2i} \ (1+TS)^{2-2i} = 0 \tag{14}$$

i.e. $$(s^2+36) \ (1+Ts)^2 +6s(1-Ts)^2 = 0$$

or $$T^2s^4 + (2T + 6T^2) \ s^3+(1+36T^2-12T)s^2$$

$$+ (72T+6)s+36 = 0 \tag{15}$$

Using the Routh-Hurwitz criterion, it can be found that the roots of equation (15) cross the imaginary axis at $\omega \tilde{=} 9.7$ for $T \tilde{=} 0.0426$. The corresponding delay (h) can be calculated from the relation (10) with $s = j\omega$ and is 0.16. This result can also be verified directly for this simple system with the substitution $s=j\omega$ into equation (13)[10], resulting in the value of ω and delay h for which the roots of the characteristic equation cross the imaginary axis.

Thus, equation (13) can be written as (keeping ζ_i and ω_i):

$$(\omega_i^2-\omega^2) + j(2\zeta_i\omega_i\omega)e^{-j\omega h} = 0 \tag{16}$$

or

$$(\omega_i^2-\omega^2+2\zeta_i\omega_i\omega \sin\omega h) + j2\zeta_i\omega_i\omega \cos\omega h = 0 . \tag{17}$$

For equation (17) to be satisfied

$$\cos \omega h = 0 \quad \text{or} \quad \omega h = \pi/2 \tag{18}$$

and

$$\omega_i^2-\omega^2+2\zeta_i\omega_i\omega = 0 \tag{19}$$

or $$\omega = \zeta_i\omega_i \pm \omega_i\sqrt{1+\zeta_i^2}$$

Taking the positive value for ω, the delay h, is given by

$$h = \frac{\pi/2}{\omega_i[\zeta_i+\sqrt{1+\zeta_i^2}\,]} . \tag{20}$$

The value of h for $\zeta_i = 0.5$ and $\omega_i = 6$ is 0.16 and thus the earlier result is verified. It is observed that an increase in damping reduces the tolerable delay (h) in the input.

The equation of motion of a single mode with inherent (natural) damping and velocity feedback can be written as:

$$\ddot{X}+2\zeta_i'\omega_i\dot{X}+\omega_i^2X = f = -2\zeta_i\omega_i\dot{X}(t-h) \tag{21}$$

where ζ_i' is the inherent damping ratio.

The corresponding characteristic equation is given by

$$s^2+2\zeta_i'\omega_i s+\omega_i^2+2\zeta_i\omega_i s e^{-sh} = 0 . \tag{22}$$

After substituting $s = j\omega$, equation (22) can be written as:

$$(\omega_i^2-\omega^2+2\zeta_i\omega_i\omega \sin\omega h) + j(2\zeta_i'\omega_i\omega+2\zeta_i\omega_i\omega\cos\omega h) = 0 \tag{23}$$

For equation (23) to be satisfied for all ω and h, we have

$$2\zeta_i'\omega_i+2\zeta_i\omega_i \cos\omega h = 0 \tag{24}$$

or

$$\cos \omega h = -\zeta_i'/\zeta_i \tag{25}$$

Thus, for $\cos\omega h = < 1$, the inherent damping must be less than damping due to control for instability. For $\zeta_i < \zeta_i'$, the system will always be stable.

With the value of ωh from equation (25) the frequency ω can be calculated as:

$$\omega = \omega_i \left[\sqrt{\zeta_i^2 - \zeta_i'^2} \pm \sqrt{1+\zeta_i^2 - \zeta_i'^2}\right] \tag{26}$$

and selecting the positive value of ω, h is given by:

$$h = \frac{\cos^{-1}(-\zeta_i'/\zeta_i)}{\omega_i\left[\sqrt{\zeta_i^2\zeta_i'^2} \pm \sqrt{1+\zeta_i^2\zeta_i'^2}\right]} \tag{27}$$

For $\zeta_i = \zeta'$ it can be seen that the delay, h, is half the undamped natural period of vibration. As the damping due to control increases, the tolerable delay (h) decreases and is in accordance with the observation made in the case without the inherent damping. The effect of inherent damping in the system is to increase the amount of delay that the system can tolerate without become unstable as compared to the case without damping

IV. Discrete Time Domain

As the controller is implemented on a digital computer, it may be more natural to consider the delayed input problem in the discrete time domain.

The equations of motion as given by equation (2) can be written in the discrete time domain as

$$X(i+1) = A_d X(i) + B_d U(i) \tag{28}$$

where

$$A_d = e^{A\Delta}, \quad B_d = \int_0^{\Delta} e^{A(t-\Delta)} B \, dt$$

Δ = discretization time.

The delayed input problem can be considered in discrete time in one of the two following ways:

i) Designing the controller of the form $U = -FX(i)$ without taking into consideration the delay and then examining the effect of delay on the stability of the closed-loop control system.

The control gain matrix F is designed such that the matrix $(A_d - B_d F)$ has the eigenvalues within the unit circle. Then the delay is introduced into the control law as:

$$U(i) = - FX(i-\ell) \tag{29}$$

and

$$X(i+1) = A_d X(i) - B_d F X(i-\ell) \, . \tag{30}$$

The stability of equation (30) can be studied using the augmented system given by

$$\underset{\tilde{Z}(i+1)}{\begin{bmatrix} X(i+1) \\ X(i) \\ \\ X(i-\ell+1) \end{bmatrix}} = \underset{\tilde{A}_d}{\begin{bmatrix} A_d & 0 & 0 & 0 & -B_d F \\ I & 0 & 0 & 0 & 0 \\ \\ 0 & 0 & 0 & I & 0 \end{bmatrix}} \underset{\tilde{Z}(i)}{\begin{bmatrix} X(i) \\ X(i-1) \\ \\ X(i-\ell) \end{bmatrix}} \tag{31}$$

or

$$\tilde{Z}(i+1) = \tilde{A}_d \tilde{Z}(i) \tag{25}$$

(ii) Designing the control by taking into account the delay in the input.[6,11]

Equation (28) can be modified as :

$$X(i+1) = A_d X(i) + B_d U(i-\ell) \tag{32}$$

The control law of the form $U(i) = -F\tilde{Z}(i)$ can be designed from the augmented system:

$$\begin{bmatrix} X(i+1) \\ U(i) \\ U(i-1) \\ \\ U(i-\ell+1) \end{bmatrix} = \begin{bmatrix} A_d & 0 & 0 & 0 & B_d \\ 0 & 0 & 0 & 0 & 0 \\ 0 & I & 0 & 0 & 0 \\ \\ 0 & 0 & 0 & I & 0 \end{bmatrix} \underset{\tilde{Z}(i)}{\begin{bmatrix} X(i) \\ U(i-1) \\ \\ U(i-\ell) \end{bmatrix}} + \begin{bmatrix} 0 \\ I \\ 0 \\ \\ 0 \end{bmatrix} U(i) \tag{33}$$

or

$$\tilde{Z}(i+1) = \tilde{A}_d Z(i) + \tilde{B}_d U(i) \, .$$

Thus the input $U(i-\ell)$ is a function of the previous inputs, $U(i-\ell-1)$, $U(i-\ell-2),\ldots$, and the previous states $X(i-\ell)$. Though this design can take delay into consideration, the sequence of the control signals: $U(i-\ell)$, $U(i-\ell+1),\ldots$ must be generated at an interval of one step and, thus, the original delay problem is not completely solved.

Conclusions

The effect of delay in the input on the stability of the continuous time controller that is designed without taking this delay into consideration is presented. The closed-loop control system of a second order plant becomes unstable for a delay of 0.16 seconds, which is only 16 percent of its natural period of motion. It is also observed that even a small amount of inherent (natural) damping in the system can increase the amount of delay that can be tolerated without the system becoming unstable. The delay problem is formulated in the discrete time domain and an analysis procedure is suggested.

Acknowledge

This research was supported by NASA Grant NSG-1414.

References

1. Outlook for Space, NASA Report - 386, Jan. 1976.

2. Industry Workshop on Large Space Structures, NASA CR-2709, Contract No. NAS-1-12436, for NASA LaRC, May, 1976.

3. Golden, C.T., Lackey, J.A., and Spear, E.E., "Configuration Development of the Land Mobile Satellite System (LMSS) Spacecraft," Large Space Systems Technology-1981, Third Annual Technical Review, NASA LaRC, Nov. 16-19, 1981, NASACP-2215, Part 2, pp. 711-766.

4. Housner, J.M., "Structural Dynamic Model and Response of the Deployable Reference Configuration Space Station," NASA TM86386, May 1985.

5. Bainum, Peter M., et al., "Modelling and Simulation of Dynamics and Control of Large Flexible Orbiting Systems," Journal of the Institution of Engineers (India), Vol. 66, Part 2, Aerospace Engineering, March 1986, pp. 52-56.

6. Kwakernaak, H. and Sivan, R., Linear Optimal Control Systems," Wiley, New York, 1972.

7. Kailath, T., "Linear Systems," Prentice-Hall Inc., Englewood Cliffs, N.J., 1980.

8. Doyle, J.C., and Stein, G., "Multivariable Feedback Design: Concepts for a Classical/Modern Synthesis," IEEE Trans on AC, Vol. AC-26, No. 1, Feb. 1981, pp. 4-16.

9. Thowsen, A., "An Analytic Stability Test for a class of Time Delay Systems," IEEE Trans. on AC, Vol. AC-26, No. 3, June, 1981, pp. 735-736.

10. Van Woerkom, P.Th.L.M.; Private Communication, Feb., 1986.

11. Reddy, A.S.S.R., and Gumustas, A.R., "Delay Digital Control of Large Space Structures," 13th IASTED International Conference on Modelling and Simulation, June 24-26, 1985, Lugano, Switzerland.

MINIMUM TIME ATTITUDE SLEWING MANEUVERS OF A RIGID SPACECRAFT

by

Feiyue Li
Graduate Research Assistant
Department of Mechanical Engineering
Howard University
Washington, D.C. 20059

and

Peter M. Bainum
Professor of Aerospace Engineering
Department of Mechanical Engineering
Howard University
Washington, D.C. 20059

To be Presented at the
AIAA 26th Aerospace Sciences Meeting
January 11-14, 1988
Reno, Nevada

Paper No. 88-0675

[illegible] OF A RIGID SPACECRAFT*

Feiyue Li† and Peter M. Bainum**
Howard University
Washington, D.C.

Abstract

The minimum time attitude slewing motion of a rigid spacecraft with its controls provided by torques and forces, which have their upper and lower limits prescribed, is considered. The two-point boundary-value problem is derived by applying the Pontryagin's Maximum Principle to the system and solved by using a quasilinearization algorithm. The nominal solutions to the problem as well as the starting values of the total slewing time and the unknown initial costates for this algorithm are generated by using Euler's eigenaxis rotation theorem. It is pointed out that one of the four initial costates associated with the quaternions can be arbitrarily selected without affecting the optimal controls and, thus, simplifying the computation. The minimum slewing time is determined by shortening the total slewing time until at least one of the controls becomes a bang-bang type. Several numerical tests for the rigidized SCOLE model are presented to show the applications of the methods.

1. Introduction

The problems of large-angle attitude maneuvers of a spacecraft have gained much consideration in recent years.[1-8] In these papers, the configurations of the spacecraft considered are: (1) completely rigid, (2) a combination of rigid and flexible parts, or (3) gyrostat-type systems. The performance indices usually include minimum torque integration, power criterion, and frequency-shaped cost functionals, etc. Also some of these papers used feedback control techniques. In this paper, we try to concentrate on the minimum time slewing problem of a rigid spacecraft.

In Ref. 2, the author studied the rapid torque-limited slewing of SCOLE about a single axis (x-axis) about which the spacecraft has a small moment of inertia. The control torque about this axis is of a bang-bang type or a bang-pause-bang type. The author computed the slewing motion on the simplified model of the rigidized SCOLE[1], then worked on the practical rigidized model (with nonzero products of inertia); hence, this leads to a large error of the attitude after the slewing. Also it seems that no details were given for the controls about the other two axes (y, z).

In the present paper, we apply optimal control theory (Maximum Principle) to the slewing motion of a general rigid spacecraft (include the rigidized SCOLE, without simplification). The slewing motion need not be restricted to a single-axis slewing. The attitude error at the end of the slewing can be made as small as required.

*Research supported by NASA Grant NSG-1414
†Graduate Research Assistant, Dept. of Mechanical Engineering, Student Member AIAA
**Professor of Aerospace Engineering; Associate Fellow AIAA

All the controls (torques and forces) are computed and the minimum slewing time is found by using the quasilinearization algorithm for the resulting two-point-boundary-value problem.

2. Attitude Description and State Equations

2.1 Attitude Description and Euler Rotation

Let $\bar{a} = [\bar{a}_1\ \bar{a}_2\ \bar{a}_3]^T$ represent a set of unit, orthogonal vectors of an inertial reference system, and $\bar{b} = [\bar{b}_1\ \bar{b}_2\ \bar{b}_3]^T$ a set of unit, orthogonal vectors of a body-fixed coordinate system of a spacecraft. Then, the attitude of the spacecraft relative to $\bar{a}$ can be described by a direction cosine matrix C with C satisfying the relation

$$\bar{b} = C\,\bar{a} \tag{1}$$

and

$$C = \begin{bmatrix} q_0^2+q_1^2-q_2^2-q_3^2 & 2(q_1q_2+q_0q_3) & 2(q_1q_3-q_0q_2) \\ 2(q_1q_2-q_0q_3) & q_0^2+q_2^2-q_3^2-q_1^2 & 2(q_2q_3+q_0q_1) \\ 2(q_1q_3+q_0q_2) & 2(q_2q_3-q_0q_1) & q_0^2+q_3^2-q_1^2-q_2^2 \end{bmatrix} \tag{2}$$

where $q = [q_0\ q_1\ q_2\ q_3]^T$ is the attitude quaternion vector and subject to a constraint equation

$$q^Tq = 1 \tag{3}$$

It can be seen that q can be used not only to represent an attitude orientation of a spacecraft, but also to describe a rotation of a rigid body (spacecraft). For example, when a rigid spacecraft rotates about an axis defined by a unit vector $\epsilon = [\epsilon_1\ \epsilon_2\ \epsilon_3]^T$ fixed in both $\bar{a}$ and $\bar{b}$, the quaternion describing this rotation is

$$q_0 = \cos(\theta/2),\quad q_i = \epsilon_i \sin(\theta/2)\quad i = 1,2,3 \tag{4}$$

where θ is the rotation angle.

The Euler rotation theorem tells us that an arbitrary orientation of a rigid body can be accomplished by rotating it about a certain eigenaxis, $\epsilon = [\epsilon_1\ \epsilon_2\ \epsilon_3]^T$, through θ angle from its initial position. By means of this theorem we can find the desired rotation quaternion, q, between the initial position q(0) and the final orientation $q(t_f)$ by the relation

$$\begin{bmatrix} q_0 \\ q_1 \\ q_2 \\ q_3 \end{bmatrix} = \begin{bmatrix} q_{00} & q_{10} & q_{20} & q_{30} \\ -q_{10} & q_{00} & q_{30} & -q_{20} \\ -q_{20} & -q_{30} & q_{00} & q_{10} \\ -q_{30} & q_{20} & -q_{10} & q_{00} \end{bmatrix} \begin{bmatrix} q_{0f} \\ q_{1f} \\ q_{2f} \\ q_{3f} \end{bmatrix} \tag{5}$$

where the second subscript "0" and "f" represent the initial time and final time, respectively.

The associated ε and θ can be obtained by the following relations

$$\theta = 2 \arccos q_0 \ , \ \varepsilon_i = q_i/\sqrt{1-q_0^2}, \ i = 1,2,3 \tag{6}$$

2.2 Kinematical and Dynamical Equations

The attitude quaternion and the angular velocity of a rigid spacecraft satisfy the following kinematical and Euler dynamical equations.

$$\dot{q} = (1/2)\ \tilde{\underline{\omega}}\ q \tag{7}$$

$$I\ \dot{\omega} = \tilde{\omega}\ I\ \omega + B\ u \tag{8}$$

where

ω _ angular velocity vector in the body system, $\omega = [\omega_1 \omega_2 \omega_3]^T$

u _ control torque and force vector, $u = [u_1 u_2 u_3 \ . \ . \ . \ u_n]^T$

and

$$\tilde{\underline{\omega}} = \begin{bmatrix} 0 & -\omega_1 & -\omega_2 & -\omega_3 \\ \omega_1 & 0 & \omega_3 & -\omega_2 \\ \omega_2 & -\omega_3 & 0 & \omega_1 \\ \omega_3 & \omega_2 & -\omega_1 & 0 \end{bmatrix}, \quad \tilde{\omega} = \begin{bmatrix} 0 & \omega_3 & -\omega_2 \\ -\omega_3 & 0 & \omega_1 \\ \omega_2 & -\omega_1 & 0 \end{bmatrix}$$

$$I = \begin{bmatrix} I_{11} & -I_{12} & -I_{13} \\ -I_{12} & I_{22} & -I_{23} \\ -I_{13} & -I_{23} & I_{33} \end{bmatrix}$$

and B is a 3xn alignment (control influence) matrix. Eq. (8) can be rewritten, by premultiplying by the inverse of I, as

$$\dot{\omega} = I^{-1}\ \tilde{\omega}\ I\ \omega + I^{-1}\ B\ u \tag{9}$$

The associated initial and terminal boundary conditions of the states, q, ω, are prescribed:

$$q(t=0),\ \omega(t=0);\ q(t_f),\ \omega(t_f) \tag{10}$$

3. Optimal Control - Two Point Boundary Value Problem

In this paper, we try to minimize the slewing time t_f,

$$t_f = \int_0^{t_f} dt \tag{11}$$

under the constraints that the elements of the control vector u have their upper and lower limits, respectively

$$u_{jmin} \le u_j \le u_{jmax}, \quad j = 1,2,3, \ \ldots, \ n \tag{12}$$

Generally speaking, minimization of t_f under the constraints (12) will result in a so-called two-point boundary-value problem in which several controls (at least one) will reach their bounds during the slewing time, t_f. To explain this point, let us first consider a well-known special case where there are only 3 control torques, u_1, u_2, u_3, about the 3 principal axes of the spacecraft, respectively (i.e. diagonal matrix I). For this case the minimum time rotation of the spacecraft about one of its principal axes will yield the following results: the control torque about this axis is of a bang-bang type, while the other two torques remain zero. Otherwise, if the slewing motion is not about a principal axis, none of the 3 controls remain zero, but we can reason that at least one of the 3 control inputs reaches its bounds, except some jumps at the switching points during the period, t_f. As for a general case where the control torques are about a body axes system which does not coincide with the principal axes (non-diagonal I) and some additional control forces, u_4, u_5, ..., u_n, are available, the control laws become more complicated.

To handle the problem in which some controls reach their bounds and others do not, we introduce an additional cost function

$$J = \frac{1}{2} \int_0^{t_f} u^T R u \ dt \tag{13}$$

where u is the control vector, R is a proper weighting matrix. From Refs. 3 and 8, we can see that, for the case of rest-to-rest (i.e. $\omega(0) = 0$, $\omega(t_f) = 0$) slewing with only 3 control inputs involved, if we use only (13) as a criterion and t_f is long enough, the control torques are approximately linear functions of time, and the controls will not reach their saturation levels. But if we shorten t_f in order to find a minimum time, some of the controls must reach their bounds and, thus, contribute more effort to the slewing. By continuing the shortening of t_f, we can get a particular value, t_f^*, during which at least one of the controls remains as bang-bang with one switching point, while others are generally not of the bang-bang type. This value, t_f^*, is called the minimum time which is required.

The motivations for using (13) as our cost function are:

1) Ease of using the quasilinearization algorithm

2) No need to determine the switching points.

3) Easy to guess the unknown initial values of the costates.

3.1 Necessary Conditions

The Hamiltonian, H, for the system (7), (9) and (13) is

$$H = (1/2)u^T R u + p^T \dot{q} + r^T \dot{\omega}$$

$$= (1/2)u^T R u + (1/2) p^T \tilde{\underline{\omega}} q + r^T (I^{-1} \tilde{\omega} I \omega + I^{-1} B\ u) \tag{14}$$

where p and r are costate vectors associated with q and ω,

$$p = [p_0 \ p_1 \ p_2 \ p_3]^T, \quad r = [r_1 \ r_2 \ r_3]^T.$$

By means of the maximum principle, the necessary conditions for minimizing J, are

$$\dot{p} = -(\partial H/\partial q) \ , \ \Longrightarrow \ \dot{p} = (1/2)\ \tilde{\underline{\omega}}\ p \tag{15}$$

$$\dot{r} = -(\partial H/\partial \omega) \ , \ \Longrightarrow \ \dot{r} = g(\omega, r) + (1/2)[q]p \tag{16}$$

where $g(\omega,r)$ is a 3x1 vector function of ω and r, and the detailed form of $g(\omega,r)$ can be found in Appendix I; $[q]$ is a 3x4 matrix

$$[q] = \begin{bmatrix} q_1 & -q_0 & -q_3 & q_2 \\ q_2 & q_3 & -q_0 & -q_1 \\ q_3 & -q_2 & q_1 & -q_0 \end{bmatrix}$$

The initial values of p, r are unknown, $p(t=0)$, $r(t=0)$.

If u is a 3x1 control torque vector and B is a 3x3 nonsingular matrix, R can be a positive-definite matrix defined by

$$R = B^T B \tag{17}$$

From

$$\frac{\partial H}{\partial u} = 0, \quad ==> \quad R\,u + B^T I^{-1} r = 0$$

$$\text{or} \quad u = -R^{-1} B^T I^{-1} r$$

$$= -B^{-1} I^{-1} r \tag{18}$$

we have[9]

$$u_j = \begin{cases} u_{jmin}, & \text{if } u_j < u_{jmin}; \\ -(B^{-1} I^{-1} r)_j, & \text{if } u_{jmin} \le u_j \le u_{jmax}; \\ u_{jmax}, & \text{if } u_j > u_{jmax}. \end{cases}$$

$$j = 1,2,3. \tag{19}$$

If u is an nx1 (n>3) vector, B is a 3xn matrix, the R formed by (17) is a semi-positive-definite matrix. To circumvent the singularity of R, we introduce a 3x1 vector, v,

$$v = B\,u \tag{20}$$

Then

$$(\partial H/\partial v) = 0, \quad ==> \quad v = -I^{-1} r \tag{21}$$

By means of pseudo-inverse of matrix B, B^+, we can get u

$$u = B^+ v = B^T(BB^T)^{-1} v$$

$$= -B^T(BB^T)^{-1}(I^{-1} r) \tag{22}$$

The control laws are

$$u_j = \begin{cases} u_{jmin}, & \text{if } u_j < u_{j\,min}; \\ -(B^+ I^{-1} r)j, & \text{if } u_{jmin} \le u_j \le u_{jmax}; \\ u_{jmax}, & \text{if } u_j > u_{jmax}. \end{cases}$$

$$j = 1,2, \ldots, n. \tag{23}$$

Note that Eq. (23) is reduced to Eq. (19) if B^{-1} exists.

In summary, we seek the function $q(t)$, $\omega(t)$, $u(t)$, $p(t)$, and $r(t)$ which satisfy the equations (7), (9), (15-16), (23) subject to the boundary conditions (10).

3.2 Properties of the Initial Values of p

The key to settle this problem is to find the unknown initial values of the costates

$$p(0) = [\,p_{00}\ p_{10}\ p_{20}\ p_{30}]^T \quad \text{and}$$

$$r(0) = [r_{10}\ r_{20}\ r_{30}]^T$$

Notice that the coefficient matrix of the right side of Eq. (15) is anti-symmetric, so,

$$p^T\dot{p} = 0 \quad \text{i.e.} \quad p^T p = \text{constant}$$

The extra constant is usually treated as an unknown and is determined by iteration. This results in more computational effort. However, as we shall prove, this unknown constant can be arbitrarily selected without changes in the optimal controls.[8]

Compare Eqs. (7) and (15), they have the same coefficient matrix on the right sides. Therefore, they have the same state transition matrix. Let Q represent this 4x4 matrix, then the q and p at any instant can be obtained by

$$q = Q\,q(0), \quad p = Qp(0) \tag{24}$$

We know that Q satisfies the following matrix differential equation

$$\dot{Q} = (1/2)\,\underset{\sim}{\omega} Q \tag{25}$$

Ref. 10 shows that Q, the solution of (25), has the form

$$Q = \begin{bmatrix} q_{11} & -q_{12} & -q_{13} & -q_{14} \\ q_{12} & q_{11} & q_{14} & -q_{13} \\ q_{13} & -q_{14} & q_{11} & q_{12} \\ q_{14} & q_{13} & -q_{12} & q_{11} \end{bmatrix} \tag{26}$$

On substituting Eq. (26) into Eq. (25) we can verify that only 4 of the 16 q_{ij} are independent. We rewrite and rearrange the first equation of (24) as

$$\begin{bmatrix} q_0 \\ q_1 \\ q_2 \\ q_3 \end{bmatrix} = \begin{bmatrix} q_{00} & -q_{10} & -q_{20} & -q_{30} \\ q_{10} & q_{00} & -q_{30} & q_{20} \\ q_{20} & q_{30} & q_{00} & -q_{10} \\ q_{30} & -q_{20} & q_{10} & q_{00} \end{bmatrix} \begin{bmatrix} q_{11} \\ q_{12} \\ q_{13} \\ q_{14} \end{bmatrix} = Q_0\,\underset{\sim}{q} \tag{27}$$

where $q_{00} = q_0(0)$, $q_{10} = q_1(0)$, etc. It is clear that the matrix, Q_0, in Eq. (27) is orthogonal, so

$$\underset{\sim}{q} = Q_0^T\,q \tag{28}$$

From Eq. (28) we get

$$q_{11}^2 + q_{12}^2 + q_{13}^2 + q_{14}^2 = 1$$

This means that Q is also orthogonal. On the other hand, we have a similar equation for p,

$$p = P_0 \underset{\sim}{q} \tag{29}$$

where P_0 has the same form as Q_0 in Eq. (27). After substituting Eq (28) into Eq. (29) and eliminating $\underset{\sim}{q}$, one arrives at

$$\begin{bmatrix} p_0 \\ p_1 \\ p_2 \\ p_3 \end{bmatrix} = \begin{bmatrix} d_0 & -d_1 & -d_2 & -d_3 \\ d_1 & d_0 & -d_3 & d_2 \\ d_2 & d_3 & d_0 & -d_1 \\ d_3 & -d_2 & d_1 & d_0 \end{bmatrix} \begin{bmatrix} q_0 \\ q_1 \\ q_2 \\ q_3 \end{bmatrix} \tag{30}$$

where the constants d_0, d_1, d_2, d_3, are given by

$$\begin{bmatrix} d_0 \\ d_1 \\ d_2 \\ d_3 \end{bmatrix} = \begin{bmatrix} q_{00} & q_{10} & q_{20} & q_{30} \\ -q_{10} & q_{00} & -q_{30} & q_{20} \\ -q_{20} & q_{30} & q_{00} & -q_{10} \\ -q_{30} & -q_{20} & q_{10} & q_{00} \end{bmatrix} \begin{bmatrix} p_{00} \\ p_{10} \\ p_{20} \\ p_{30} \end{bmatrix} \tag{31}$$

Eq. (30) represents the relationship between the quaternion and the associated costates. Eq. (30) can be rewritten as

$$\begin{bmatrix} p_0 \\ p_1 \\ p_2 \\ p_3 \end{bmatrix} = \begin{bmatrix} q_0 & -q_1 & -q_2 & -q_3 \\ q_1 & q_0 & q_3 & -q_2 \\ q_2 & -q_3 & q_0 & q_1 \\ q_3 & q_2 & -q_1 & q_0 \end{bmatrix} \begin{bmatrix} d_0 \\ d_1 \\ d_2 \\ d_3 \end{bmatrix} \tag{32}$$

Substituting of Eq. (32) into Eq. (16) results in

$$\dot{r} = g(\omega,r) - (1/2)\, C\, d \tag{33}$$

where $d = [d_1\ d_2\ d_3]^T$, C is just the attitude matrix given by Eq. (2). It can be seen that r is independent of d_0, from Eq. (33), and u depends only on r, from Eq. (23). Therefore, u is also independent of d_0. This means the arbitrary selection of the value of d_0 yields the same extremum control, u. Now we can explain the results in Ref. 11. In view of Eq. (31), we have

$$d_0^2+d_1^2+d_2^2+d_3^2 = p_{00}^2+p_{10}^2+p_{20}^2+p_{30}^2 \tag{34}$$

If we set $d_0 = 0$ the norm of the initial costates in Eq. (34) reaches its minimum, the solution of which is considered in Ref. [3]. From Eq. (31) we can also know that $d_0 = 0$ means

$$p(0)^T q(0) = 0$$

which is the orthogonality condition obtained in Ref. 11

4. Initial Values of Costates and the Slewing Time

By means of Euler's eigenaxis rotation theorem, from the known attitudes at the initial and final time, q(0) and $q(t_f)$, we can find a unit vector (eigenaxis), ε, which is fixed in both the body axes and inertial coordinate system, and a rotation angle, θ^*. Then the attitude changes from q(0) to $q(t_f)$ can be realized by rotating the spacecraft about the axis, ε, through the angle, θ^*.

Theoretically, there are many ways through which we can change the attitude from its initial value, q(0), to its final value, $q(t_f)$. For example, this change of attitude can be achieved by successively rotating the spacecraft about the x,y, z axes (i.e. 1-2-3 rotations) through certain displacements in the angles, θ_1, θ_2, θ_3, respectively. To do this way, we need to speed up (and slow down) the spacecraft 3 times, and the total rotation angle is, $\theta_1+\theta_2+\theta_3$. On the other hand, for the Euler rotation, we only need to rotate the spacecraft about ε once through the angle θ^* which is less than the total angle required by any other way. Since the Euler rotation is simple and requires a smaller angle, it may take less time and consume less energy (torques and forces). Therefore, in view of our cost functions, (11) and (13), it is reasonable to think that the optimal slewing is near the Euler rotation. We shall call this rotation the "expected rotation," which is determined only from the initial and final attitude of the spacecraft and will be used in obtaining a set of approximate unknown initial values of the costates and the starting solution of the quasilinearization algorithm.

4.1 Initial Values of Costates

Before starting the quasilinearization algorithm, we need to guess the unknown initial values of the costates, p and r. Considering the analytical solution about a single principal axis maneuver in Ref. 3 we define a rotation angle $\theta(t)$, about an arbitrary axis ε.

$$\theta(t) = \theta(0)+\dot{\theta}(0)t + \frac{1}{2}\ddot{\theta}(0)t^2 + \frac{1}{6}\dddot{\theta}(0)t^3 \tag{35}$$

where $\theta(0)$, $\dot{\theta}(0)$, $\ddot{\theta}(0)$, and $\dddot{\theta}(0)$ are constants to be determined.

For simplicity, here we only consider the solution of θ with the following boundary conditions

$$\theta(0) = 0,\quad \dot{\theta}(0) \neq 0,\ \theta(t_f) = \theta^*\quad \dot{\theta}(t_f) = 0 \tag{36}$$

These conditions correspond to the boundary conditions of the states

$$q(0),\ \omega(0) \neq 0,\ q(t_f),\ \omega(t_f) = 0$$

Substituting Eq. (36) into Eq. (35) yields

$$\ddot{\theta}(0) = (6\theta^*/t_f^2) - (4\dot{\theta}(0)/t_f) \tag{37a}$$

$$\dddot{\theta}(0) = -(12\theta^*/t_f^3) + (6\dot{\theta}(0)/t_f^2) \tag{37b}$$

For the Euler's rotation, the angular velocity and its derivatives are expressed as follows

$$\omega = \varepsilon\dot{\theta}, \quad \dot{\omega} = \varepsilon\ddot{\theta}, \quad \ddot{\omega} = \varepsilon\dddot{\theta} \tag{38}$$

To approximately determine the initial values of p and r, we need to use the dynamical Eqs. (9) and (33). Upon using Eqs. (20) and (21), substituting v (u) into Eq. (9) and solving for r, we get

$$r = I\,\tilde{\omega}\,I\omega - I^2\dot{\omega} \tag{39}$$

and the derivatives

$$\dot{r} = \frac{d}{dt}\,(I\,\tilde{\omega}\,I\,\omega) - I^2\ddot{\omega} \tag{40}$$

At the same time, from Eq. (33), and noting that $C^T = C^{-1}$,

$$d = 2\,C^T\,[g(\omega, r) - \dot{r}\,] \tag{41}$$

At the time t=0, by putting Eqs. (37-38) into Eqs. (39-41), we can get the approximate values of r(0) and d. As for p(0), we can set $p_0(0) = 0$ (since d_0 can be arbitrarily chosen) and solve for d_0 and $p_i(0)$, i=1,2,3, by using Eq. (32).

Now we determine $\dot{\theta}(0)$ from known initial value $\omega(0)$. Generally, $\omega(0)$ is not equal to $\varepsilon\dot{\theta}(0)$ since ε is independent of $\omega(0)$. Let e be the difference between them

$$e = \varepsilon\dot{\theta}(0) - \omega(0)$$

To find a minimum value of e^Te, we differentiate e^Te with respect to $\dot{\theta}(0)$ and note that $\varepsilon^T\varepsilon = 1$, we get

$$\dot{\theta}(0) = \varepsilon^T\omega(0) \tag{42}$$

By using the initial values p(0) and r(0) obtained above, and integrating the differential equations (7), (9), (15-16), with Bu in Eq. (9) replaced by v in Eqs. (20) and (21), we can get a set of values, q(t), ω(t), p(t), and r(t), $0 \le t \le t_f$, which will be used as the starting values of the quasilinearization method.

4.2 Initial Value of t_f

The starting value $t_f^{(0)}$ needs to be made as close to the minimum time, t_f^*, as possible. This can be done by using the techniques similar to those described above. Suppose the slewing motion is an Euler rotation about a vector, ε, through an angle, θ(t). Then, by putting the first two equations of Eq. (38) and Eq. (20) into Eq. (8), we get

$$I\,\varepsilon\,\ddot{\theta} = \dot{\theta}^2\,\tilde{\varepsilon}\,I\,\varepsilon + v \tag{43}$$

For simplicity, we only consider the case $v_{jmin} = -v_{jmax}$. Then, let $c_j = v_{jmax}$ and $v_j = c_j\tau_j$; the above vector equation can be expressed as the following 3 similar equations for θ(t):

$$a_i\,\ddot{\theta} = b_i\,\dot{\theta}^2 + c_i\,\tau_i \qquad i = 1,2,3 \tag{44}$$

where a_i, b_i, and c_i are constants, τ_i is the normalized control about the i^{th} body axis and

$$|\tau_i| \le 1 \qquad i = 1,2,3 \tag{45}$$

Each equation of Eq. (44) with the boundary condition Eq. (36) can be treated as a minimum time control problem with the constraint (45). It is easy to see that the control for this problem is of a bang-bang type and the the problem can be solved analytically to get the minimum time t^*_{fi} (i=1, 2,3) as functions of θ^* and $\dot{\theta}(0)$. The results are shown in Appendix II.

Since the only minimum time, t_f^*, that every equation of Eq. (44) can accept at the same time is the longest one, we use the largest one as our initial guess for t_f.

We choose a quasilinearization algorithm to solve the two point boundary value problem because this method needs only to solve linear differential equations and it converges quadratically.

In the quasilinearization algorithm, the linearized state and costate equations are solved using the method of particular solutions.[12] The computational values of u, which satisfy Eq. (23), are determined by a technique similar to that used in Ref. 9. The minimum slewing time is obtained by the following procedure. For an assumed given slewing time, t_f, as a result of the iterations, the routine arrives at the (converged) values for the initial costates. Then, a check is made as to whether one of the control inputs is of a bang-bang type. If yes, this slewing time is designated the minimum time. If not, the assumed t_f should be shortened and the iteration cycle restarted in order to determine new values for the initial costates and new time histories for the control effort.

5. Numerical Results

Finally, we apply these methods described in the previous sections to the SCOLE slewing motion. Fig. 1a shows the SCOLE configuration. It is composed of a Space Shuttle and a large reflecting antenna. The antenna is attached to the Shuttle by a flexible beam. Since we only consider the motion of the rigid SCOLE in this paper, the flexibility of the beam is ignored. The X, Y, Z axes are the spacecraft axes corresponding to roll, pitch and yaw axes, respectively. The controls considered in this paper include three moments about the X, Y, Z axes of the system and two forces applied at the center of the reflector in the X, Y directions only. The inertia parameters of the SCOLE and the saturation levels of the controls are:

I_{11} = 1,132,508, I_{22} = 7,007,447, I_{33} = 7,113,962 slug - ft^2

I_{12} = -7,555, I_{23} = 115,202, I_{31} = 52,293

Torques: $|u_i|_{max}$ = 10,000 ft-lb, i = i,2,3.

Reflector actuators: $|f_j|_{max}$ = 800 lb., j= 1.2,

We have done some numerical simulations for the following cases: (a) A diagonal inertia matrix I is used. The control is assumed to be provided only by torquers on the Shuttle. No control forces on the reflector are assumed. The expected rotation is a rotation about one of the three principal axes, through 20 deg., from rest to rest. The result is exactly the same as that of the theoretical analysis discussed earlier in this paper, i.e., the control torque about the slewing axis is of a bang-bang type while the others remain zero.

(b) Extend the inertia matrix in case (a) to a non-diagonal form. The expected rotation is a rotation about one of the three spacecraft axes and the rotation angle is 20 deg.

Figs. 2-3 give the control torques and attitude angles (1-2-3 Euler angles) for the expected rotations "X-axis slewing" and "Z-axis slewing," respectively. Fig. 2a shows that u_x is nearly of a bang-bang type, while u_y, u_z are not. The non-zero contributions of the u_y and u_z are due to the offset of the inertia distribution of the SCOLE configuration (non-diagonal matrix I). Similar situations are shown in Fig. 3a, where u_z is nearly of a bang-bang type and the others are not.

The starting value of $t_f^{(0)}$ for these slewings (X- and Z- axes) are $t_f^{(0)}$= 12.5749 sec. and $t_f^{(0)}$= 31.5166 sec., respectively, by using the method in section 4.2. The minimum time, t_f^*, we actually obtained are t_f^* = 12.57 sec. and t_f^* = 31.33 sec., respectively. These results indicate that the estimated values for t_f^* are very accurate.

In Fig. 2b, θ_x changes from zero to 20 deg., but θ_y and θ_z change very little during the slewing and finally approach zero. The non-zero changes in θ_y and θ_z are also due to the offset of the structural distribution of the SCOLE.

In Fig. 3b, unlike the case in Fig. 2b, the θ_x changes greatly. This change is due to the differences in the moments of inertia about the X-axis and Y-axis.

Fig. 4 shows the control torques for the "X-axis slewing" with a slewing time t_f= 15.37 sec., which is 2.8 sec. more than the minimum time t_f^* = 12.57 sec. (Fig. 2). The controls are almost linear functions of time (rest-to-rest slewing). u_x is less than the saturation level, and u_y, u_z are nearly zero. From Fig. 4 and Fig. 2a, we see that much more control effort (approximate 50%) is needed if we increase the slewing time a little. Another feature of using a longer slewing time in the computation is that it needs less number (4 times) of iterations for convergence than by using minimum slewing time t_f^* (12 times). These properties suggest that, in practical applications of this problem, it is not necessary to seek the minimum time, t_f^*, and the associated extremum controls. It is enough to know approximate values of the t_f^* and the controls. The results of Fig. 5 for the "Z-axis slewing" are similar to those of Fig. 4.

(c) Following the case (b), we now add two control force actuators on the reflector, f_x and f_y.

The associated alignment matrix, B, in Eq. (8) is

$$B = \begin{bmatrix} 1 & 0 & 0 & 0 & 130 \\ 0 & 1 & 0 & -130 & 0 \\ 0 & 0 & 1 & 32.5 & 18.75 \end{bmatrix}$$

Figs. 6 show the control torques, forces and attitude angles for the "X-axis slewing" motion. The slewing time t_f^* is greatly shortened, t_f^* = 3.988 sec. (about one third of the slewing time without the forces, f_x and f_y).

Figs. 7 and 8 show the controls and attitude angle changes for the "Z-axis slewing." For the sake of comparison, we use 2 different t_f in the computation, t_f= 27.5 sec., and t_f^*= 20.0 sec. (minimum time; recall that t_f^* =31.33 sec. without f_x and f_y). By comparing Figs. 7 with Figs. 8 we can see that the control torques approach the bang-bang type when the slewing time is shortened, and the maximum amplitude of the control forces increases gradually. From Fig. 7c and Fig. 8c, we can also see the obvious increases in θ_x and θ_y. This is due to the increases in u_x, u_y, f_x, and f_y.

(d) Now we consider a general case. Suppose the SCOLE is in an Earth orbit and we need the line of sight to be directed toward the center of the Earth. The orbital coordinate system (x,y,z) is shown in Fig. 1b. Suppose, before the slewing, the Y axis of the spacecraft coincides with the orbital y axis, and the angular difference between X and x (or Z and z) axes is α= 7.897224212 deg. Thus, the initial attitude quaternion of the spacecraft is $q(0)= [\cos(\alpha/2)\ 0\ \sin(\alpha/2)\ 0]^T$. According to Ref. 1, the unit vector along the line of sight in the rigid SCOLE coordinate system is $\hat{R}_{LOS}$

$$= [0.1112447155\ -0.2410302170\ 0.9641208678]^T$$

The direction cosines of the orbital z axis in the body system at the initial time are $\hat{z}/_B = [\sin\alpha\ 0\ \cos\alpha]^T$. The angle between $\hat{R}_{LOS}$ and $\hat{z}/_B$ at the initial time is $\theta_{LOS}(0) = \hat{R}_{LOS} \cdot \hat{z}/_B$= 20 deg. The eigen axis of the expected rotation in the body system is determined by

$$\epsilon = (\hat{R}_{LOS} \times \hat{z}/_B)/|\hat{R}_{LOS} \times \hat{z}/_B|$$

Thus, the quaternion for this rotation is

$$q_0 = \cos(20^\circ/2),\ q_i = \epsilon_i \sin(20^\circ/2),\ i = 1,2,3$$

From (5) we can get the final attitude quaternion, $q(t_f)$. Fig. 9 shows the control torques, reflector forces, and attitude angles for this slewing motion. The θ_{LOS} in Fig. 9c is the angle between the line of sight and the line of the target direction (from the spacecraft to the center of the Earth).

6. Concluding Remarks

(1) There is a good agreement between the guessed value of t_f and the value of t_f to which the algorithm converges in the case (b).

(2) The guessed initial values of the costates here: p(0), r(0) are adequate for the algorithm to converge. If the slewing time, t_f, is sufficiently larger than the minimum time,

t_f^*, then, the converged values of p(0) and r(0) are very close to the guessed values and less number (4 times) of iterations is needed (Fig. 4). The same situation was observed in Ref. 8

(3) The control profiles obtained in this paper give us a good reference for future use. For example, an extension to the minimum time slewing motion of the SCOLE model containing both rigid and flexible components is planned.

References

1. Taylor, L.W. and Balakrishnan, A.V., "A Mathematical Problem and a Spacecraft Control Laboratory Experiment (SCOLE) used to Evaluate Control Laws for Flexible Spacecraft ... NASA/IEEE Design Challenge," Jan., 1984.
2. Lin, J.G., "Rapid Torque-Limited Line-of-sight Pointing of SCOLE (Spacecraft Control Laboratory Experiment) Configuration," AIAA/AAS Astrodynamics Conference, Williamsburg, Va., August, 1986, AIAA Paper 86-1991.
3. Junkins, J.L. and Turner, J.D., "Optimal Continuous Torque Attitude Maneuvers," Journal of Guidance and Control, Vol. 3, No. 3, May-June, 1980, pp. 210-217.
4. Skaar, S.B. and Kraige, L.G., "Large-Angle Spacecraft Attitude Maneuvers Using an Optimal Reaction Wheel Power Criterion," The Journal of the Astronautical Sciences, Vol. 32, No. 1, Jan. - March 1984, pp. 47-61.
5. Chen, J. and Kane, T.R., "Slewing Maneuvers of Gyrostat Spacecraft." The Journal of the Astronautical Sciences, Vol. 28, No. 3, July-Sept. 1980, pp. 267-281.
6. Turner, J.D. and Junkins, J.L., "Optimal Large-Angle Single-Axis Rotational Maneuvers of Flexible Spacecraft, Journal of Guidance and Control, Vol. 3, No. 6, Nov.- Dec. 1980, pp. 578-585.
7. Chun, H.M. and Turner, J.D., "Frequency-Shaped Large-Angle Maneuvers," AIAA 25th Aerospace Sciences Meeting, Jan. 12-15, 1987, Reno, Nevada, AIAA Paper 87-0174.
8. Bainum, P.M. and Feiyue Li, "Optimal Torque Control SCOLE Slewing Maneuvers," 3rd Annual SCOLE Workshop, Nov. 17, 1986, NASA Langley Research Center, Hampton, Virginia.
9. Yeo, B.P., Waldron, K.J. and Goh, B.S., Optimal Initial Choice of Multipliers in the Quasilinearization Method for Optimal Control Problems with Bounded Controls," Int. J. Control, 1974, Vol. 20, No. 1, pp. 17-33.
10. Morton, H.S. Jr., Junkins, J.L. and Balnton, J.N., "Analytical Solutions for Euler Parameters," Celestial Mechanics, Vol. 10, No. 3, 1974, pp. 287-301.
11. Vadali, S.R., Kraige, L.G. and Junkins, J.L., "New Results on the Optimal Spacecraft Attitude Maneuver Problem," J. Guidance and Control, Vol. 7, No. 3, May-June, 1984, pp. 378-380.
12. Miele, A., and Iyer, R.R., "General Technique for Solving Nonlinear Two-Point Boundary-Value Problems Via the Method of Particular Solutions," Journal of Optimization Theory and Applications, Vol. 5, No. 5, 1970, pp. 382-399.

Appendix I The Term $g(\omega, r)$ in Eq. (16)

The term $I^{-1}\tilde{\omega}I\omega$ in dynamical equation (9) can be replaced by

$$I^{-1}\tilde{\omega}I\omega = [a_{ij}:b_{ij}][\omega_1^2\ \omega_2^2\ \omega_3^2\ \ \omega_2\omega_3\ \ \omega_3\omega_1\ \ \omega_1\omega_2]^T = [\ A:B]\ \bar{\bar{\omega}}$$

where the a_{ij} and b_{ij} (the elements of 3x3 matrices A and B) are constants associated with the inertia parameters of the spacecraft. Then the term $r^T I^{-1}\tilde{\omega}I\omega$ of the Hamiltonian, H, in Eq. (14) has the form

$$h = r^T I^{-1}\tilde{\omega}I\omega = [R_1\ R_2\ R_3\ R_4\ R_5\ R_6]^T\ \bar{\bar{\omega}}$$

where R_i are

$$[R_1R_2R_3]^T = A^T r,\quad [R_4R_5R_6]^T = B^T r$$

The term $g(\omega, r)$ in Eq. (16) is obtained by

$$g(\omega,r) = -(\partial h/\partial\omega) = -\begin{bmatrix} 2R_1 & R_6 & R_5 \\ R_6 & 2R_2 & R_4 \\ R_5 & R_4 & 2R_3 \end{bmatrix}\begin{bmatrix}\omega_1\\ \omega_2\\ \omega_3\end{bmatrix}$$

Appendix II Solution of Eq. (44)

Eq. (44) can be rewritten as

$$a_i\ddot{\theta} = b_i\dot{\theta}^2 + c_i\tau_i \qquad (44)$$

For simplicity, we only consider the solutions for the following boundary conditions

$$\theta(0) = 0,\ \dot{\theta}(0) = 0;\ \theta(t_f) = \theta^*,\ \dot{\theta}(t_f) = 0 \qquad (II\text{-}1)$$

Suppose $a_i \neq 0$, $b_i \neq 0$ and let $b=b_i/a_i$, $c=c_i/a_i$ (suppose $c>0$), we can rewrite Eq. (44) as

$$\ddot{\theta} = b\dot{\theta}^2 + c\tau \qquad (II\text{-}2)$$

Since the control for this problem is of a bang-bang type with only one switching point, then, by integrating Eq. (II-2) and using (II-1), we get

$$\dot{\theta} = \sqrt{c(e^{2b\theta}-1)/b},\ \text{for } \tau=1; \qquad (II\text{-}3)$$

$$\dot{\theta} = \sqrt{c(1-e^{2b(\theta-\theta^*)})/b},\ \text{for } \tau=-1 \qquad (II\text{-}4)$$

By equating Eqs. (II-3) and (II-4), we get $\theta=\theta_s$ and $\dot{\theta}=\dot{\theta}_s$ at the switching point, t=ts,

$$\theta_s = (1/2b)\log[2/(1+e^{-2b\theta^*})]\quad \dot{\theta}_s = \sqrt{c(e^{2b\theta_s}-1)/b}$$

Finally, by integrating (II-3,4) and using (II-1), we get

$$t_s = \begin{cases} \cosh^{-1}(e^{-b\theta_s}) / \sqrt{-bc}, & b<0; \\ [(\pi/2)-\sin^{-1}(e^{-b\theta_s})]/\sqrt{bc}, & b>0 \end{cases}$$

and

$$t_f = \begin{cases} t_s + [(\pi/2) - \sin^{-1}(e^{b(\theta \mp \theta_s)})/\sqrt{-bc}, & b<0 \ ; \\ t_s + \cosh^{-1}(e^{b(\theta \mp \theta_s)})/\sqrt{bc}, & b>0 \end{cases}$$

For the case $\dot{\theta}(0) \neq 0$, more complicated solutions can be obtained, but are not given here.

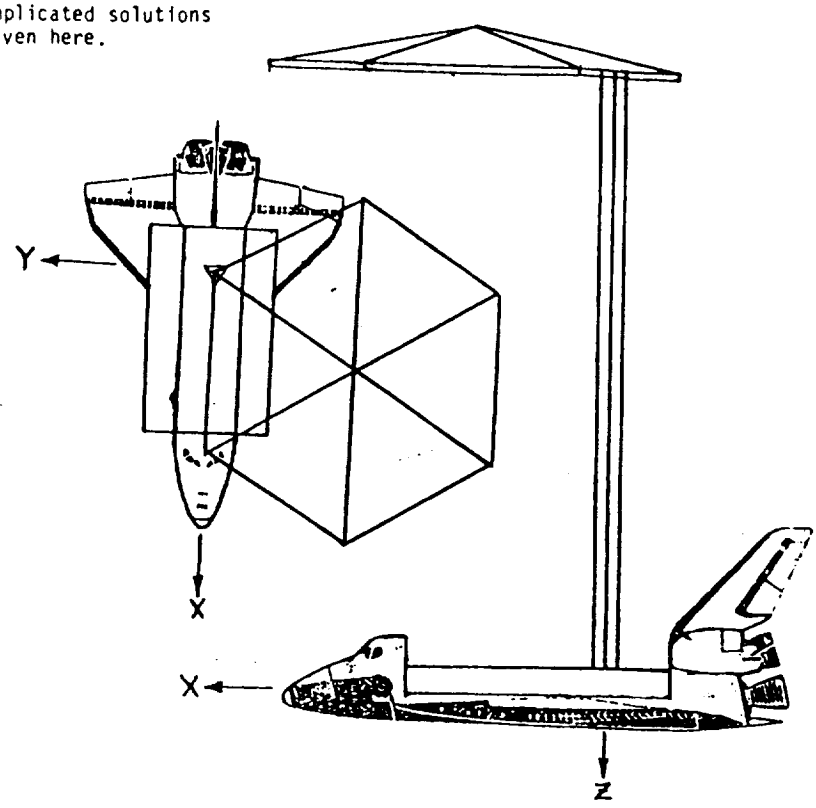

Fig. 1a Spacecraft Control Laboratory Experiment Configuration (SCOLE)

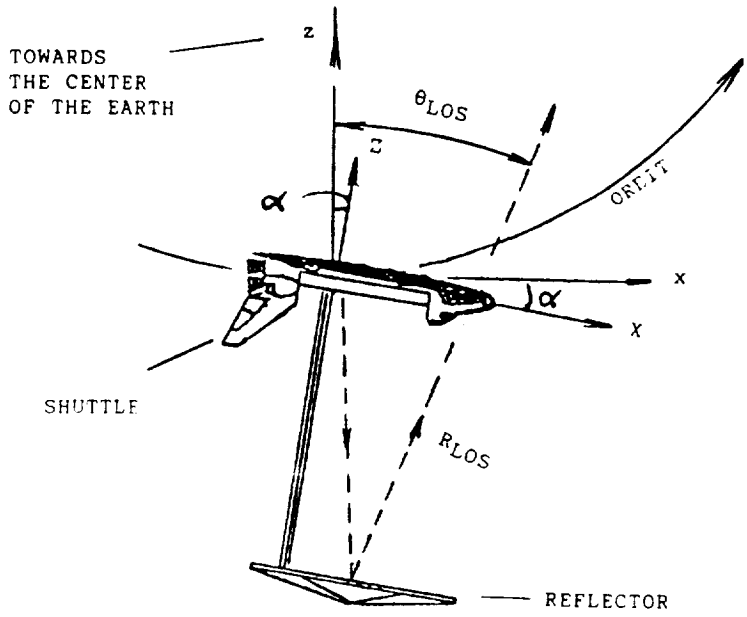

Fig. 1b. Attitude of the SCOLE Showing Antenna Line of Sight

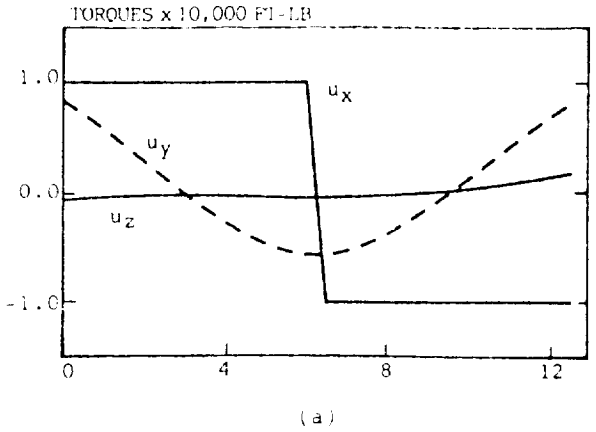

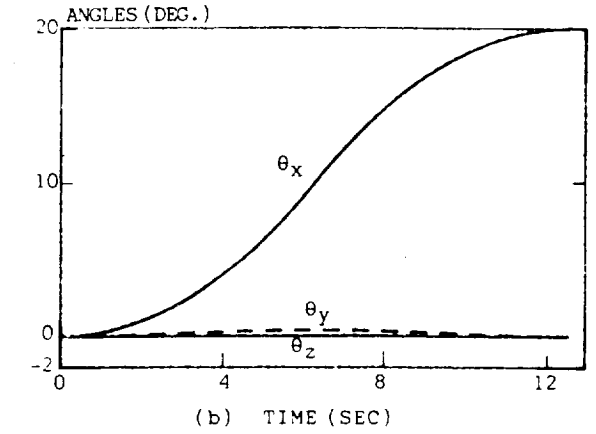

Fig. 2. X-Axis Slewing, t_f = 12.57 Sec.

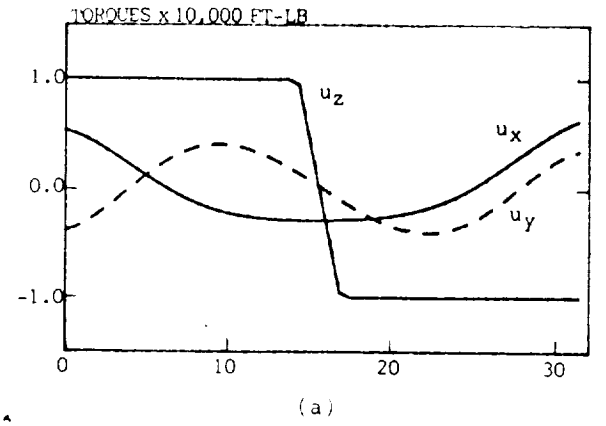

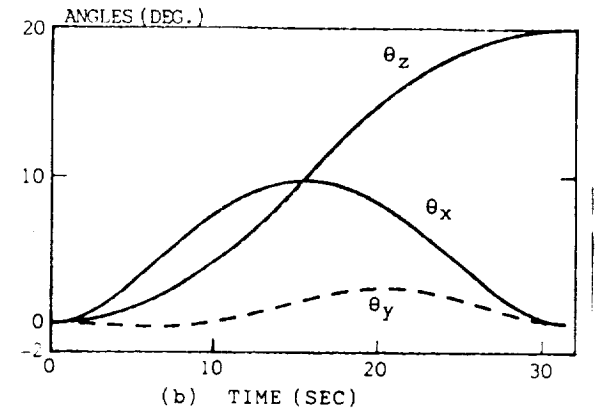

Fig. 3. Z-Axis Slewing, t_f = 31.33 Sec.

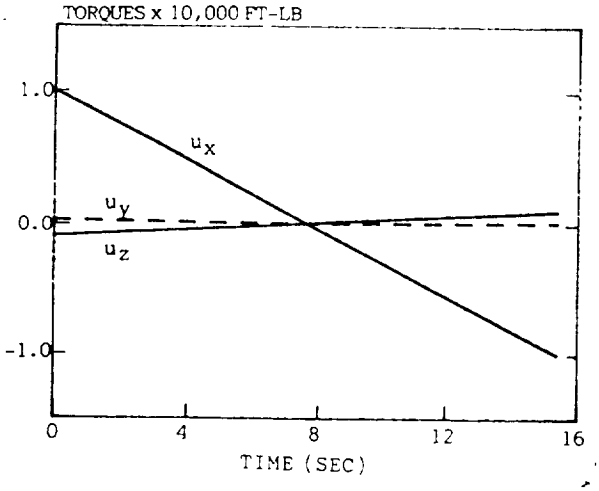

Fig. 4. X-Axis Slewing, t_f = 15.37 Sec.

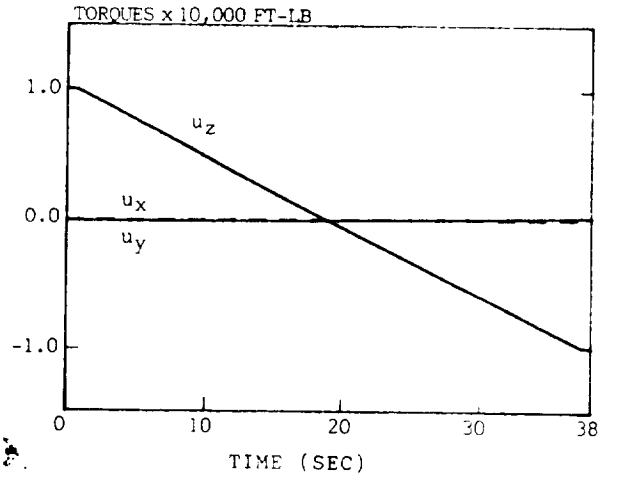

Fig. 5. Z-Axis Slewing, t_f = 38 Sec.

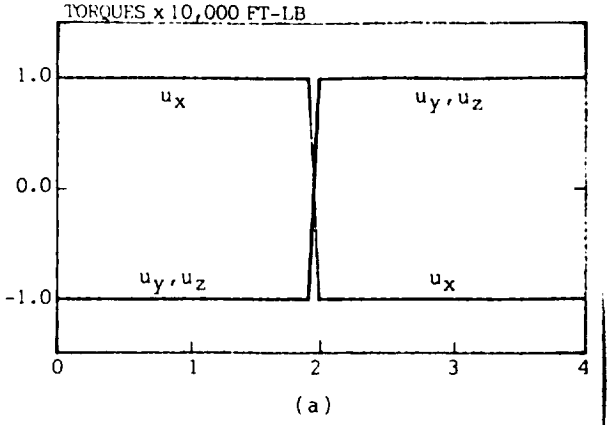

(a)

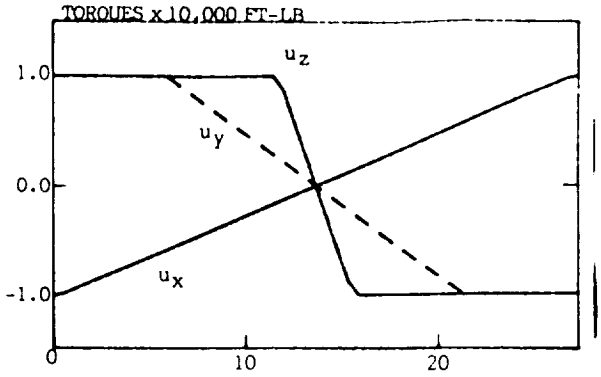

(a)

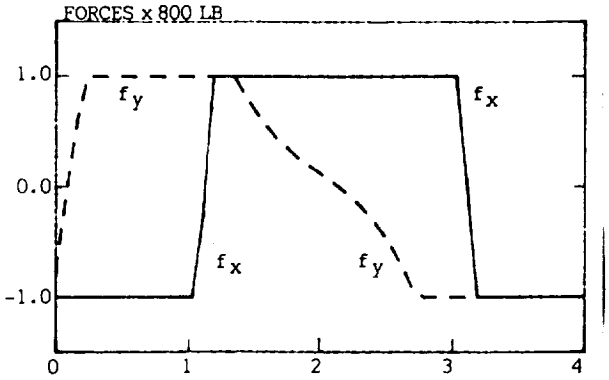

(b)

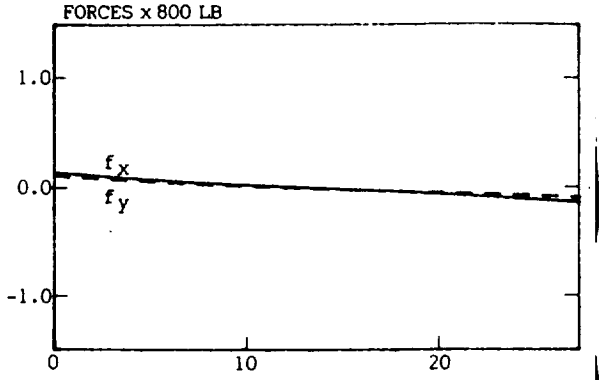

(b)

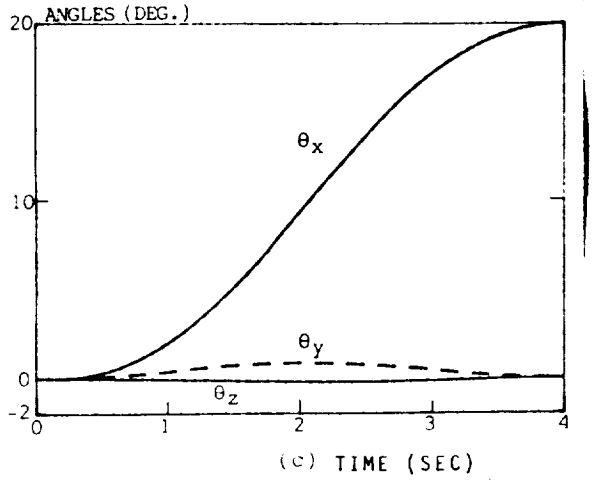

(c) TIME (SEC)

Fig. 6. X-Axis Slewing, t_f = 3.988 Sec.

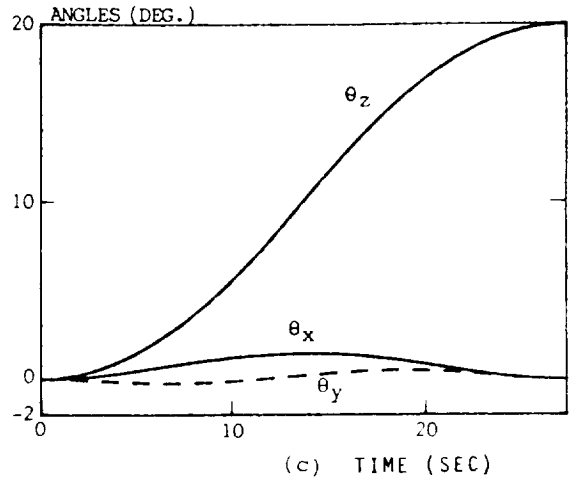

(c) TIME (SEC)

Fig. 7. Z-Axis Slewing, t_f = 27.5 Sec.

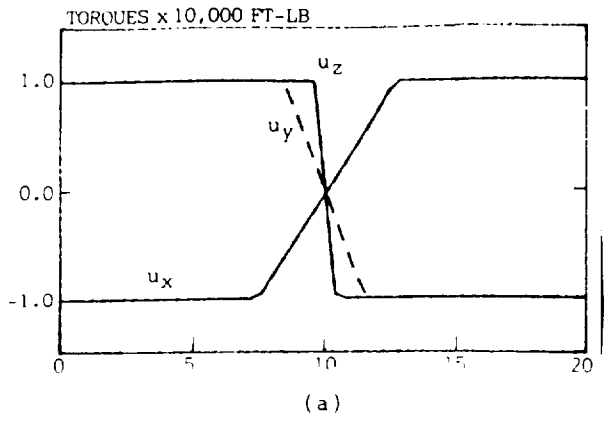

(a)

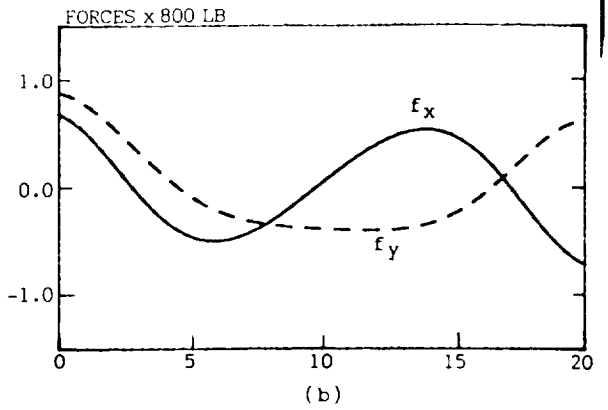

(b)

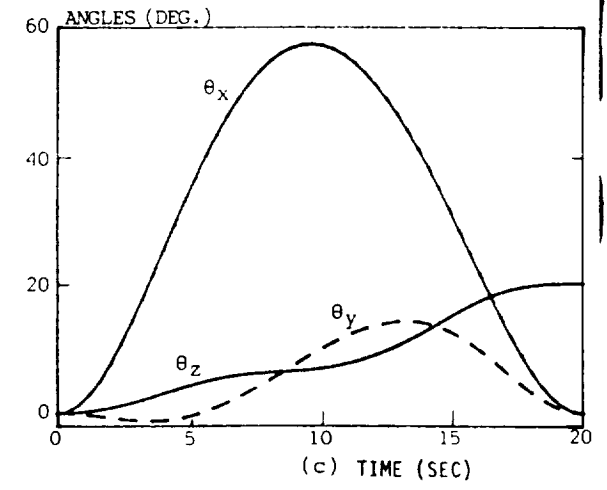

(c) TIME (SEC)

Fig. 8. Z-Axis Slewing, t_f = 20 Sec.

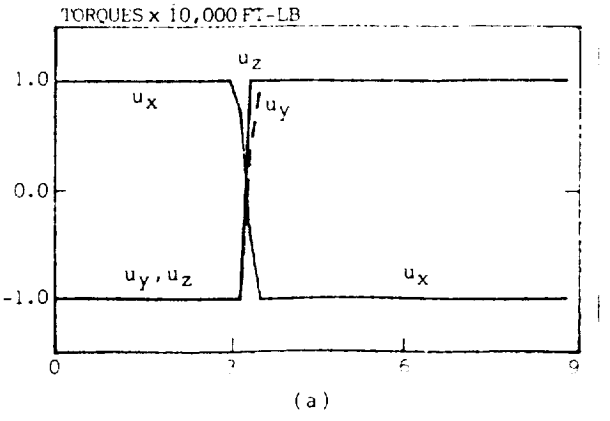

(a)

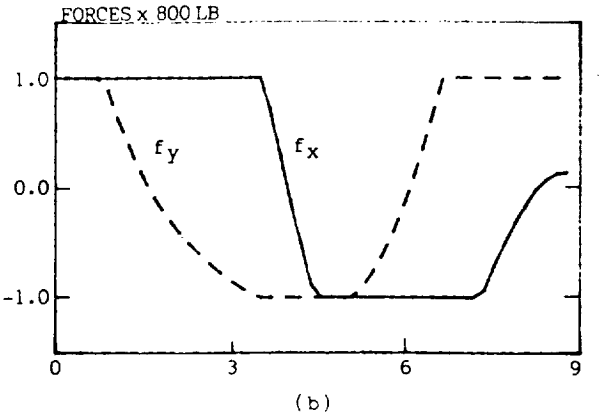

(b)

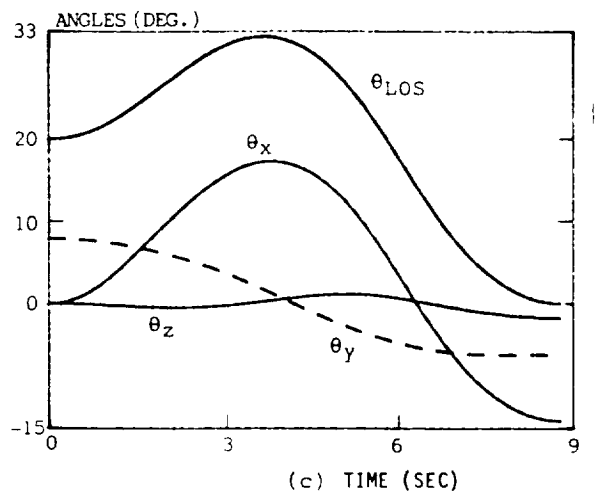

(c) TIME (SEC)

Fig. 9. SCOLE - Example Slewing, t_f = 8.77 Sec.

HOWARD UNIVERSITY

N89-13467

PRINCIPAL INVESTIGATOR: Dr. Peter M. Bainum
CO-INVESTIGATOR: Dr. A.S.S.R. Reddy
STUDENTS: Cheick Modibo Diarra and Feiyue Li
TECHNICAL MONITOR: Mr. John Young (LaRC)

The Dynamics and Control of the In-Orbit SCOLE Configuration - NASA-NSG 1414

ABSTRACT

The study of the dynamics of the Spacecraft Control Laboratory Experiment (SCOLE)[1] is extended to emphasize the synthesis of control laws for both the linearized system as well as the large amplitude slewing maneuvers required to rapidly reorient the antenna line of sight. For control of the system through small amplitude displacements from the nominal equilibrium position LQR techniques are used to develop the control laws. Pontryagin's maximum principle is applied to minimize the time required for the slewing of a general rigid spacecraft system. The minimum slewing time is calculated based on a quasi-linearization algorithm for the resulting two point boundary value problem.[2] The effect of delay in the control input on the stability of a continuously acting controller (designed without considering the delay) is studied analytically for a second order plant. System instability can result even for delays which are only a small fraction of the natural period of motion.[3]

REFERENCES

1. Taylor, L.W. and Balakrishnan, A.V., "A Mathematical Problem and a Spacecraft Control Laboratory Experiment (SCOLE) used to Evaluate Control Laws for Flexible Spacecraft ... NASA/IEEE Design Challenge," Jan. 1984.

2. Li, Feiyue and Bainum, P.M., "Minimum Time Attitude Slewing Maneuvers of a Rigid Spacecraft," accepted for presentation, AIAA 26th Aerospace Sciences Meeting, Reno, Nevada, Jan. 11-14, 1988.

3. Reddy, A.S.S.R. and Bainum, P.M., "Stability Analysis of Large Space Structure Control Systems with Delayed Input," 6th VPI & SU/AIAA Symposium on Dynamics and Control of Large Structures, Blacksburg, Va., June 29 - July 1, 1987.

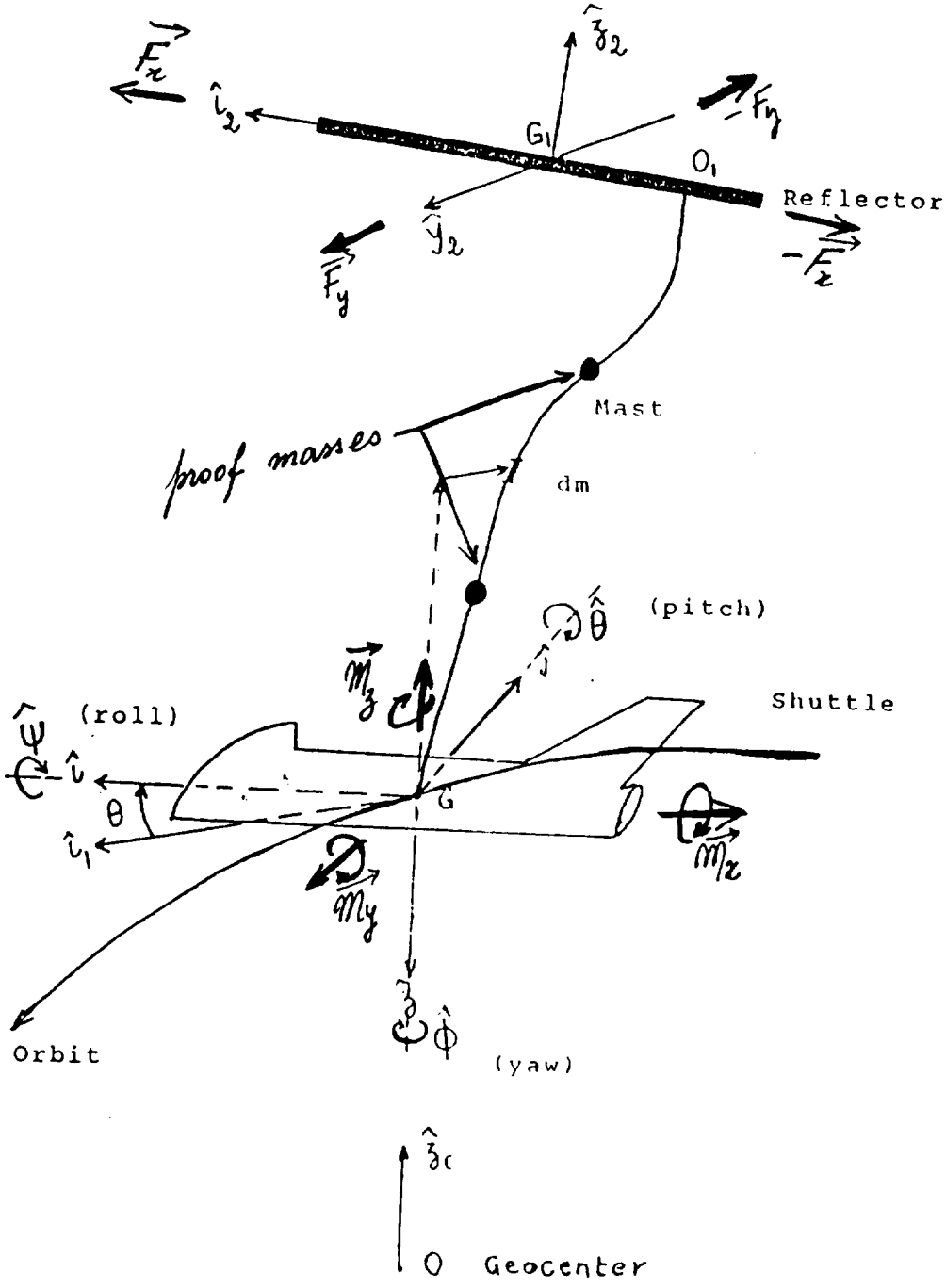

FIGURE III-1: THE 3-D GEOMETRY OF THE SCOLE CONFIGURATION IN ITS DEFORMED STATE

. Equations of Motion

· Derived using a Newton-Euler approach

. Assumptions

- Reflector and Shuttle rigid
- Mast has constant cross-section
- It is assumed to undergo small elastic deformations only
- Its modal shapes in orbit are assumed to be the same as those of an identical non-rotating beam.

Stability Analysis (Rigidized SCOLE)

A stability analysis of the rigidzed SCOLE was conducted for the following configurations:

a) Rigid - no offset. Pitch motion decouples from roll and yaw in the linear ranges. System not stable

b) Rigid - with offset parallel to roll axis. Pitch motion still decouples from roll and yaw in the linear range. System unstable.

c) Rigid - With both offsets (parallel to roll and pitch axes). The motions in all 3 degrees of freedom are coupled. System found to be unstable.

.Control Laws

Assumption: All the states of the system are available. It was suggested by J.G. Lin that an intuitively appealing practical approach to achieve the LOS pointing objective is a two-stage procedure. (a) Slew as if rigid then, (b) damp-out flexible dynamics.

.The linear regulator theory used here to control
-the linear model of the rigidized SCOLE,
-The linear model of the actual SCOLE configuration including the first four flexible modes of the mast.

Next

Preliminary slew maneuvers of rigidized SCOLE.

SCOLE: TRANSIENT RESPONSES

6.0 DEG. INITIAL PERTURBATION IN ROLL FROM EQUILIBRIUM

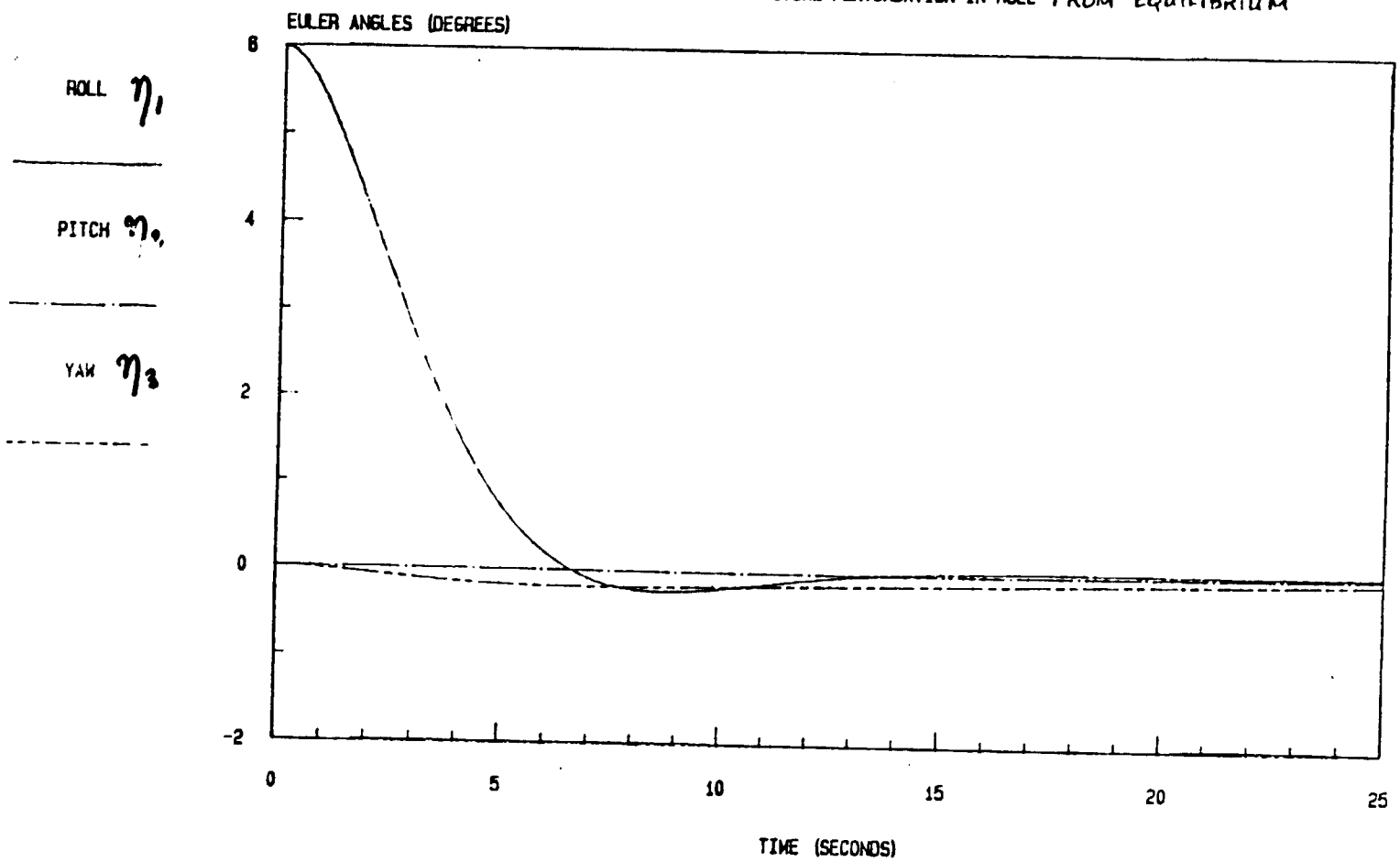

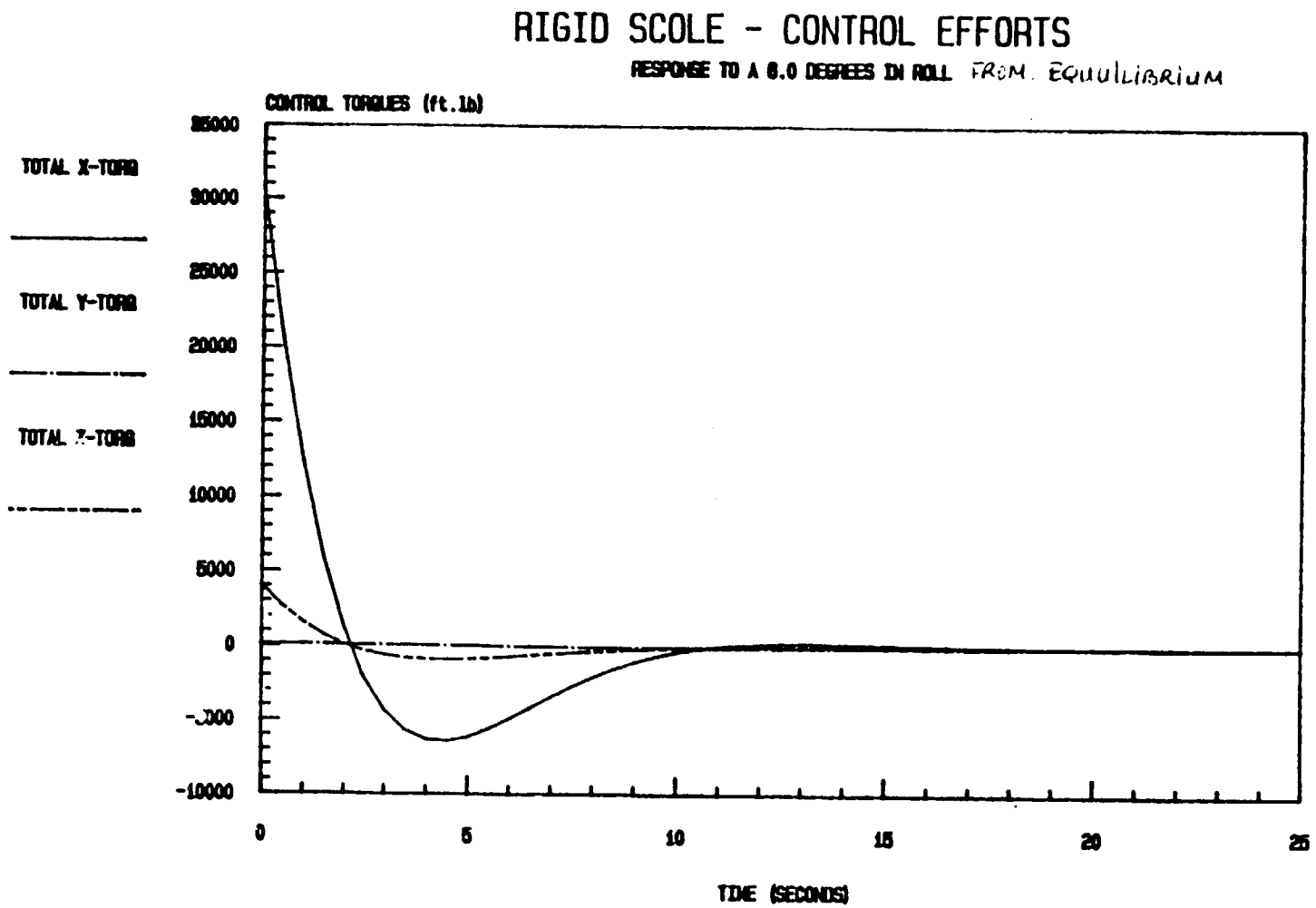
RIGID SCOLE - CONTROL EFFORTS
RESPONSE TO A 8.0 DEGREES IN ROLL FROM EQUILIBRIUM
CONTROL TORQUES (ft.lb)
TOTAL X-TORQ
TOTAL Y-TORQ
TOTAL Z-TORQ
35000
30000
25000
20000
15000
10000
5000
0
-5000
-10000
0
5
10
15
20
25
TIME (SECONDS)

RIGID SCOLE - CONTROL EFFORTS

RESPONSE TO A 8.0 DEGREES IN ROLL FROM EQUILIBRIUM

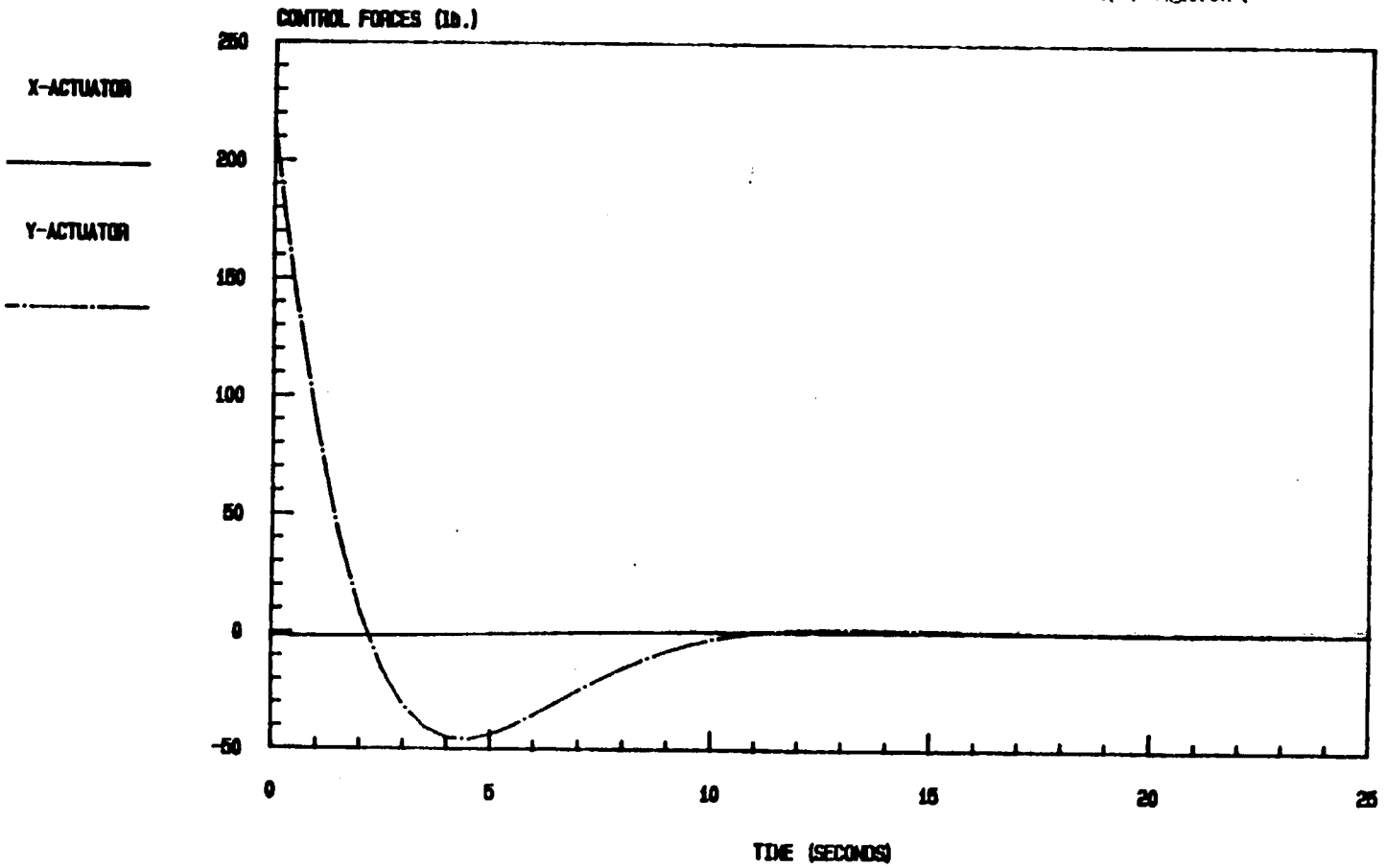

RIGID SCOLE - CONTROL EFFORTS

RESPONSE TO A 8.0 DEGREES IN ROLL FROM EQUILIBRIUM

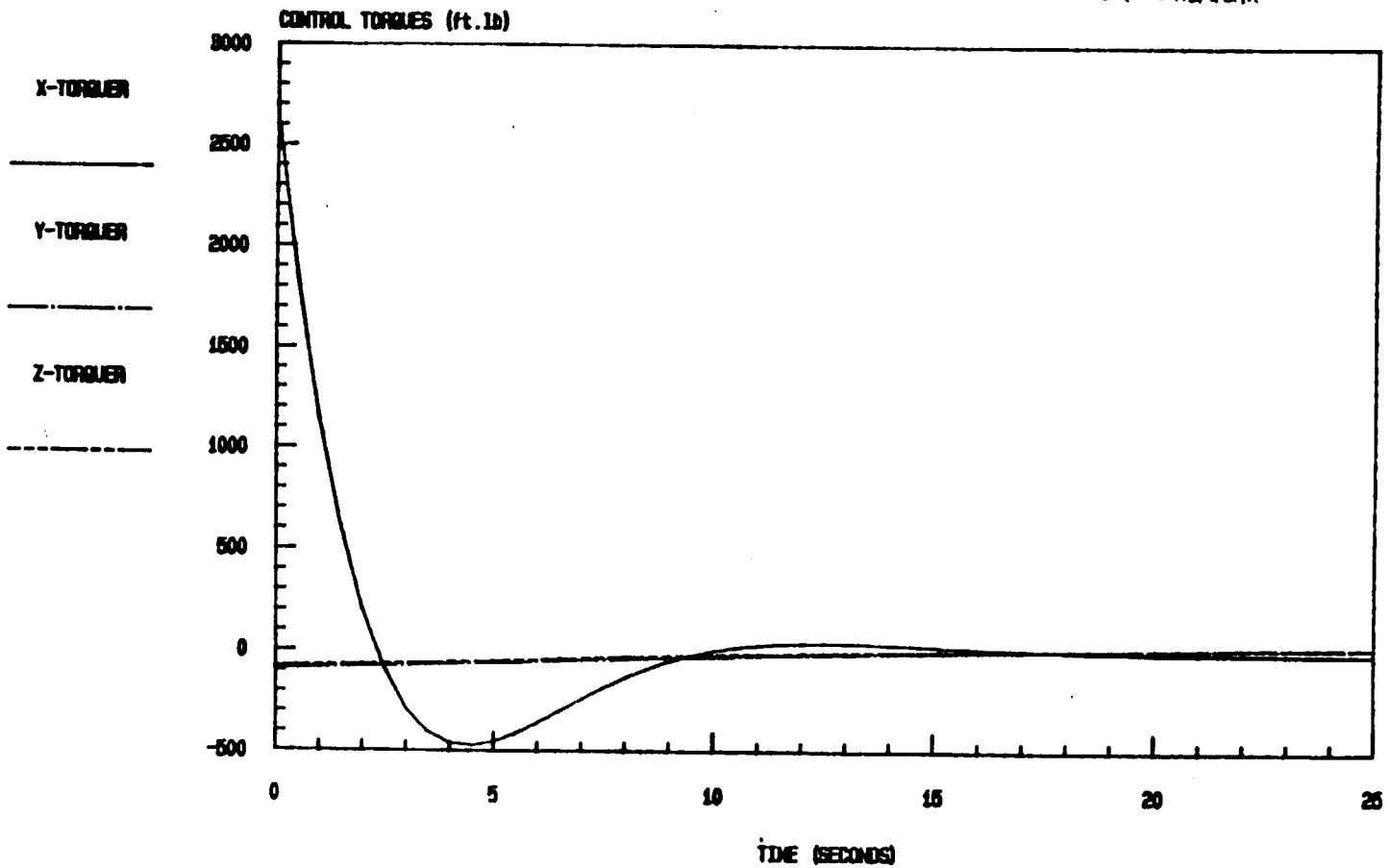

LINEAR MODEL OF SCOLE WITH FLEXIBILITY

TRANS. RESP. TO AN INITIAL 8deg. IN ROLL FROM EQUIL.

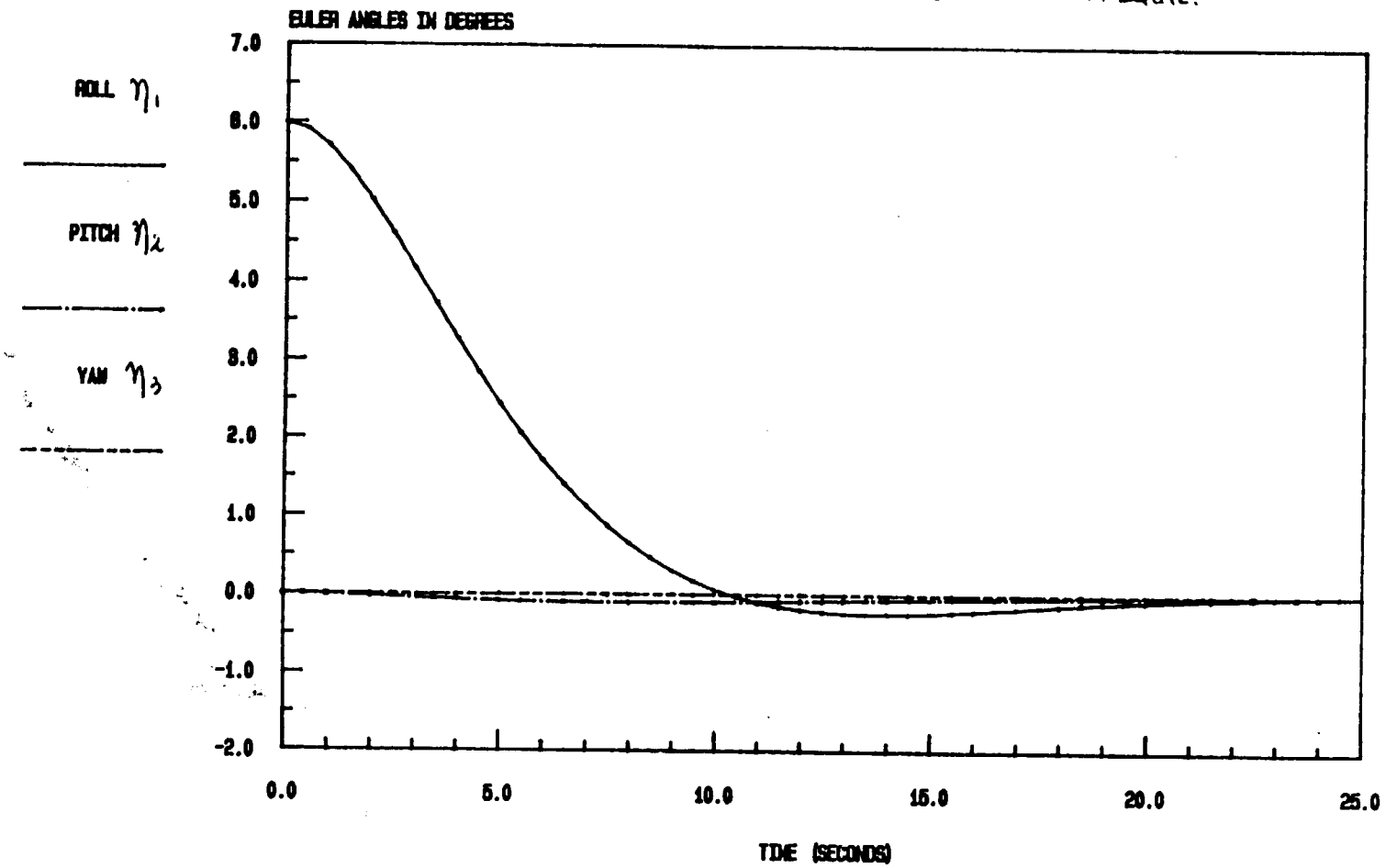

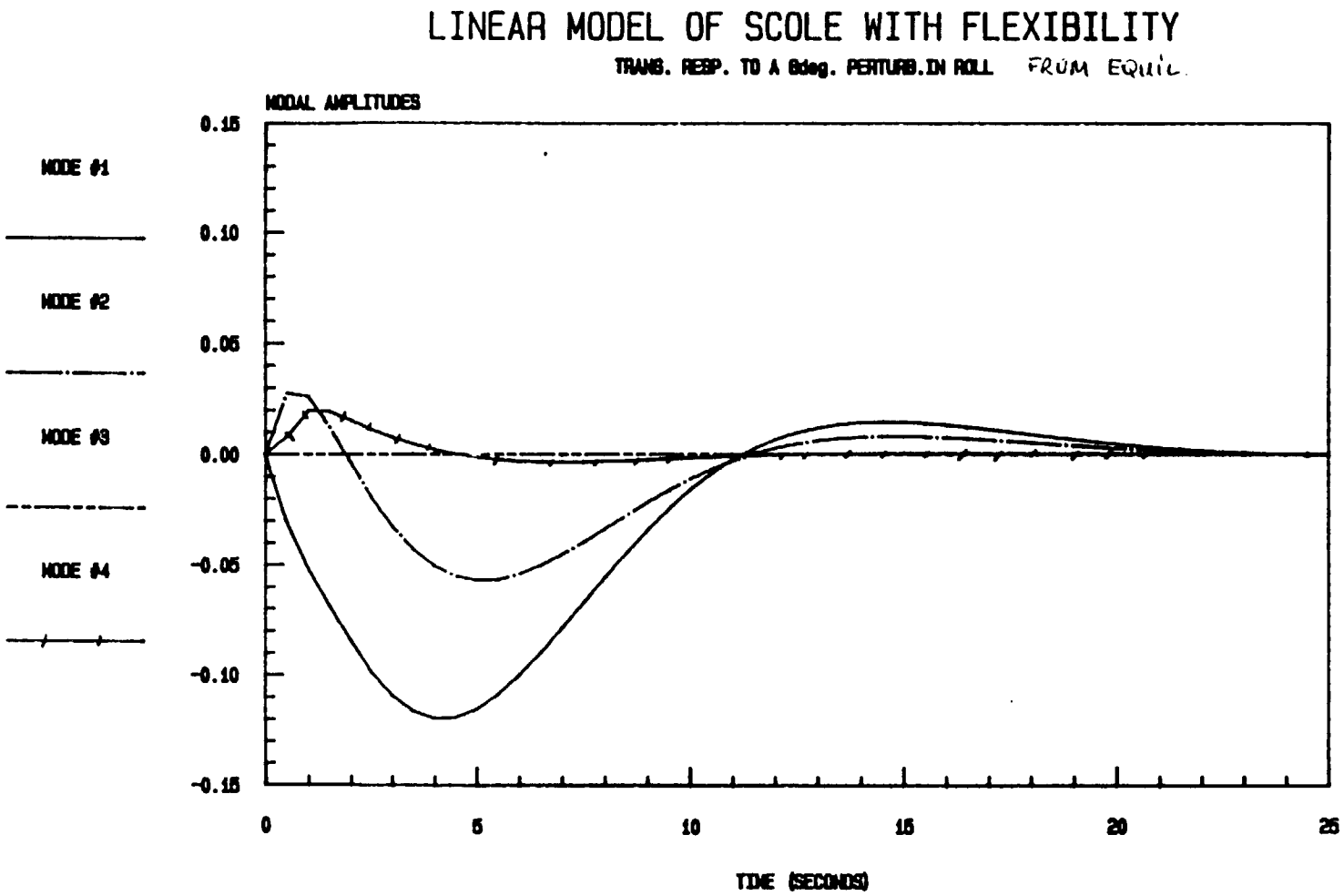
LINEAR MODEL OF SCOLE WITH FLEXIBILITY
TRANS. RESP. TO A 8deg. PERTURB.IN ROLL FROM EQUIL.
MODAL AMPLITUDES
MODE #1
MODE #2
MODE #3
MODE #4
0.15
0.10
0.05
0.00
-0.05
-0.10
-0.15
0
5
10
15
20
25
TIME (SECONDS)

SCOLE: TRANSIENT RESPONSES

6.0 DEG. INITIAL PERTURBATION IN PITCH FROM EQUILIBRIUM

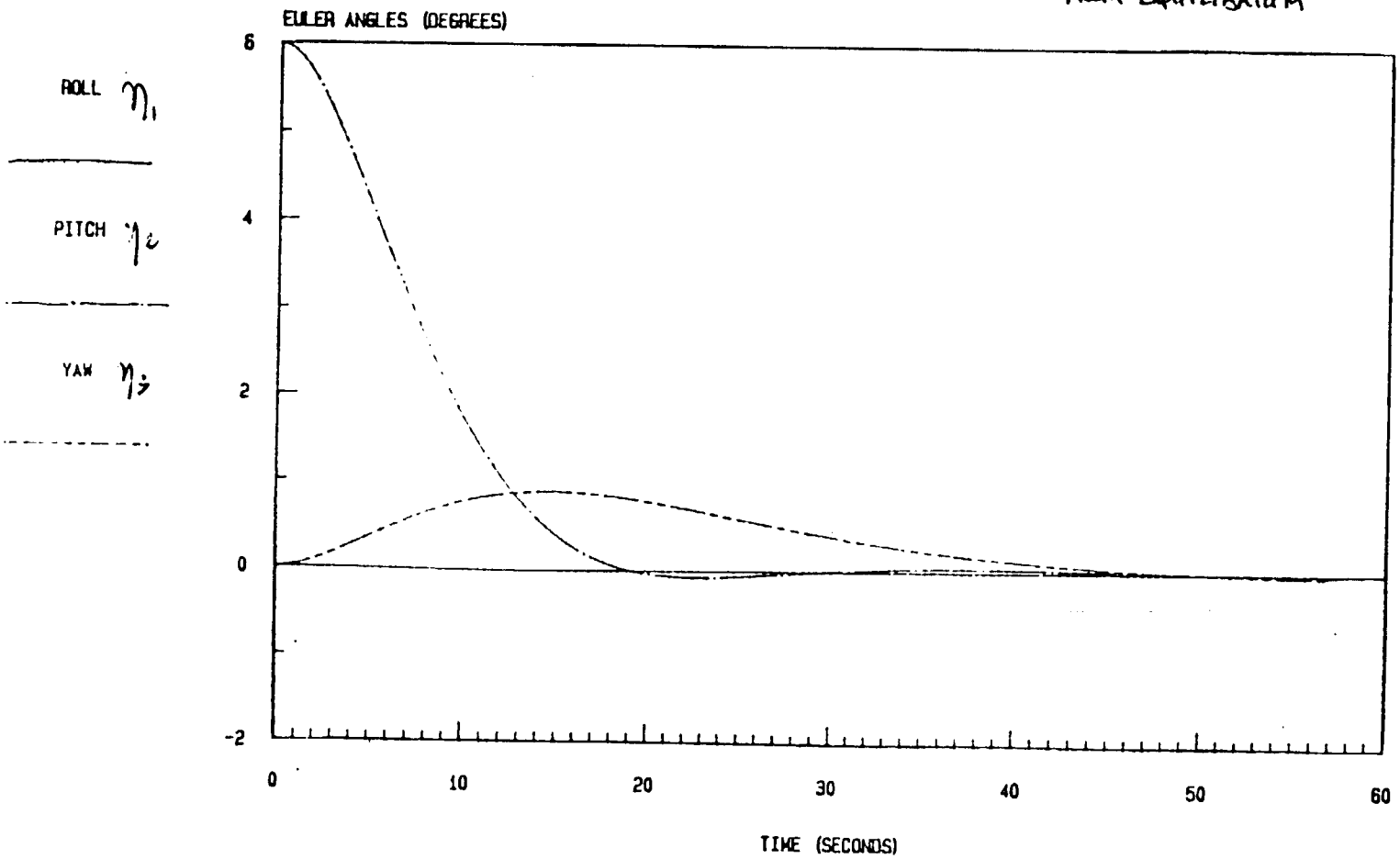

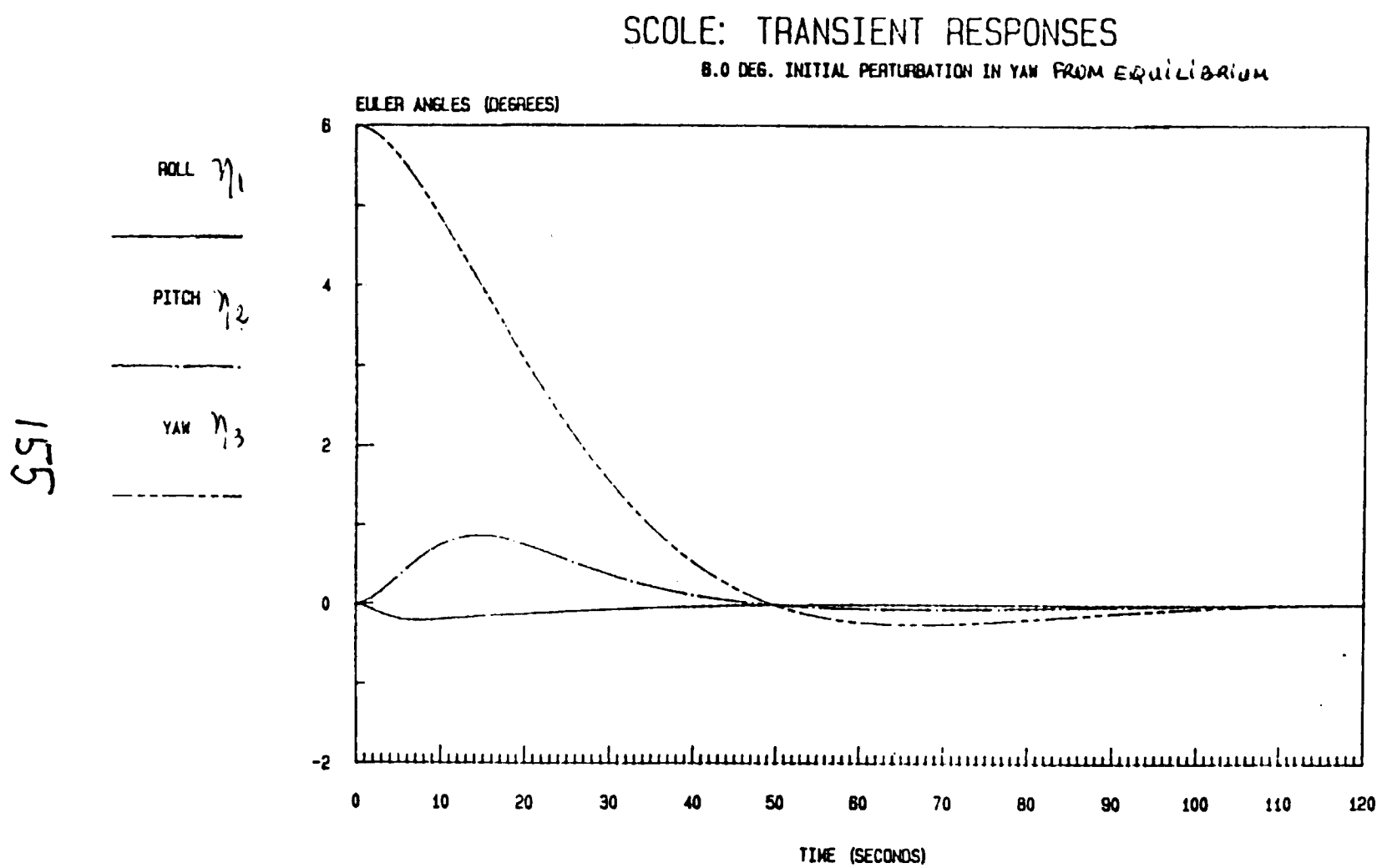
SCOLE: TRANSIENT RESPONSES
8.0 DEG. INITIAL PERTURBATION IN YAW FROM EQUILIBRIUM
EULER ANGLES (DEGREES)
ROLL η_1
PITCH η_2
YAW η_3
6
4
2
0
-2
0
10
20
30
40
50
60
70
80
90
100
110
120
TIME (SECONDS)

LINEAR MODEL OF SCOLE WITH FLEXIBILITY

TRANS. RESP. TO A 8deg. PERTURB. IN PITCH FROM EQUILIBRIUM

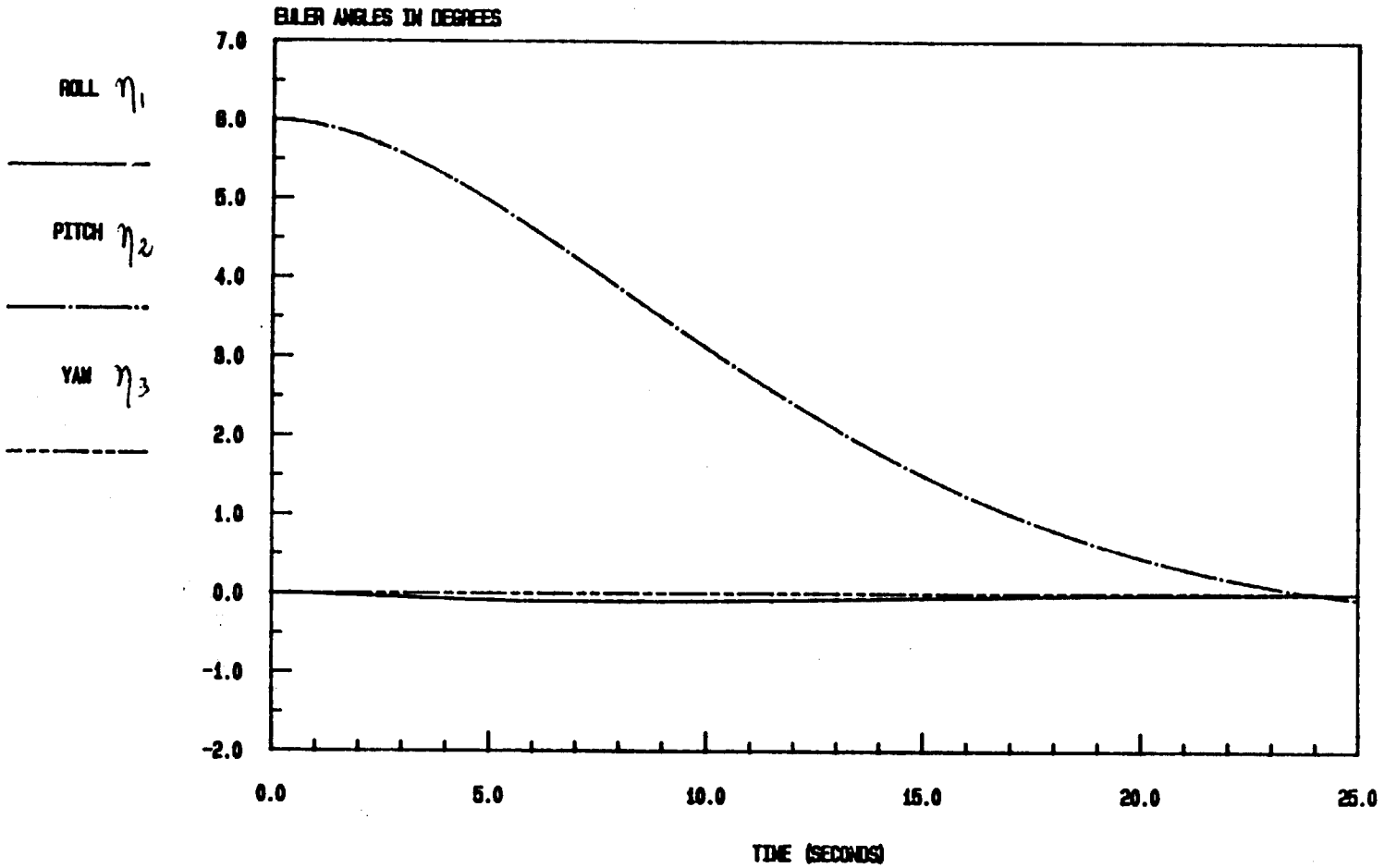

LINEAR MODEL OF SCOLE WITH FLEXIBILITY

TRANS. RESP. TO A 8deg. PERTURB.IN PITCH FROM EQUILIBRIUM

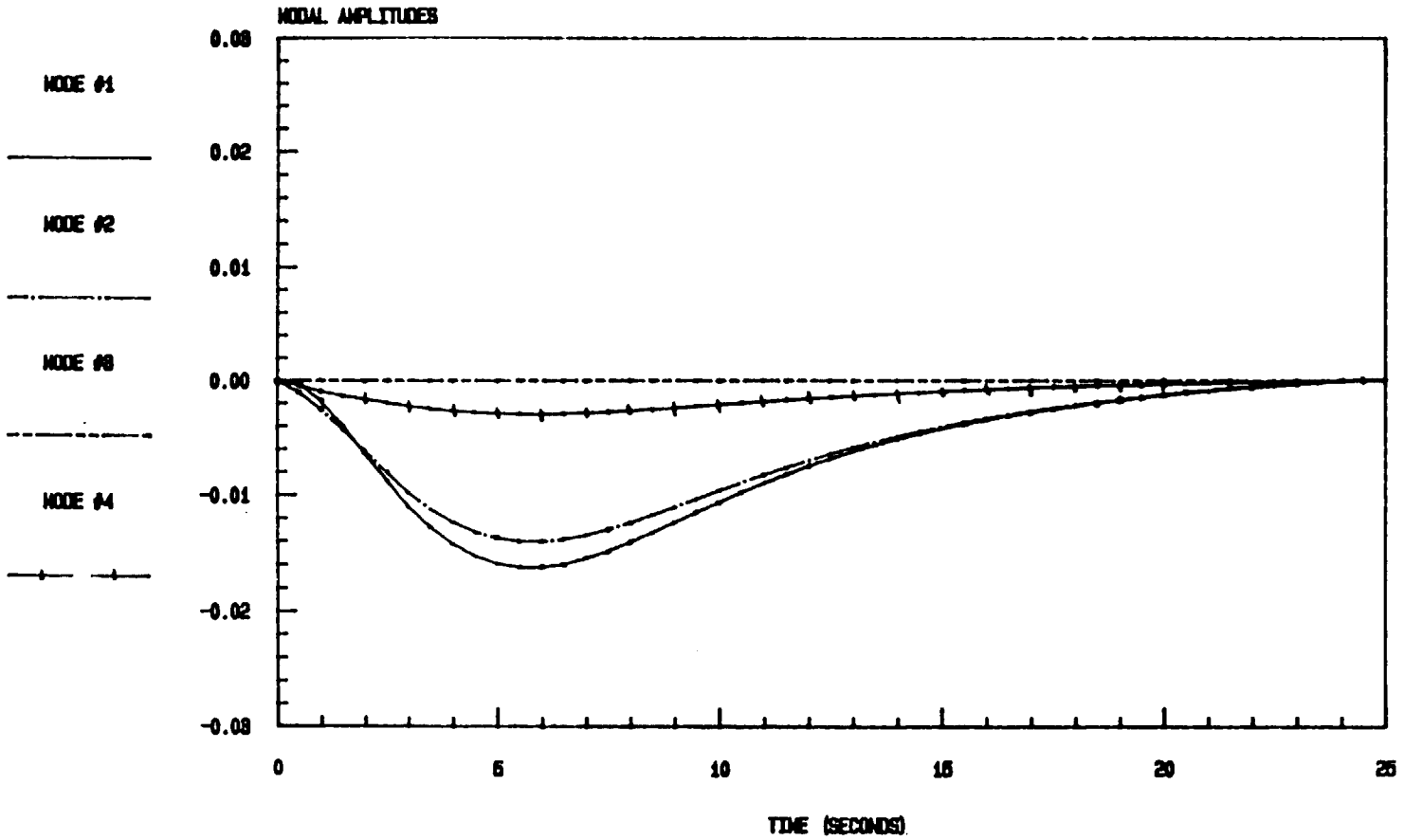

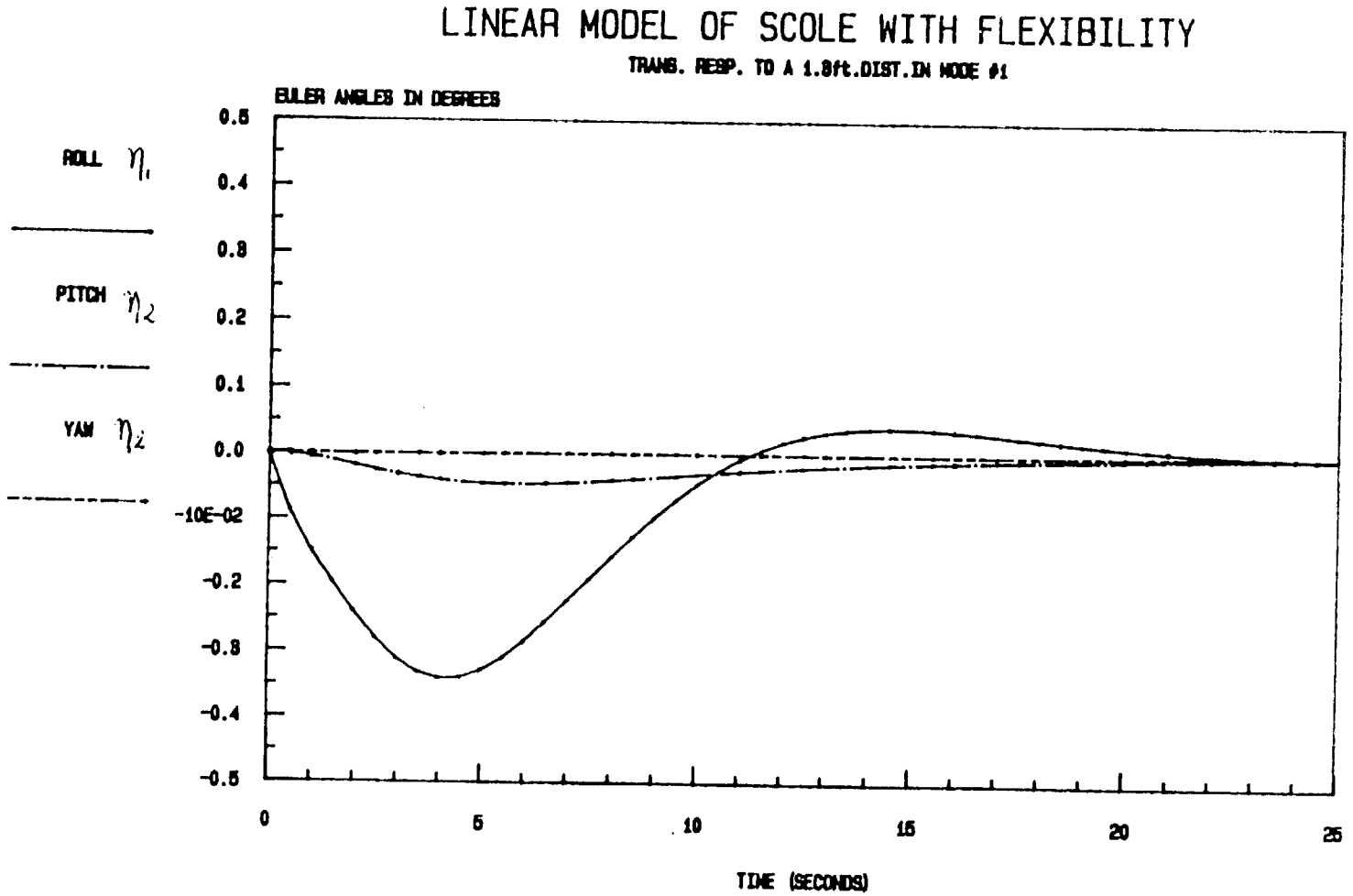
LINEAR MODEL OF SCOLE WITH FLEXIBILITY
TRANS. RESP. TO A 1.0ft.DIST.IN MODE #1
EULER ANGLES IN DEGREES
ROLL η_1
PITCH η_2
YAW η_3
0.5
0.4
0.3
0.2
0.1
0.0
-10E-02
-0.2
-0.3
-0.4
-0.5
0
5
10
15
20
25
TIME (SECONDS)

LINEAR MODEL OF SCOLE WITH FLEXIBILITY

TRANS. RESP. TO A 1.0ft.DIST.IN MODE #1

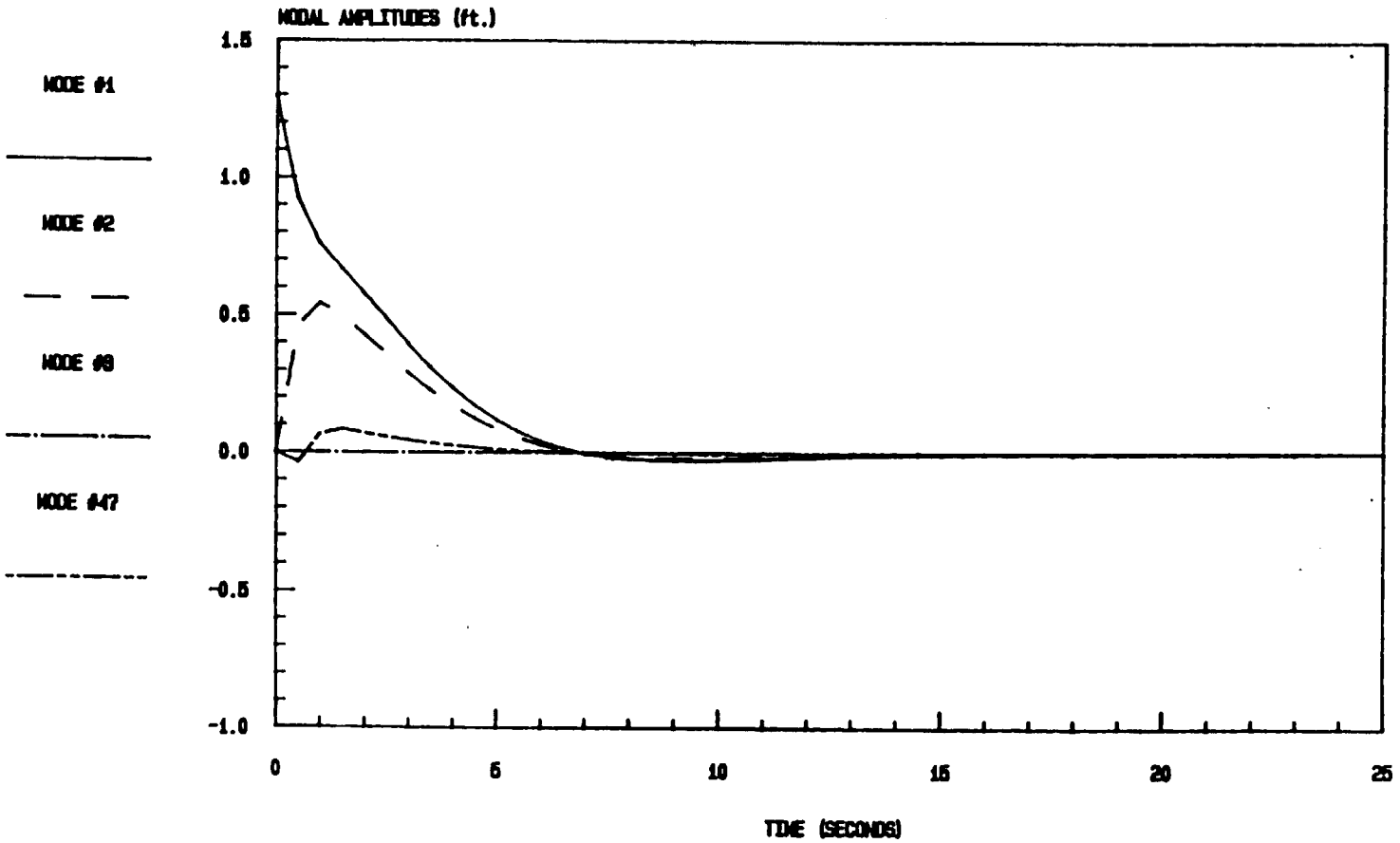

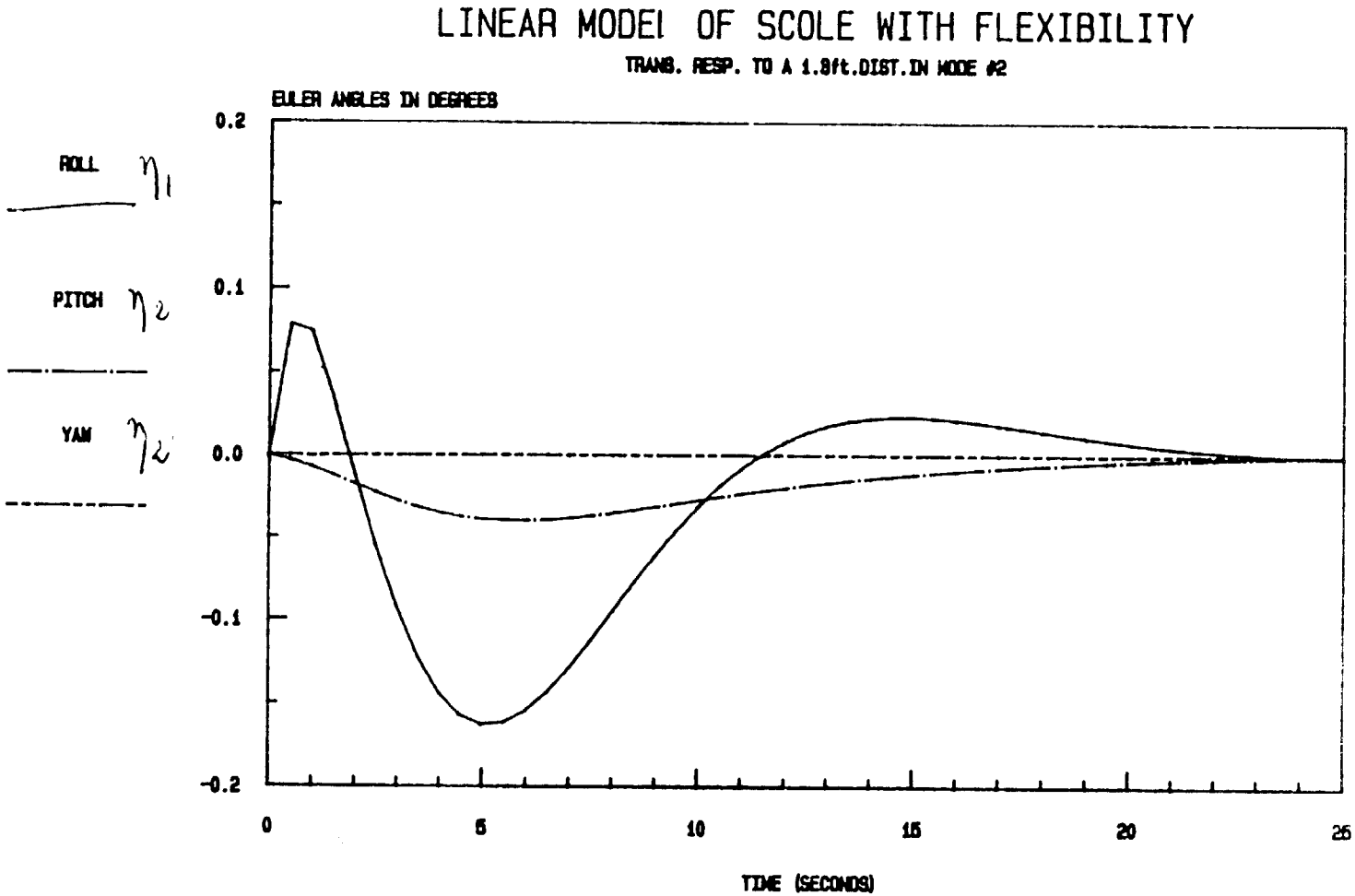
LINEAR MODEl OF SCOLE WITH FLEXIBILITY
TRANS. RESP. TO A 1.8ft.DIST.IN MODE #2
EULER ANGLES IN DEGREES
ROLL η_1
PITCH η_2
YAW η_2'
0.2
0.1
0.0
-0.1
-0.2
0
5
10
15
20
25
TIME (SECONDS)

LINEAR MODEL OF SCOLE WITH FLEXIBILITY

TRANS. RESP. TO A 1.8ft.DIST.IN MODE #2

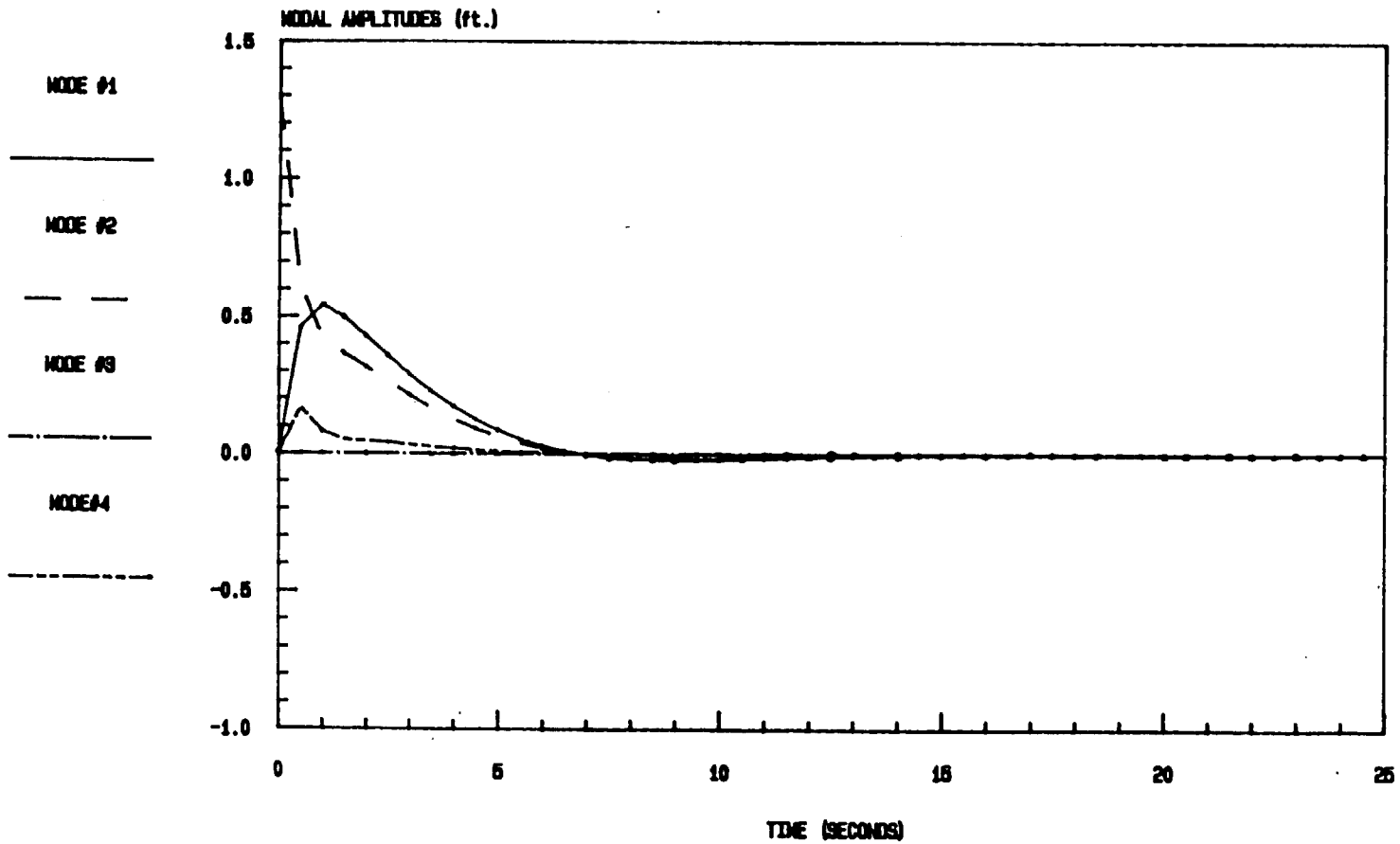

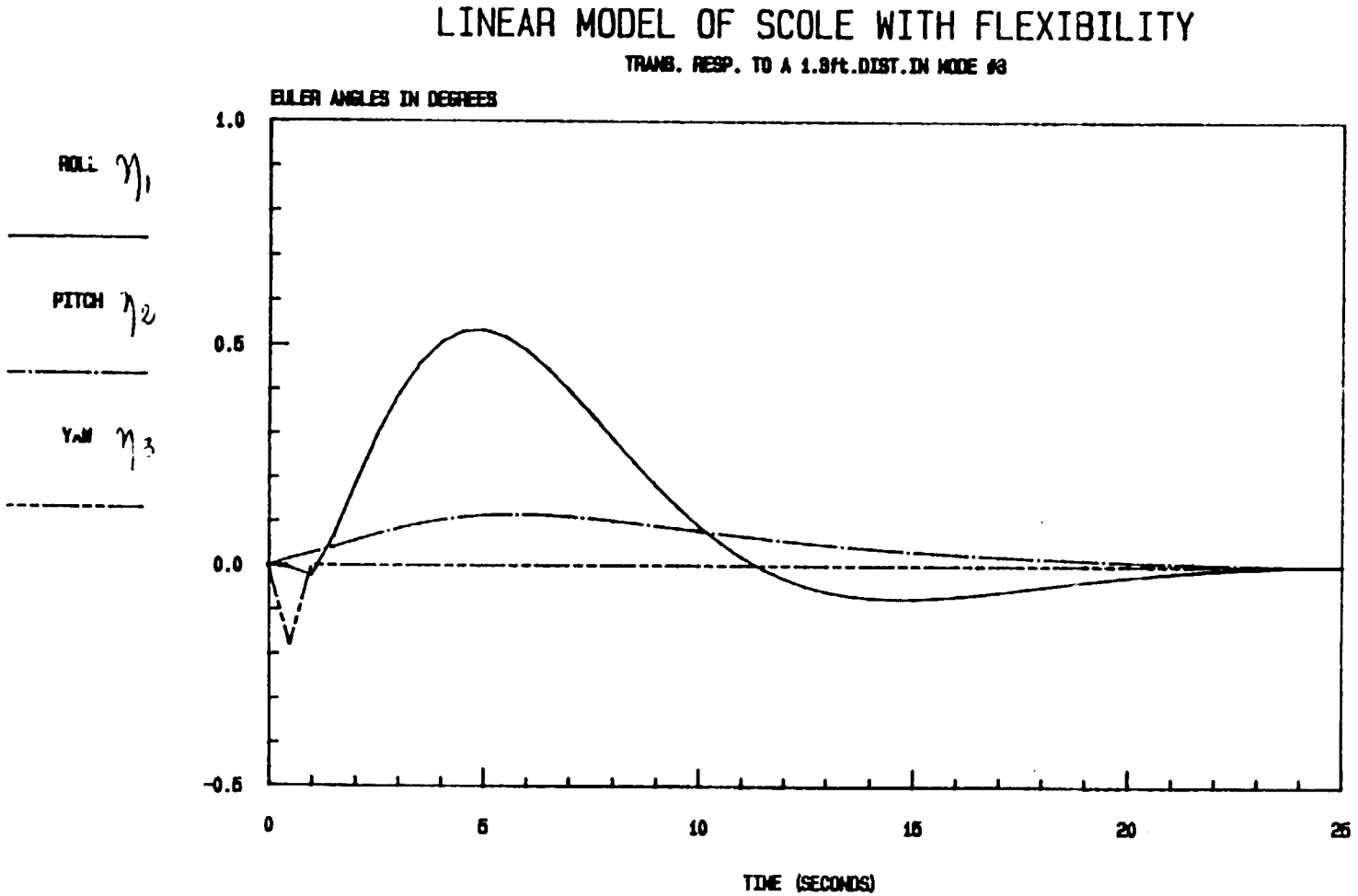
LINEAR MODEL OF SCOLE WITH FLEXIBILITY
TRANS. RESP. TO A 1.0ft.DIST.IN MODE #3
EULER ANGLES IN DEGREES
ROLL η_1
PITCH η_2
YAW η_3
1.0
0.5
0.0
-0.5
0
5
10
15
20
25
TIME (SECONDS)

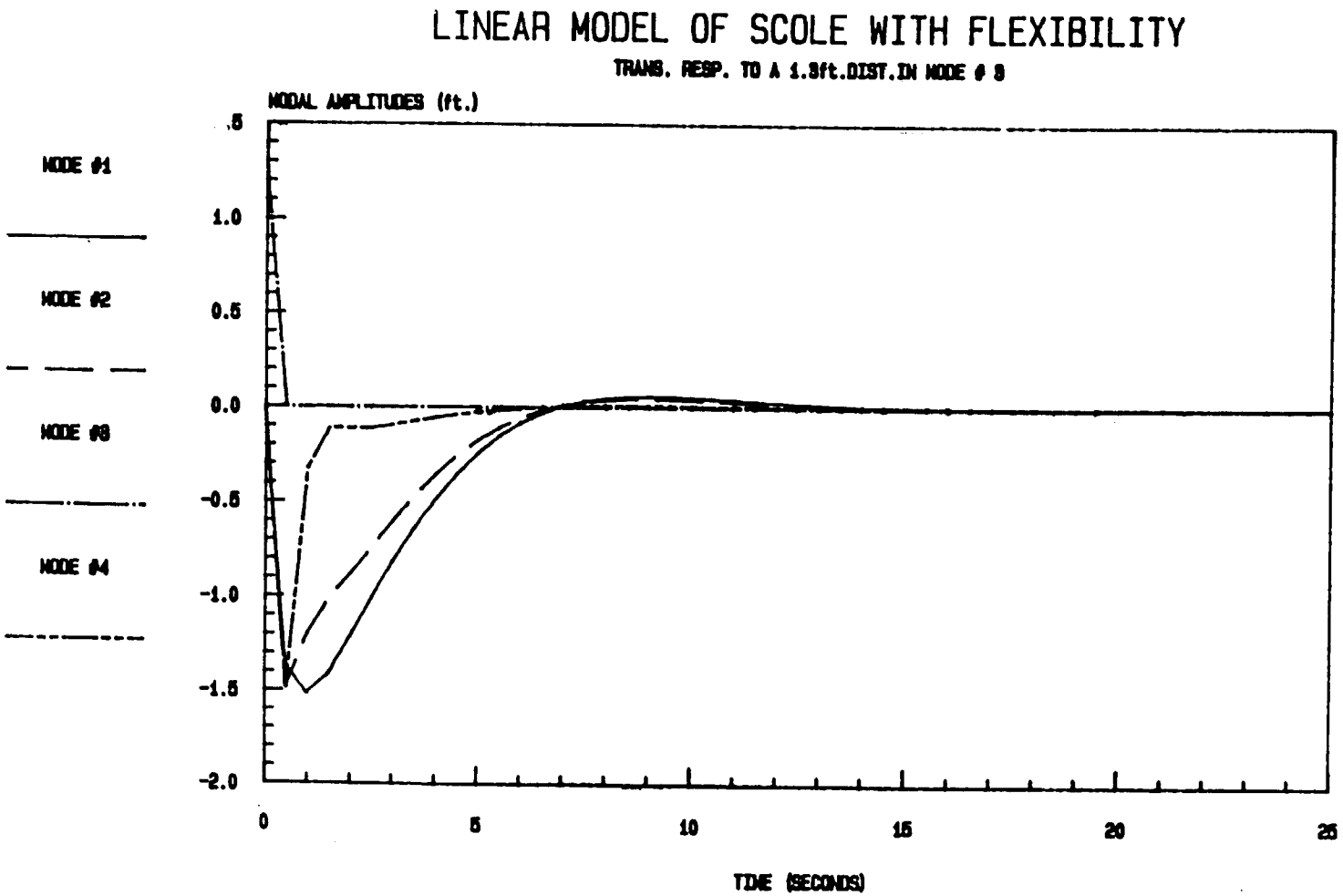
LINEAR MODEL OF SCOLE WITH FLEXIBILITY
TRANS. RESP. TO A 1.0ft.DIST.IN MODE # 8
MODAL AMPLITUDES (ft.)
MODE #1
MODE #2
MODE #8
MODE #4
1.5
1.0
0.5
0.0
-0.5
-1.0
-1.5
-2.0
0
5
10
15
20
25
TIME (SECONDS)

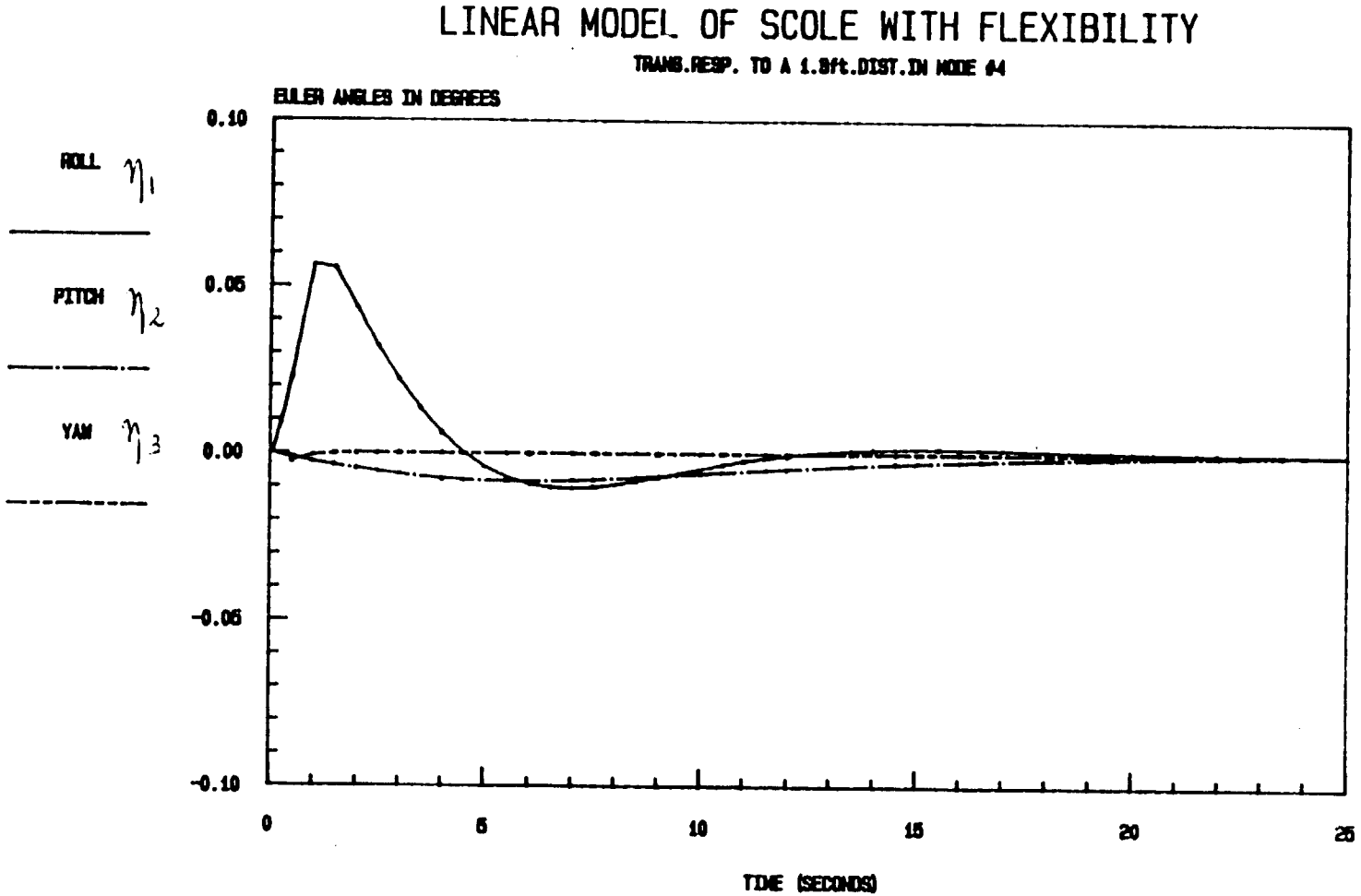
LINEAR MODEL OF SCOLE WITH FLEXIBILITY
TRANS.RESP. TO A 1.0ft.DIST.IN MODE #4
EULER ANGLES IN DEGREES
ROLL η_1
PITCH η_2
YAW η_3
0.10
0.05
0.00
-0.05
-0.10
0
5
10
15
20
25
TIME (SECONDS)

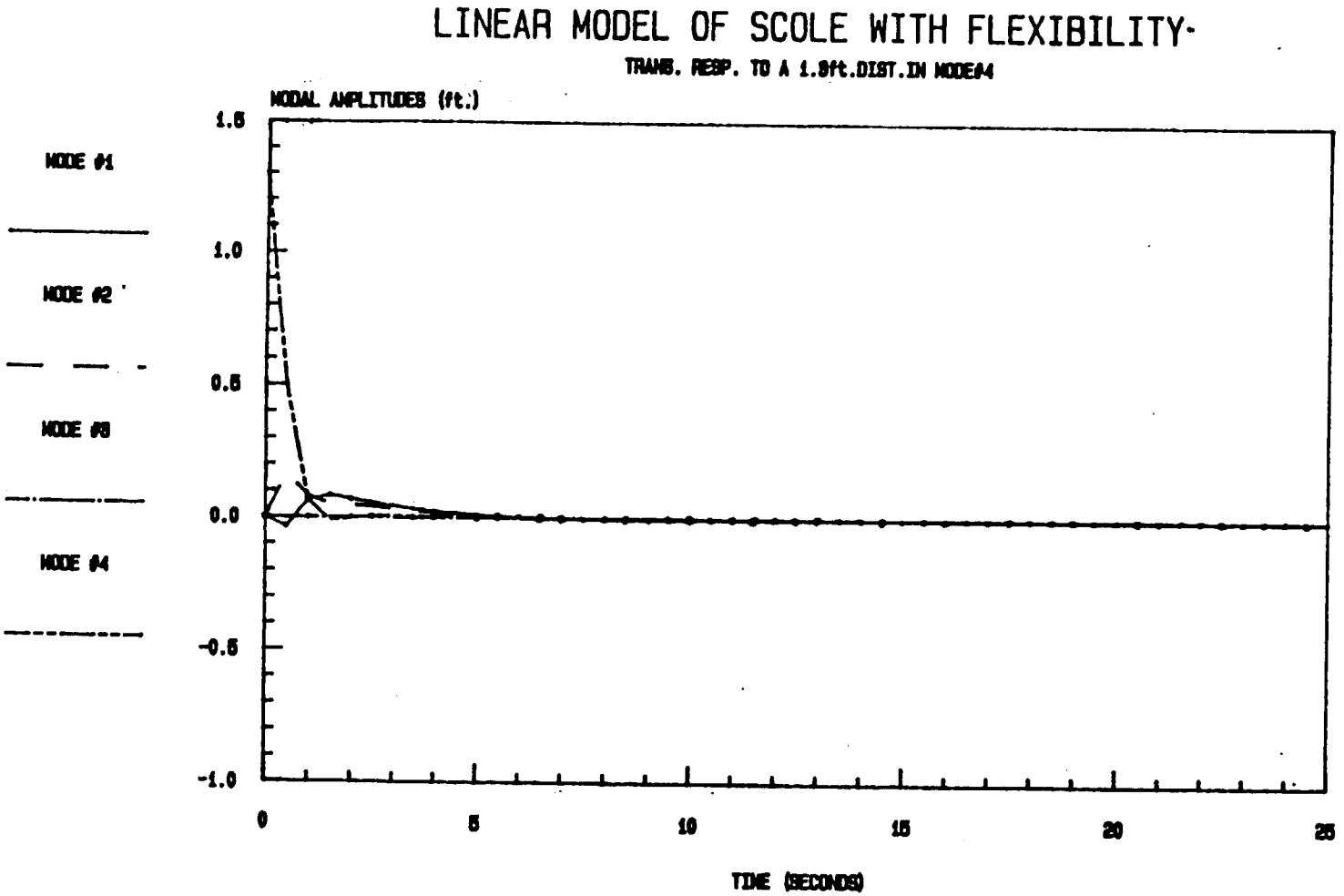
LINEAR MODEL OF SCOLE WITH FLEXIBILITY·
TRANS. RESP. TO A 1.0ft.DIST.IN MODE#4
MODAL AMPLITUDES (ft.)
MODE #1
MODE #2
MODE #3
MODE #4
1.5
1.0
0.5
0.0
-0.5
-1.0
0
5
10
15
20
25
TIME (SECONDS)

MINIMUM TIME ATTITUDE SLEWING MANEUVERS OF A RIGID SPACECRAFT

OBJECTIVE

- DEVELOP COMPUTATIONAL TECHNIQUES TO SLEW A GENERAL RIGID SPACECRAFT (INCLUDING RIGIDIZED SCOLE) FROM AN ARBITRARY INITIAL ATTITUDE TO A FINAL REQUIRED ATTITUDE PRECISELY, AND SATISFYING THE FOLLOWING CONDITIONS:
  - IN MINIMUM TIME
  - THE CONTROLS HAVE SATURATION LEVELS

METHODOLOGY

- THE MAXIMUM PRINCIPLE FROM OPTIMAL CONTROL THEORY IS APPLIED TO THE EULER'S DYNAMICAL EQUATIONS AND THE QUATERNION KINEMATICAL EQUATIONS OF THE SYSTEM TO DERIVE THE NECESSARY CONDITIONS FOR THE CONTROLS. THIS LEADS TO THE TWO-POINT BOUNDARY-VALUE PROBLEM.
- AN INTEGRAL OF A QUADRATIC FUNCTION OF THE CONTROLS IS USED AS A COST FUNCTION, BUT THE INTEGRATION PERIOD OF THIS INTEGRAL, CALLED THE SLEWING TIME, IS TO BE CHANGED UNTIL IT REACHES ITS MINIMUM VALUE.
- THE RESULTING TPBVP IS SOLVED BY A QUASILINEARIZATION ALGORITHM (METHOD OF PARTICULAR SOLUTIONS).
- EULER'S EIGENAXIS ROTATION THEOREM IS USED TO APPROXIMATELY DETERMINE THE INITIAL VALUES OF THE COSTATES AND THE SLEWING TIME AS WELL AS THE NOMINAL SOLUTIONS WHICH ARE UESD TO START THE QUASILINEARIZATION ALGORITHM.
- THE MINIMUM SLEWING TIME IS DETERMINED BY SHORTENING THE TOTAL SLEWING TIME UNTIL AT LEAST ONE OF THE CONTROLS BECOMES A BANG-BANG TYPE.

SPACECRAFT CONTROL LAB EXPERIMENT (SCOLE)

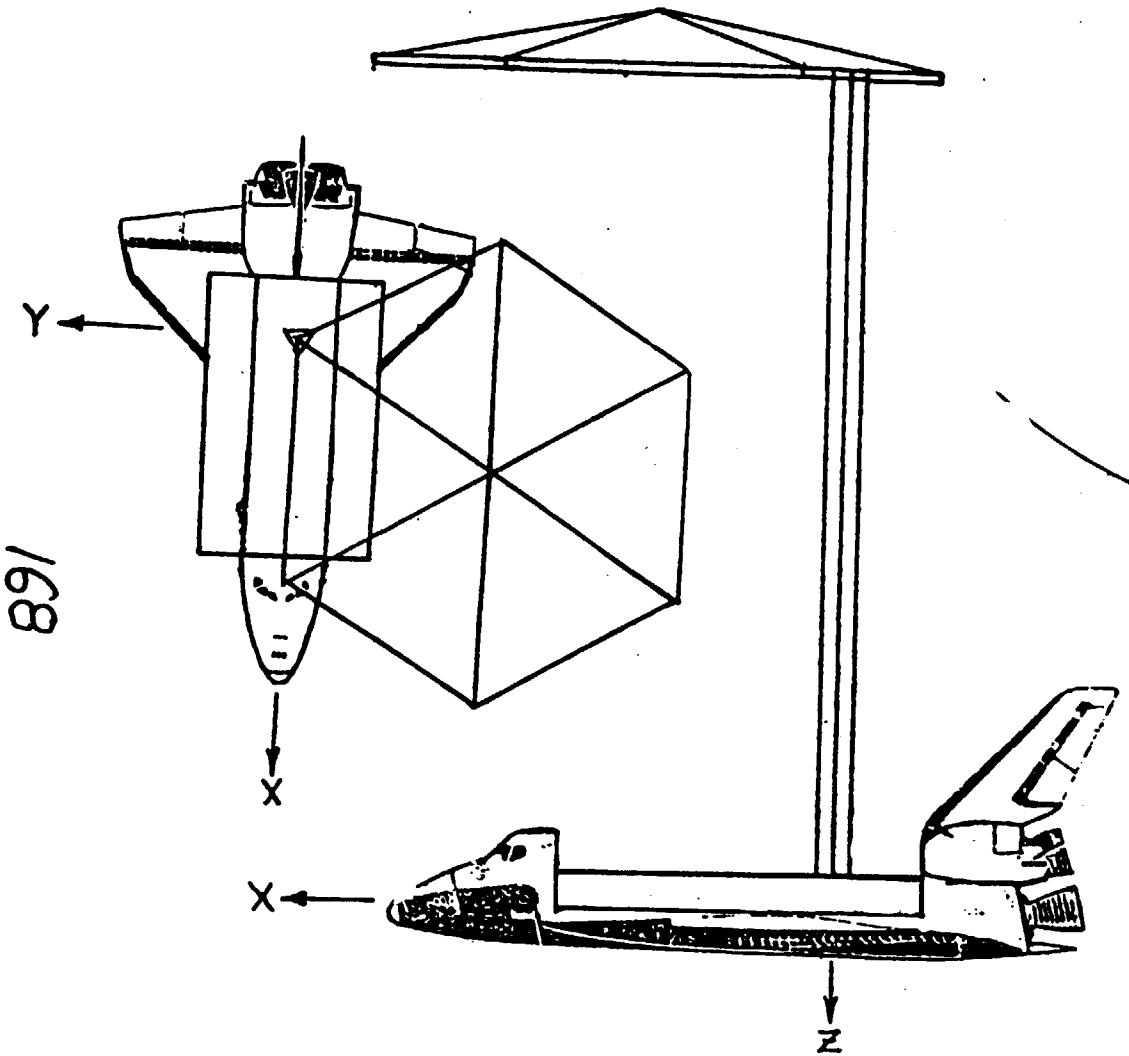

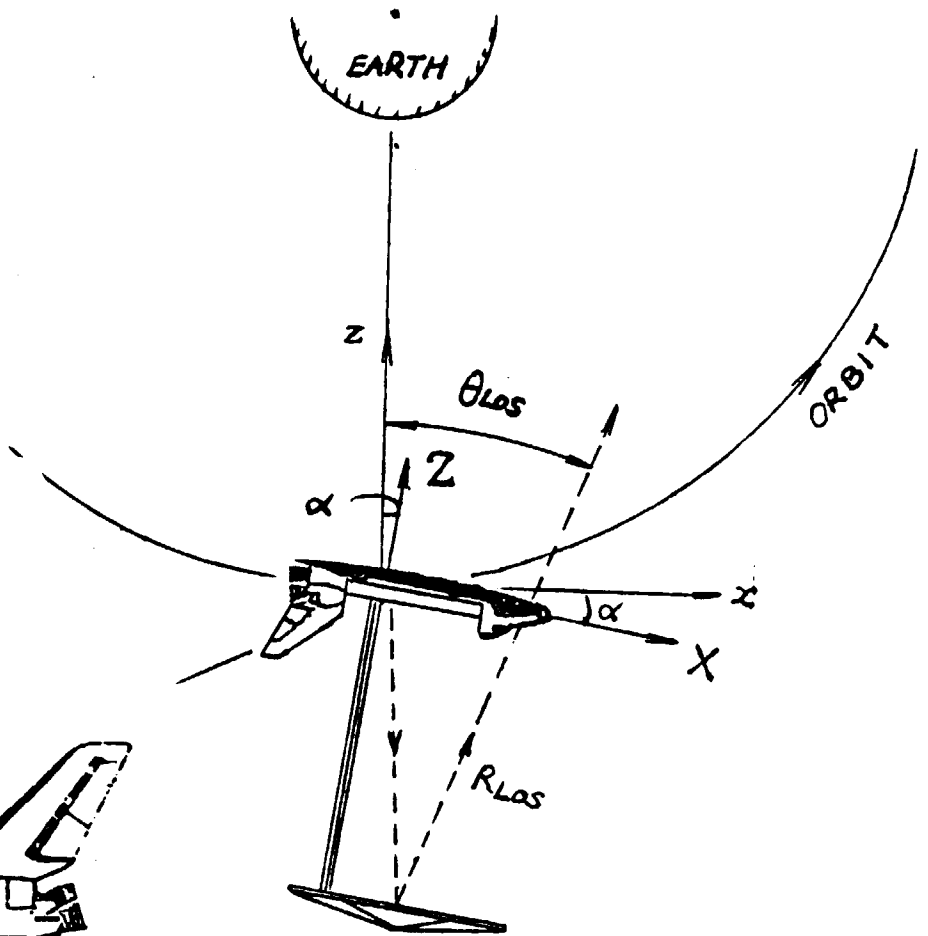

ATTITUDE OF THE SCOLE

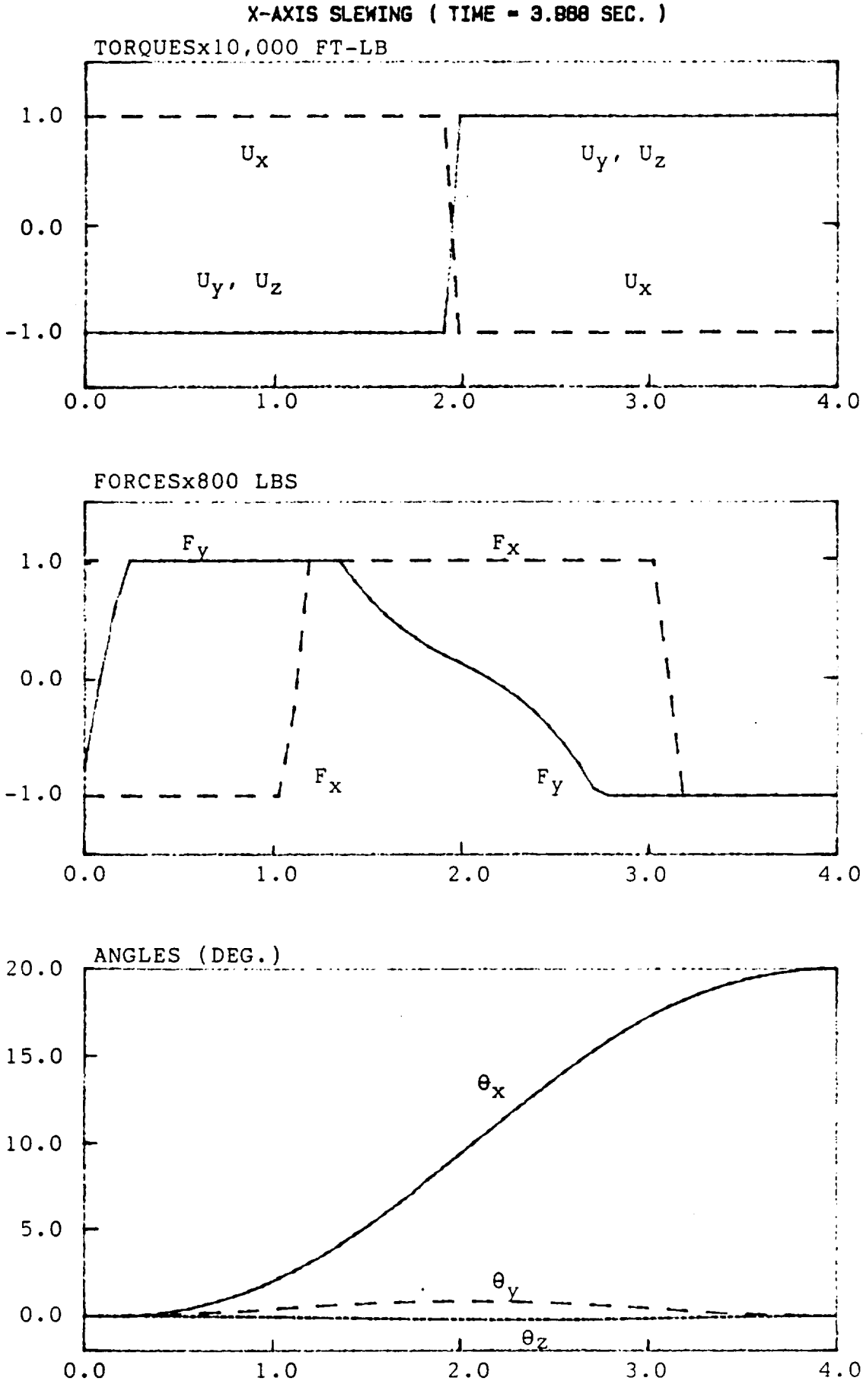
X-AXIS SLEWING (TIME = 3.888 SEC.)
TORQUESx10,000 FT-LB
1.0
0.0
-1.0
U_x
U_y, U_z
U_y, U_z
U_x
0.0
1.0
2.0
3.0
4.0
FORCESx800 LBS
1.0
0.0
-1.0
F_y
F_x
F_x
F_y
0.0
1.0
2.0
3.0
4.0
ANGLES (DEG.)
20.0
15.0
10.0
5.0
0.0
θ_x
θ_y
θ_z
0.0
1.0
2.0
3.0
4.0
TIME (SEC.)

EXAMPLE-SLEWING (TIME = 8.77 SEC.)

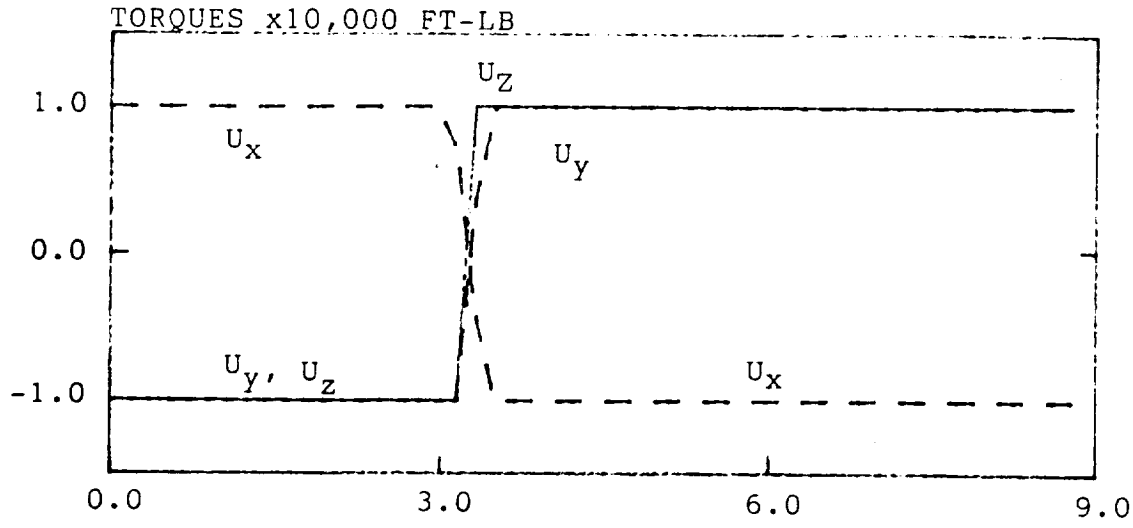

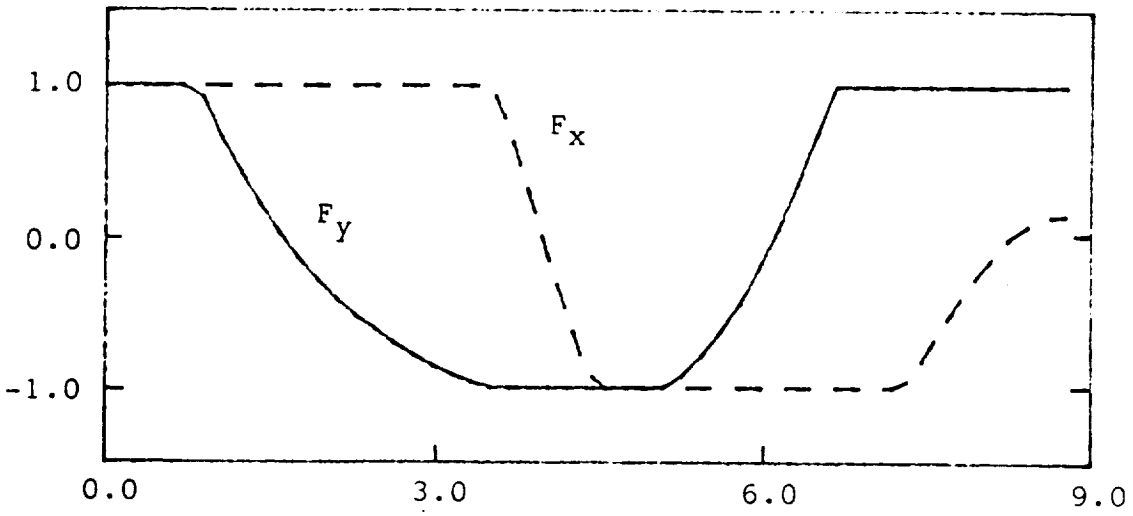

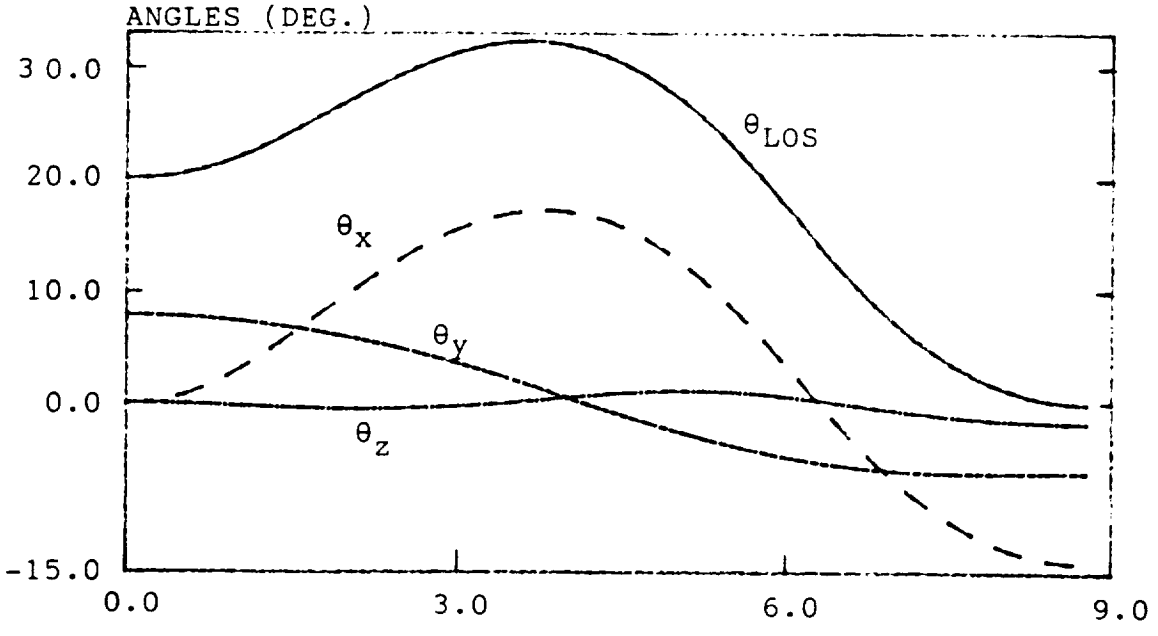

CONCLUDING REMARKS

- THE SLEWING MOTION NEED NOT BE RESTRICTED TO A SINGLE AXIS MANEUVER.
- THE GUESSED STARTING VALUE OF THE SLEWING TIME IS VERY CLOSE TO THE CONVERGED VALUE FOR THE SCOLE EXAMPLES AND SUBROUTINE USED HERE.
- THE GUESSED INITIAL VALUES OF THE COSTATES ARE ADEQUATE FOR THE ALGORITHM TO CONVERGE.
- THE METHODS USED HERE MAY BE IMPLEMENTED FOR PRACTICAL CONTROL SOURCES WHICH MAY HAVE MORE CONSTRAINTS.
- AN EXTENSION TO THE MINIMUM TIME SLEWING MOTION OF THE SCOLE MODEL CONTAINING BOTH RIGID AND FLEXIBLE COMPONENTS IS PLANNED.

Appendix - Chapter II

Stability Analysis of Second Order System with Delayed State Feedback

As a second order differential equation describes the dynamics of a single mode of any large space structure, the stability analysis of such a system with delayed state feedback is analyzed and the amount of delay that can be tolerated by the system without becoming unstable is arrived at analytically.

The differential equation of second order with state feedback can be written as:

$$\ddot{x}_i + 2\zeta_i'\omega_i\dot{x}_i + \omega_i^2 x_i = -k_r x_i(t-h) - k_p \dot{x}_i(t-h) \qquad (1)$$

where

x_i = i^{th} modal coordinate

ω_i = i^{th} natural frequency

ζ_i' = i^{th} mode inherent damping ratio

k_r = rate feedback gain

k_p = position feedback gain

h = time delay

The feedback gains k_r, k_p are designed for the required stability and transient response specifications without taking the delay into consideration.

The inherent damping ratio, ζ_i' and the feedback gains, k_r and k_p; will give rise to five possible combinations as shown in Table 1 and are thus analyzed separately for mathematical convenience and easy understanding.

Case I: $\zeta_i' = 0$, $k_p = 0$ and $k_r > 0$

The differential equation of the system can be written as:

$$\ddot{x}_i + \omega_i^2 x_i = - k_r \dot{x}_i(t-h) \tag{3}$$

Case	ζ_i'	k_r	k_p
I	= 0	> 0	= 0
II	> 0	> 0	= 0
III	= 0	> 0	> 0
IV	> 0	= 0	≠ 0
V	> 0	> 0	≠ 0

Note: The remaining three combinations are neither feasible nor of interest.

Table 1: Feasible Combinations of ζ_i', k_r, k_p for Stability Analysis

and the corresponding characterstic equation is given by:

$$s^2 + \omega_i^2 + 2\zeta_i\omega_i s e^{-sh} = 0 \tag{4a}$$

where $k_r = 2\zeta_i\omega_i$.

The value of h for which the roots of equation (3) cross the imaginary axis can be evaluated by substituting $s = j\omega$.

Thus

$$\omega_i^2 - \omega^2 + j2\zeta_i\omega_i\omega \sin\omega h + 2\zeta_i\omega_i\omega\cos\omega h = 0 \tag{4b}$$

For equation (4b) to be satisfied

$$\sin\omega h = 0$$

and $$\omega_i^2 - \omega^2 + 2\zeta_i\omega_i\omega \cos\omega h = 0 \tag{5}$$

Thus $\omega h = \pi/2$

and $$h = \frac{\pi/2}{\omega_i \left[\zeta_i + \sqrt{1+\zeta_i^2}\right]} \tag{6}$$

Case II: $\zeta_i' > 0$, $k_r = 2\zeta_i\omega_i$ and $k_p = 0$

The characteristic equation of the system described by equation (1) is given by

$$(\omega_i^2-\omega^2+2\zeta_i\omega_i\omega\sin\omega h) + j(2\zeta_i'\omega_i\omega+2\zeta_i\omega_i\omega\cos\omega h) = 0 \tag{7}$$

Thus $\cos\omega h = -\zeta_i'/\zeta_i$

and $$h = \frac{\cos^{-1}(\zeta_i'/\zeta_i}{\omega_i \left[\sqrt{\zeta_i^2-\zeta_i'^2} + \sqrt{1+\zeta_i^2-\zeta_i'^2}\right]} \tag{8}$$

For the case where $\zeta_i<\zeta_i'$ thesystem will always be stable since no value of h exists for which the roots of (7) cross the imaginary axis. A plot of $\omega_i h$ versus ζ_i for various values of ζ_i' is shown in Figure 2.1.

Case III: $\zeta_i' = 0$, $k_p = k_r > 0$

The characteristic equation is given by

$$s^2+\omega_i^2+k_r s e^{-sh}+k_p e^{-sh} = 0 \tag{9}$$

or $$(\omega_i^2-\omega_i^2+\omega k_r\sin\omega h+k_p\cos\omega h) + j(\omega k_r\cos\omega h-k_p\sin\omega h) = 0 \tag{10}$$

Thus $$\tan\omega h = \frac{\omega k_r}{k_p}$$

and $$\omega^2 = \frac{1}{2}\left[(2\omega_i^2+k_r^2) + \sqrt{[k_r^4+4\omega_i^2k_r^2+4k_p^2]}\right] \tag{11}$$

Plots of $h\omega_i$ versus k_r/ω_i for various values of k_p/ω_i^2 are shown in Figure 2.2. It can be seen here that these are many combinations of k_p and k_r for which the roots of Eq. (10) can cross the imaginary axis - i.e. value of $h\omega_i$ which leads to instability.

Case IV: $\zeta_i' > 0,\ k_r = 0,\ k_p \neq 0$

The characteristic equation is given by

$$(\omega_i^2 - \omega^2 + k_p \cos\omega h) + j(2\zeta_i' \omega_i \omega - k_p \sin\omega h) = 0 \tag{12}$$

Thus

$$\sin\omega h = \frac{2\zeta_i' \omega_i \omega}{k_p} \tag{13}$$

and

$$\omega^2 = \omega_i^2(1-2\zeta_i'^2) + \omega_i^2\sqrt{[(1-2\zeta_i'^2)^2 + (k_p/\omega_i^2)^2]} \tag{14}$$

The plots of $h\omega_i$ versus k_p/ω_1^2 for various values of ζ_i' are shown in Figure 2.3

Case V: $\zeta_i' > 0,\ k_r > 0,\ k_p \neq 0$

The characteristic equation is given by

$$(\omega_i^2 - \omega^2 + \omega k_r \sin\omega h + k_p \cos\omega h) + j(2\zeta_i' \omega_i \omega + \omega k_r \cos\omega h - k_p \sin\omega h) = 0 \tag{15}$$

By equating the imaginary part to zero, ωh can be evaluated as

$$\omega h = \sin^{-1}\underbrace{\left(\frac{2\zeta_i' \omega_i \omega}{\sqrt{k_p^2 + \omega k_r^2}}\right)}_{y} - \tan^{-1}\left(\frac{\omega k_r}{k_p}\right) \tag{16}$$

after substituting ωh in the real part of equation (15), the following equation in the single unknown variable ω can be obtained

$$\omega_i^2 - \omega^2 + \omega k_r \sin\left(\sin^{-1}y - \tan^{-1}\left(\frac{\omega k_r}{k_p}\right)\right) + k_p \cos\left(\sin^{-1}y - \tan^{-1}\left(\frac{\omega k_r}{k_p}\right)\right) = 0 \tag{17}$$

Using equations (17) and (16), the limiting value for given values of ζ_i', k_r, k_p and ω_i can be determined. As the equation (17) is nonlinear, numerical procedures may have to be used and thus the generalized plots similar to the other cases may be obtained.

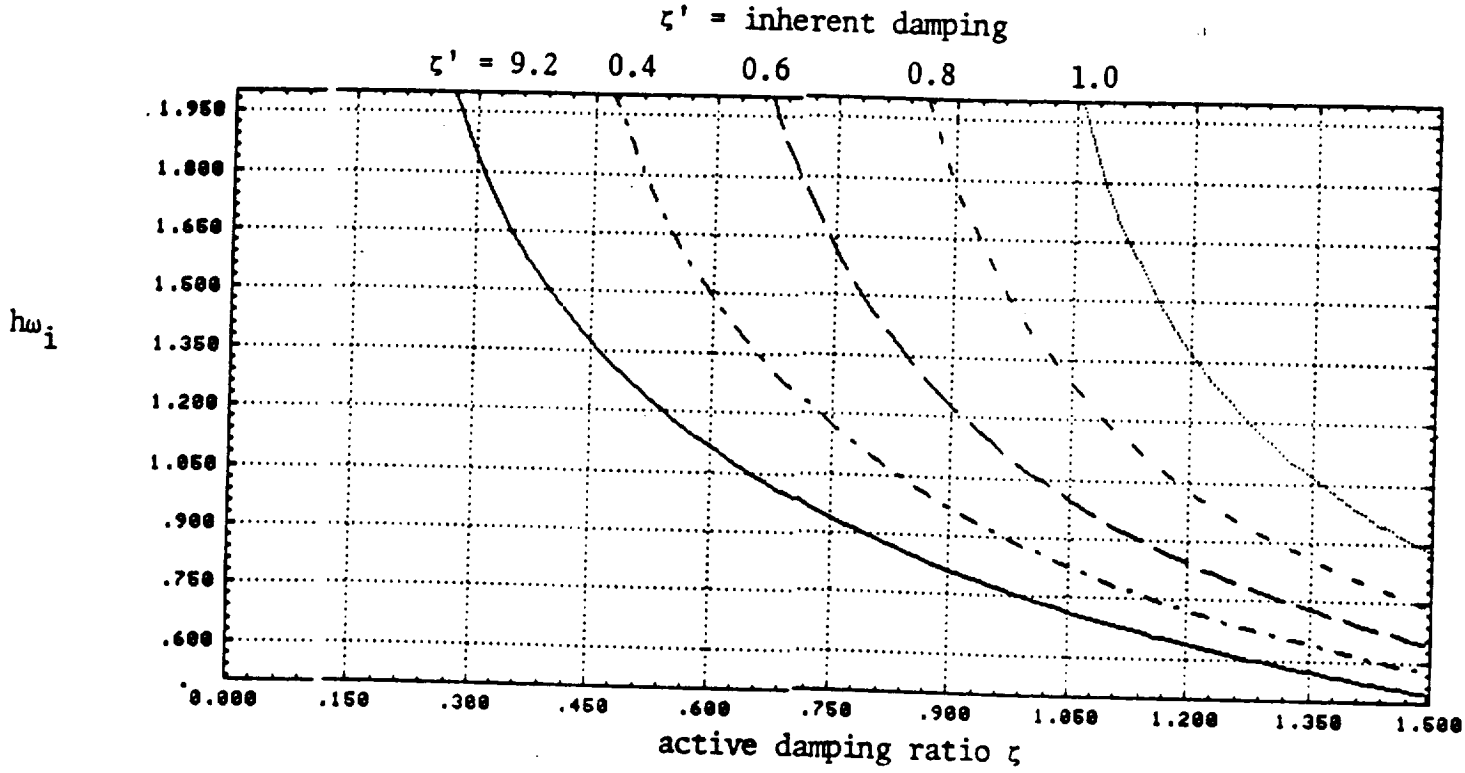

Figure 2.1: Plots of $h\omega_i$ vs ζ_i correspondence to Case II with ζ_i' as a parameter.

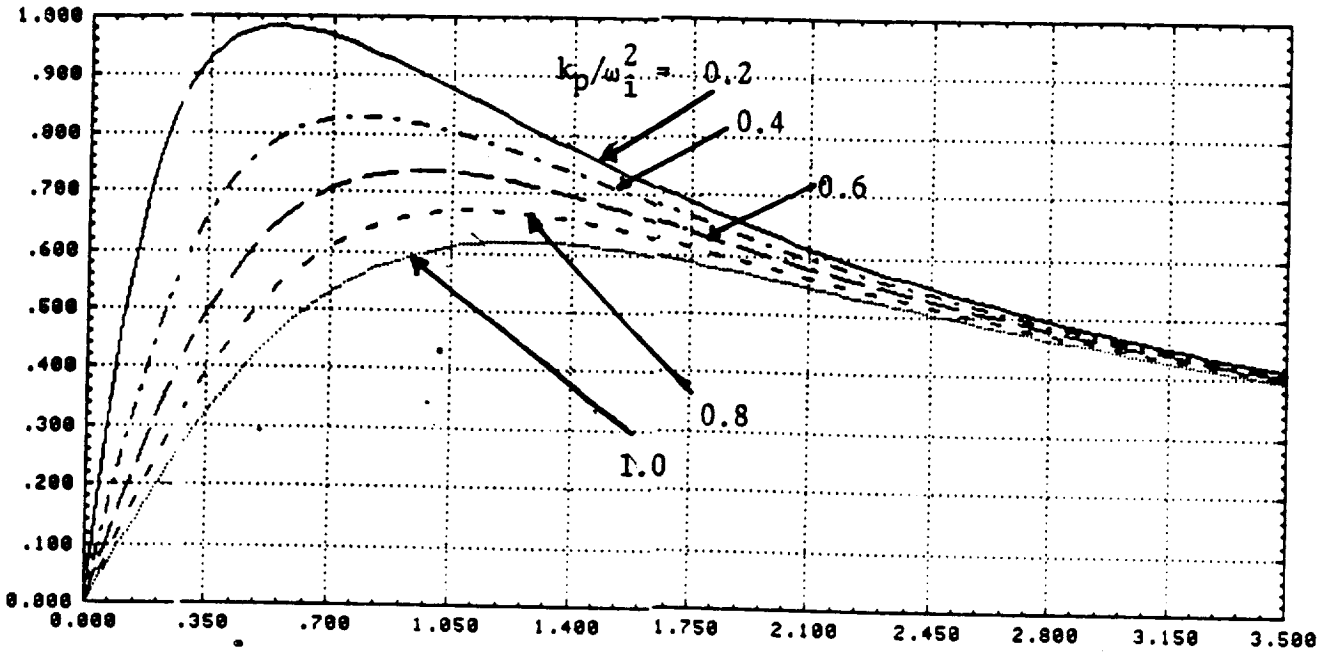

Figure 2.2 Plot of $h\omega_i$ vs k_r/ω_i corresponding to Case III with k_p/ω_i^2 as a parameter

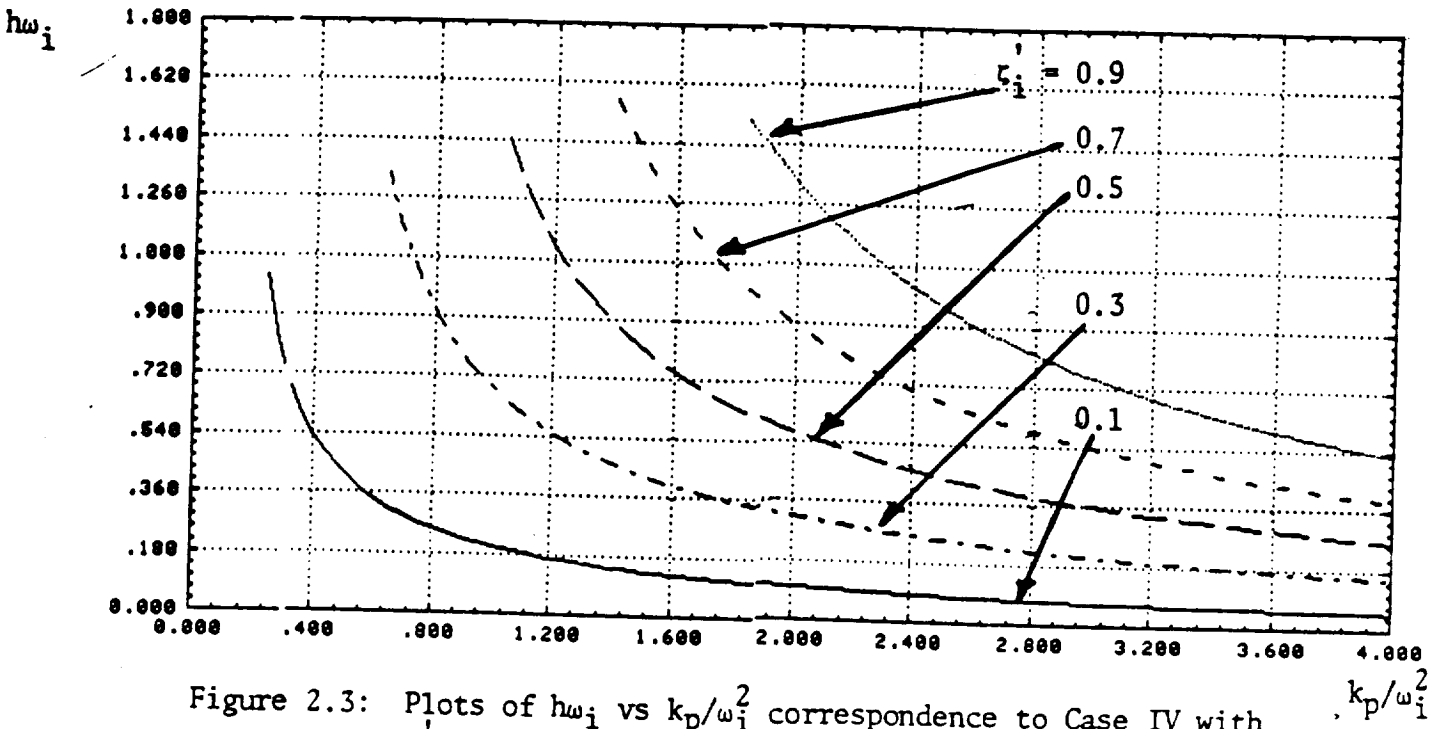

Figure 2.3: Plots of $h\omega_i$ vs k_p/ω_i^2 correspondence to Case IV with ζ_i' as a parameter

$\hbar\omega_i$

INITIAL TEST RESULTS ON STATE ESTIMATION ON THE SCOLE MAST

D. SPARKS, JR.

NASA LANGLEY RESEARCH CENTER
M/S 161
HAMPTON, VA 23665
(804)-865-4591

Abstract

Modal state estimation tests are performed on the SCOLE mast for the fixed Shuttle platform case. Kalman filter state estimation results from a five mode computer model of the SCOLE mast, developed from a finite element analysis, are compared with those state estimates obtained from laboratory tests. Two comparison runs are presented, one an excitation of the first two bending modes, another, an excitation of the first torsional mode of the mast. Results from both runs show poor agreement in modal estimation between the computer model simulations and the laboratory test data. At present, the reason(s) for this poor performance is unknown. Both the laboratory hardware and software and the computer model are being checked for possible sources of errors. Further computer simulations as well as laboratory testing will be performed.

MODEL OF SCOLE MAST

- ⊙ MODAL DATA FORM FINITE ELEMENT ANALYSIS OF MAST
- ⊙ FIVE DECOUPLED MODES (FREQUENCIES .443-4.345 HZ)
- ⊙ ACTUATORS: FOUR JETS AND THREE REACTION WHEELS
- ⊙ SENSORS: SIX LINEAR ACCELEROMETERS AND 3 AXIS RATE GYRO
- ⊙ MODAL STATE AND OUTPUT EQUATIONS:

$$X(k+1) = AX(k) + BU(k)$$

$$Y(k) = CX(k) + DU(k)$$

- ⊙ STATES ESTIMATED BY KALMAN FILTER

KALMAN FILTER

⊙ EQUATIONS IN BASIC FORM:

$$\tilde{X}(k+1) = A\hat{X}(k) + BU(k)$$

$$\hat{X}(k+1) = \tilde{X}(k+1) + G(Y(k) - \hat{Y}(k))$$

$\tilde{X}$ - PREDICTED STATE

$\hat{X}$ - ESTIMATED STATE

G - KALMAN FILTER GAIN MATRIX

⊙ KALMAN FILTER GAINS ASSUMED CONSTANT

- SENSOR NOISE INTENSITIES ESTIMATED FROM MANUFACTURERS' DATA

⊙ ABOVE FORM USED IN SOFTWARE FOR LABORATORY TESTS

SIMULATION AND TEST PARAMTERES

RUNS USED FORCING FUNCTION TO EXCIT SCOLE MAST

$$F = A \sin(\omega T)$$

RUN	EXCITATION TIME	FREQUENCY	AMPLITUDE	DURATION
1	10 sec	.443 HZ	5.0	30 sec
2	10 sec	1.504 HZ	2.0	30 sec

⊙ COMPUTER SIMULATIONS USED SAME VALUES

C-5

EAL 1ST BENDING MODE (MODE 1)

VIBRATIONAL MODE. FREQ (HZ) . 4426 X10 +00

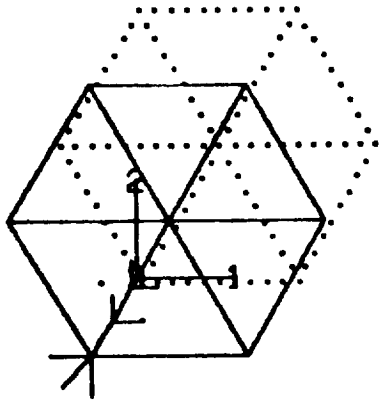

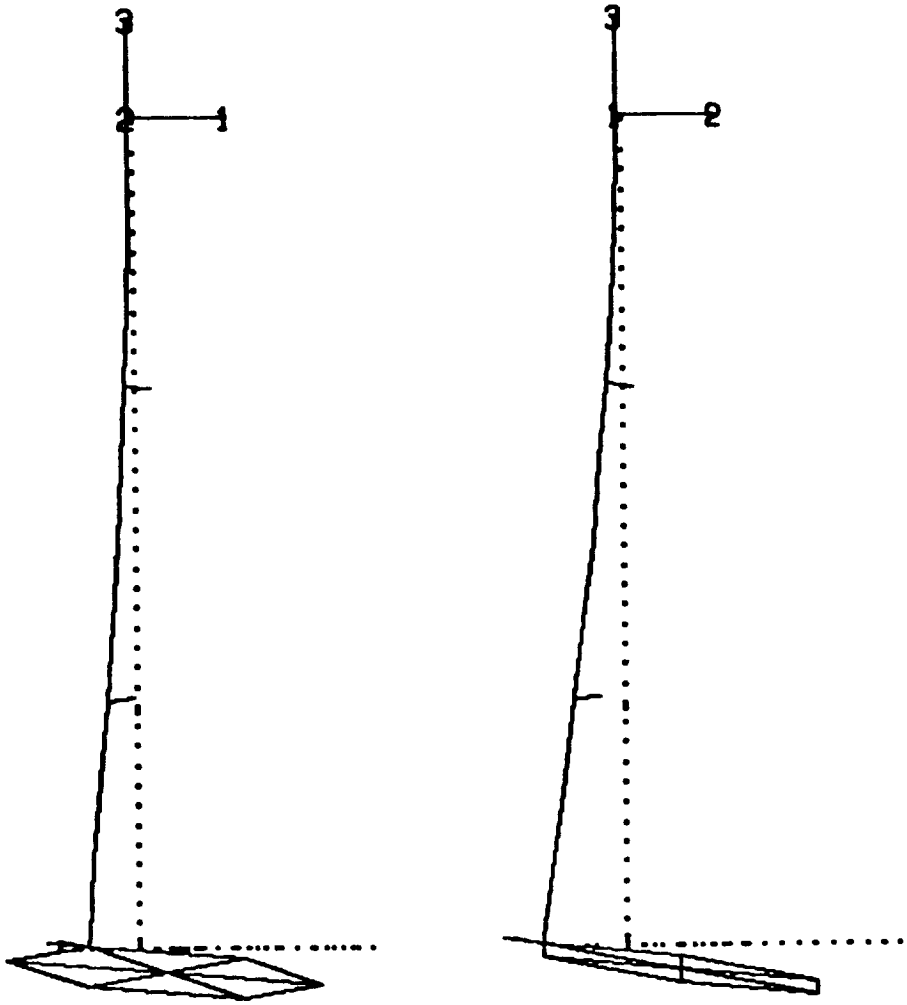

SPEC
1.1

SCOLE VIBRATIONAL MODE SHAPE 1

RUN #1 X - WHEEL INPUT

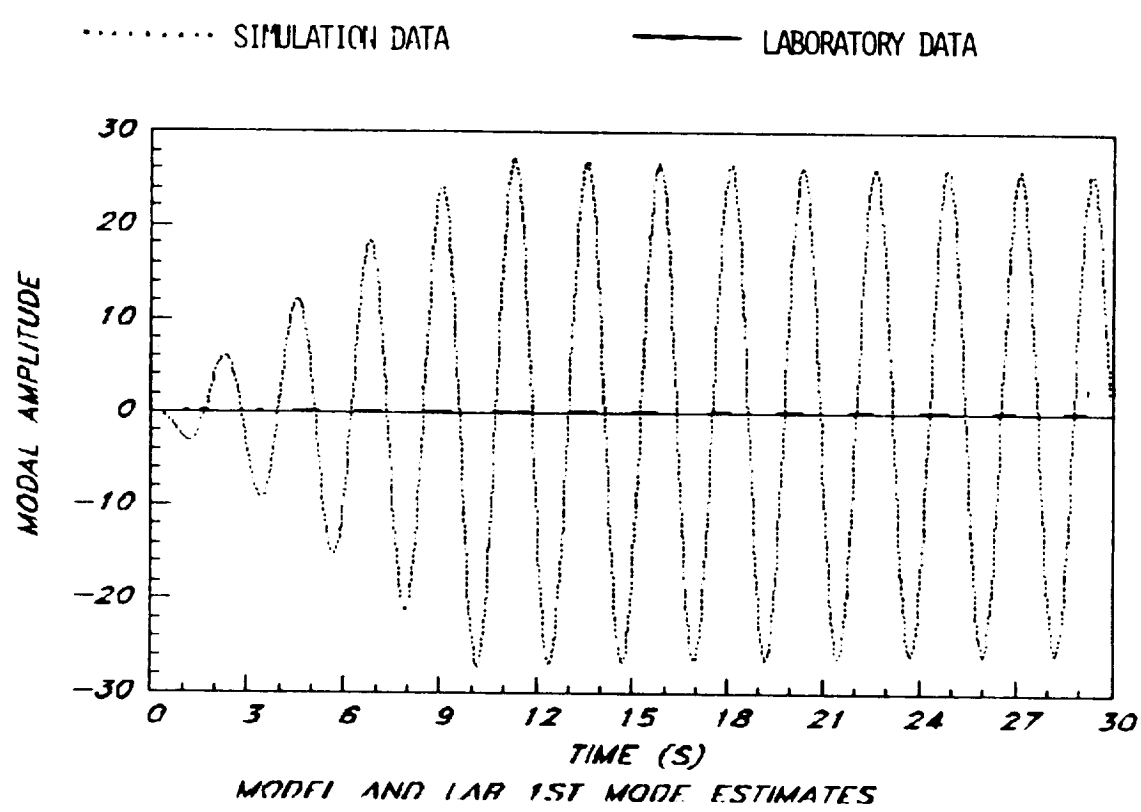

MODEL AND LAB 1ST MODE ESTIMATES

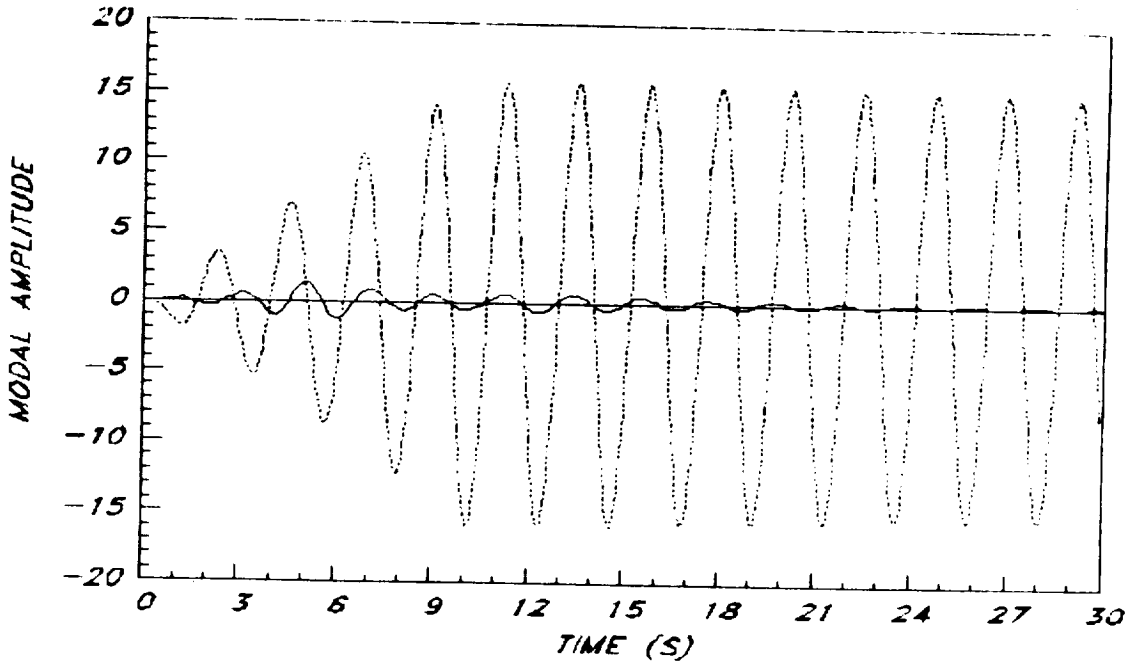

MODEL AND LAB 2ND MODE ESTIMATES

EAL 1ST TORSIONAL MODE (MODE 3)

VIBRATIONAL MODE, FREQ (HZ) . 1504 X10 +01

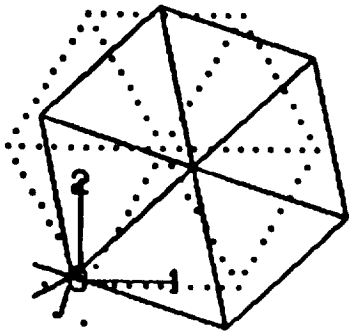

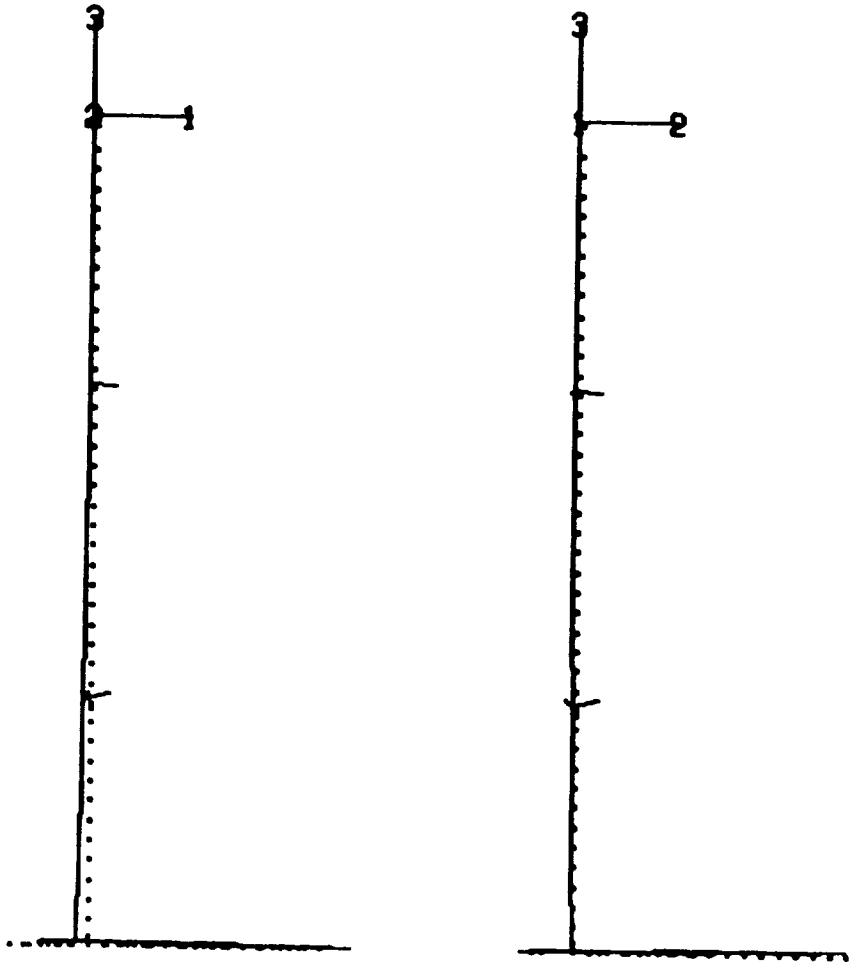

SPEC
3 1

SCOLE VIBRATIONAL MODE SHAPE 3

RUN # 2 z - WHEEL INPUT

..... SIMULATION DATA —— LABORATORY DATA

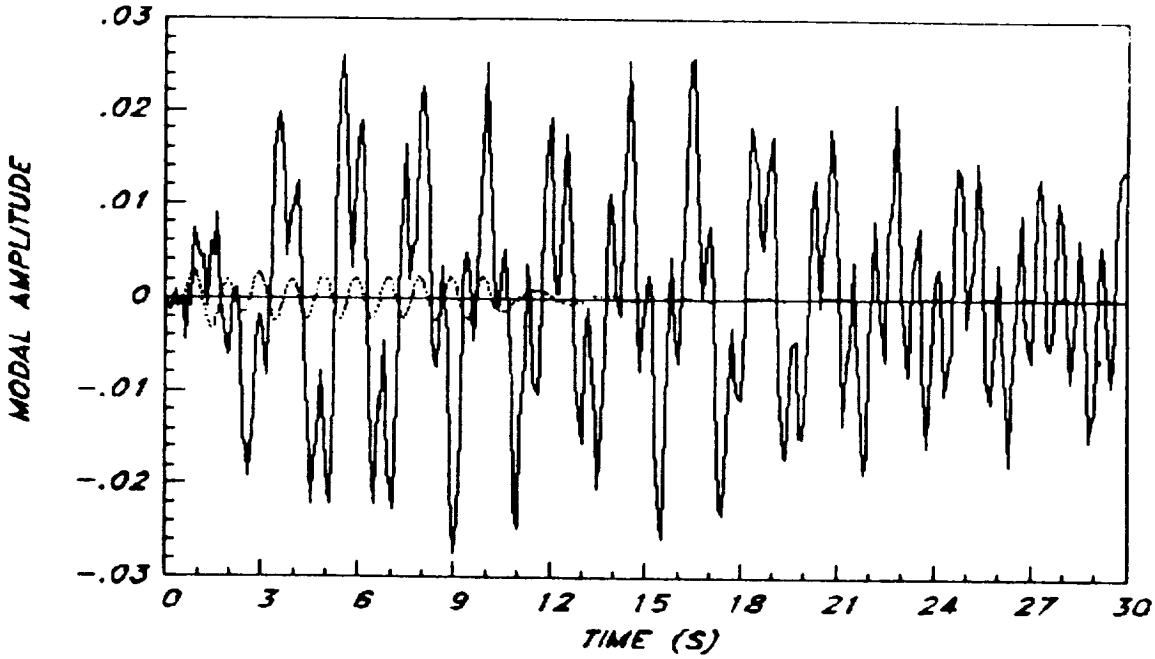

MODEL AND LAB 2ND MODE ESTIMATES

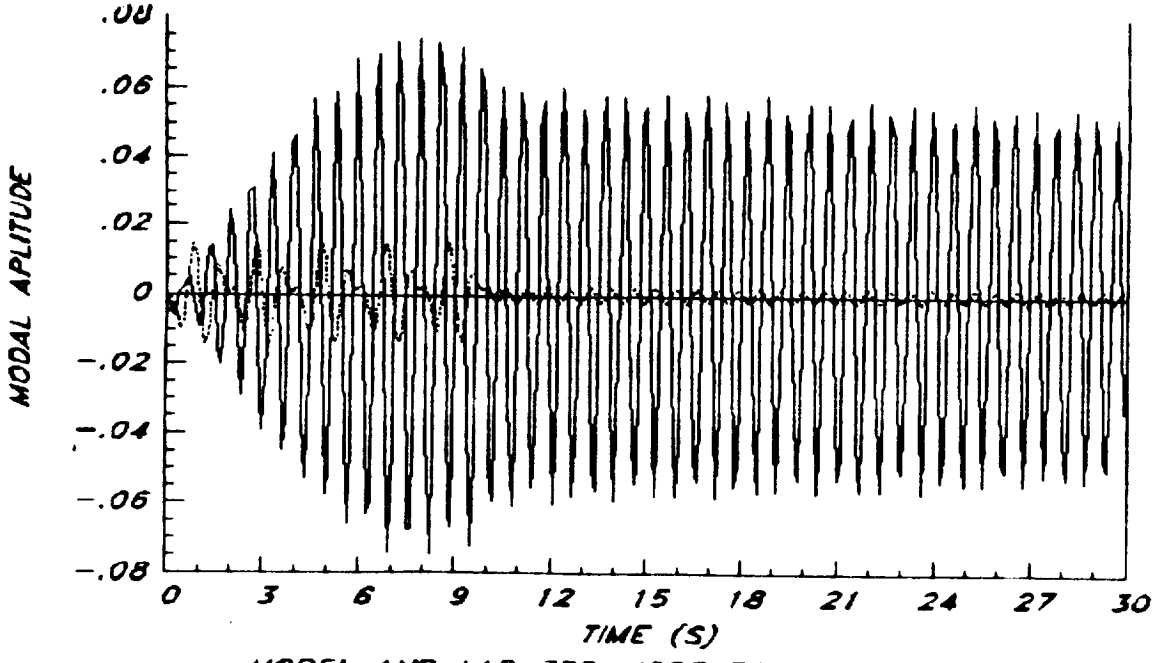

MODEL AND LAB 3RD MODE ESTIMATES

COMMENTS

- LABORATORY AND COMPUTER SIMULATIONS OF MODE ESTIMATES ARE VERY DIFFERENT !

- ONLY GENERAL AGREEMENT BETWEEN LABORATORY AND COMPUTER SIMULATION IS IN WHICH MODES ARE "DOMINANT" FOR THE RESPECTIVE FORCING FUNCTIONS

- CONFIDENCE IN LINEAR COMPUTER SIMULATION MODEL

SUMMARY

- MORE LABORATORY TESTS ARE REQUIRED

- RE-CHECK LABORATORY APPARATUS (SOFTWARE AND HARDWARE)

- PARAMETER IDENTIFICATION AND RE-DEFINING MODEL OF SCOLE
  SIMPLE LINEAR DECOUPLED MODAL MODEL MAY NOT BE
  SUFFICIENT FOR PROPER LABORATORY EXPERIMENTS

SLEWING AND VIBRATION CONTROL OF THE SCOLE

JIGUAN GENE LIN

CONTROL RESEARCH CORPORATION
LEXINGTON, MA 02173

OUTLINE

I. Introduction

II. Structural Vibrations in SCOLE Excited by
Time-Minimized Rapid Slewing

-- Bang-Pause-Bang (BPB) Control (800 lb)
-- Bang-Bang (BB) Control (0, 80, 25 lbs)

How bad? Always that bad?
No Force means Least Excitation?

III. Active Damping of BPB-Excited Vibrations
using **High-Perforamance Modal Dashpots**

Direct Velocity Output Feedback really cannot
control excessive vibrations effectively, quickly?

IV. Comments

V. Conclusions

VI. Recommendations

- SCOLE Primary control task is:
  Rapidly Slew or change the Line-of-Sight (LOS), and
  Settle or Damp Structural Vibrations to a required degree

- The Objective is:
  Minimize the time required to Slew and Settle,
  until LOS remains within a specified angle.

- 2-Stage approach:
  First: Slew the whole structure like a rigid body,
  -- in a minimum time,
  -- under the limited control moments and forces
  Then: Damp the excited structural vibrations

- Some previous results on Stage-1 design

Case	Strategy (lb-ft) →	Moment (lb) →	Force (deg) →	LOS error (sec) →	Slew Time
F10	BB	10,000	0	.150	12.604
F11	**BPB**	**10,000**	**800**	**.086**	**4.892**
F12	BB	10,000	800	.097	3.756

- Objective of Current Study
  Stage-2 design: Active Control of Excited Vibrations

Structural Vibrations Excited by Bang-Bang-Type Rapid Slew Maneuvers

Force (lb)	Moment (lb-ft)	Strategy (sec)	Slew Time (sec)	LOS Error (deg)	Deflect. (ft)	Att. Dev. (deg)
800	10,000	.867 (B) 3.158 (P) .867(-B)	4.892 (Note 1)	89.8 or 133.3	+114 -113	+88.35 -86.96
0	same	6.307 (B) 6.307(-B)	12.614	6.25	+5.06 -5.18	+3.83 -4.02
80	same	4.416 (B) 4.416(-B)	8.832	24.7	+20.59 -10.83	+15.98 -8.31
25	same	5.479 (B) 5.479(-B)	10.959	0.51	+0.25 -0.30	+0.16 -0.30

Note 1. Time of application is 1.734 sec, only 35.32% of the slew time.

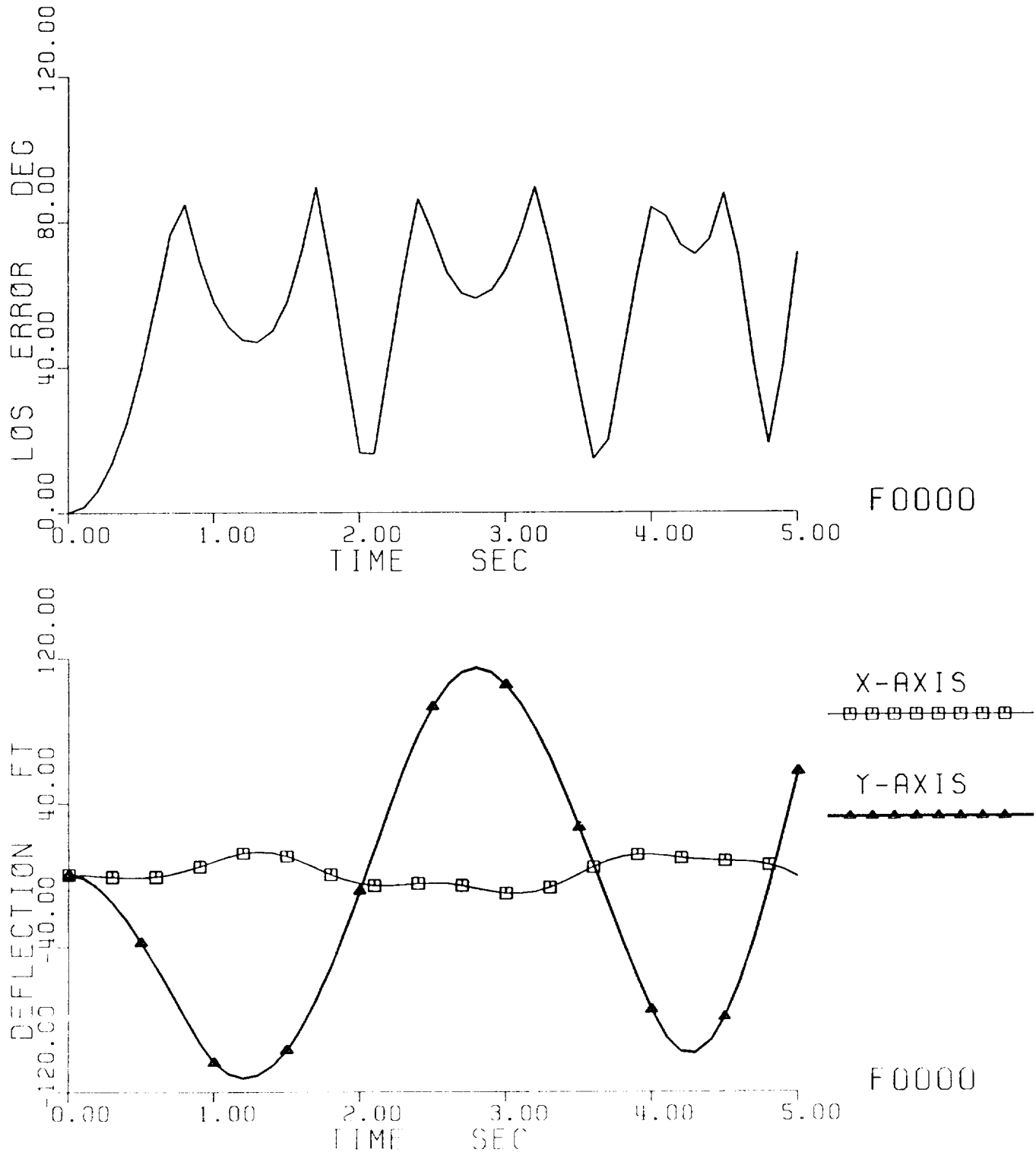

Fig. 3-1 Vibratory responses to Rapid Time-minimized Bang-Pause-Bang Slew;
a. Line-of-sight error and Mast tip deflection.

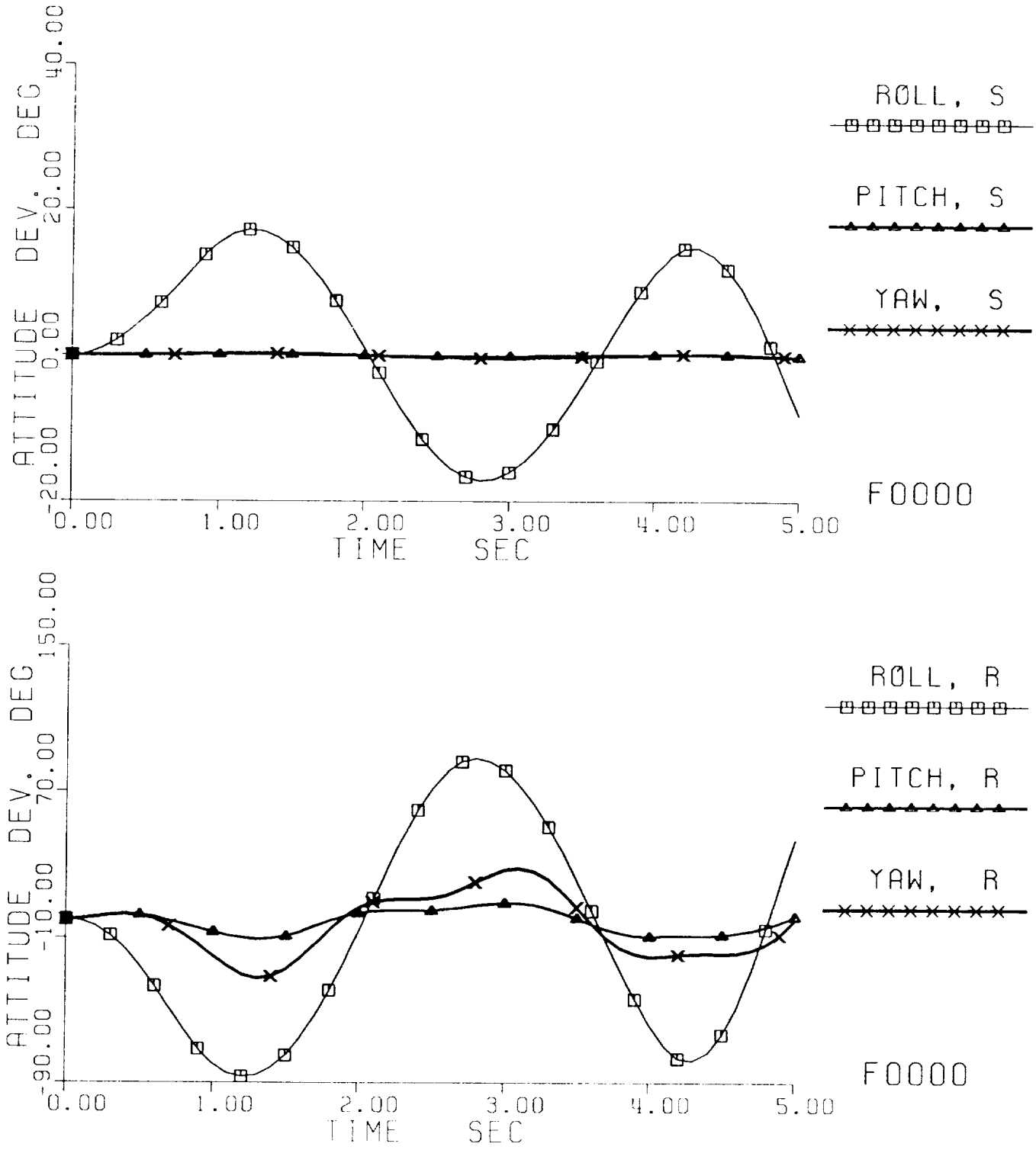

Fig. 3-1 Vibratory responses to Rapid Time-minimized Bang-Pause-Bang Slew;
b. Attitude deviations at the Shuttle (S) and the Reflector (R) ends.

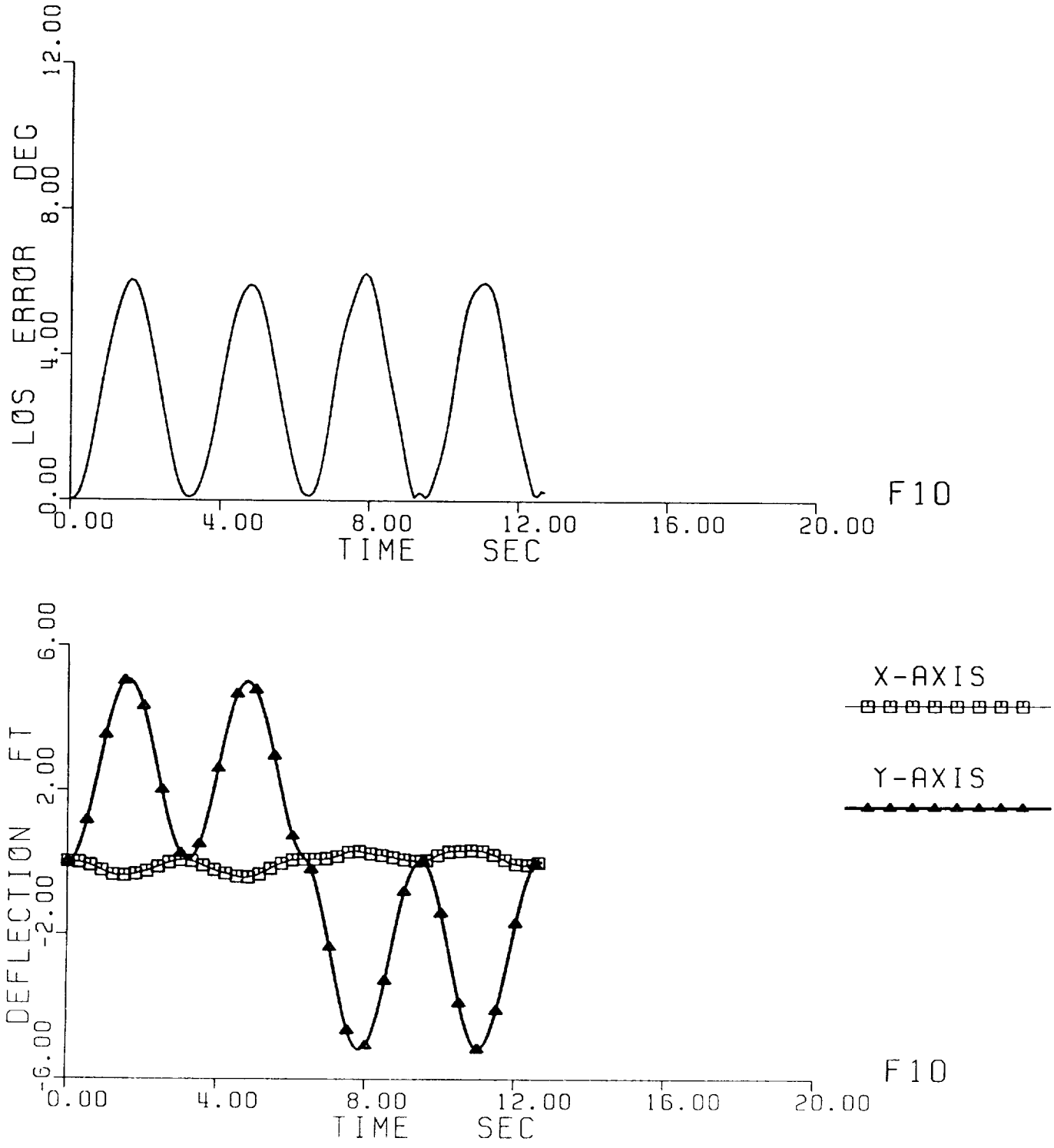

Fig. 3-2 Vibratory responses to Rapid Time-minimized Bang-Bang Slew: 0 lb;
a. Line-of-sight error and Mast tip deflection.

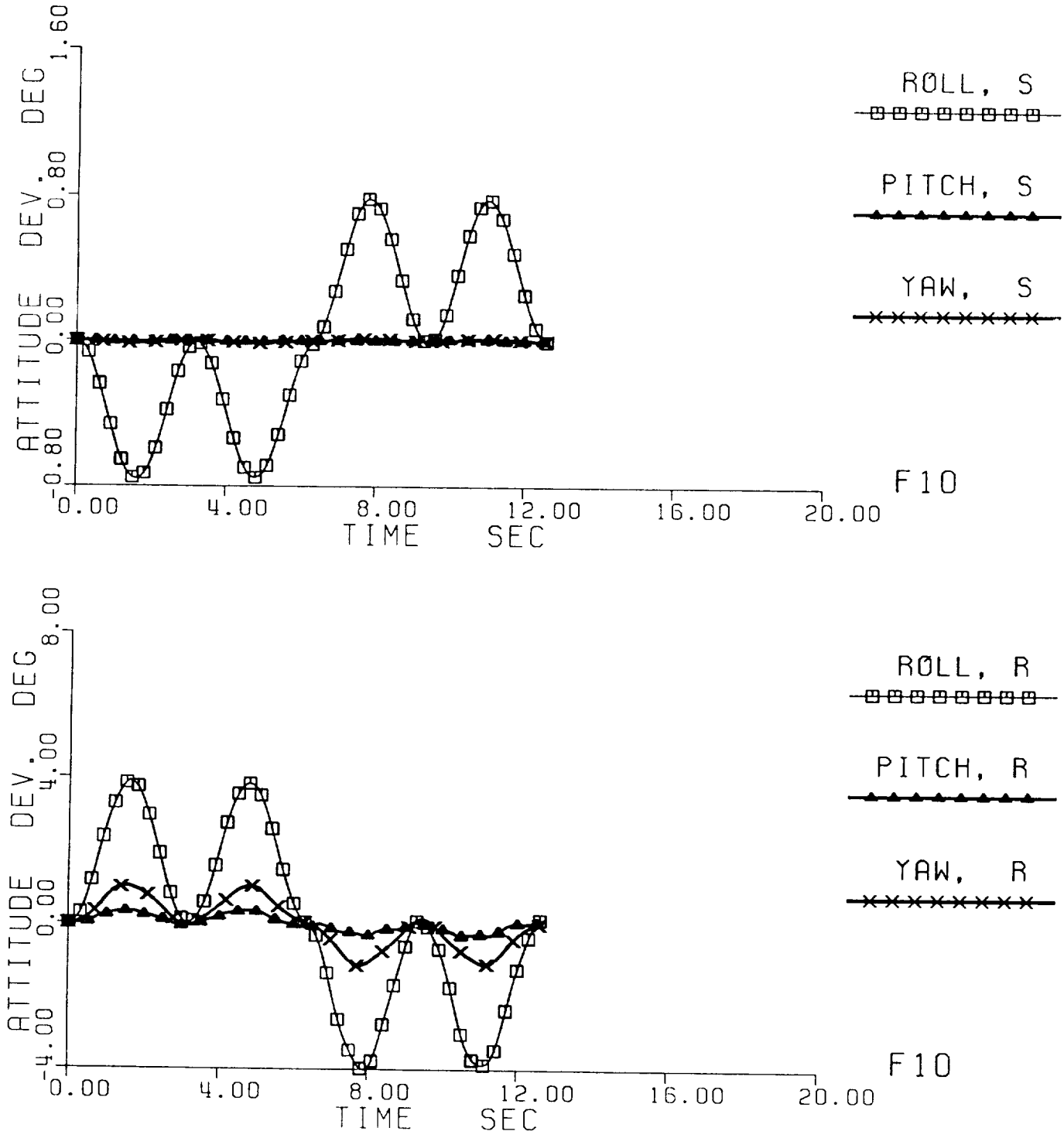

Fig. 3-2 Vibratory responses to Rapid Time-minimized Bang-Bang Slew: 0 lb;
b. Attitude deviations at the Shuttle (S) and the Reflector (R) ends.

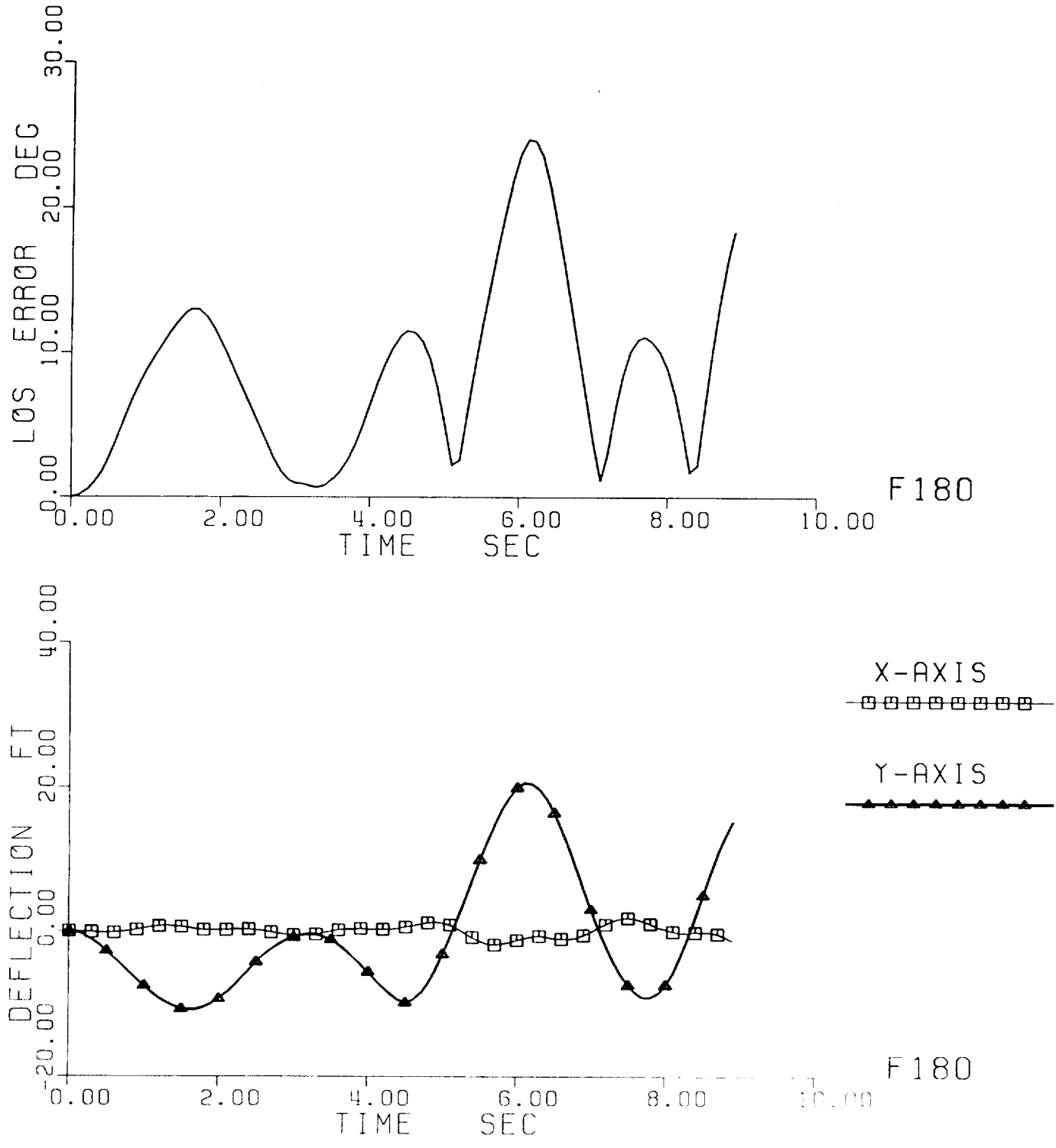

Fig. 3-3 Vibratory responses to Rapid Time-minimized Bang-Bang Slew: 80 lb;
a. Line-of-sight error and Mast tip deflection.

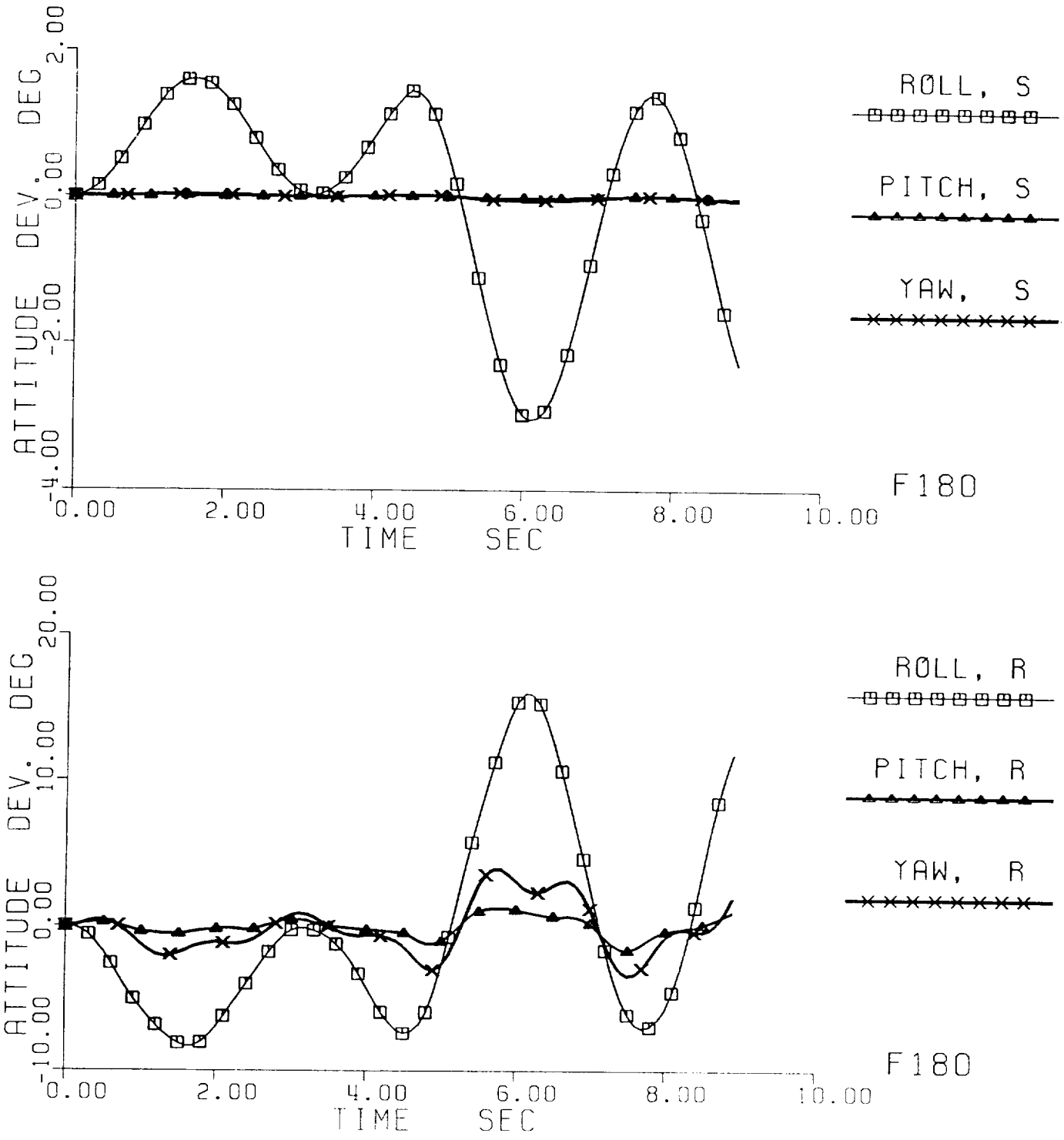

Fig. 3-3 Vibratory responses to Rapid Time-minimized Bang-Bang Slew: 80 lb; b. Attitude deviations at the Shuttle (S) and the Reflector (R) ends.

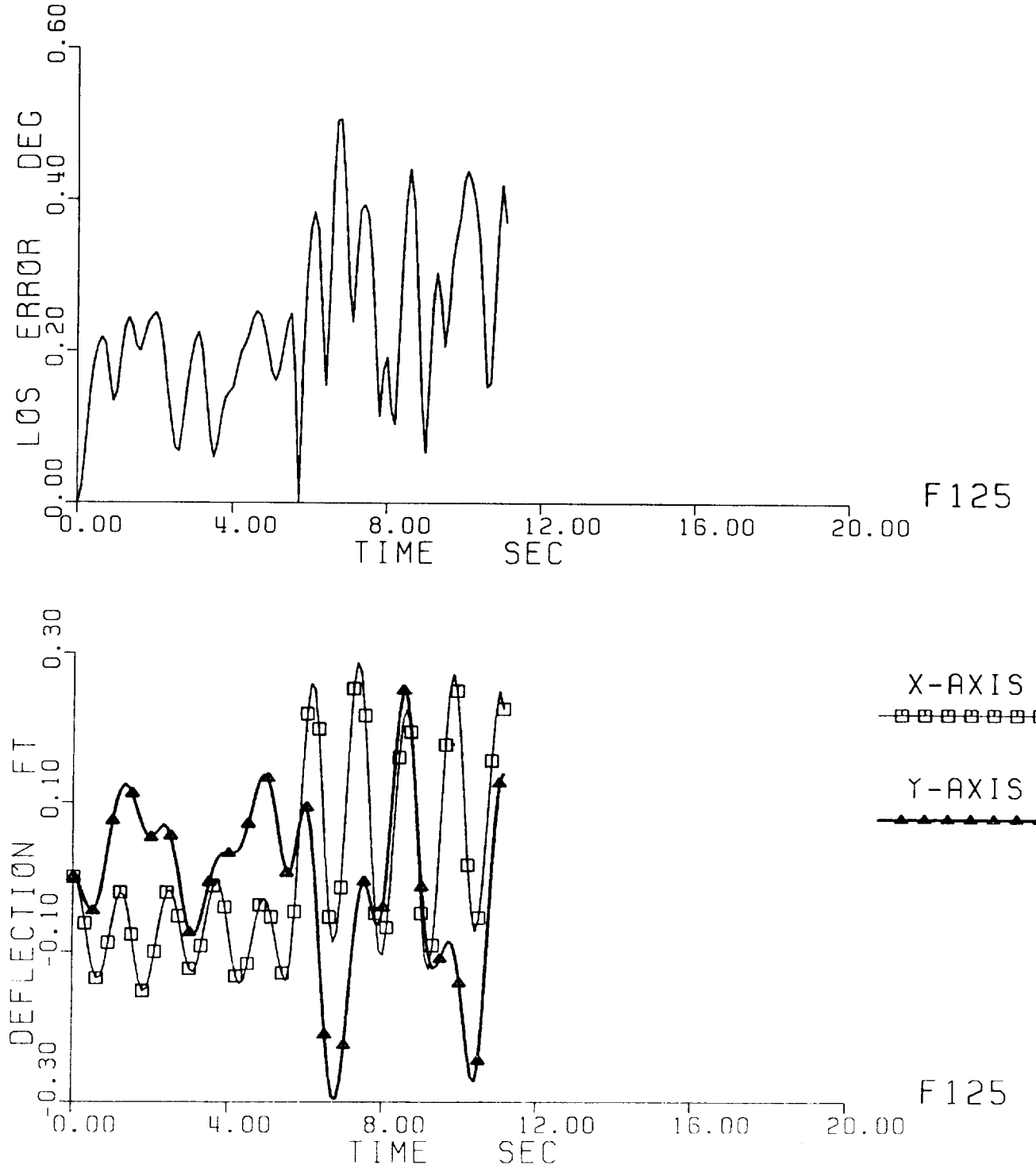

Fig. 3-4 Vibratory responses to Rapid Time-minimized Bang-Bang Slew: 25 lb;
a. Line-of-sight error and Mast tip deflection.

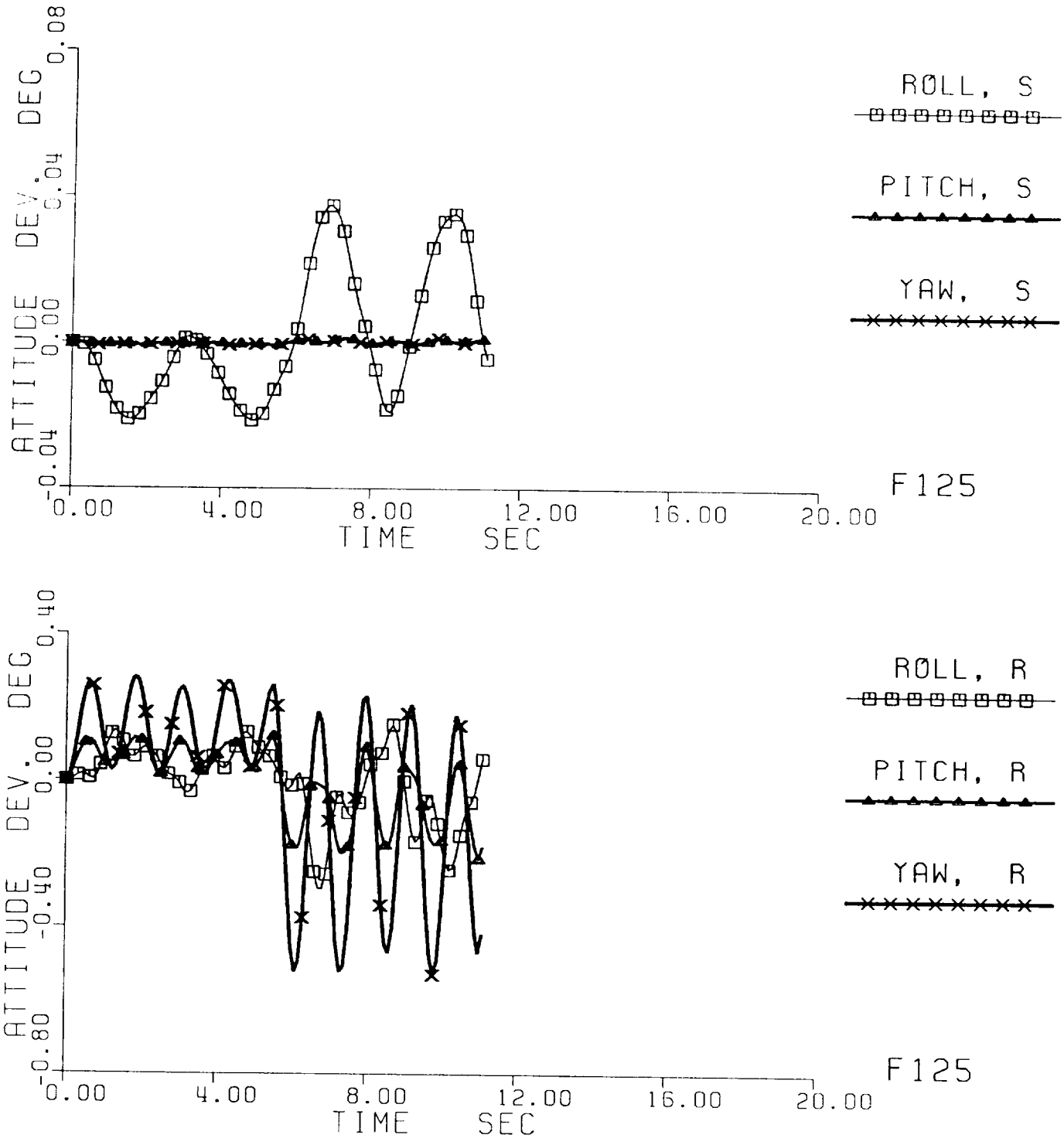

Fig. 3-4 Vibratory responses to Rapid Time-minimized Bang-Bang Slew: 25 lb;
b. Attitude deviations at the Shuttle (S) and the Reflector (R) ends.

- USING NO FORCES ON REFLECTOR DOES NOT MEAN LEAST EXCITATION!

- IF LOS ERROR IS THE ONLY CONCERN, STOP USING 800LB FORCE;
  USE 25LB (VERNIER THRUSTER LEVEL) INSTEAD.
  -- BUT TIME IS EQUALLY IMPORTANT!!!

- ADDITIONAL TIME OF VARIOUS LENGTH IS STILL REQUIRED
  FOR DAMPING OUT THE EXCITED VIBRATIONS.

- **VIBRATION CONTROL CHALLENGE:**

CAN EXCESSIVE VIBRATIONS,
SUCH AS EXCITED BY THE 800LB RAPID SLEWING,
BE EFFECTIVELY SUPPRESSED TO A REASONABLE LEVEL
QUICKLY, SAY, IN 5 SEC?

MODAL-DASHPOT DESIGN MD1

PART 1: LINEAR VELOCITY FEEDBACK

$$\begin{bmatrix} U_7 \\ U_8 \end{bmatrix} = - G_{LVR} \begin{bmatrix} Y_{15} \\ Y_{16} \end{bmatrix}$$

$$\begin{bmatrix} U_7 \\ U_8 \end{bmatrix} = F_4 = \begin{bmatrix} \text{APPLIED FORCE ON REFLECTOR IN X-DIRECTION} \\ \text{APPLIED FORCE ON REFLECTOR IN Y-DIRECTION} \end{bmatrix}$$

$$\begin{bmatrix} Y_{15} \\ Y_{16} \end{bmatrix} = \begin{bmatrix} \text{RATE OF XZ-DEFLECTION AT REFLECTOR END} \\ \text{RATE OF YZ-DEFLECTION AT REFLECTOR END} \end{bmatrix}$$

$$G_{LVR} = \begin{bmatrix} .58420630E+01 & .43392044E+00 \\ .42038249E+00 & .69796355E+01 \end{bmatrix}$$

ADDITIONAL DAMPING RATIO DESIGNED = 0.6737, MODE 2
= 0.6, MODE 1

2% SETTLING TIME OF 3 SEC IS DESIGNED FOR MODE 2

MODAL-DASHPOT DESIGN MD1

PART 2: ANGULAR VELOCITY FEEDBACK

$$\begin{bmatrix} U_4 \\ U_5 \\ U_6 \end{bmatrix} = - G_{AVR} \begin{bmatrix} Y_{10} \\ Y_{11} \\ Y_{12} \end{bmatrix}$$

$$\begin{bmatrix} U_4 \\ U_5 \\ U_6 \end{bmatrix} = M_4 = \begin{bmatrix} \text{APPLIED MOMENT ON REFLECTOR ABOUT X-AXIS} \\ \text{APPLIED MOMENT ON REFLECTOR ABOUT Y-AXIS} \\ \text{APPLIED MOMENT ON REFLECTOR ABOUT Z-AXIS} \end{bmatrix}$$

$$\begin{bmatrix} Y_{10} \\ Y_{11} \\ Y_{12} \end{bmatrix} = \begin{bmatrix} \text{RATE OF REFLECTOR ROLL ATTITUDE DEVIATION} \\ \text{RATE OF REFLECTOR PITCH ATTITUDE DEVIATION} \\ \text{RATE OF REFLECTOR YAW ATTITUDE DEVIATION} \end{bmatrix}$$

$$G_{AVR} = \begin{bmatrix} .24172707E+04 & .16653096E+03 & .45158162E+03 \\ .15734103E+03 & .21781213E+04 & -.72768193E+03 \\ .13433660E+04 & -.22055215E+04 & .42951681E+04 \end{bmatrix}$$

ADDITIONAL DAMPING RATIO DESIGNED = 0.03, MODES 3,4,5

INHERENT DAMPING RATIO ASSUMED = 0.003 ALL MODES

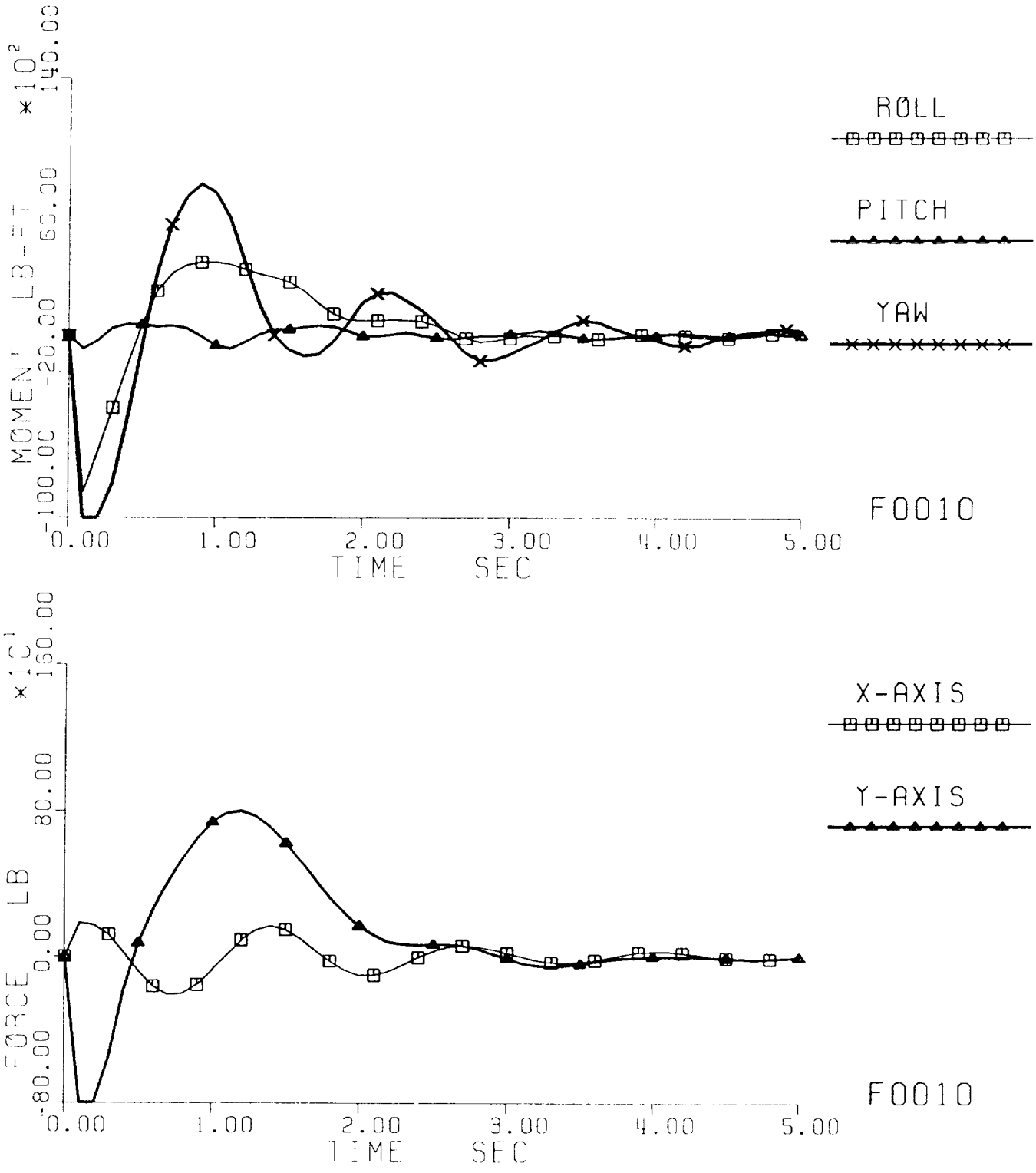

Fig. 6-1 Simulation results of vibration control design MD1;
a. Histories of applied moments and forces at the Reflector.

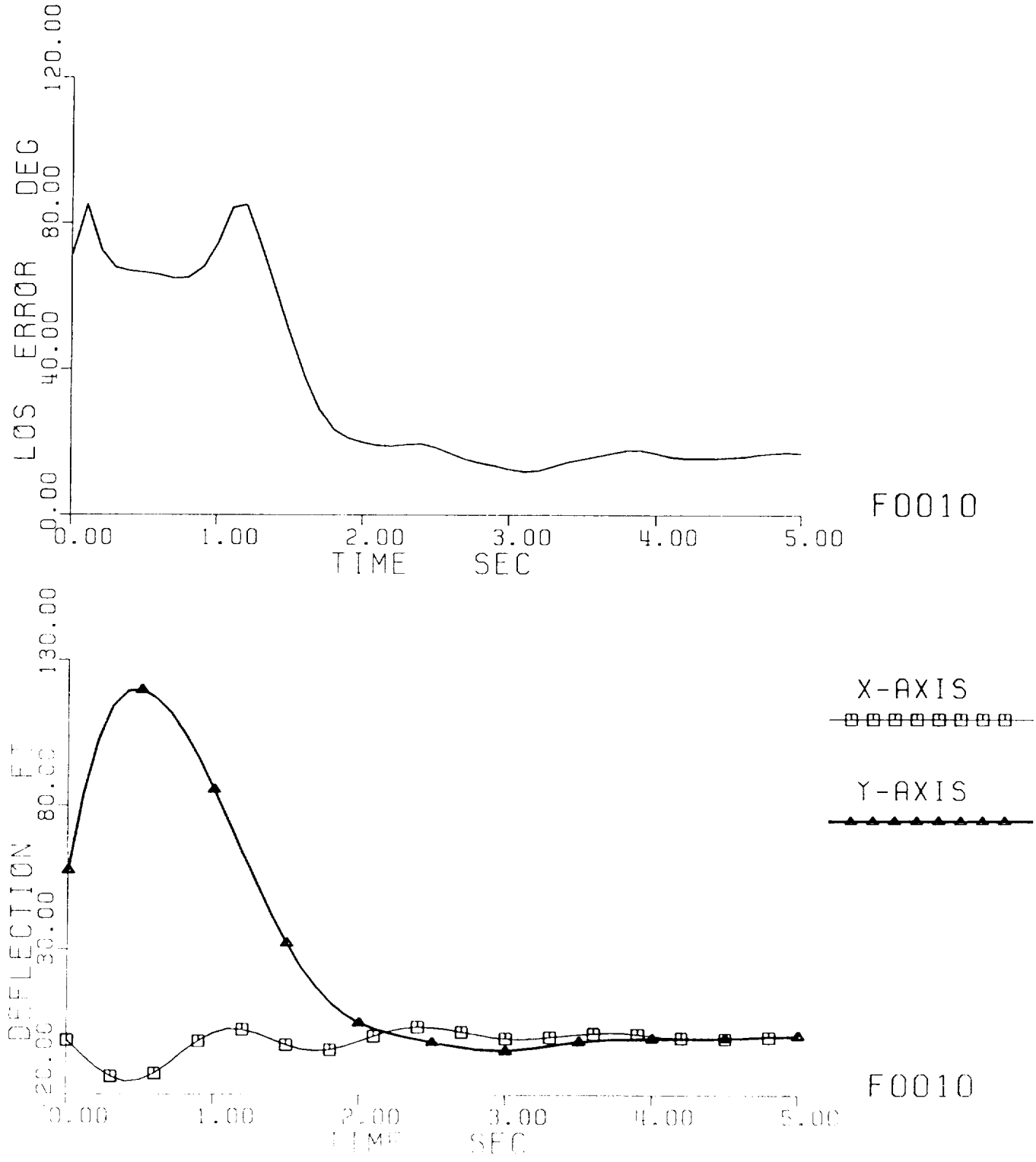

Fig. 6-1 Simulation results of vibration control design MD1;
b. Histories of line-of-sight error and Mast tip deflection.

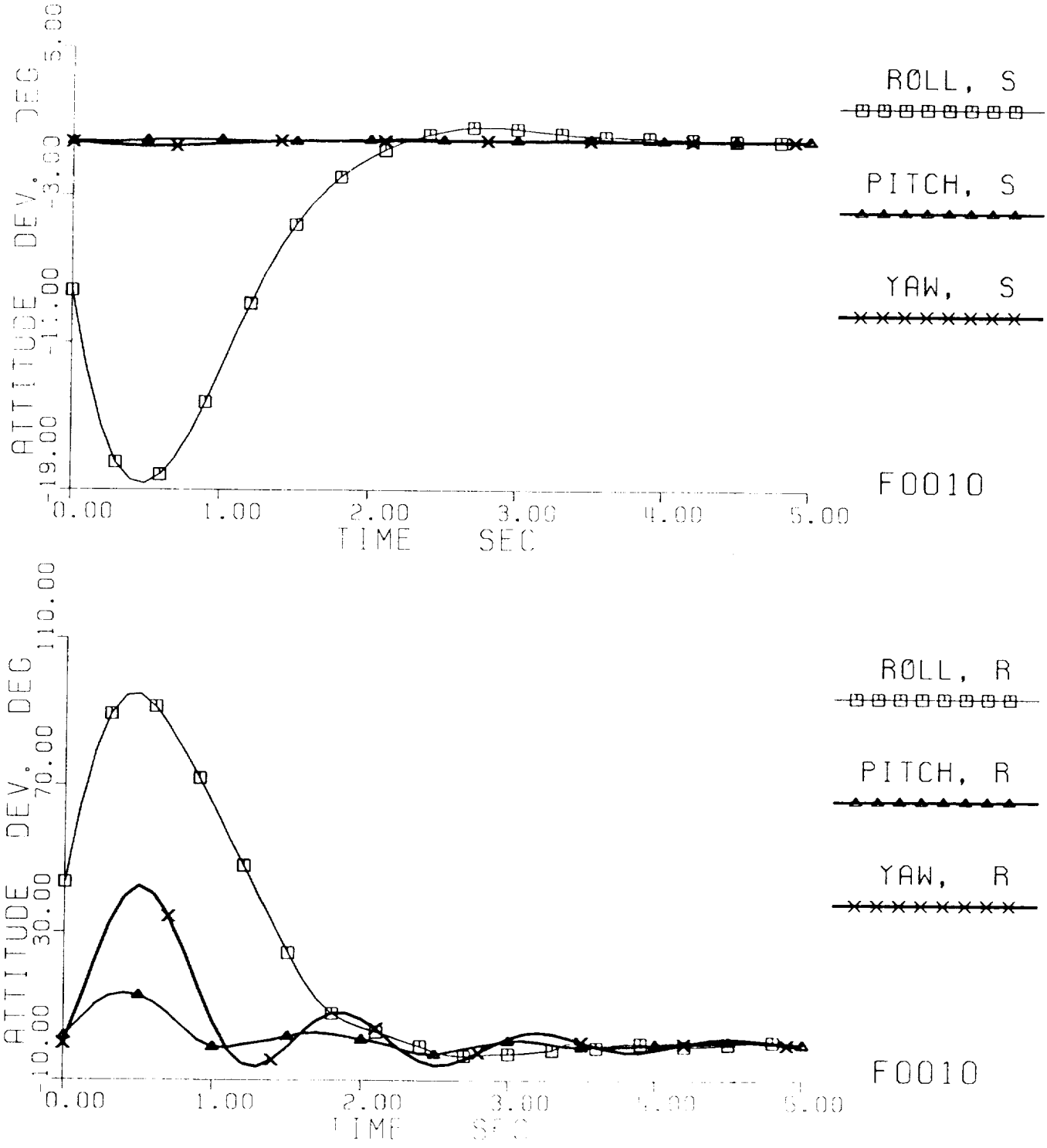

Fig. 6-1 Simulation results of vibration control design MD1;
c. Histories of attitude deviations at Shuttle (S) and Reflector (R) ends

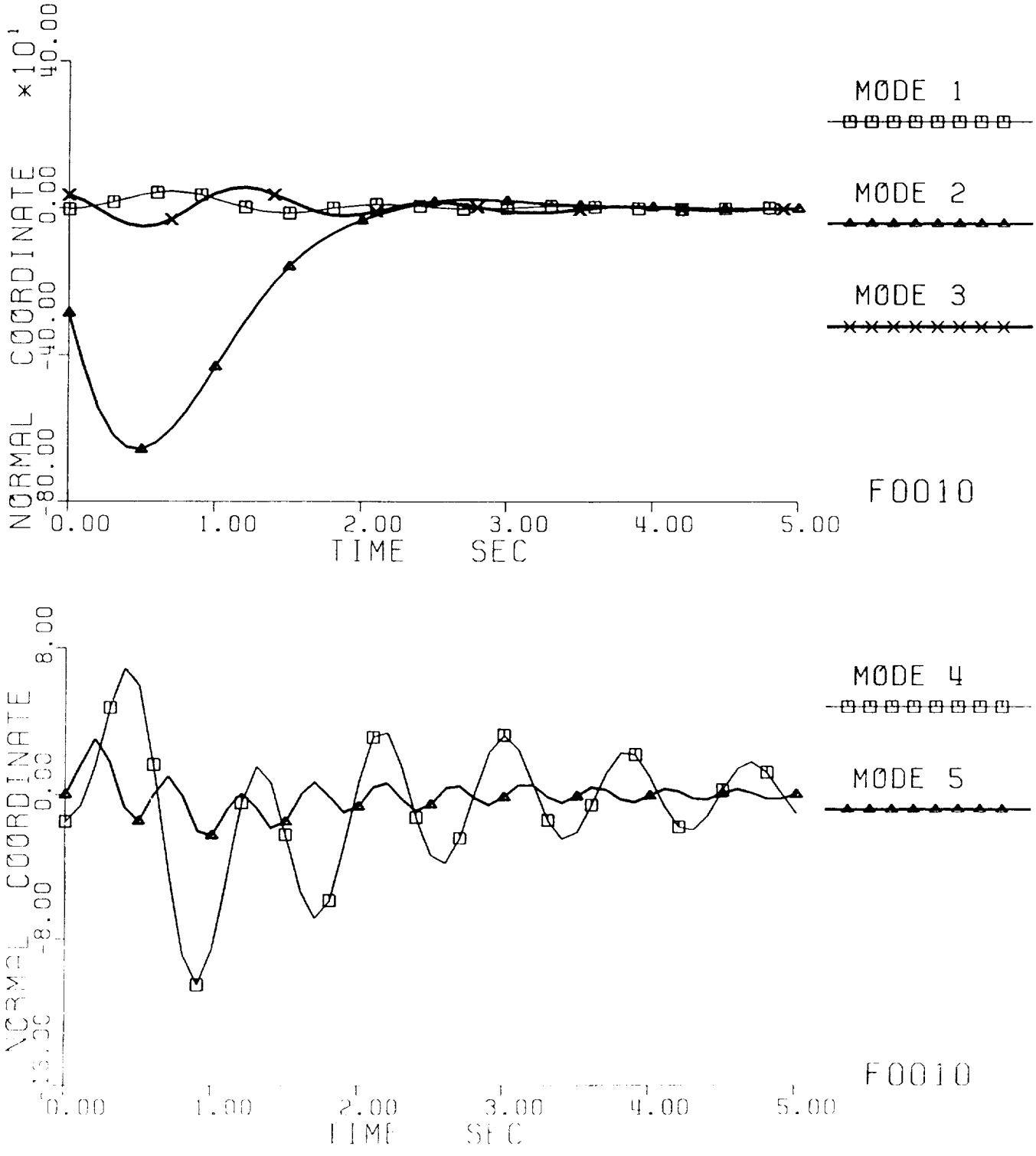

Fig. 6-1 Simulation results of vibration control design MD1;
d. Histories of normal coordinates of the 10 modes.

SUMMARY -- MD1

LOS ERROR $< 18.46^{0}$ $T = 2.5$ SEC

$< 17.46^{0}$ $T > 2.5$ SEC

$\doteq 11.79^{0}$ $T = 3.1$ SEC

DEFLECTION $\leq \pm 5$ FT $T \doteq 2$ SEC

$\leq \pm 0.5$ FT $T = 4.2$ SEC

2% SETTLING TIME $\leq$ 2.9 SEC

LAST PEAK REFLECTOR ATTITUDE DEVIATION:

ROLL $\doteq 0.460^{0}$

PITCH $\doteq 0.546^{0}$

YAW $\doteq 1.360^{0}$

SUMMARY -- MD1A

ADDITIONAL DAMPING RATIO RE-DESIGNED = 0.6, MODE 2
CORRESPONDING 2% SETTLING TIME FOR MODE 2 IS 3.38 SEC

$$G_{LVR} = \begin{bmatrix} .58420557E+01 & .45784262E+00 \\ .42061494E+00 & .62209375E+01 \end{bmatrix}$$

LOS ERROR $\leq$ 16.66° (↓) T $\geq$ 1.8 SEC

$\doteq$ 9.57° (↓) T = 3.1 SEC

DEFLECTION $\leq \pm$ 7.35 FT (↑) T = 1.3 SEC

$\leq \pm$ 0.75 FT (↑) T = 3.7 SEC

2% SETTLING TIME $\doteq$ 3 SEC

LAST PEAK REFLECTOR ATTITUDE DEVIATION:

ROLL $\doteq$ 0.714° (↑)

PITCH $\doteq$ 0.582°

YAW $\doteq$ 1.399°

COMMENTS

- THE MODAL DASHPOT DESIGN MET THE VIBRATION CONTROL CHALLENGE FAIRLY WELL: **EFFECTIVE, FAST SUPPRESSION OF EXCESSIVE VIBRATIONS**

- FOR COMPLETE SUPPRESSION AND PRECISION POINTING AFTER THE QUICK SUPPRESSION,
  EITHER: INCREASE THE MODAL DASHPOT FEEDBACK GAINS
  OR: SWITCH TO INTEGRATED DESIGN OF **LQG/LTR AND MODAL DASHPOTS**

- DIRECT VELOCITY OUTPUT FEEDBACK CONTROLLERS NEED NOT BE OF "LOW AUTHORITY", LOW PERFORMANCE.
  -- ADDITIONAL DAMPING RATIO CAN BE DESIGNED TO BE AS HIGH AS TO THE OPTIMAL VALUE 0.707, IF NEACESSARY; INSTEAD OF RESTRICTING TO ONLY ABOUT 0.1

- NO MORE HIGH-GAIN PROBLEMS OF ORIGINAL CANAVIN DEDIGN

- SPILLOVER IS MINIMAL: PERFORMANCE DEGRADATION UN-NOTICEABLE
  SPILLOVER IS BENEFICIAL: CONCOMITANT ACTIVE DAMPING OF UNMODELED MODES

- SYSTEMATIC DESIGN METHOD FOR MODAL DASHPOTS WORKS!

CONCLUSIONS

- 2-STAGE APPROACH IS FEASIBLE AND PROMISING FOR RAPID SLEWING AND PRECISION POINTING OF SCOLE

- NOT ALL BANG-BANG TYPE OF TIME-MINIMIZED SLEW MANEUVERS WILL EXCITE LARGE STRUCTURAL VIBRATIONS IN SCOLE

- MODAL DASHPOTS CAN BE A CONCENTRATED HIGH-POWER VIBRATION CONTROL, AS WELL AS THE USUAL DIFFUSE ("BROAD-BAND"), LOW-POWER ("LOW-AUTHORITY") CONTROL

RECOMMENDATIONS

- LIMIT THE MAGNITUDE OF APPLIED FORCES ON REFLECTOR TO
  EITHER 25 LB
  -- LEVEL OF VERNIER THRUSTERS ON THE REAL SPACE SHUTTLE
  OR 150 LB
  -- LEVEL EQUIVALENT TO THE COLD-GAS JETS OF LABORATORY SCOLE

- TO COMPLETE STAGE 2, ADD AN INTEGRATED DESIGN OF
  LQG/LTR (LINEAR-QUADRATIC-GAUSSIAN/LOOP-TRANSFER-RECOVERY)
  AND **MODAL DASHPOTS**

- VALIDATE THE 2-STAGE APPROACH USING THE SCOLE LABORATORY FACILITY WITH A COMPREHENSIVE SEQUENCE OF INTEGRATED DESIGNS AND EXPERIMENTS COUPLING NONLINEAR RIGID-BODY MOTIONS WITH FLEXIBLE-BODY DYNAMICS

PLACING DYNAMIC SENSORS AND ACTUATORS ON FLEXIBLE SPACE STRUCTURES

Gregory A. Norris and Robert E. Skelton

Purdue University

ABSTRACT

Input/Output Cost Analysis involves decompositions of the quadratic cost function into contributions from each stochastic input and each weighted output. In the past, these suboptimal cost decomposition methods of sensor and actuator selection (SAS) have been used to locate perfect (infinite bandwidth) sensors and actuators on large scale systems. This paper extends these ideas to the more practical case of imperfect actuators and sensors with dynamics of their own. NASA's SCOLE examples demonstrate that *sensor and actuator dynamics affect the optimal selection and placement of sensors and actuators.*

1.0 INTRODUCTION

The objective of this paper is to develop and evaluate a method for the selection of sensors and actuators in the control of finite-dimensional linear systems using imperfect sensors and actuators -- devices which do not provide instantaneous responses, but have nontrivial dynamics of their own. In addition, the plant noise and the measurement noise is assumed correlated. This important case allows the use of accelerometers as sensors (this always yields correlated plant and measurement noise). Application of the generalized method to practical control problems demonstrates that correlatedness of the noise and the dynamics of the actuator and sensor devices can significantly affect the optimal selection of both the number and location of sensors and actuators.

Consider as a starting point the following familiar dynamic system model:

$$\dot{x}_p = A_p x_p(t) + B_p[f(t) + w(t)] \tag{1.1a}$$

$$y_p(t) = C_p x_p(t)\ ,\ z(t) = M_p x_p(t) + v(t) \tag{1.1b}$$

$$E\{w(t)w^T(\tau)\} = \delta(t-\tau)W\ ,\ E\{v(t)v^T(\tau)\} = \delta(t-\tau)V\ ,\ E\{w(t)v^T(\tau)\} = \delta(t-\tau)U \tag{1.1c}$$

where $x_p \in R^{n_x}$, $f \in R^{n_u}$, $w \in R^{n_w}$, $z,v, \in R^{n_z}$ and (A_p,C_p) observable, (A_p,B_p) controllable and (A_p,M_p) detectable. The vectors w(t) and v(t) are respectively zero mean white noise characterizations of the actuator and sensor noise.

In control of large space structures, the locations of sensors and actuators becomes a critically significant "degree of freedom" in control design [14, 20]. Among over 60 more recent contributions to the SAS problem, only [4], [7], [10], [11], and [12] consider noisy actuators (W, V nonzero). In all cases, the disturbances are modelled as Gaussian, white, and *uncorrelated* (W, V diagonal, U = 0). Most of the SAS literature takes no account of *actuator or sensor dynamics*. Two exceptions are McClamrock [19], and Howell and Baxter, [6]. In [1] the authors extend the cost decomposition approach [2] to

accommodate noise correlation between sensor and actuator noise sources (W, V not diagonal, $U \neq 0$). A key conclusion in [1] is that the proper sensor/actuator selection and placement can be drastically affected by noise correlation. For example, the deletion of a noise source (by making an actuator or sensor noise free) may *degrade* performance contrary to the usual expectations when noise sources are uncorrelated.

Very fast actuator dynamics may be neglected in stability considerations, [9]. A more thorough discussion of the effect of *actuator dynamics* is given by Goh and Caughey [8]. The analysis of [8] and [9] demonstrates that plant frequencies occurring above the actuator bandwidth can lead to closed loop instability, even for co-located sensors and actuators. Goh and Caughey *do not* address the problem of *selection* of dynamic actuators. That is the goal of this paper.

This paper is organized as follows. First the system model is augmented to include sensor and actuator dynamics. The closed-loop input and output costs are then developed for the fully augmented system, and they are used to define expressions which reflect the effectiveness of each *dynamic* actuator or sensor in minimizing the cost function. Finally, the method is illustrated by application both to small scale numerical examples and to NASA's SCOLE flexible space structure model. It is found that in the selection of noisy actuators and sensors, finite dynamics can *significantly* affect selection results.

2.0 MODELING DYNAMIC ACTUATORS AND SENSORS

In [2] the results of Closed-Loop Input/Output Cost Analysis (CIOCA) were developed and applied to the Sensor and Actuator Selection problem (SAS) for systems of the form (1.1) under closed-loop control. In [1] the control f(t) is the vector of optimal state estimate feedback controls:

$$f(t) = Gx_c(t)\ ,\ G = -R^{-1}B_p^T K. \tag{2.1a}$$

$$\dot{x}_c = A_p x_c(t) + B_p f(t) + F[z(t) - M_p x_c(t)]\ ,\ F = [PM_p^T + B_p U]V^{-1}\ , \tag{2.1b}$$

$$0 = KA_p + A_p^T K - KB_p R^{-1} B_p^T K + C_p^T Q C_p \tag{2.2a}$$

$$0 = [A_p - B_p U V^{-1} M_p]P + P[A_p - B_p U V^{-1} M_p]^T - PM_p^T V^{-1} M_p P \tag{2.2b}$$

$$+ B_p W B_p^T - B_p U V^{-1} U^T B_p^T$$

which minimizes the cost function

$$V = E_\infty\{\|y_p(t)\|^2 Q + \|u(t)\|^2 R\}\ ,\ E_\infty \triangleq \lim_{t\to\infty} E[\cdot] \tag{2.3}$$

where $x_c \in R^{n_x}$ is the vector of state estimates. The conclusion from [1] for this problem (1.1), (2.1) (2.2) is that when $U \neq 0$, the sensor/actuator selection results can be drastically different.

2.1 Adding Actuator Dynamics

First the system (1.1) is augmented to include stable, observable, controllable actuator dynamics of arbitrary order.

$$\dot{x}_a = A_a x_a + B_a(u+w_u)\ ,\ (A_a,B_a) \text{ controllable} \tag{2.4a}$$

$$f = C_a x_a,\ (A_a,C_a) \text{ observable},\ x_a \in R^{n_a},\ f \in R^{n_a} \tag{2.4b}$$

Figure 2.1 presents schematic representations for actuator models of varying degrees of complexity; Figure 2.1a represents the non-dynamic actuator, while Figure 2.1b represents the general model for a dynamic actuator with white noise. Note that for the non-dynamic actuator the noise w(t) is purely additive with the input u(t). In the case of dynamic actuators the analyst may consider the actuator's output (into the system) to

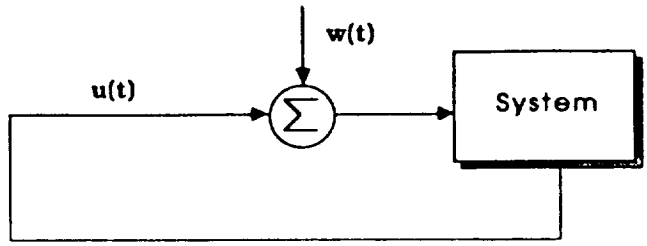

Figure 2.1a

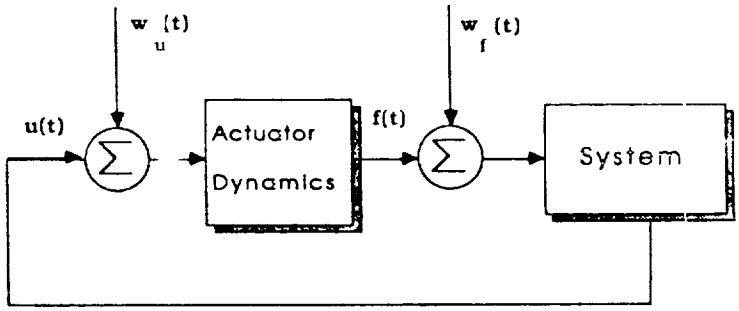

Figure 2.1b

Figure 2.1: Actuator Models

include additive actuator output noise $w_f(t)$, or actuator command noise $w_u(t)$ which is filtered by the dynamics of the actuator, or both. Both types of noise are assumed possible in our development.

Augmenting the system states x_p of the original system (2.1) with a vector of actuator states x_a, we obtain:

$$\dot{x} = Ax + Bu + Dw\,,\quad y = Cx\,,\quad z = Mx + v = z_p \tag{2.5a}$$

$$x = \begin{bmatrix} x_p \\ x_a \end{bmatrix},\ y = \begin{bmatrix} y_p \\ f \end{bmatrix},\ w = \begin{bmatrix} w_f \\ w_u \end{bmatrix},\ A = \begin{bmatrix} A_p & B_pC_a \\ 0 & A_a \end{bmatrix},\ D = \begin{bmatrix} B_p & 0 \\ 0 & B_a \end{bmatrix},$$

$$W = \begin{bmatrix} W_f & U_{fu} \\ U_{fu}^* & W_u \end{bmatrix},\ C = \begin{bmatrix} c_p & 0 \\ 0 & C_a \end{bmatrix},\ B = \begin{bmatrix} 0 \\ B_a \end{bmatrix},\ M^T = \begin{bmatrix} M_p^T \\ 0 \end{bmatrix}$$

where $f = C_a x_a$, (A_a, C_a) is observable, and $Re\left[\lambda_i(A_a)\right] < 0$, $\quad i = 1, 2, \cdots n_a$. (A_a, B_a) is controllable.

First note that since x_p is observable from y_p, (i.e., (A_p, C_p) is observable) and x_a is observable from f (i.e., (A_a, C_a) is observable) then from the definitions (2.5) x must be observable from y, that is:

$$(A,C) \text{ is observable} \tag{2.6a}$$

Also note that the actuator dynamics are assumed stable, so that the system (2.1) has not been augmented with any unstable states. Therefore, detectability of (A_p, M_p) together with stable A_a yields

$$(A,M) \text{ detectable.} \tag{2.6b}$$

Finally, Theorem 1 states the conditions for controllability of the system (2.1) augmented with actuator dynamics (2.5). Proof of the theorem is contained in the Appendix.

Theorem 1

Consider the controllable system

$$\dot{x}_p = A_p x_p + B_p(f+w_f)\,, \quad (A_p,B_p) \text{ controllable} \tag{2.7a}$$

$$x_p \in R^{nx_p} \tag{2.7b}$$

augmented with controllable and observable actuator dynamics of arbitrary order

$$\dot{x}_a = A_a x_a + B_a(u+w_u)\,, \quad (A_a,B_a) \text{ controllable} \tag{2.7c}$$

$$f = C_a x_a, \quad (A_a,C_a) \text{ observable}, \quad x_a \in R^{nx_a}, \quad f \in R^{nu} \tag{2.7d}$$

to form the composite system

$$\dot{x} = Ax + Dw + Bu \tag{2.7e}$$

$$A = \begin{bmatrix} A_p & B_pC_a \\ 0 & A_a \end{bmatrix}\,, \quad D = \begin{bmatrix} B_p & 0 \\ 0 & B_a \end{bmatrix}\,, \quad B = \begin{bmatrix} 0 \\ B_a \end{bmatrix}\,, \quad x = \begin{bmatrix} x_p \\ x_a \end{bmatrix}\,, \quad w = \begin{bmatrix} w_f \\ w_u \end{bmatrix} \tag{2.7f}$$

The system states x_p *are controllable from* u(t) *if the number of poles minus the number of zeros is the same for each individual actuator's transfer function.*

Remark 1: Note that full controllability of the augmented-system state vector x is not guaranteed under the conditions of the theorem.

Remark 2: The conditions of the theorem are always met for first order dynamic actuators, (assuming no direct input/output "feedthrough" for the actuators), since each actuator will have one pole and no zeros.

Remark 3: As long as the original system states x_p are controllable through some minimum set of actuators meeting the criteria of the theorem above, then controllability of x_p will be maintained with the *addition* of actuators of *any order and any number of transfer zeros.*

Remark 4: Finally, note that the usefulness of the theorem stems from the fact that by meeting certain *mildly* restrictive conditions, the actuator dynamics can be guaranteed not to destroy controllability of the original system states, *regardless of the pole/zero locations of the plant.*

2.2 Adding Sensor Dynamics

Next the system (2.5) is augmented to include stable, observable, controllable sensor dynamics of arbitrary order.

$$\dot{x}_s = A_s x_s + B_s(M_p x_p + v_{in}), \quad (A_s, B_s) \text{ controllable} \tag{2.8a}$$

$$z = C_s x_s + v_{out}, \quad (A_s, C_s) \text{ is observable}, \quad x_s \in R^{n_s} \tag{2.8b}$$

$$Re[\lambda_i(A_s)] < 0, \quad i = \{1, 2, \cdots n_s\} \tag{2.8c}$$

Figure 2.2 presents schematic representations for actuator models of varying degrees of complexity; Figure 2.2a represents the non-dynamic sensor, while Figure 2.2b represents the general model for a dynamic sensor with white noise. Note from both eqn (2.8) and Figure 2.2b that (similarly to the case of actuator dynamics), adding sensor dynamics leads to the possibility of both sensor input noise and sensor output noise. The i_{th} sensor's input noise $(v_{in})_i$ is filtered by the dynamics of the i_{th} sensor, while the output noise $(v_{out})_i$ is purely additive with the sensor output. Both types of noise are assumed possible in our development.

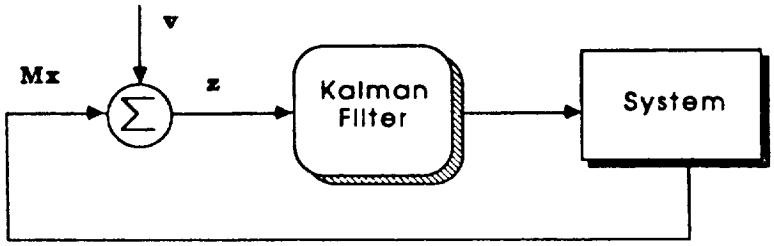

Figure 2.2a

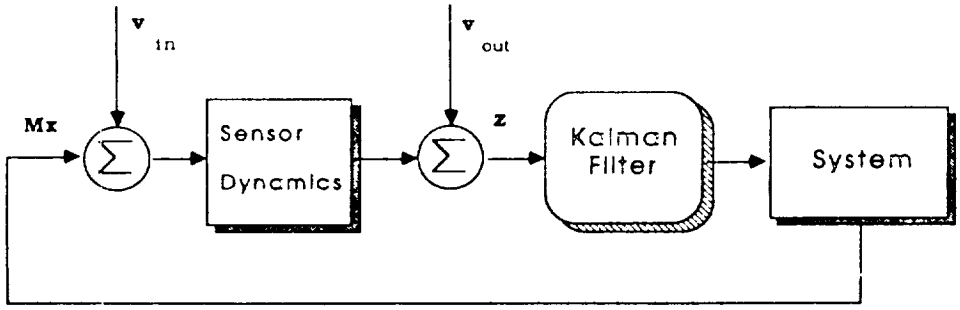

Figure 2.2b

Figure 2.2: Sensor Models

The fully augmented system equations have the following form:

$$\dot{x} = Ax + Bu + Dw \tag{2.9a}$$

$$y = Cx \tag{2.9b}$$

$$z = Mx + v \tag{2.9c}$$

$$x^T = [x_p^T, x_a^T, x_s^T], \quad y^T = [y_p^T, f^T], \quad w^T = [w_f^T, w_u^T, v_{in}^T], \quad v = v_{out}$$

$$D = \begin{bmatrix} B_p & 0 & 0 \\ 0 & B_a & 0 \\ 0 & 0 & B_s \end{bmatrix}, \quad A = \begin{bmatrix} A_p & B_pC_a & 0 \\ 0 & A_a & 0 \\ B_sM_p & 0 & A_s \end{bmatrix}, \quad C = \begin{bmatrix} C_p & 0 & 0 \\ 0 & C_a & 0 \end{bmatrix} \text{ or } C = [C\ 0]$$

$$B = \begin{bmatrix} 0 \\ B_a \\ 0 \end{bmatrix}, \quad V = V_{out}, \quad W = \begin{bmatrix} W & U \\ U^* & V_{in} \end{bmatrix}, \quad M = [0\ 0\ C_s]$$

The response $y_p(s)$ of the plant to the input f(s) is given by

$$y_p(s) = H_p(s)f(s) \tag{2.10a}$$

where

$$H_p(s) = C_p(sI - A_p)^{-1}B_p. \tag{2.10b}$$

is the plant transfer function. The response Mx(s) of the actuator/plant system (2.9) to the input u(s) is given by

$$Mx(s) = H(s)u(s), \tag{2.11a}$$

where

$$H(s) = M(sI - A)^{-1}B. \tag{2.11b}$$

Finally, the response z(s) of the sensors to an input Mx(s) is given by

$$z(s) = H_s(s)Mx(s)\,, \tag{2.12a}$$

where

$$H_s(s) = C_s(sI - A_s)^{-1}B_s \tag{2.12b}$$

is the transfer function for the sensor dynamics. Minimal systems are controllable and observable. Thus, given minimality of the plant/actuator system [(A,B) controllable and (A,M) observable], then measurability of the full augmented system is guaranteed [(A, M) observable] if there are no pole/zero cancellations between H(s) and $H_s(s)$.

2.3 Defining the Cost Function

With the properties of the augmented system established, optimal control design for the augmented system is now considered. Recall that the standard LQG cost function (2.3) for the unaugmented system (2.1) includes a penalty on the output regulation error y(t), as well as a penalty on the control energy u(t). However, in the augmented system (2.5), while the actuator *command* is given by u(t), the actuator *response* f(t) (contained in the augmented output vector y) is distinct from u(t) due to actuator dynamics. A true measure of control energy is more appropriately stated in terms of a weighted sum of the variances of f(t) rather than of u(t). It can readily be shown, however, that even in the presence of a weighting on the actuator outputs, f(t), some nonzero weighting on the actuator inputs u(t) is necessary to avoid an infinite gain solution to the optimization problem. For this reason, and in view of the relation of f(t) to the design goals as discussed above, minimization of cost functions of the form

$$V = E_\infty \left[\|y(t)\|_Q^2 + \|u(t)\|_R^2 \right] \tag{2.13}$$

and

$$Q = \text{diag}[Q_o, Q_a], \quad Q > 0 \tag{2.14}$$

provides a stable optimal closed-loop solution.

3.0 SELECTION OF DYNAMIC SENSORS AND ACTUATORS

3.1 Closed-Loop Input/Output Cost Analysis

In order to write the expressions for the closed-loop input and output costs, it is first necessary to put the fully augmented system, under closed loop steady-state optimal state-estimate feedback control, in the following state space form:

$$\dot{\mathbf{x}}(t) = \mathbf{A}\mathbf{x}(t) + \mathbf{D}w(t) \tag{3.1a}$$

$$\mathbf{y}(t) = \mathbf{C}x(t) \tag{3.1b}$$

$$V = E_\infty V_o(t),\ V_o(t) = \mathbf{y}^*(t)\mathbf{Q}\mathbf{y}(t)\,, \tag{3.1c}$$

where

$$\mathbf{x}^T = [x^T, x_c^T],\quad \mathbf{y}^T = [y]^T \quad \mathbf{w}^T = [w^T, v^T] \tag{3.1d}$$

$$\mathbf{A} = \begin{bmatrix} A & BG \\ FM & A+BG-FM \end{bmatrix},\ \mathbf{D} = \begin{bmatrix} D & 0 \\ 0 & F \end{bmatrix},\ \mathbf{C} = \begin{bmatrix} C & 0 \\ 0 & G \end{bmatrix},\ \mathbf{Q} = \begin{bmatrix} Q & 0 \\ 0 & R \end{bmatrix},\ \mathbf{W} = \begin{bmatrix} W & U \\ U^* & V \end{bmatrix} \tag{3.1e}$$

$$G = -R^{-1}B^TK,\ 0 = KA + A^TK - KBR^{-1}B^TK + C^TQC \tag{3.1f}$$

$$F = [PM^T + DU]V^{-1},\ 0 = [A - DUV^{-1}M]P + P[A - DUV^{-1}M]^T \tag{3.1g}$$

$$-PM^TV^{-1}MP + DWD^T - DUV^{-1}U^TD^T$$

For the system (3.1) the output costs V_t^y, defined by

$$V_i^y = (1/2)\{E_\infty(\partial V_o/\partial y_i)y_i\} \tag{3.2a}$$

are calculated as follows [2]

$$V_i^y = [CXC^TQ]_{ii} \tag{3.2b}$$

where X is the steady state covariance satisfying

$$0 = AX + XA^T + DWD^T \tag{3.2c}$$

and where the output costs satisfy the cost decomposition property

$$\sum_{i=1}^{n_y} V_i^y = V \ . \tag{3.2d}$$

The input costs are defined by

$$V_i^w = (1/2)\{E_\infty(\partial V_o/\partial w_i)w_i\} \tag{3.3a}$$

and are found from [2]

$$V_i^w = [D^TSDW]_{ii} \tag{3.3b}$$

where S satisfies

$$0 = A^TS + SA + C^TQC \tag{3.3c}$$

and where the input costs also satisfy the cost decomposition property

$$\sum^{n_w} V_i^w = V \ . \tag{3.3d}$$

The input and output costs represent the *in situ* contributions that the noise inputs and the system outputs make in the cost function. We may also wish to know the amount by which the cost function will be reduced if a noise input is eliminated. This amount, ΔV_i^w, is defined as

$$\Delta V_i^w = V - V_{Ri} \tag{3.4}$$

where V_{Ri} is the value of the cost function after the i_{th} *noise input* is eliminated, (but the controller is not redesigned) and ΔV_i^w is the cost reduction due to eliminating w_i. A positive value for ΔV_i^w indicates that elimination of the i_{th} input will *reduce* the cost, while negative ΔV_i^w indicates that a cost *increase* will follow noise elimination. It was shown in [1] that the ΔV_i^w may be positive or negative in the presence of noise correlation. Partitioning the matrices W and D facilitates direct solution for the cost reduction [2], yielding

$$\Delta V_i^w = 2V_i^w - d_i^* S d_i W_{ii} . \tag{3.5}$$

The closed-loop covariance X may be written

$$X = \begin{bmatrix} P+N & N \\ N & N \end{bmatrix} \tag{3.6}$$

where P satisfies eqn (3.1g) and where N satisfies:

$$0 = N(A+BG)^T + (A+BG)N + FVF^T \tag{3.7}$$

Also, S has the following form

$$S = \begin{bmatrix} K+L & -L \\ -L & L \end{bmatrix} \tag{3.8}$$

where K satisfies eqn (3.1f) and where L satisfies

$$0 = L(A-FM) + (A-FM)^T L + G^T R G \tag{3.9}$$

For notational convenience the steady state covariance X is partitioned as follows:

$$X = [P+N] = \begin{bmatrix} X_p & X_{12} & X_{13} \\ X_{12}^T & X_a & X_{23} \\ X_{13}^T & X_{23}^T & X_S \end{bmatrix} \tag{3.10}$$

Using the notation of (3.10) and the special structure of the closed-loop system matrices in eqn (3.13) we write the following expressions for the output costs

$$V_i^{y_p} = [C_p X_p C_p^T Q_p]_{ii} \quad i = 1, \cdots ny_p \tag{3.11a}$$

$$V_i^{f} = [C_a X_a C_a^T Q_a]_{ii} \quad i = 1, \cdots nu \tag{3.11b}$$

$$V_i^{u} = [GNG^T R]_{ii} \quad i = 1, nu \tag{3.11c}$$

and for the input costs

$$V_i^{w} = [D^T(K+L)DW]_{ii} \qquad i = 1, \cdots nw \tag{3.12a}$$

$$V_i^{v_{in}} = [D^T(K+L)DW]_{nw+i,nw+i} \quad i = 1, \cdots nz \tag{3.12b}$$

$$V_i^{v_{out}} = [F^T LFV]_{ii} \qquad i = 1, \cdots nz \tag{3.12c}$$

and the input cost reductions

$$\Delta V_i^{w} = [D^T(K+L)DW - D^T LFU^T]_{ii} \qquad i = 1, \cdots nw \tag{3.13a}$$

$$\Delta V_i^{v_{in}} = [D^T(K+L)DW - D^T LFU^T]_{nw+i,nw+i} \quad i = 1, \cdots nz \tag{3.13b}$$

$$\Delta V_i^{v_{out}} = [F^T LFV - F^T LFV - F^T LBU]_{ii}. \quad i = 1, \cdots nz \tag{3.13c}$$

3.2 Dynamic Actuator Effectiveness Values

Now that the closed-loop input and output costs have been determined for systems with dynamic sensors and actuators, it remains to use the CIOCA results to define expressions which reflect the effectiveness of each sensor and actuator in the cost function. This section defines the effectiveness values for dynamic actuators. The approach taken in [1] and [2] for non-dynamic actuators was to subtract the contribution the i_{th} actuator's *noise* in the cost function from the contribution of its *control* signal, and to label this difference the "effectiveness" of the i_{th} actuator, V_i^{act}. That is,

$$V_i^{act} = V_i^u - \Delta V_i^w \tag{3.14}$$

This subtracts the "bad" from the "good" contributions of the actuator to measure its effectiveness. The results of applying (3.14) to sensor and actuator selection for a range of small and large scale examples in [2], [3], [4], [17] and [18] have demonstrated the utility of this approach.

Extending the definition (3.14) for applicability to systems with dynamic actuators, we proceed as follows. In (3.1) there are two noise sources associated with each actuator: command noise, w_u, which is filtered by the actuator dynamics; and output noise, w_f, which is additive with the actuator output. Thus, the noise contribution associated with the i_{th} actuator is given by the sum of $\Delta V_i^{w_u}$ and $\Delta V_i^{w_f}$.

The beneficial control cost for each actuator is not immediately evident. First, recall that *it is the actuator output* f(t), *not its input* u(t), *which drives the system.* Next, note that the contribution of the i_{th} actuator's *output* in the cost function, V_i^f, includes the effects of noise w_{ui}. That is, even in the open loop ($u \equiv 0$), $V_i^f \neq 0$ for $[W_u]_{ii} > 0$ with dynamics. Hence, to define the ***beneficial*** (control) portion of V_i^f it is necessary to subtract the portion of V_i^f which is due to noise. This can not be accomplished exactly,

since the actuator command u(t) and the command noise $w_u(\tau)$ are correlated for $t > \tau$. An approximation is obtained, however, by solving for V_i^f when $u \equiv 0$ (that is, in the open loop). We define the contribution of w_{ui} to V_i^f and the contribution of u_i to V_i^f as follows, using the open loop covariance of the actuator states $\underline{X}_a$:

$$[V_i^f]^w = [C_a \underline{X}_a C_a^T Q_a]_{ii} \tag{3.15a}$$

and

$$[V_i^f]^u = V_i^f - [V_i^f]^w = [C_a(X_a - \underline{X}_a)C_a^T Q_a]_{ii} \tag{3.15b}$$

where $\underline{X}_a$ solves

$$0 = A_a \underline{X}_a + \underline{X}_a A_a^T + B_a W_u B_a^T . \tag{3.15c}$$

Finally, the input costs and the decomposition of the output cost V_i^f are combined in an effectiveness formula for dynamic actuators which is motivated by the results of [1] and [2]:

$$V_i^{act} = [V_i^f]^u - \Delta V_i^{wf} - \Delta V_i^{w_u} . \tag{3.16}$$

Note that in the absence of command input noise, $[V_i^f]^w$ and $V_i^{w_u}$ are both zero. Also, in the absence of actuator dynamics, $f_i(t)$ is equivalent to $u_i(t)$. Thus the expression (3.16) reduces to the original effectiveness formula of [1] in the absence of actuator dynamics. Note also that (3.16) is applicable whether or not the actuator noise signals are correlated with other noise sources, and it is applicable to systems with actuator dynamics of arbitrary order.

3.3 Dynamic Sensor Effectiveness Values

Unlike the actuator noise, (which has a direct path to the output, independently of the conrollers influence) the noise associated with sensors reaches the system only

through the controller. Since the gains in the Kalman filter of the LQG controller represent an optimal trade-off of each sensor's (beneficial) measurement information versus the (performance degrading) impact of its noise, then a ΔV_i^v of large magnitude is indicative of a *highly effective sensor.* That is, the fact that a sensor's noise is being allowed to heavily affect the cost means that its measurement information is even more critical to performance. For this reason, the following effectiveness formula for non-dynamic sensors, generalized to accommodate the possibility of noise correlation, was presented in [1]:

$$V_i^{sen} \triangleq |\Delta V_i^v| \ . \tag{3.17}$$

For dynamic sensors there are two possible noise inputs associated with each sensor. As in the non-dynamic case, both noise inputs reach the system dynamics through the Kalman filter. Thus a straightforward extension of (3.17) to dynamic sensors is

$$V_i^{sen} = |\Delta V_i^{v_{in}}| + |\Delta V_i^{v_{out}}| \ . \tag{3.18}$$

Note that this formula is applicable in the presence of sensor dynamics of arbitrary order, and applies whether or not any of the noise sources are correlated with one another.

This section concludes with the suggestion that (3.16) and (3.18) provide effective measures of the contribution of each actuator and sensor in a closed loop optimal LQG control (with sensor and actuator dynamics properly included).

4.0 SELECTION OF DYNAMIC ACTUATORS FOR SCOLE

In this section the actuator selection problem is solved for a model of NASA's SCOLE (Spacecraft Control Laboratory Experiment) system. The SCOLE configuration consists of a flexible antenna suspended from the Space Shuttle cargo bay by a 130 ft.

flexible beam (see Figure 4.6). The effectiveness values for proof mass actuators (PMA's) located along the beam are calculated and plotted versus position for both dynamic and non-dynamic actuators in order to evaluate the dynamic actuator selection method and to determine the effect of actuator dynamics on our results.

4.1 PROBLEM DEFINITION

A certain 2-dimensional SCOLE model includes four flexible modes and no rigid body modes [15-18]. Approximate open-loop mode shapes for the four flexible modes are presented in Figure 4.7, and the results of an open loop modal cost analysis are presented in Table 4.2. A detailed discussion of the model development is given in [16] and [18]. The two sensors retained in the model (using the CIOCA method of selection for non-dynamic sensors) are angular position and rate measurements located at the center of mass of the reflector [18]. Since there are no accelerometers presents, then the sensor and actuator noise is uncorrelated. Noise intensity data for the sensors is given in Table 4.3.

The set of admissible actuators includes both a control moment gyro (CMG) located at the reflector center of mass and a set of PMAs distributed along the flexible beam. The actuator selection problem is to determine the optimal location for two PMA devices along the beam. To this end, the admissible set of PMAs was defined as 20 actuators spaced at distances of 6.25 feet apart on the 130-foot beam from a point 10.75 feet above the shuttle end of the beam to a point 129.5 feet from the shuttle. The PMA locations are

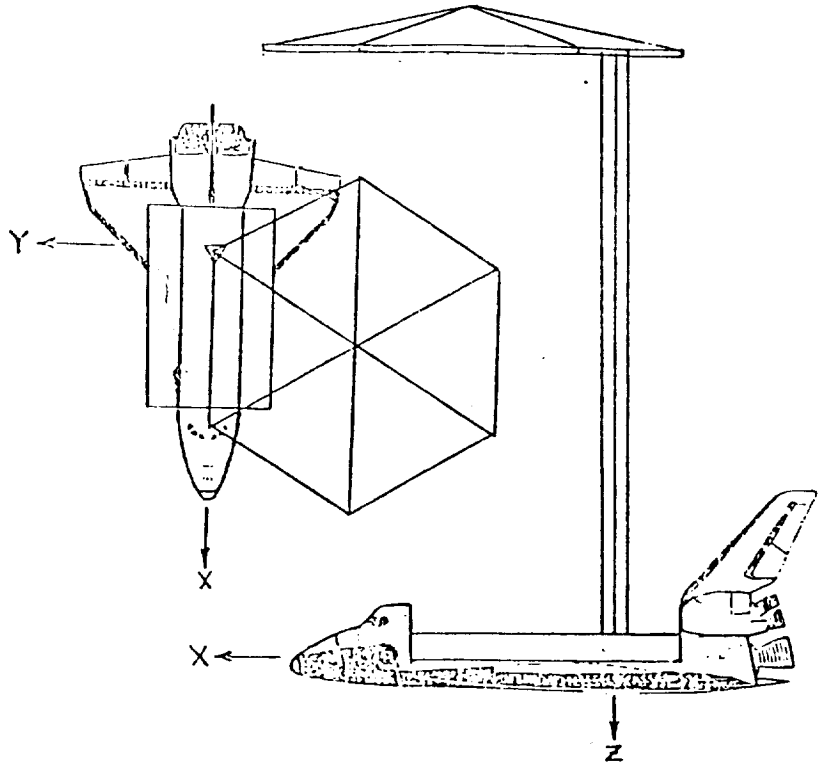

Figure 1.3: SCOLE Configuration

4.6

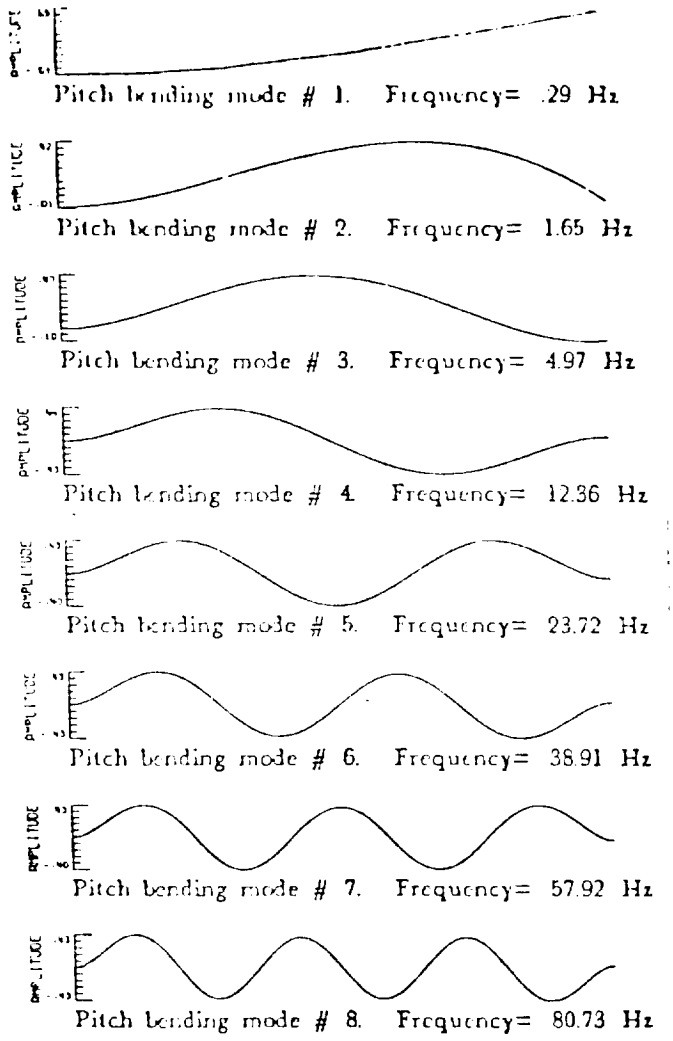

Figure 1.4: Flexible Pitch-Direction Mode Shapes for 2-Dimensional SCOLE

Table 4.2: 2-Dimensional SCOLE Elastic Modal Cost Analysis

Mode#	Frequency (Hz)	Modal Cost	Percent Total
1	.289E+00	.547E+01	.466E+02
2	.164E+01	.626E+01	.533E+02
3	.497E+01	.105E-01	.895E-01
4	.124E+02	.180E-04	.153E-03
5	.237E+02	.201E-06	.171E-05
6	.389E+02	.692E-08	.590E-07
7	.580E+02	.470E-09	.400E-08
8	.810E+02	.506E-10	.431E-09
9	.108E+03	.748E-11	.638E-10
10	.139E+03	.142E-11	.121E-10
11	.175E+03	.322E-12	.274E-11
12	.215E+03	.849E-13	.723E-12
13	.259E+03	.243E-13	.207E-12

Table 4.3: Noise Specifications for SCOLE Actuators and Sensors

			Actuators	
Type	Dynamic Range	Noise Intensity	Type	Noise Intensity
PMA	10 lb	.0001 $(lb)^2$	Accelerometers	$v_a = .0025\ (deg/sec^2)^2$
CMG	10^5 ft–lb	10,000. $(ft–lb)^2$	Angular Position	$10^{-6}\ (deg)^2$
				$.004\ (deg/sec)^2$

thus selected by evaluating the relative effectiveness of each of the 20 PMA locations.

4.2 RESULTS FOR NON-DYNAMIC ACTUATORS

The PMA selection problem for non-dynamic actuators was solved first, for later comparison with the dynamic actuator selection results. In all cases (dynamic and non-dynamic) the actuator effectiveness values are calculated following controller design which achieves a specified output variance and minimizes the amount by which the actuators exceed their specified variances. This type of controller is designed by an iterative selection of the control and output weights using the Output Variance Assignment (OVA) algorithm (DeLorenzo and Skelton, [3]). The variance specification for each actuator was equal to 10 times the intensity of its noise (see Table 4.3).

The actuator effectiveness values based upon standard Closed Loop Input/Output Cost Analysis (CIOCA) [2] for non-dynamic actuators are presented in Figure 4.8. The figure portrays PMA effectiveness results for four different controllers, each achieving a different steady-state line-of-sight (LOS) error variance. The results provide a vivid illustration of how the controller objectives can profoundly influence the actuator selection results. For lower gain controllers (lower LOS error) the theory determines that the upper tip is the most desirable PMA location. However, as the gain increases (controller designed for smaller LOS error) the center of the beam becomes the optimal location.

The results of Figure 4.8 are readily explained via modal analysis. The mode shape figures for the four flexible modes retained in the 2-dimensional SCOLE model were presented in Figure 4.7. Recall that mode #1, which accounts for 46.6 percent of the open loop modal cost, has a maximum amplitude at the reflector-end tip of the beam (i.e., at 130 ft.). Mode number #2, which accounts for 53.3 percent of the open loop modal

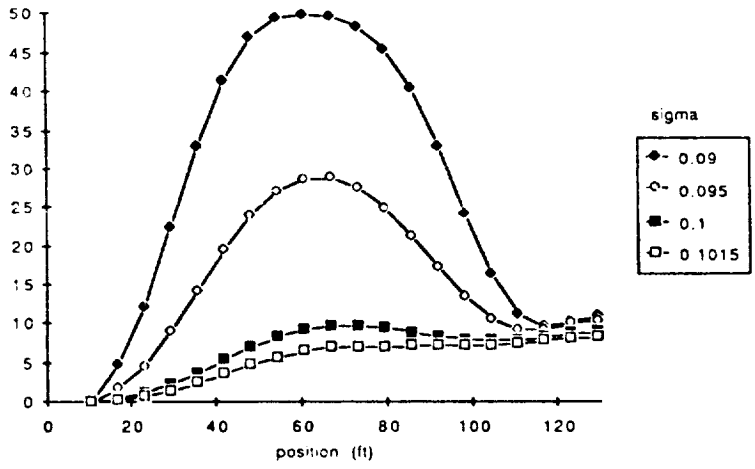
50
45
40
35
30
25
20
15
10
5
0
0
20
40
60
80
100
120
position (ft)
sigma
0.09
0.095
0.1
0.1015

4.8

cost, has a maximum amplitude near the 90 ft. point. And mode #3, which accounts for only approximately 0.1 percent of the open loop modal cost, has a peak amplitude near the center of the beam.

Next note from Figure 4.8 that as the gain is increased in order to achieve a smaller steady state LOS error variance, the most effective location for PMAs shifts from the tip of the beam to the midpoint. This corresponds to a shift from the peak of mode #1 to the peak of mode #3. The shift occurs *even though* with higher gain the *noise* in the PMAs near the beam midpoint becomes the *most detrimental* to performance (Figure 4.9). In fact, Figure 4.9 indicates the reason for the shift in optimal PMA location: with higher gain the third mode becomes the least damped by the control of the CMG, and becomes therefore a significant mode to be controlled by the PMAs. Figure 4.10 and Table 4.4 indicate the motion of the closed-loop eigenvalues from their open loop locations under varying levels of gain (output performance).

Since the control cost of each PMA ($V_i^u = E_\infty r_i u_i^2$) is equal to its effectiveness value V_i^{act} minus the cost contribution of its noise, V_i^w, then it is clear from Figures 4.8 and 4.9 that the PMAs are being used primarily to control mode #3 (i.e., near the middle of the beam). However mode #3 is the most lightly damped mode in the closed loop. This is true in spite of the fact that in all cases the input variances of both the CMG and PMAs, when normalized by their variance specifications, are of like order of magnitude (see Figure 4.11).

The results demonstrate the interesting result that while the PMAs are being used at a level similar to the CMGs (in relation to their specified variance levels), they nontheless make a small contribution to the closed-loop modal damping. This claim is verified by deleting all PMAs from the system and again using OVA to achieve a specified LOS error of 0.1 (arc sec)^2, and comparing the resulting closed-loop modal and

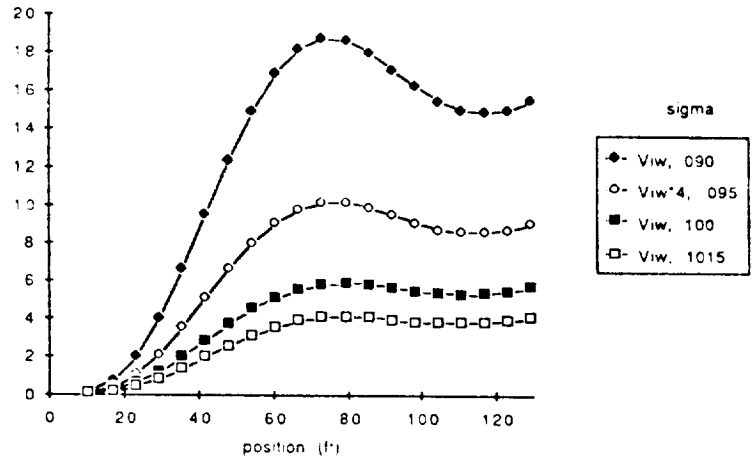
20
18
16
14
12
10
8
6
4
2
0
0
20
40
60
80
100
120
position (ft)
sigma
Viw, 090
Viw*4, 095
Viw, 100
Viw, 1015

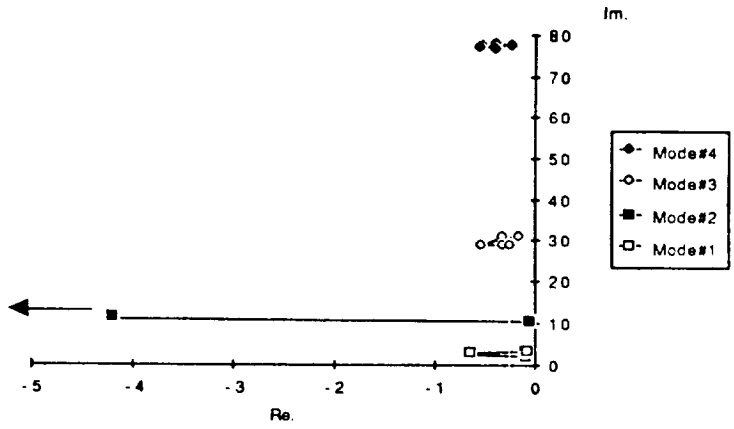

4.10

Table 4.4: Modal Characteristics of [A+BG] as a Function of Output Performance

	Open Loop	.1015 $(deg)^2$	.10 $(deg)^2$	.095 $(deg)^2$	.09 (no PMAs)	.10 $(deg)^2$
ω_1(r/s)	1.8	3.14	3.14	3.14	3.14	3.135
ζ_1	.005	.028	.027	.0255	.025	.01
τ_1 (sec)	111.1	11.4	11.8	12.5	12.74	31.9
ω_2(r/s)	10.3	56.	62.	93.	160.	63
ζ_2	.005	.675	.68	.6926	.702	.68
τ_2(sec)	19.4	.026	.024	.015	.009	.023
ω_3(r/s)	31.	29.	28.9	28.8	28.8	28.9
ζ_3	.005	.0217	.0185	.011	.009	.016
τ_3(sec)	6.45	1.6	1.87	3.16	3.95	2.16
ω_4(r/s)	78	77.4	77.	77.	77.	77.3
ζ_4	.005	.0065	.007	.0072	.0052	.0068
τ_4(sec)	2.56	2.0	1.86	1.8	2.5	2.49
Steady-State Normalized CMG Variance	--	46.04	60.6	183.6	591.1	65.2

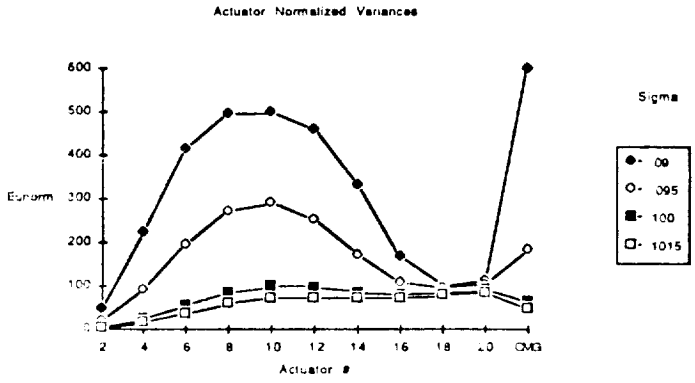
Actuator Normalized Variances
600
500
400
300
200
100
0
2
4
6
8
10
12
14
16
18
20
Actuator #
Sigma
00
095
100
1015

performance data with that obtained from a full set of PMAs and an output variance of 0.1 (arc sec)^2 (see Table 4.4).

4.3 RESULTS FOR DYNAMIC ACTUATORS

In this section we add actuator dynamics to the SCOLE model and then re-solve the actuator selection problem solved above. The actuator dynamics are given in NASA's original SCOLE document [15] to be first-order with a time constant of 0.1 seconds. That is, for each actuator (both PMA and CMG) the response of the actuator $f_i(t)$ to its input signal $u_i(t)$ is governed by

$$f_i(s)/u_i(s) = [1/(.1s+1)] \tag{4.7a}$$

or

$$\dot{f}_i = -10f_i + 10u_i \,. \tag{4.7b}$$

There are several possibilities for the characteristics of the white noise associated with the actuators; white noise may be an *input* to (and thus be filtered by) the actuator, or it may be additive with the actuator *output* (thus unfiltered), or *both*. In this example *four* different actuator noise models are considered. Recalling that the non-dynamic actuators had additive white noise with intensity W, the following noise cases were studied for dynamic actuators:

1. white actuator input noise of intensity $W_u = W$;

2. white actuator output noise of intensity $W_f = W$;

3. both input and output noise, each white and of intensity W;

4. both input and output noise, each white and of intensity W/2.

The sensors are assumed non-dynamic (without phase lag).

First we examine the effect of actuator dynamics on the maximal theoretically achievable accuracy. From [3], the lower bound y_i^* on the steady-state variance of the i_{th} output is given by

$$y_i^* = [CPC^T]_{ii} \qquad i = 1, ..., ny . \tag{4.8}$$

The values of the lower bound on the LOS error for the fourth-order 2-D SCOLE model under study were calculated for the four different actuator noise cases listed above, as well as for the non-dynamic actuator model examined earlier. The results are shown below.

Table 4.5: Maximal Accuracy for Different Actuator Noise Cases

Noise Case	No Dynamics	W_u=W	W_f=W	W_f=W_u=W	W_f=W_u=W/2
Max. Acc. (arc sec)^2	.086921	.0691	.086921	.10072	.07926

From Table 4.5 it is clear that the addition of actuator dynamics along with retention of the white noise input to the system states (actuator output noise only, W_f=W) *does not change* the theoretical maximal accuracy; that is, y^* is equal for the non-dynamic and the $W_f = W$ case. Also from the table, filtering of the actuator noise by passing it through finite actuator dynamics clearly improves the maximal accuracy. Finally it is noted that for case (3), $W_f = W_u = W$, the minimal LOS error is greater than that obtained by all but one of the controllers in the non-dynamic case. Thus for purposes of comparison only cases (1), (2) and (4) are studied in further detail.

For each of the three actuator noise cases a controller was designed (using OVA) which assigned the steady state LOS error variance to 0.1 (arc sec)^2 and minimized the sum of the normalized actuator variances among those actuators whose variances exceed their specifications (normalized variances greater than unity). For each final controller, the dynamic actuator effectiveness values for the PMAs are plotted in Figure 4.12 versus the actuators' position along the 130 ft. flexible beam.

For each of the noise cases the most effective actuator location is toward the reflector-end of the beam, with the highest effectiveness values corresponding to actuators located at the beam tip. Recalling the mode shape figures for the open loop flexible modes, the results in Figure 4.12 indicate that the PMAs are used by the optimal controller primarily for control of mode #1, which accounted for 46.6 percent of the open loop modal cost. It is interesting to compare Figure 4.12 with the plot of effectiveness values for non-dynamic actuators (Figure 4.8); note that the most effective non-dynamic actuators for the controller which achieved LOS error = 0.1 (arc sec)^2 were located near the center of the beam (70 ft from the shuttle). Hence, the optimal beam locations for PMAs in controllers which are achieving the same output performance are affected by the actuator dynamics.

CONCLUSIONS

The Closed-Loop Input/Output Cost Analysis (CIOCA) method of sensor and actuator selection (SAS) has been extended for application to systems with dynamic sensors and actuators -- that is, systems in which the response of the sensors and actuators to their inputs is not instantaneous but governed by deterministic dynamics. The extended SAS method is applicable to systems in which the deterministic sensor and actuator dynamics are of arbitrary order. Application to simple numerical examples

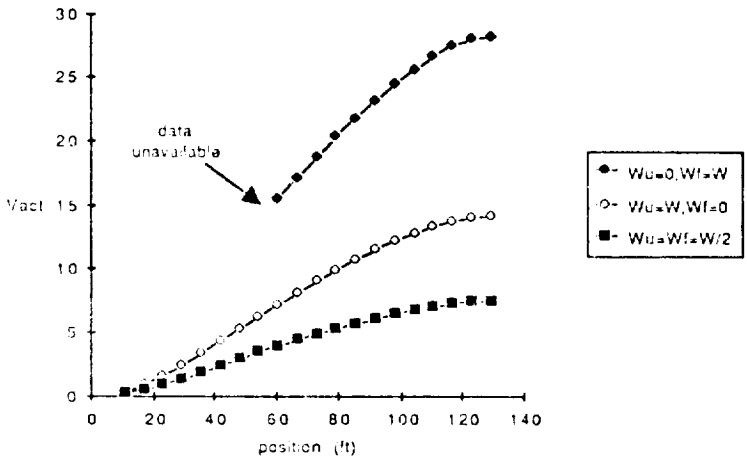
30
25
20
15
10
5
0
Vact
data
unavailable
0
20
40
60
80
100
120
140
position (ft)
Wu=0,Wf=W
Wu=W,Wf=0
Wu=Wf=W/2

demonstrates the utility of the SAS method. The examples also demonstrated that even uniform sensor dynamics can affect the optimal selection of sensors. Application of the actuator selection method in detail to NASA's SCOLE space structure demonstrated that even uniform actuator dynamics can affect the optimal selection of actuators.

LIST OF REFERENCES

[1] Skelton, R.E., and Norris, G.A., "Selection of Noisy Sensors and Actuators in the Presence of Correlated Noise," *Journal of Control Theory and Advanced Technology,* to appear.

[2] Skelton, R.E., and DeLorenzo, M.L., "Selection of Noisy Actuators and Sensors in Linear Stochastic Systems," *Journal of Large Scale Systems, Theory and Applications,* Vol. 4, April 1983, pp. 109-136.

[3] Skelton, R.E., and DeLorenzo, M.L., "Space Structure Control Design by Variance Assignment," *Journal of Guidance and Control,* Vol. 8, July-August 1985, pp. 454-462.

[4] DeLorenzo, M.L., "Selection of Noisy Sensors and Actuators for Regulation of Linear Systems," Ph.D. Thesis, School of Aeronautics and Astronautics, Purdue University, West Lafayette, IN, May 1983.

[5] Skelton, R.E., and Hughes, P.C., "Modal Cost Analysis for Linear Matrix-Second-Order Systems," *Journal of Dynamic Systems, Measurement, and Control,* Vol. 102, Sept. 1980.

[6] Howell, K.C., and Baxter, M.J., "Some Considerations of Actuator Dynamics in the Attitude Control of a Flexible Beam," (AIAA/AAS Paper 86-2124).

[7] Chiu, JD. and Skelton, R.E., "Optimal Selection of Inputs and Outputs in Linear Stochastic Systems," *J. Astronautical Sciences,* Vol. XXXI, No. 3, pp. 399-414, July-Sept. 1983.

[8] Goh, C.J., and Caughey, T.K., "On the Stability Problem Caused by Finite Actuator Dynamics in the Collocated Control of Large Space Structures," *Int. J. Control,* Vol. 41, No. 3, 1985, pp. 787-802.

[9] Balas, M.J., "Feedback Control of Flexible Systems," *IEEE Transactions on Automatic Control,* Vol. AC-23, No. 4, 1978, pp. 673-679.

[10] Malandrakis, C.G., "Optimal Sensor and Controller Allocation for a Class of Distributed Parameter Systems," *Int. J. Syst. Sci.,* Vol. 10, No. 5, pp. 463-480, Sept. 1980.

[11] Ichikawa, A. and Ryan, E.P., "Filtering and Control of Distributed Parameter Systems with Point Observations and Inputs," *Proc. of the 2nd IFAC Symp. on Control of D.P.S.,* pp. 347-357, Coventry, Jul. 1977.

[12] Ichikawa, A. and Ryan, E.P., "Sensor and Controller Location Problems for Distributed Parameter Systems," *Automatica,* Vol. 15, No. 3, pp. 347-352, May 1979.

[13] Hughes, P.C., "Space Structure Vibration Modes: How Many Exist? Which ones are Important?" *IEEE Control Systems Magazine,* February 1987, pp. 22-28.

[14] Schaechter, D.B., "Control Technology Development," *NASA Langley Research Center LSS Tech.,* Mar 1982, pp. 297-311.

[15] Taylor, L.W., and Balakrishnan, A.V., "A Mathematical Problem and a Spacecraft Control Laboratory Experiment (SCOLE) Used to Evaluate Control Laws for Flexible Spacecraft ... NASA/IEEE Design Challenge," January 1984, unpublished, available from Lawrence W. Taylor, Jr., Spacecraft Control Branch, NASA Langley Research Center, Hampton, VA, 23665.

[16] Hotz, A.F., Collins, E., and Skelton, R.E., "Linearized Dynamic Model for the NASA/IEEE SCOLE Configuration," NASA Contractor Report 172394, Langley Research Center, Hampton, VA, Sept. 1984.

[17] King, A.M., Norris, G.A., and Skelton, R.E., "Controller Design for Vibration and Shape Control of an Offset Reflector Satellite," contractor report to SPARTA, Inc., May 1986.

[18] Norris, G.A., "Selection of Non-Ideal Noisy Actuators and Sensors in the Control of Linear Systems," Master's Thesis, School of Aeronautics and Astronautics, Purdue University, West Lafayette, IN, May 1987.

[19] McClamrock, H. "Control of Large Space Structures Using Electro-Mechanical Actuators," CSDL-P-1607, The Charles Starke Draper Lab., Inc., Cambridge, Mass., July 1982.

Proof of Theorem 1

Let $\alpha = (nx_p+nx_a)$. The composite system (2.7e) has a controllability matrix $W_c \in R^{\alpha\times(\alpha\cdot nu)}$ of the following form

$$W_c = \begin{bmatrix} W_{c1} \\ W_{c2} \end{bmatrix} = \begin{matrix} 0 & B_oC_aB_a & (A_pB_oC_aB_a+B_oC_aA_aB_a) & \cdots & (A_p^{\alpha-2}B_oC_aB_a+A_p^{\alpha-3}B_oC_aA_aB_a+\cdots+B_oC_aA_a^{\alpha-2}B_a) \\ B_a & A_aB_a & A_a^2B_a & \cdots & A_a^{\alpha-1}B_a \end{matrix} \tag{A.1}$$

Now noting that $C_aA_a^iB_a = M_i$ is the ith Markov parameter for the system of actuator dynamics (2.7c,d), W_{c1} may be rewritten

$$W_{c1} = [0\ B_oM_o\ (A_pB_oM_o+B_oM_1)\ (A_p^2B_oM_o+A_pB_oM_1+B_oM_2)\cdots$$

$$\cdots(A_p^{\alpha-2}B_oM_o+A_p^{\alpha-3}B_oM_1+\cdots+B_oM_{\alpha-2})] \tag{A.2}$$

The columns of W_c span the controllable subspace of the composite system. Linear independence of all the rows in W_c implies full controllability of the composite system. However, controllability of the original system states, x_p, requires only that the columns of W_{c1} span the state space for x_o. This in turn will hold if and only if the matrix W_{c1} has rank nx_p.

The proof of the Theorem begins with the proof that (A.3) implies (A.4):

$$\{\det M_k \neq 0,\ M_i = 0,\ i = 0, 1, ..., k-1\} \tag{A.3}$$

$$\text{rank}[W_{c1}] = n_{x_p} \text{ (or range space of } W_{c1} \text{ has dimension } n_{x_p}) \tag{A.4}$$

Note that the last block of W_{c1} has the form

$$W_{c1(\alpha)} = (A_p^{\alpha-2}B_oM_o+A_p^{\alpha-3}B_oM_1 + \cdots + B_oM_{\alpha-2}) \tag{A.5}$$

Now let $k \leq \alpha-2$ be the index of the first nonzero Markov parameter, M_k. (In this case

the first k+1 blocks of W_{c1} are zero.) Next, use is made of two results from linear algebra ("R [K]" denotes "range space of K"),

$$\{\det K \neq 0\} \Rightarrow \{R[JK] = R[J]\} \tag{A.6a}$$

$$R[J+K] \subset R[J] + R[K] \tag{A.7b}$$

(where "$\subset$" means "is contained in") to demonstrate the following results which hold when M_k is nonsingular

$$R[B_o] = R[B_o M_k] \tag{A.8}$$

$$\begin{aligned} R[B_o\, A_p B_o] &= R[B_o] + R[A_p B_o] \\ &= R[B_o M_k] + R[A_p B_o M_k] \\ &= R[B_o M_k] + R[A_p B_o M_k + B_o M_{k+1} - B_o M_{k+1}] \\ &\subset R[B_o M_k] + R[A_p B_o M_k + B_o M_{k+1}] + R[B_o M_{k+1}] \\ &= R[B_o M_k] + R[A_p B_o M_k + B_o M_{k+1}] \end{aligned}$$

$$\therefore R[B_o\, A_p B_o] \subset R[B_o M_k\, A_p B_o M_k + B_o M_{k+1}] \tag{A.9}$$

Eqns (A.8) and (A.9) lead by induction to the main result

$$R[B_o\, A_p B_o \cdots A_o^{\alpha-k-2} B_o] \subset R[B_o M_k\, A_p B_o M_k + B_o M_{k+1} \cdots A_p^{\alpha-k-2} B_o M_k + \cdots B_o M_{\alpha-2}]$$

that is,

$$R[B_o\, A_p B_o \cdots A_p^{\alpha-k-2} B_o] \subset R[W_{c1}]\,. \tag{A.10}$$

Condition (A.3) leads to (A.10). Thus, given (A.3) together with (A_p,B_o) controllable, the columns of W_{c1} are guaranteed to span the nx_p-dimensional state space for x_p as long as

$$\alpha-k-2 \geq nx_o-1 .$$

that is, as long as

$$k \leq nx_a - 1 . \tag{A.11}$$

In fact, the index k of the first nonzero Markov parameter for the system (2.7) will always satisfy (A.11). To show this, simply note that by observability of (A_a,B_a), the observability matrix W_{oa} for (2.7) has full column rank:

$$\text{rank}(W_{oa}) = nx_a \tag{A.12}$$

From (A.12),

$$\{W_{oa}B_a = 0\} \Rightarrow \{B_a = 0\} \Rightarrow \{\text{Contradiction of } (A_a,B_a) \text{ controllable}\} \tag{A.13}$$

Thus,

$$W_{oa}B_a = [M_o^T, M_1^T, ..., M_{n\gamma-1}^T]^T \neq 0 \tag{A.14}$$

and so the validity of (A.11) is guaranteed for (2.7) completing the proof that

$$\{[(A_p,B_o) \text{ controllable}] \;\&\; [M_k \neq 0, M_i = 0, i = 0, 1, ..., k-1]\} \tag{A.15}$$

$$\Rightarrow \{x_p \text{ controllable u}\}$$

The usefulness of (A.15) stems from the fact that by meeting certain *mildly* restrictive conditions the actuator dynamics can be guaranteed not to destroy *controllability of the original system states* x_p, regardless of the pole/zero location for the plant.

It remains to prove the equivalence of the condition (A.3) and the requirements on the individual actuators' numbers of poles and zeros. First, note that since each actuator is a single input, single output (SISO) system, then the Markov parameters M_i for the lumped actuator dynamics (2.7) are diagonal matrices of the following form:

$$M_i = \text{diag}\,[m_{1i}, m_{2i}, m_{3i}, ..., m_{nui}] \tag{A.16}$$

where m_{ji} is the (scalar) i_{th} Markov parameter for the j_{th} actuator. Thus the condition (A.3) is met if and only if the index i of the first nonzero markov parameter is equal among all the actuators.

The input/output transfer function for any n_{th} order SISO system has the form:

$$T(s) = (c_{n-1}s^{n-1}+c_{n-2}s^{n-2} + \cdots + c_o)/(s^n+d_{n-1}s^{n-1}+\cdots+d_o) \tag{A.17}$$

The scalar Markov parameters m_i for the SISO system with transfer function (A.20) may be shown to be given by:

$$m_o = c_{n-1}$$

$$m_1 = c_{n-2} - d_{n-1}n_o$$

$$\begin{array}{ll} n_2 = c_{n-3} - d_{n-2}\ n_o - d_{n-1}n_1 & \\ \vdots \qquad\qquad\qquad\quad \vdots & \\ n_n = c_o - d_1 \qquad -d_2n_1 - \cdots - d_{n-1}n_{n-2} & \end{array} \tag{A.18}$$

From (A.18), n_i is the first nonzero Markov parameter for a system when the number of zeros in its transfer function is

$$z = n - i - 1 \tag{A.19}$$

Letting n_j and z_j equal the number of poles and zeros for the j_{th} actuator, respectively, (A.19) yields the conclusion that

$$\{\det M_k \neq 0,\ M_i = 0,\ i = 0,\ 1,\ \ldots,\ k-1\} \Leftrightarrow \{(n_j - z_j) = (n_i - z_i) \bigvee\ i,j, \in (1,2,\ldots,nu)\} \quad (A.20)$$

Thus it is concluded that

$$\{(n_j - z_j) = (n_i - z_i) \bigvee\ i,j, \in (1,2,\ldots,nu)\} \Rightarrow \{x_p \text{ is controllable u}\}. \quad (A.21)$$

SCOLE 87/1

OPTIMIZATION-BASED DESIGN OF CONTROL SYSTEMS FOR FLEXIBLE STRUCTURES

E. Polak, T. E. Baker, T-L. Wuu and Y-P. Harn

Department of Electrical Engineering and
Computer Sciences
University of California
Berkeley, Ca. 94720

Presented at
The 4th Annual SCOLE Workshop
Air Force Academy
Colorado Springs, Colorado
November 16, 1987

This research was supported by the National Science Foundation grant ECS-8517362; the Air Force Office Scientific Research grant 86-0116; and the Office of Naval Research contract N00014-86-K-0295.

ABSTRACT

The purpose of this presentation is to show that it is possible to use nonsmooth optimization algorithms to design both closed-loop finite dimensional compensators and open-loop optimal controls for flexible structures modeled by partial differential equations.

An important feature of our approach is that it does not require modal decomposition and hence is immune to instabilities caused by spillover effects. Furthermore, it can be used to design control systems for structures that are modeled by mixed systems of coupled ordinary and partial differential equations.

DESIGN OF STABILIZING FEEDBACK-SYSTEM COMPENSATORS

The optimization-based design of finite dimensional compensators for systems modeled by coupled systems of ordinary and partial differential equations is made possible by a generalization of the following necessary and sufficient stability test for linear systems described by ordinary differential equations.

THE DYNAMICAL SYSTEM

Consider a parametrized, linear, time-invariant, interconnected, finite dimensional dynamical system, $\Sigma(\mathbf{p})$, described by a set of state equations:

$$\begin{aligned} \dot{\mathbf{x}}(t) &= \mathbf{A}(\mathbf{p})\mathbf{x}_i(t) + \mathbf{B}(\mathbf{p})\mathbf{u}(t), \\ \mathbf{y}(t) &= \mathbf{C}(\mathbf{p})\mathbf{x}(t) + \mathbf{D}(\mathbf{p})\mathbf{u}(t), \end{aligned} \tag{1}$$

We shall denote the characteristic polynomial of $\Sigma(\mathbf{p})$ by $\chi(s,\mathbf{p})$ and assume that the coefficients of $\chi(s,\mathbf{p})$ are continuously differentiable in $\mathbf{p}$.

S-STABILITY

When, it is desired to ensure not only exponential stability of a closed loop system, but also to exercise some control over the location of its poles, it is convenient to make use of the following definition of S-stability.

Definition *(S-stability):* Consider a linear, time-invariant, finite dimensional dynamical system Σ of the form (1). Let $\mathbf{S}$ be an open unbounded subset of $\mathbb{C}$ which is symmetrical with respect to the real axis, and such that $\mathbf{S}^c \supset \mathbb{C}_+$, where $\mathbf{S}^c$ is the complement of $\mathbf{S}$ and $\mathbb{C}_+$ is the closed right half of the complex plane.

We say that the system Σ is **S–stable** if all the zeros of its characteristic polynomial are in S. ■

A MODIFIED NYQUIST STABILITY CRITERION

Theorem : Let $S \subset \mathbb{C}$ be as specified in the Definition and let $B \subset \mathbb{C}$ be any simply connected set satisfying $(0,0) \notin B$. Suppose that $D(s,q) \in \mathbb{C}[s]$ is a parametrized polynomial of degree N, whose coefficients depend on the parameter vector $q \in \mathbb{R}^{n_D}$ in such a way that for every $\chi(s) \in P_N$ satisfying $Z[\chi(s)] \subset S$, there exists a $q_\chi \in \mathbb{R}^{n_D}$ such that

(i) $Z[D(s,q_\chi)] \subset S$, (2a)

(ii) $\chi(s)/D(s,q_\chi) \in B, \ \forall \ s \in \partial S.$ (2b)

Then, given a polynomial $\chi(s) \in P_N$, $Z[\chi(s)] \subset S$ if and only if there exists a $q_\chi \in \mathbb{R}^{n_D}$ such that (2a,b) hold. ■

PROOF OF MODIFIED NYQUIST STABILITY CRITERION

(= = =>) Suppose that $\mathbf{Z}[\chi(s)] \subset \mathbf{S}$. Then, by assumption, there exists a $q_\chi \in \mathbb{R}^{n_D}$ such that (2a), (2b) hold.

(<= = =) Next, suppose that (2a), (2b) hold. Then, because **B** is a simply connected set which does not contain the origin, the locus traced out in the complex plane by $\chi(s)/D(s,q_\chi)$, for $s \in \partial S$, does not encircle the origin. It now follows from (2a) and the Argument Principle that $\mathbf{Z}[\chi(s)] \subset \mathbf{S}$. ■

Comment : It is clear from the Theorem that an acceptable parametrization of the polynomial $D(s,q)$ depends on the shape of the set **S** and the choice of the set **B**. A further requirement is imposed by semi-infinite optimization: the parametrization must be such that it is easy to ensure that the zeros of $D(s,q)$ are in **S**. ■

OPTIMIZATION-BASED CONTROL SYSTEM DESIGN

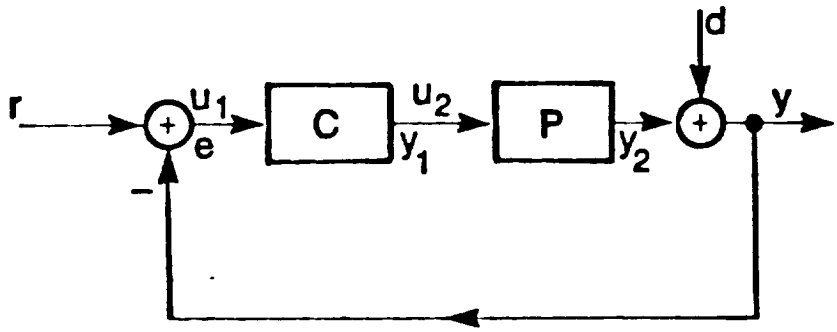

SYSTEM DYNAMICS

$$\frac{d}{dt}\begin{bmatrix} z_P^1 \\ z_P^2 \\ z_P^3 \end{bmatrix} = \begin{bmatrix} -3 & -4 & -2 \\ 1 & 0 & 0 \\ 0 & -2 & -4 \end{bmatrix}\begin{bmatrix} z_P^1 \\ z_P^2 \\ z_P^3 \end{bmatrix} + \begin{bmatrix} 1 & 0 \\ 0 & 0 \\ 0 & 1 \end{bmatrix}\begin{bmatrix} u_2^1 \\ u_2^2 \end{bmatrix},$$

$$\begin{bmatrix} y_2^1 \\ y_2^2 \end{bmatrix} = \begin{bmatrix} 1 & 4 & 3 \\ 0 & 2 & 3 \end{bmatrix}\begin{bmatrix} z_P^1 \\ z_P^2 \\ z_P^3 \end{bmatrix}.$$

$$\frac{d}{dt}\begin{bmatrix} z_C^1 \\ z_C^2 \end{bmatrix} = \begin{bmatrix} x^1 & x^2 \\ x^3 & x^4 \end{bmatrix}\begin{bmatrix} u_1^1 \\ u_1^2 \end{bmatrix}, \qquad \begin{bmatrix} y_1^1 \\ y_1^2 \end{bmatrix} = \begin{bmatrix} x^5 & x^6 \\ x^7 & x^8 \end{bmatrix}\begin{bmatrix} z_C^1 \\ z_C^2 \end{bmatrix}.$$

DESIGN VECTOR: $x = [\, x^1, x^2, \ldots, x^8 \,]$.

DESIGN CRITERIA

1. The feedback system must be exponentially stable.

2. The system should have a good step input response.

3. There should be little interaction between channels.

4. Plant should not be saturated by command input effects.

5. System should have high output disturbance rejection.

MODIFIED NYQUIST STABILITY CONSTRAINT

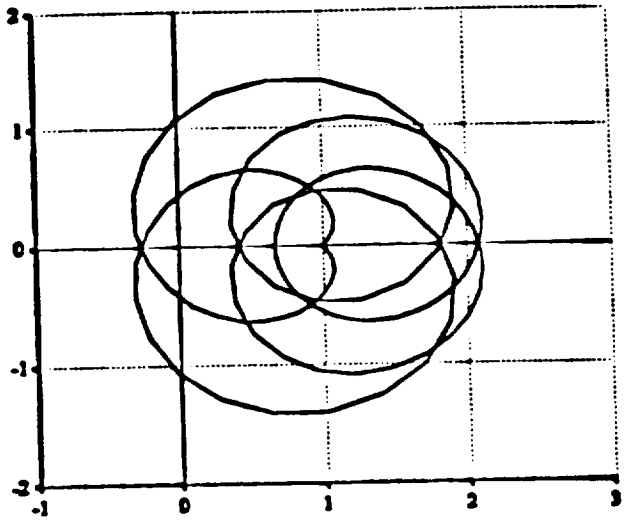

Initial Design

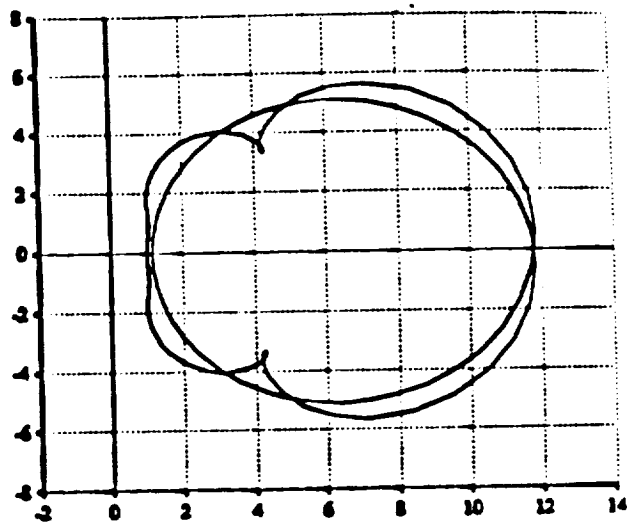

Final Design

STEP RESPONSES

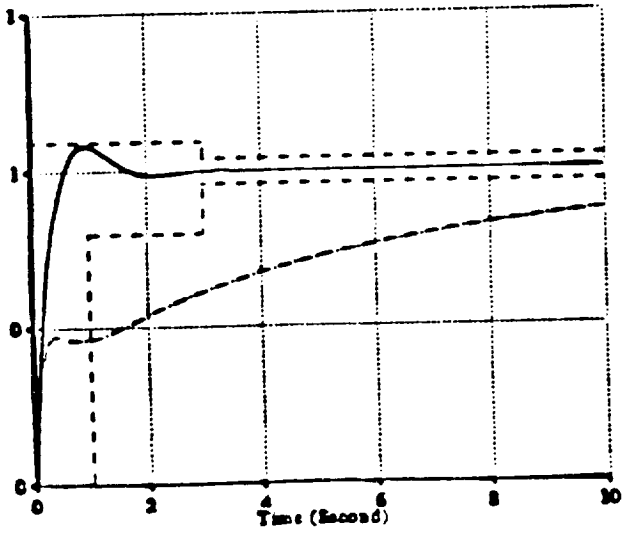

Channel 1

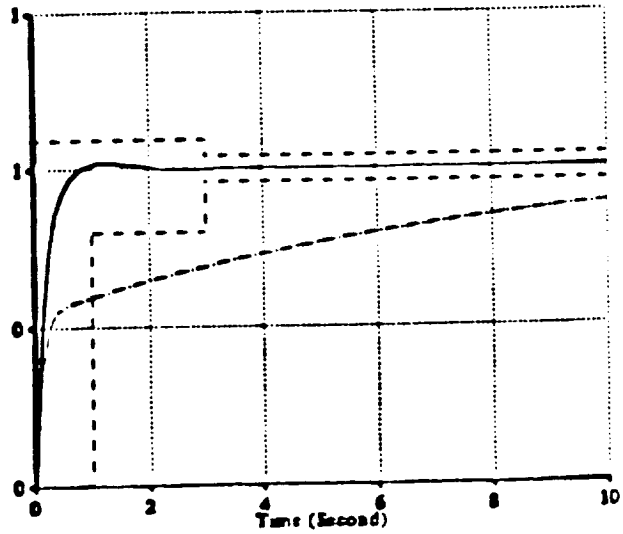

Channel 2

CHANNEL INTERACTION CONSTRAINT

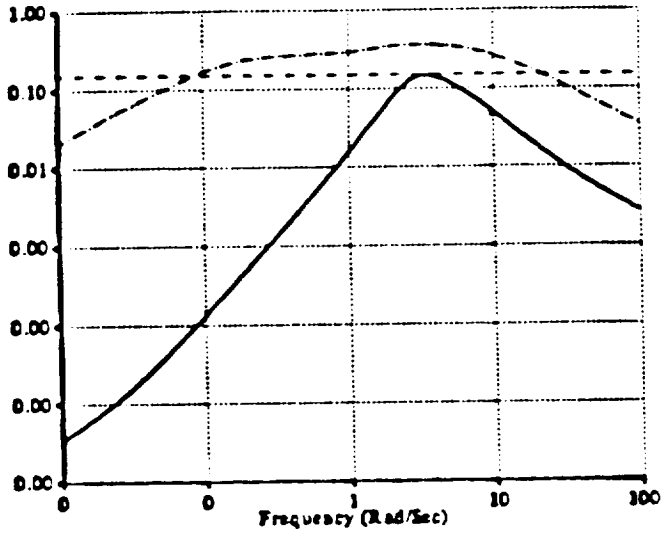

Magnitude of $H_{y^2r^1}(j\omega, x)$

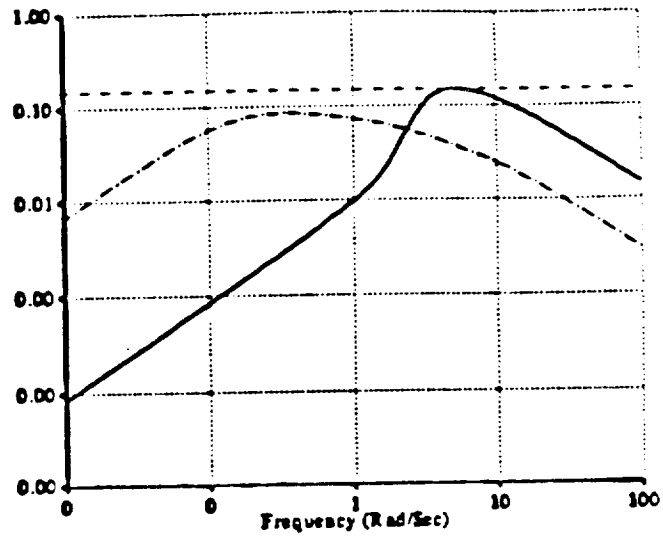

Magnitude of $H_{y^1r^2}(j\omega, x)$

COMMAND INPUT SATURATION CONSTRAINT

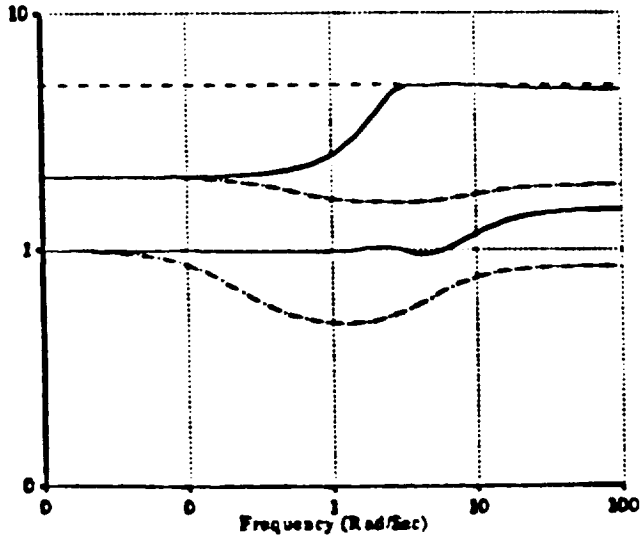

Singular Values of $H_{u_2r}(j\omega, x)$

OUTPUT DISTURBANCE SUPPRESSION CONSTRAINT

Must accept some disturbance amplification outside operating bandwidth:

$$\bar{\sigma}[H_{yd}(j\omega, x) \leq 1.05, \forall\, \omega \in [1, 1000]$$

COST: OUTPUT DISTURBANCE SUPPRESSION

Suppress disturbance effects inside operating bandwidth:

$$f(x) \triangleq \max_{\omega \in [0.001, 1]} \bar{\sigma}[H_{yd}(j\omega, x)$$

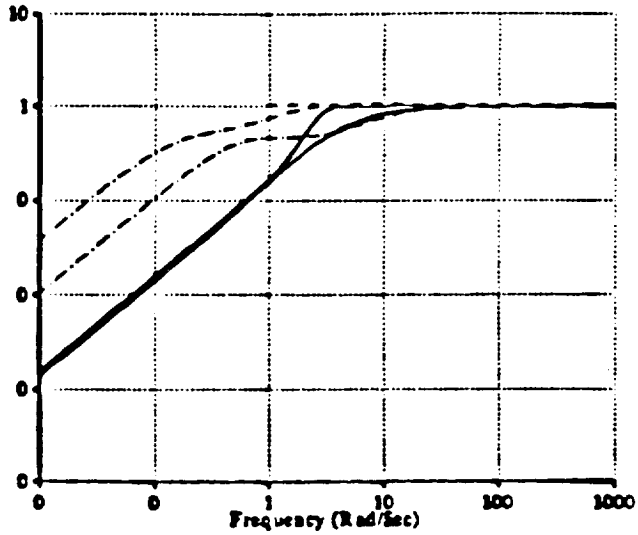

Singular Values of $H_{yd}(j\omega, x)$

INTEGRATED STRUCTURE-CONTROL-SYSTEM DESIGN

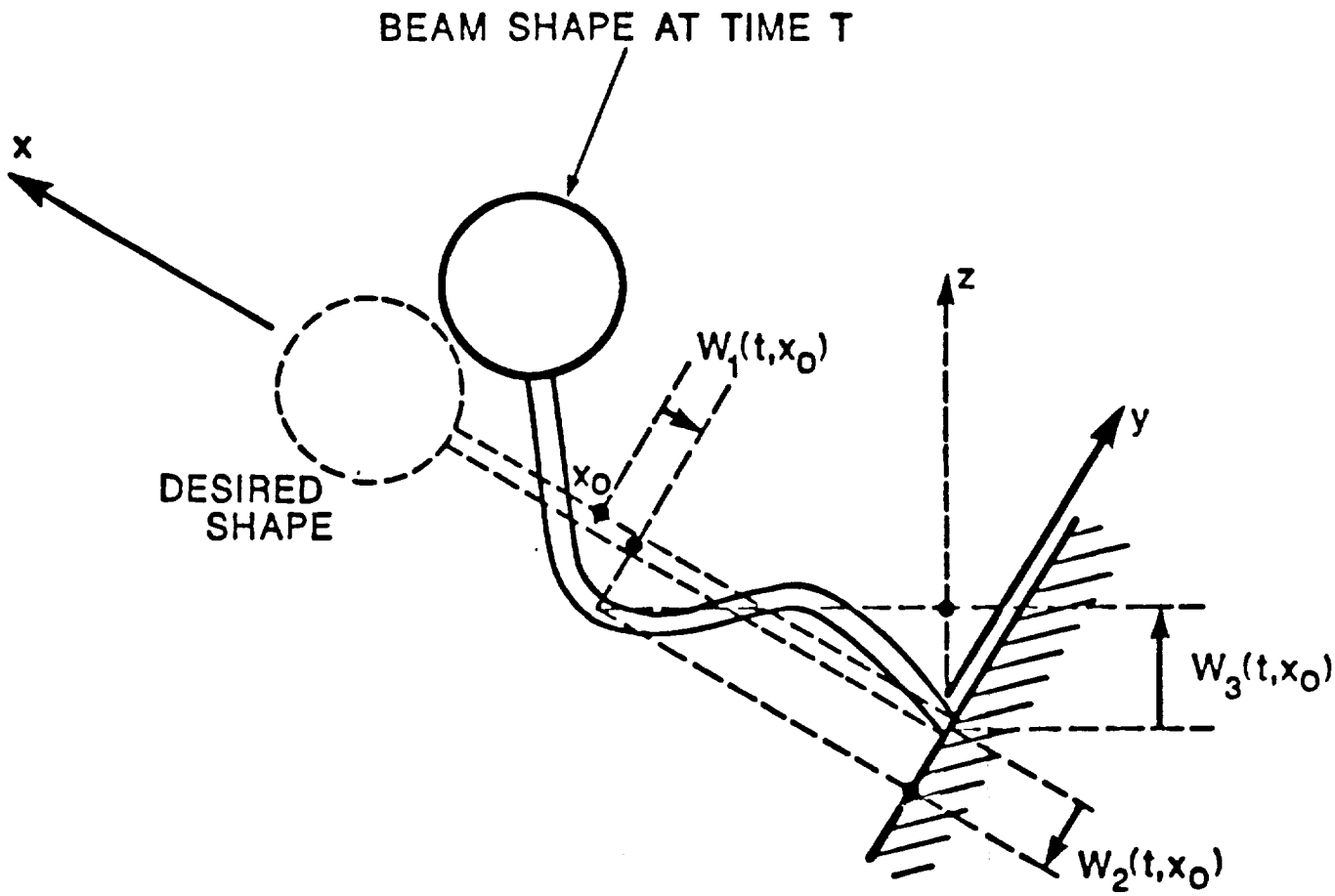

Vibrating Beam

DYNAMICS

- **GENERAL MODEL: Euler-Bernoulli Model, Kelvin-Voigt or Proportional Damping, Coupled Axial and Flexural Linear PDE's.**

- **Control Forces $F^i(t)$, Actuator Positions a^i, Sensor Positions s^i.**

- **SIMPLIFIED MODEL: Decoupled Motion Formulation:**

$$mu_{tt}(t\ ,\ x) + CIu_{txxxx} + EIu_{xxxx}(t\ ,\ x) = \sum_{i=1}^{n_i} b_i(x - a_i)F^i(t)\ .$$

$$y^i(t) = \int_0^1 c_i(\zeta - s^i)u(t\ ,\ \zeta)d\zeta \quad \text{or} \quad y^i(t) = \int_0^1 d_i(\zeta - s^i)\dot{u}(t\ ,\ \zeta)d\zeta\ .$$

BOUNDARY CONDITIONS

$$u(t\ ,\ 0) = 0\ ,\quad u_x(t\ ,\ 0) = 0,\ \ Ju_{ttx}(t\ ,\ 1) + CIu_{txx}(t\ ,\ 1) + EIu_{xx}(t\ ,\ 1) = 0\ ,$$

$$M u_{tt}(t\ ,\ 1) - CIu_{txxx}(t\ ,\ 1) - EIu_{xxx}(t\ ,\ 1) = 0.$$

DESIGN CRITERIA

1. The feedback system must be exponentially stable.

2. Control system compensator should be finite dimensional.

3. Actuators should not be saturated by command input effects.

4. System should have high mechanical disturbance rejection.

5. Average power use should be low.

6. Structure weight should be low.

7. Structure should remain in elastic range.

DESIGN VARIABLES

- **CONTROL SYSTEM COMPENSATOR**

(i) Coefficients of compensator differential equation.

- **STRUCTURE**

(i) Positions of actuators and sensors.

(ii) Parameters of damping devices.

(iii) Parameters of composite materials.

(iv) Parameters determining shape of structure.

PRELIMINARY RESULTS

1. **The control system can be stabilized using a *finite dimensional* proportional-plus-integral controller which ensures good disturbance rejection. The use of our modified Nyquist stability criterion in the design of a stabilizing controller requires only evaluations of the system frequency response. Since the frequency response at a given frequency can be computed in some cases by formula and in the more general cases by solving two-point linear boundary value problems,** *there is no need for modal decomposition* and hence *there are no spillover effects.* As in the finite dimensional case, time and frequency domain constraints can be treated simultaneously and, in an *integrated design approach* structural parameters and constraints can also be introduced into the optimization problem.

2. **If** *a sequential design approach* is used, an infinite dimensional compensator can be designed using an H^∞ frequency domain constraint formulation which results in a convex optimization problem and automatically ensures exponential stability with stability margin.

3. **An infinite dimensional controller designed as above can be approximated by a finite dimensional controller without spillover effects.**

4. **A special semi-infinite optimization algorithm has been developed which is highly effective for design with H^∞ frequency domain design constraints.**

A FLEXIBLE ARM OPTIMAL SLEWING PROBLEM

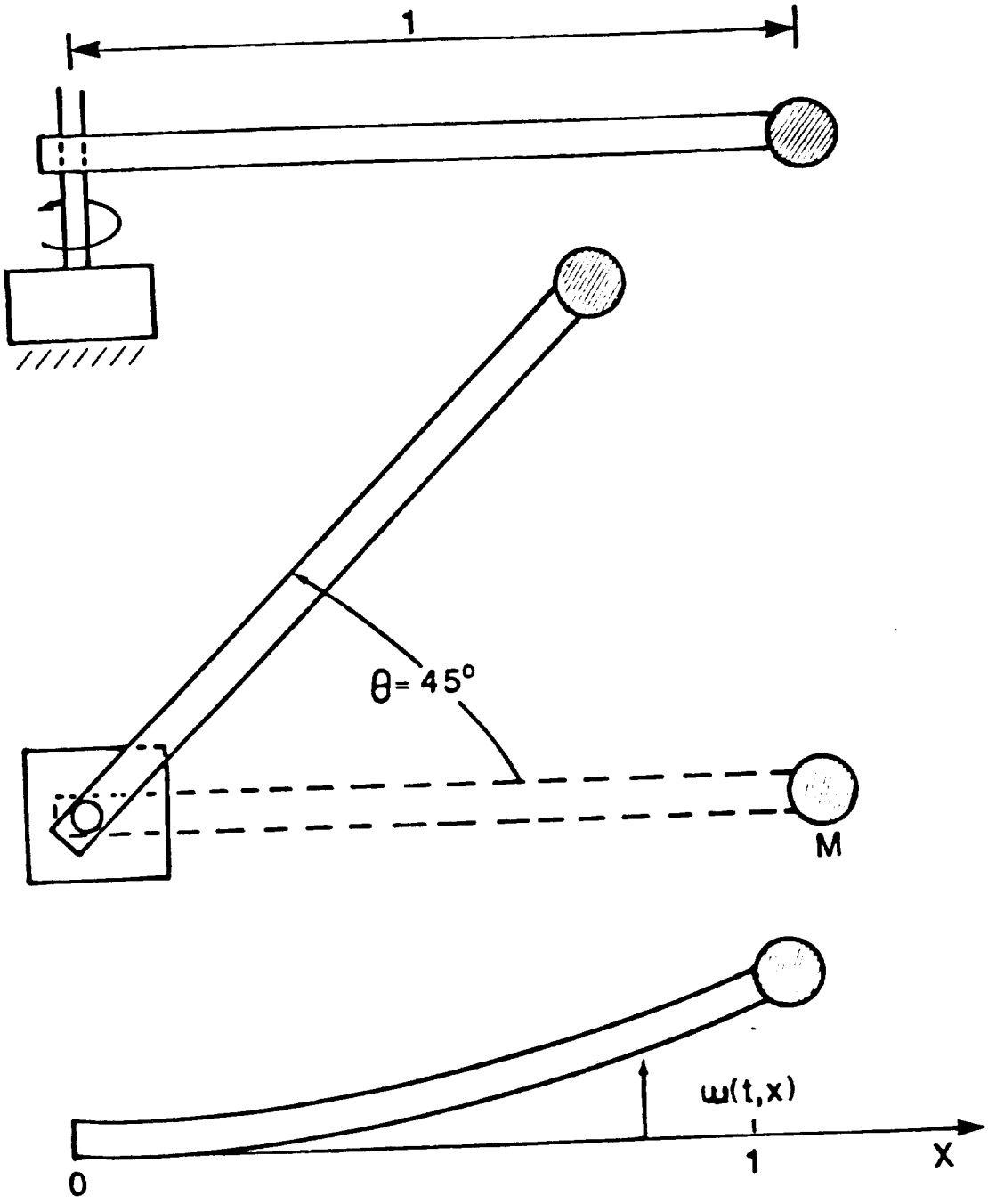

THE DYNAMICAL SYSTEM

Hollow aluminum tube: one meter long, 2.0 cm diameter, 1.6 mm thick. Attached mass weighs 1 kg. We assume that motor torque $\mathbf{u}(t)$ can be directly controlled.

Standard Euler-Bernoulli tube equations with Kelvin-Voigt visco-elastic damping:

$$\mathbf{m}w_{tt}(t,x) + \mathbf{CI}w_{txxxx}(t,x) + \mathbf{EI}w_{xxxx}(t,x) - \mathbf{m}\Omega^2(t)w(t,x) = -\mathbf{m}u(t)x, \quad x \in [0,1] \tag{1a}$$

with boundary conditions:

$$w(t,0) = 0, \quad w_x(t,0) = 0, \quad \mathbf{CI}w_{txx}(t,1) + \mathbf{EI}w_{xx}(t,1) = 0. \tag{1b}$$

$$\mathbf{M}(\Omega^2(t)w(t,1) - w_{tt}(t,1) - u(t)) + \mathbf{CI}w_{txxx}(t,1) + \mathbf{EI}w_{xxx}(t,1) = 0 \tag{1c}$$

where $\mathbf{w}(t,x)$ is displacement of tube from *shadow tube* (which remains undeformed during the motion), $\mathbf{u}(t)$ is motor torque, and $\Omega(t)$ rad/sed is angular velocity. Above: $\mathbf{m} = .2815$ kg/m, $\mathbf{C} = 6.89\times10^7$ pascals/sec., $\mathbf{E} = 6.89\times10^9$ pascals, $\mathbf{I} = 1.005 \times 10^{-8}\mathbf{m}^4$, The tube is very lightly damped (0.1 per cent).

THREE OPTIMAL SLEWING PROBLEMS

$\mathbf{P}_1$:

Minimize the time required to rotate the tube 45 degrees, from rest to rest, subject to the torque not exceeding 5 newton-meters.

$\mathbf{P}_2$:

Minimize the total energy required to rotate the tube 45 degrees, from rest to rest, subject to the torque not exceeding 5 newton-meters and the maneuver time not exceeding a given bound.

$\mathbf{P}_3$:

Minimize the time required to rotate the tube 45 degrees, from rest to rest, subject to the torque not exceeding 5 newton-meters and an upper bound on the potential energy due to deformation of the tube throughout the entire maneuver.

THE DYNAMICAL SYSTEM

MATHEMATICAL FORMULATION OF THE THREE PROBLEMS

• To avoid technical problems associated with variable intervals and problems due to discretization, augment dynamics by one state variable and introduce scale factor $\mathbf{T} > 0$ so that problem becomes defined on *normalized time* interval $[0, 1]$, with $\mathbf{T}$ also equal to final time.

• *Tube is at rest* when the total energy = energy due to rigid body motion + energy due to vibration and deformation = 0.

(i) To ensure a slewing motion of 45°, we define

$$\mathbf{g}^1(\mathbf{u}, \mathbf{T}) \triangleq (\Theta - \Pi/4)^2 \tag{2}$$

(ii) Rigid body energy at final time is proportional to the square of the angular velocity.

$$\mathbf{g}^2(\mathbf{u}, \mathbf{T}) \triangleq \Omega(\mathbf{T})^2. \tag{3}$$

(iii) Kinetic energy due to tube vibration at normalized time 1 is

$$g^3(t,u) \triangleq \frac{m}{2}\int_0^1 w_t(1,x)^2 dx. \tag{4}$$

(iv) Potential energy due to tube deformation at normalized time 1 is

$$g^4(1,u) \triangleq \frac{EI}{2}\int_0^1 w_{xx}(1,x)^2 dx. \tag{5}$$

- Potential energy due to deformation of the tube at normalized time **t**:

$$P(t,u) \triangleq \frac{EI}{2}\int_0^1 w_{xx}(t,x)^2 dx. \tag{6}$$

(v) To limit tube deformation for all $t \in [0,1]$ we define

$$g^5(u,T) \triangleq \int_0^T [\max\{ P(t,u) - f(t) , 0 \}]^2 \tag{7}$$

(vi) To ensure slewing time does not exceed T_f seconds, we define

$$g^6(u,T) \triangleq T - T_f. \tag{8}$$

FINAL PROBLEM FORM

$$\mathbf{P}_1: \quad \min_{T \in \mathbb{R}_+,\, u \in G} \{\, g^0(u,T) \mid g^j(u,T) - \varepsilon \le 0,\ j \in \{1,2,3,4\} \,\},$$

where $g^0(u,T) \triangleq T$, $\mathbb{R}_+ \triangleq \{\, \gamma \in \mathbb{R} \mid \gamma > 0 \,\}$ and

$$G \triangleq \{\, u \in L_\infty[0,1] \mid |u(t)| \le 5,\ t \in [0,1] \,\}.$$

$$\mathbf{P}_2: \quad \min_{T \in \mathbb{R}_+,\, u \in G} \{\, g^0(u,T) \mid g^j(u,T) - \varepsilon \le 0,\ j \in \{1,2,3,4,6\} \,\},$$

where $g^0(u,T) \triangleq \int_0^1 \|u(t)\|^2\, dt$.

$$\mathbf{P}_3: \quad \min_{T \in \mathbb{R}_+,\, u \in G} \{\, g^0(u,T) \mid g^j(u,T) - \varepsilon \le 0,\ j \in \{1,2,3,4,5\} \,\},$$

where $g^0(u,T) \triangleq T$.

- All g^j are continuously differentiable in $L_\infty[0,1]$.

THE DYNAMICAL SYSTEM

COMPUTATIONAL RESULTS

IMPLEMENTATION. Because we cannot solve the system PDEs exactly, we cannot evaluate $\mathbf{g}^j(\mathbf{u},\mathbf{T})$ or $\nabla\mathbf{g}^j(\mathbf{u},\mathbf{T})$ exactly. Furthermore, since $\mathbf{u}$ is an infinite dimensional design vector, it can only be entered into a computer in discretized form. We use an *implementable* algorithm which adjusts integration precision and control discretization adaptively. To discretize the PDE in space, we use the finite element method. Since the PDE is fourth order in space, it is necessary to use elements of at least second order. We have chosen Hermite splines as basis elements. The input $\mathbf{u} \in \mathbf{G}$ is discretized in time and Newmark's method is applied to evaluate the resulting system of ordinary differential equations.

LINEARIZATION. The results presented are for the case in which the $\Omega^2(\mathbf{t})$ terms are neglected in equation (1). Similar results have been obtained by performing experiments when the $\Omega^2(\mathbf{t})$ terms are included.

SCOLE 87/24

OPTIMAL CONTROL FOR MINIMUM-TIME PROBLEM

WITH TORQUE CONSTRAINTS ONLY

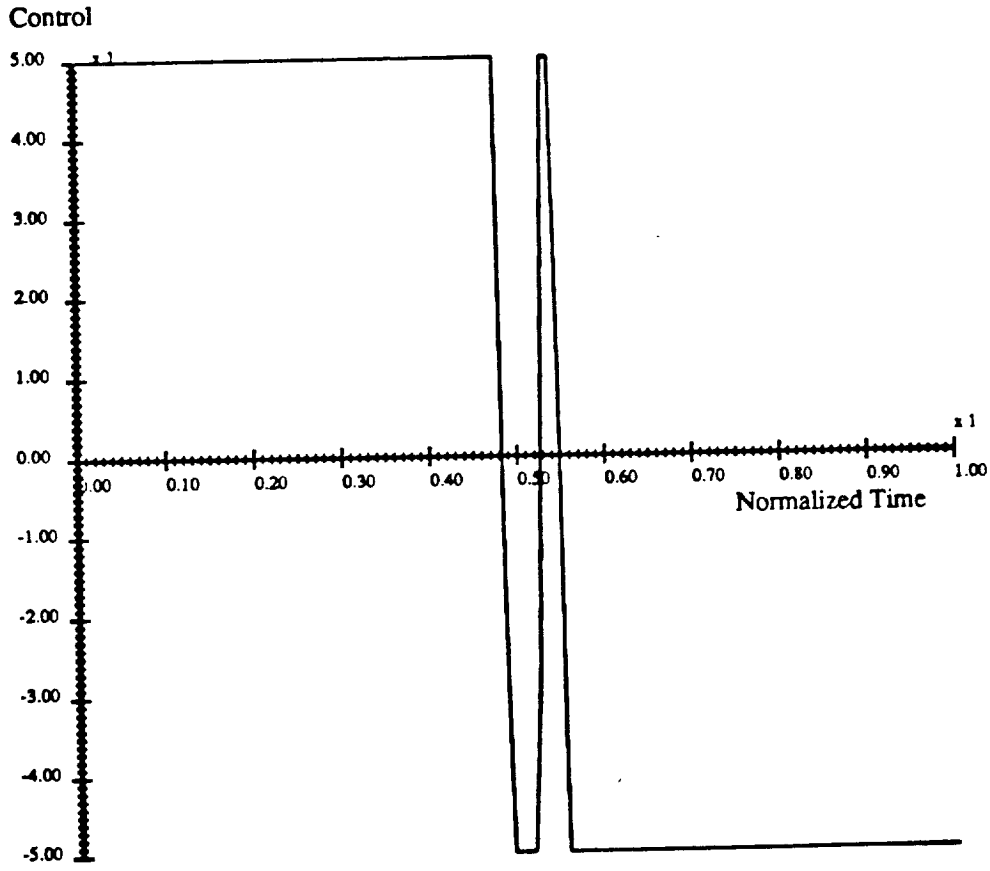

C 4

TIP DISPLACEMENT FOR MINIMUM-TIME PROBLEM

WITH TORQUE CONSTRAINTS ONLY

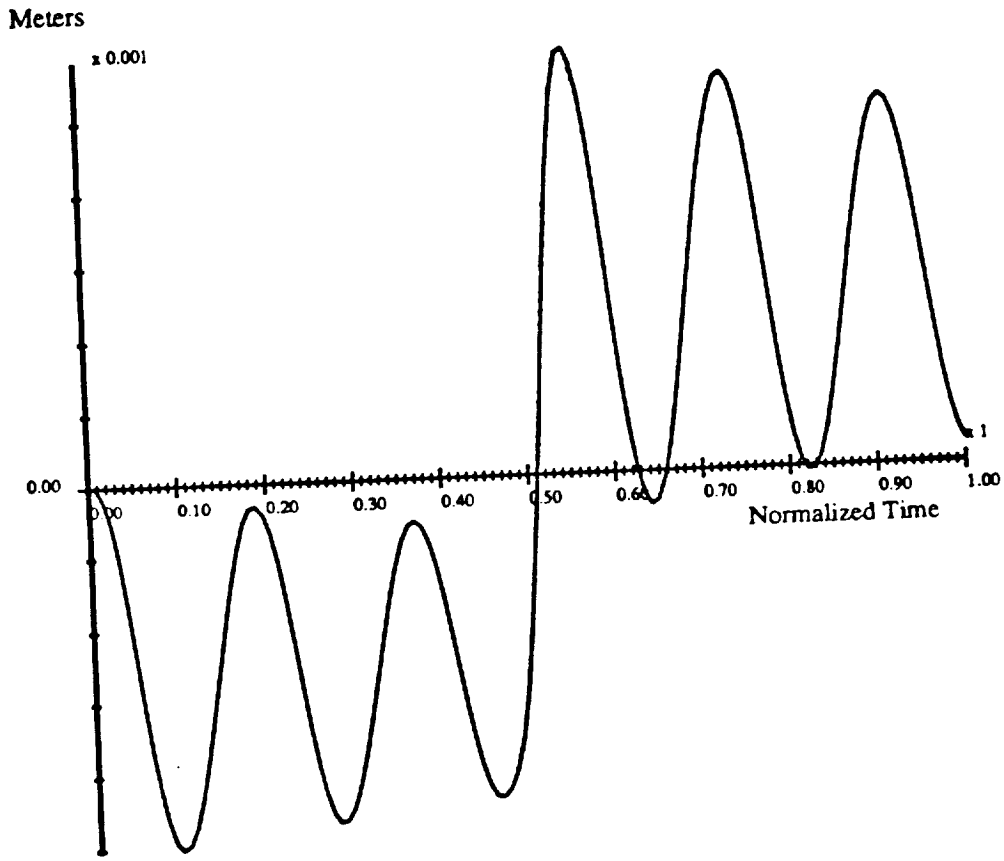

DEVIATION FROM SHADOW BEAM FOR MINIMUM-TIME PROBLEM WITH TORQUE CONSTRAINTS ONLY

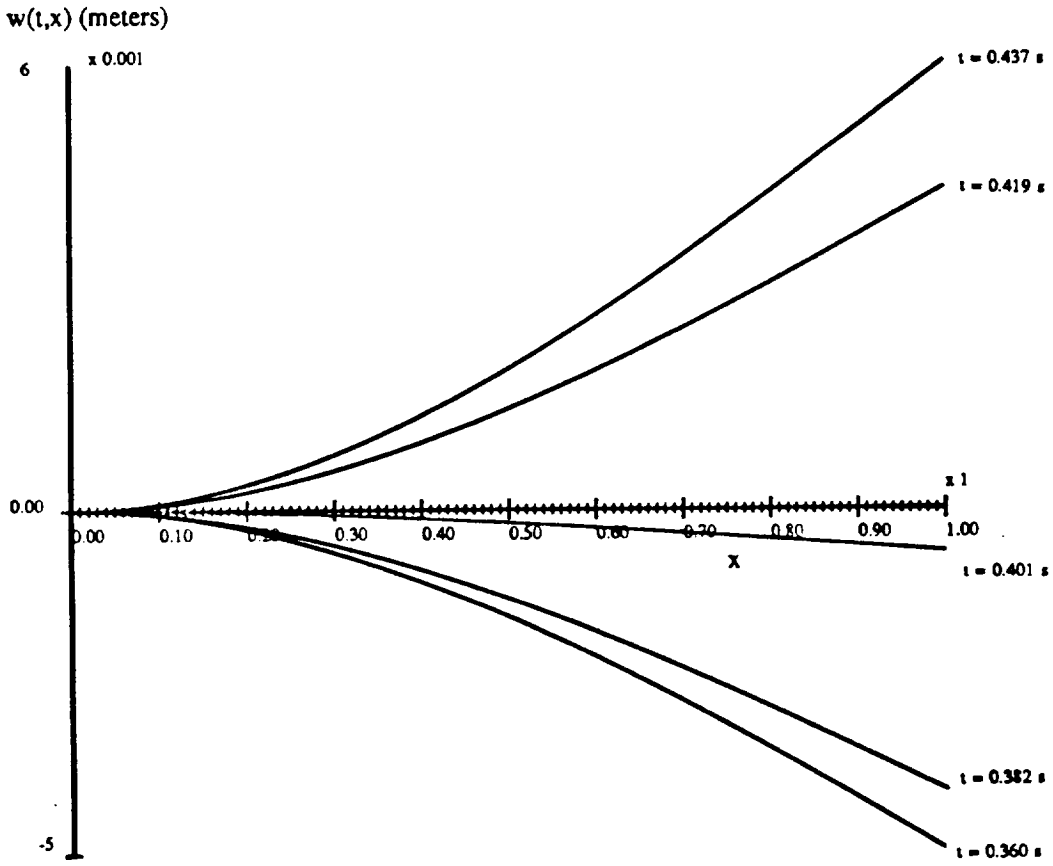

CONSTRAINT VIOLATION FOR MINIMUM-TIME PROBLEM WITH TORQUE CONSTRAINTS ONLY: DISCRETIZATION EFFECTS

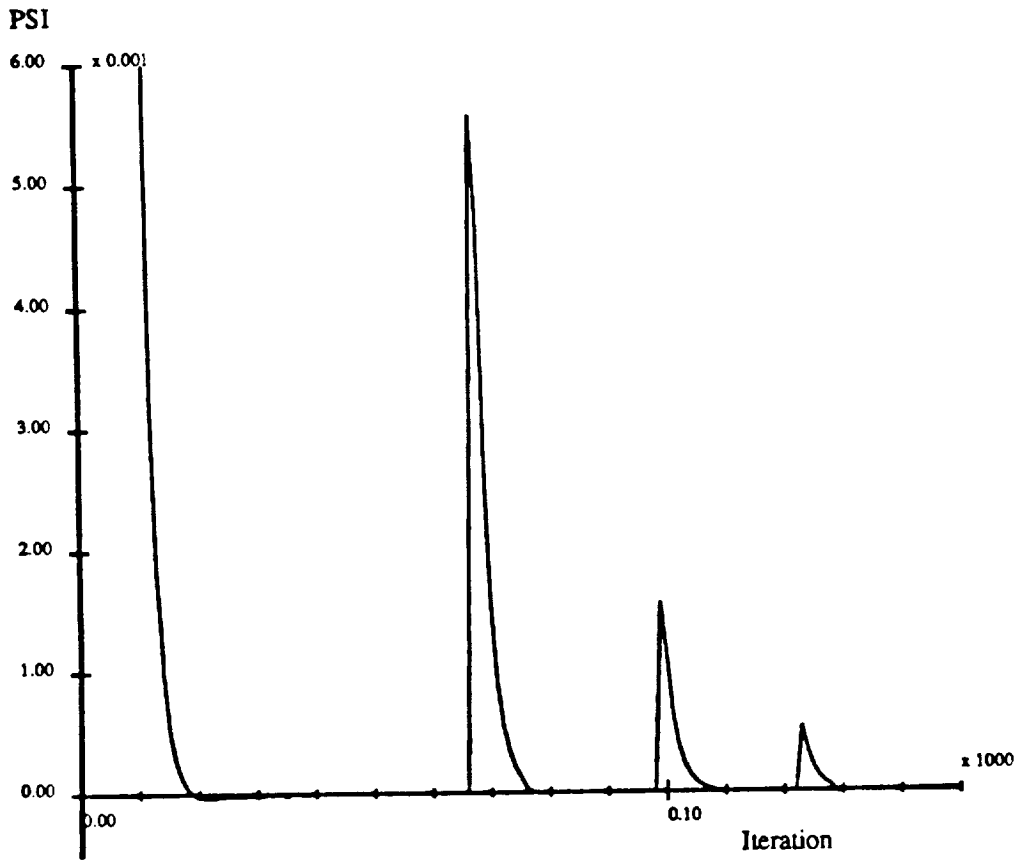

OPTIMAL TORQUE

FOR MINIMUM-CONTROL-ENERGY PROBLEM

WITH TORQUE CONSTRAINTS AND FINAL TIME ≤ 0.8 SEC.

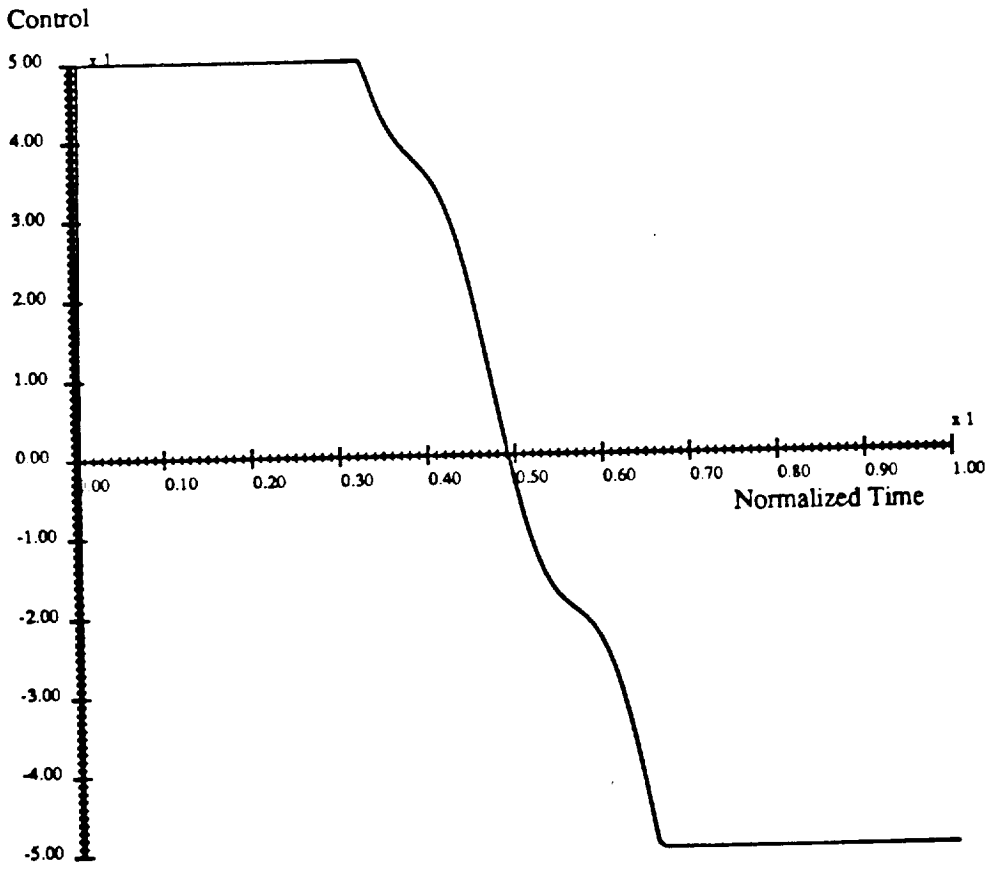

SCOLE 87/29

OPTIMAL TORQUE

FOR MINIMUM-CONTROL-ENERGY PROBLEM

WITH TORQUE CONSTRAINTS AND FINAL TIME ≤ 1.0 SEC.

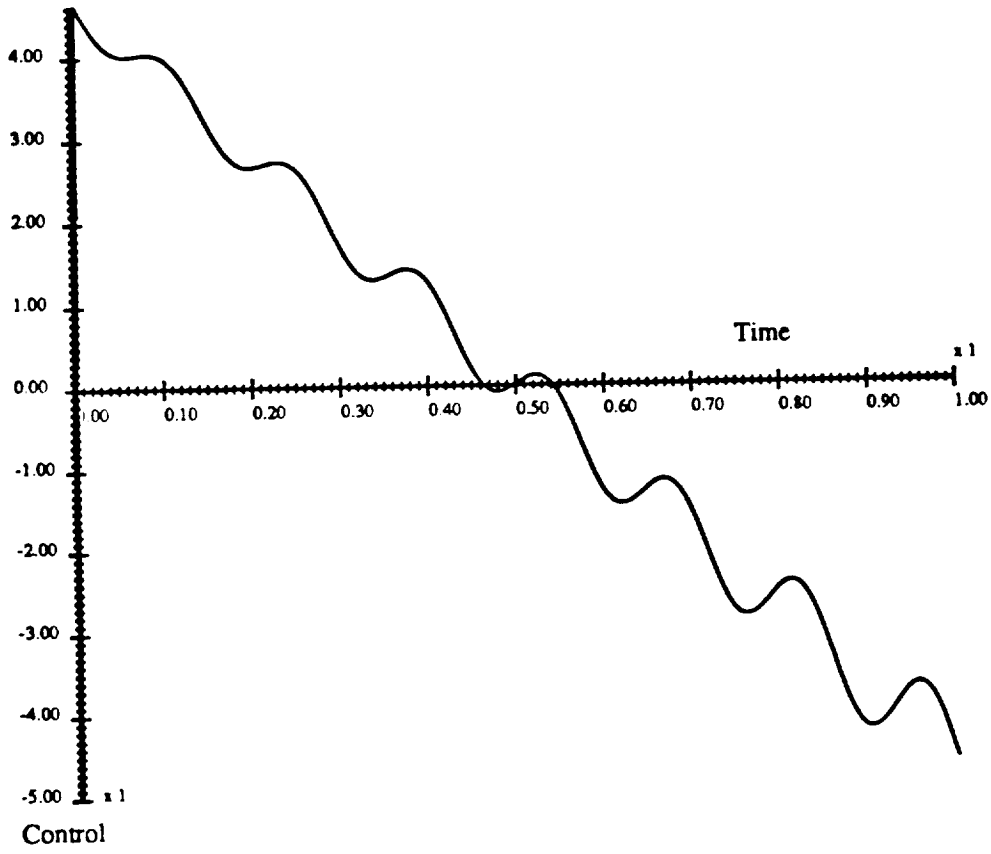

POTENTIAL ENERGY FOR MINIMUM TIME PROBLEM

WITH TORQUE CONSTRAINTS ONLY

Curve A is potential energy

Parabola B is deformation constraint.

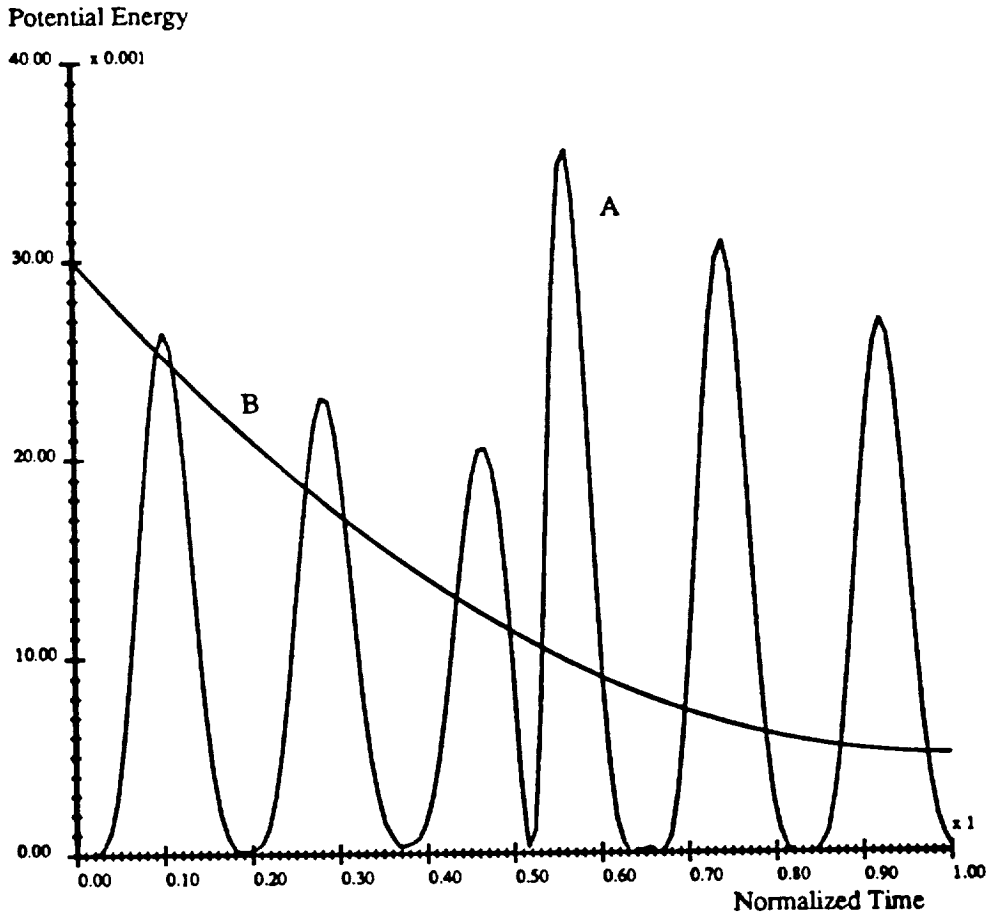

POTENTIAL ENERGY FOR MINIMUM-TIME PROBLEM WITH TORQUE AND POTENTIAL ENERGY CONSTRAINTS

Curve A is potential energy

Parabola B is deformation constraint.

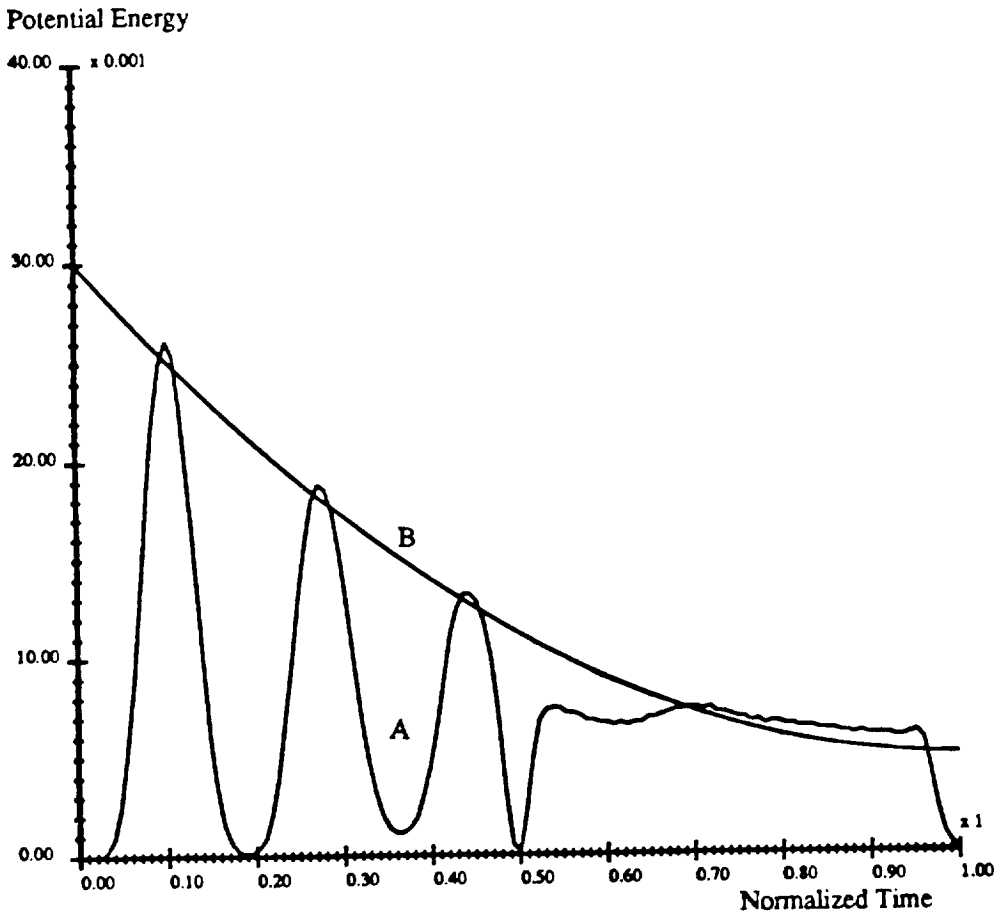

OPTIMAL CONTROL FOR MINIMUM-TIME PROBLEM WITH TORQUE AND POTENTIAL ENERGY CONSTRAINTS

Note: The optimal final time is 0.8177 seconds, an increase of only 3.7 percent over the solution of $\mathbf{P}_1$.

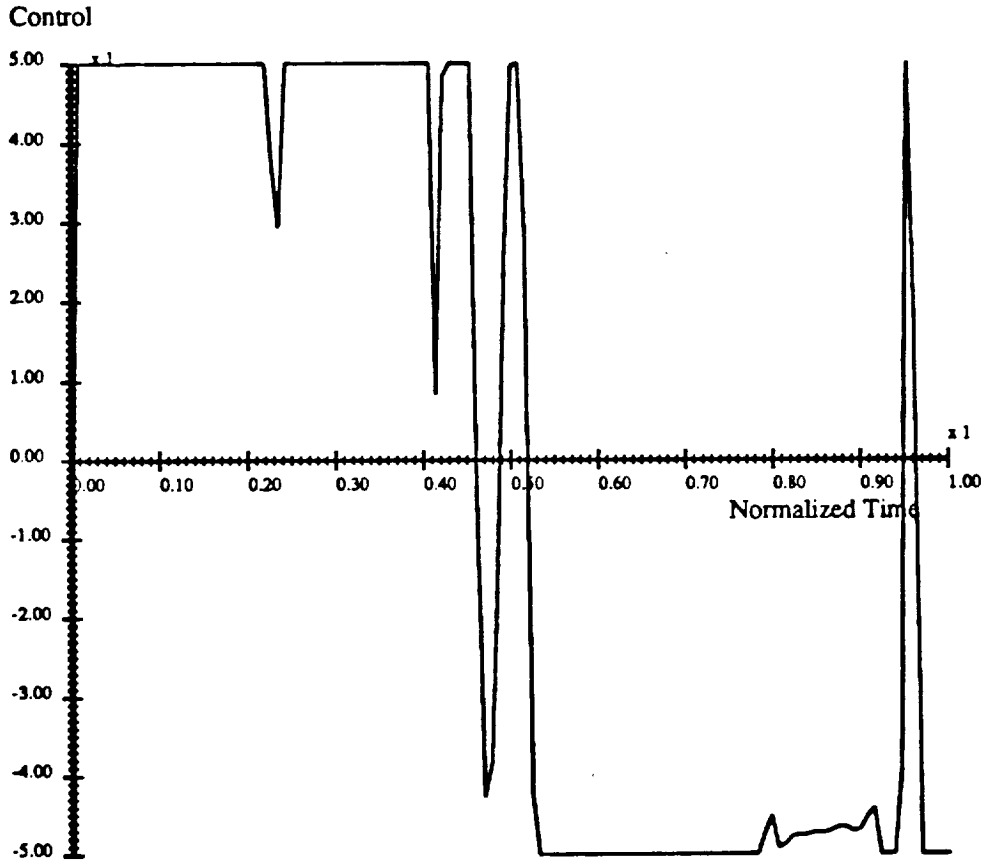

EFFECT OF ACTUATOR DYNAMICS ON CONTROL OF BEAM FLEXURE DURING NONLINEAR SLEW OF SCOLE MODEL

SHALOM ("MIKE") FISHER

NAVAL RESEARCH LABORATORY

NOVEMBER 16, 1987

Simulation of Two Aspects of Physical Limitations on Regulation of Beam Flexure

- One foot travel limitation on displacement of proof-mass actuators
- Time delay of 0.1 second in application of controls

goal is to assess magnitude of induced errors:

compared to ideal, how much flexure during slew and settling

DISCOS SIMULATION:

BODIES CONNECTED BY HINGES

FINITE ELEMENT MODEL OF BEAM PROVIDED BY NASTRAN

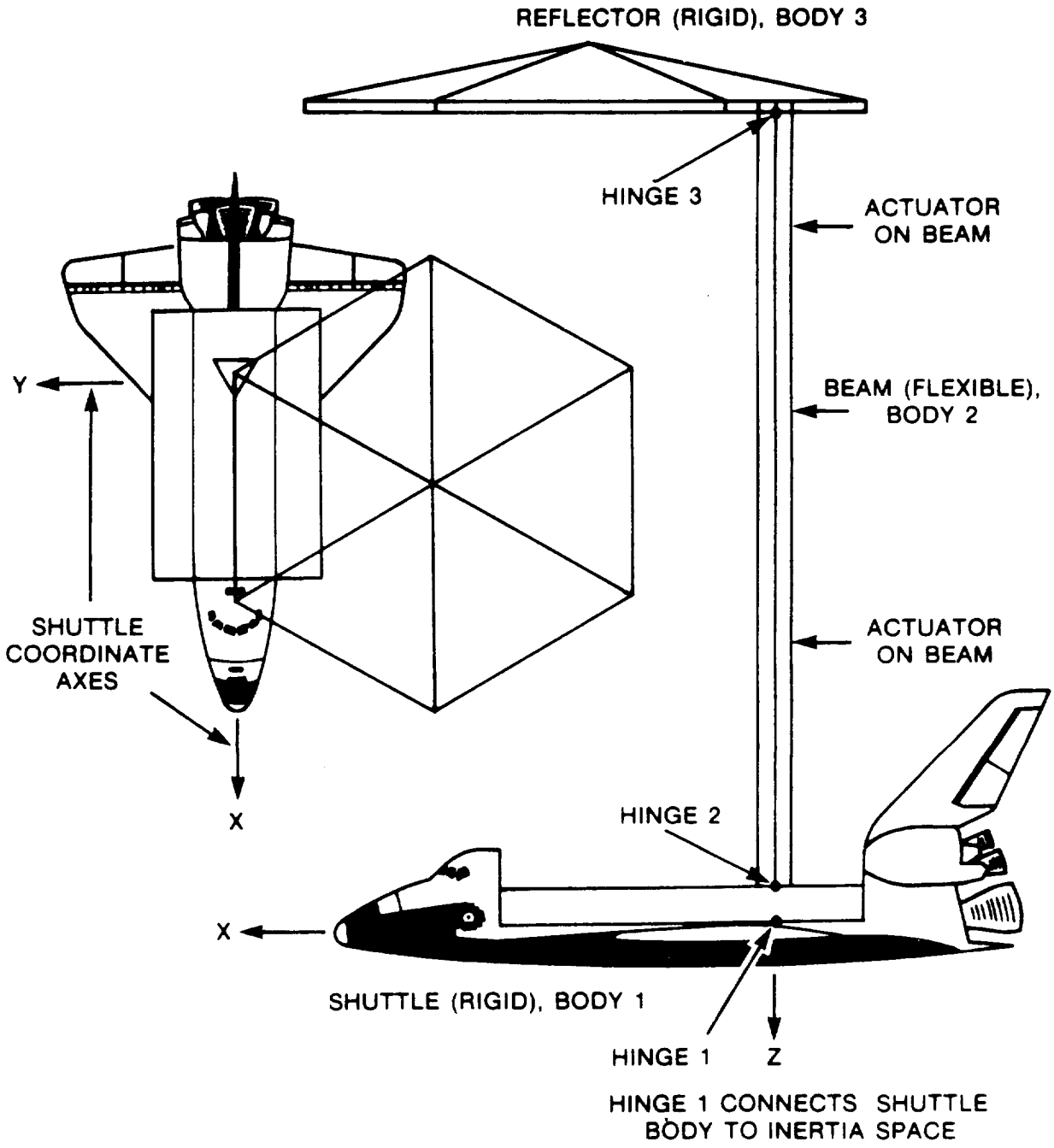

Fig. 1—Scole Configuration

TWO PARTS OF SIMULATION

1. Open-loop commanded slew
   10,000 ft-lb thrusters on shuttle body
   50 lb force on reflector
   bang-bang control law
   thrusters on full for 5.65 seconds, then reverse full
   slew completed in 11.30 seconds (20^0)

2. Regulation of beam flexure during slew and after (settling)
   Linear quadratic regulator (LQR)
   vernier thrusters (60 ft-lb torque) on shuttle and reflector
   2 sets of 2 axes proof-mass actuators on beam
   each set of actuators has 10 lb force in both "x" and "y"
   maximum of 1 ft travel distance of proof-mass

PROCEDURES OF THIS ANALYSIS

- NASTRAN finite element model for flexible beam
  12 vibration modes of beam
  Reflector and shuttle body assumed to be rigid

- Nonlinear DISCOS simulation of 20 degree slew

- Closed-loop linear quadratic regulator (LQR)

- Regulator uses:
  1. Proof mass actuators on beam
     Maximum force is 10 lbs.
     Maximum stroke is 1 foot.

  2. Thruster moments on shuttle body
     Thruster forces on reflector

LQ REGULATOR FOR FLEXIBLE BEAM

- Purpose: To maintain the flexible beam in a nominally unbent position during the large angle slew
- Method: Linear quadratic regulator (LQR) matrices computed offline
- Linearized system equation: $\dot{x}(t) = \mathbf{A}x(t) + \mathbf{B}u(t)$

  $x(t)$: components are modal amplitudes and rates

  $\mathbf{A}$: system matrix

  $\mathbf{B}$: control distribution matrix

  $u(t)$: input forces, applied at points on the beam
- Cost functional to be minimized:

$$J = \int_0^\infty [x^T(s)\mathbf{Q}x(s) + u^T(s)\mathbf{R}u(s)]ds$$

LQ Regulator (continued)

- Objectives in minimizing cost functional:

  1. Maximize regulator performance
  2. 10 lb limitation on regulator force

- Solve control algebraic Ricatti equation:

$$0 = \mathbf{Q} + \mathbf{A}^T\mathbf{P} + \mathbf{PA} - \mathbf{PBR}^{-1}\mathbf{B}^T\mathbf{P}$$

set $\mathbf{Q} = \mathbf{I}$ and $\mathbf{R} = r\mathbf{I}$, with $r = 10^{-6}$

- Input force vector u(t) is given by:

$u(t) = -\mathbf{R}^{-1}\mathbf{B}^T\mathbf{P}\,\tilde{x}(t)$: u(t) is recalculated at each time step

$\tilde{x}(t)$ incorporates time lag: $\tilde{x}(t) = x(t - h)$ with h = time delay

$\tilde{x}(t)$ can include a reduced set of modes

ASSESS EFFECTS OF 1 FT TRAVEL LIMIT

COMPARISON RUNS : Simulate 20^0 slew, t = 0 to 30 seconds

RUN #1	No limit on proof-mass travel distance
RUN #2	1 foot limit imposed
Run #3	No proof-mass actuators

RESULTS

Runs #1 and #2, maximum flexure amplitude is about 0.009^0

Run #3 maximum flexure is about 0.010^0

Somewhat less damping in run #2 than in run #1

Significantly less damping in run #3 than in the other runs.

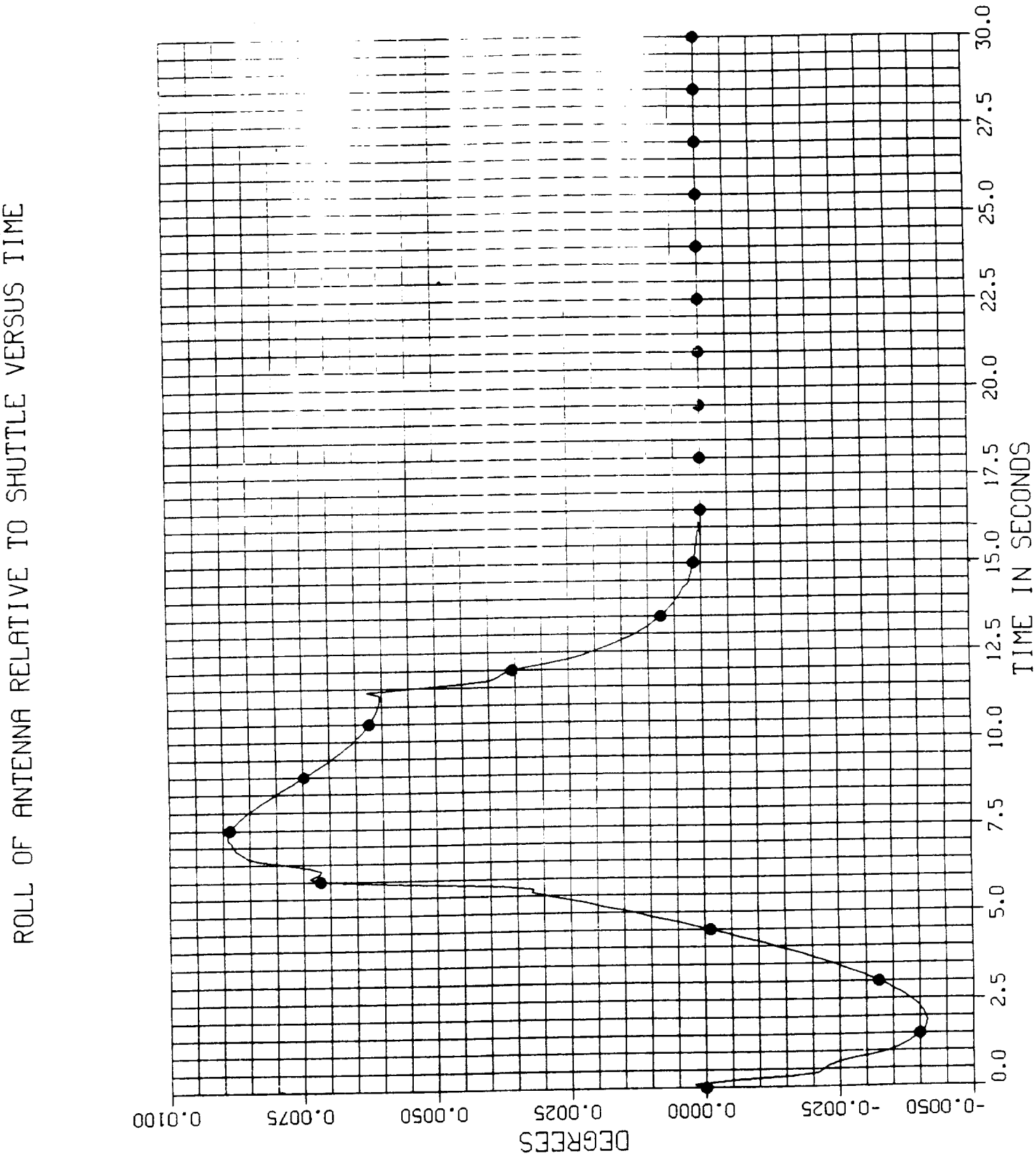

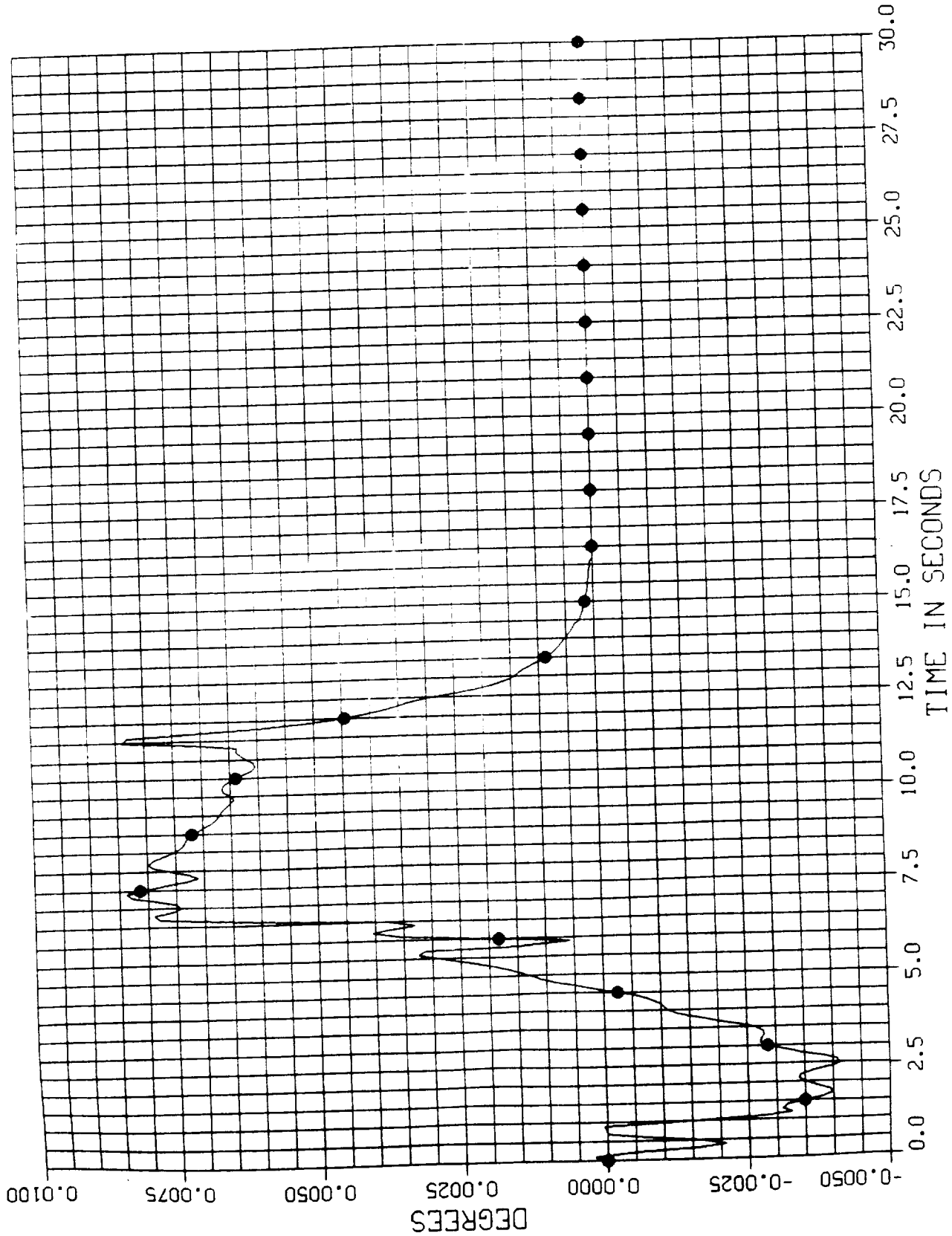

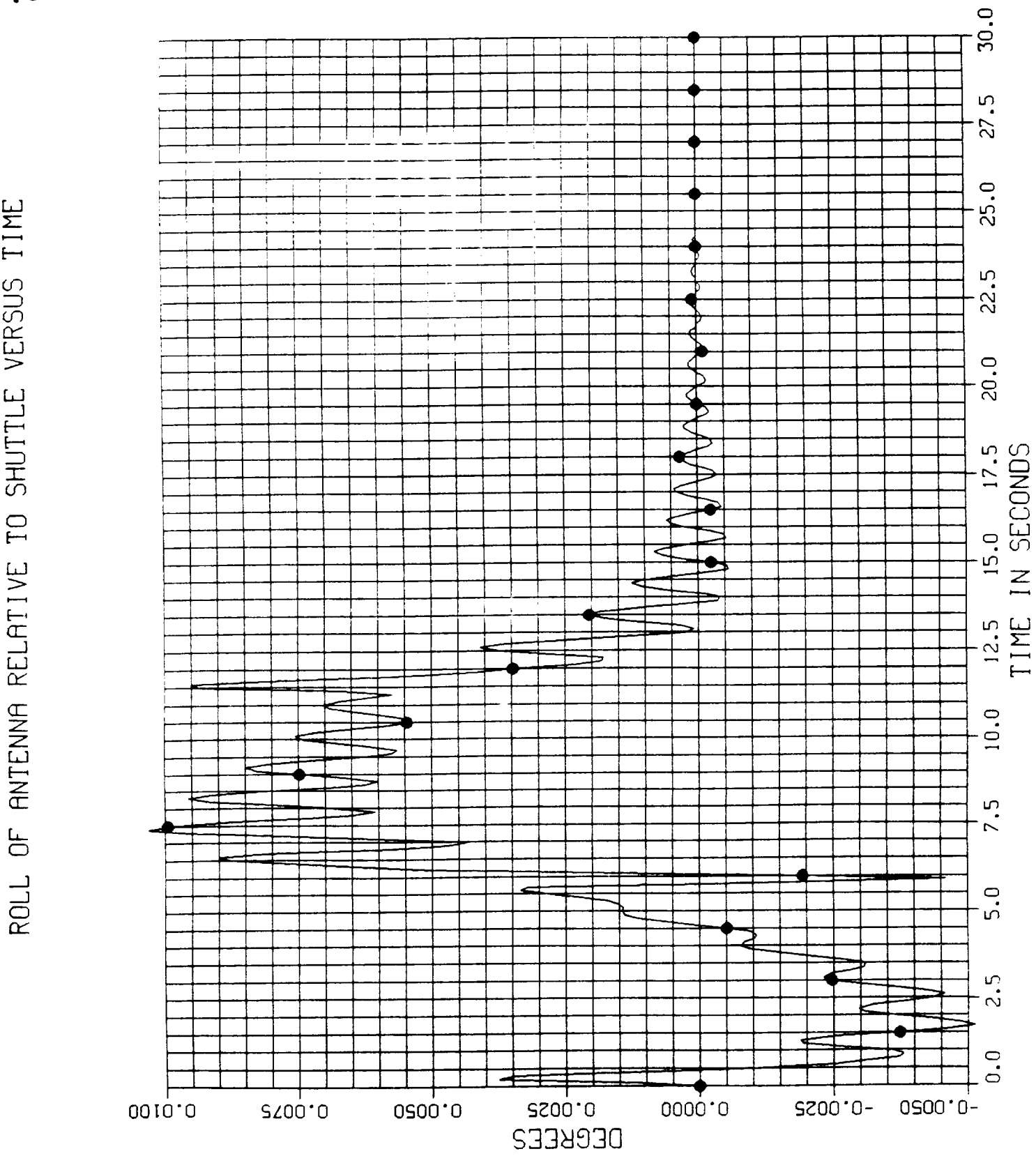

MODAL CONTROLLABILITY WITH TIME DELAY

MODE #	ω in radians	τ in seconds	max h $\tau/4$ criterion	max h $\tau/6$ (Reddy & Bainum)
1	1.746	3.60	0.90	0.576
2	1.969	3.195	0.80	0.511
3	5.105	1.232	0.31	0.197
4	7.410	0.848	0.21	0.136
5	12.848	0.489	0.12	0.078
6	29.459	0.213	0.053	0.034
7	34.263	0.183	0.046	0.029
8	74.670	0.084	0.021	0.013
9	78.883	0.080	0.020	0.013
10	106.281	0.059	0.015	0.009
11	142.467	0.044	0.011	0.007
12	145.618	0.043	0.010	0.007

COMPARISON OF CONTROL EFFECTIVENESS

h = .1 sec

	No regulator	No time delay	Modes 1-4	Modes1-5
Max flexure	0.4^0	0.0085^0	0.08^0	0.115^0
Steady-state	0.4^0	0 at 16 sec	0.036^0	0.05^0

ROLL OF ANTENNA RELATIVE TO SHUTTLE VERSUS TIME

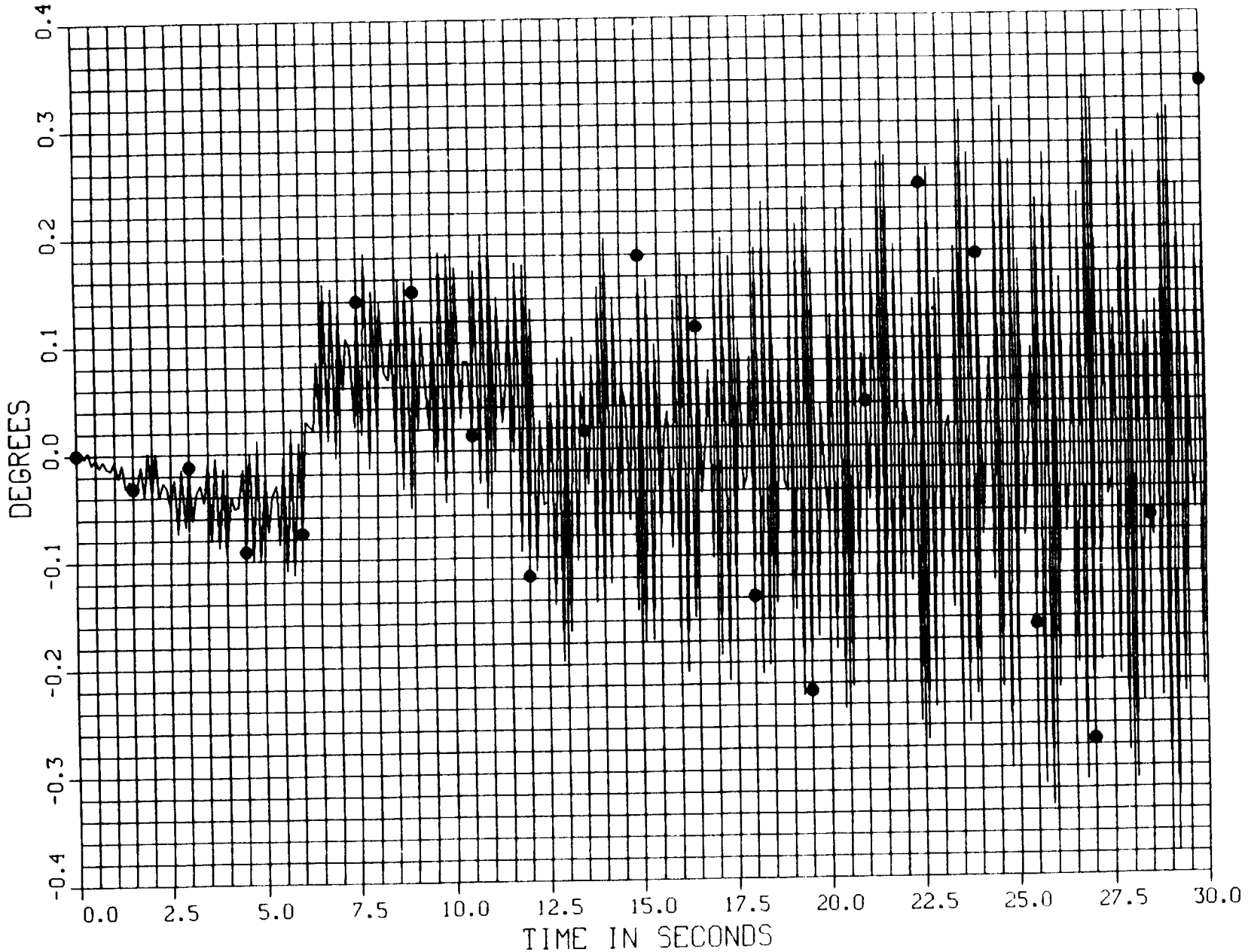

ROLL OF ANTENNA RELATIVE TO SHUTTLE VERSUS TIME

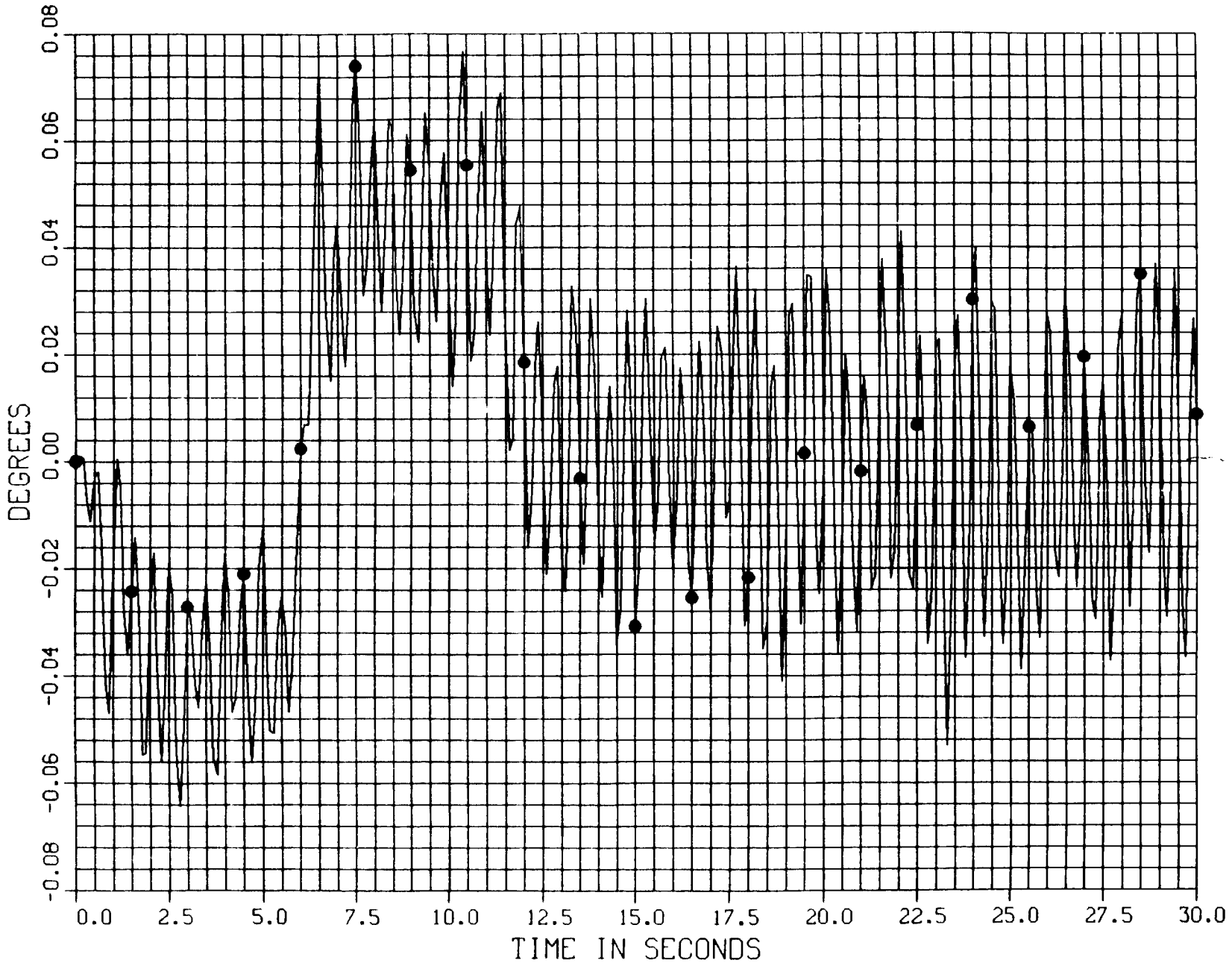

ROLL OF ANTENNA RELATIVE TO SHUTTLE VERSUS TIME

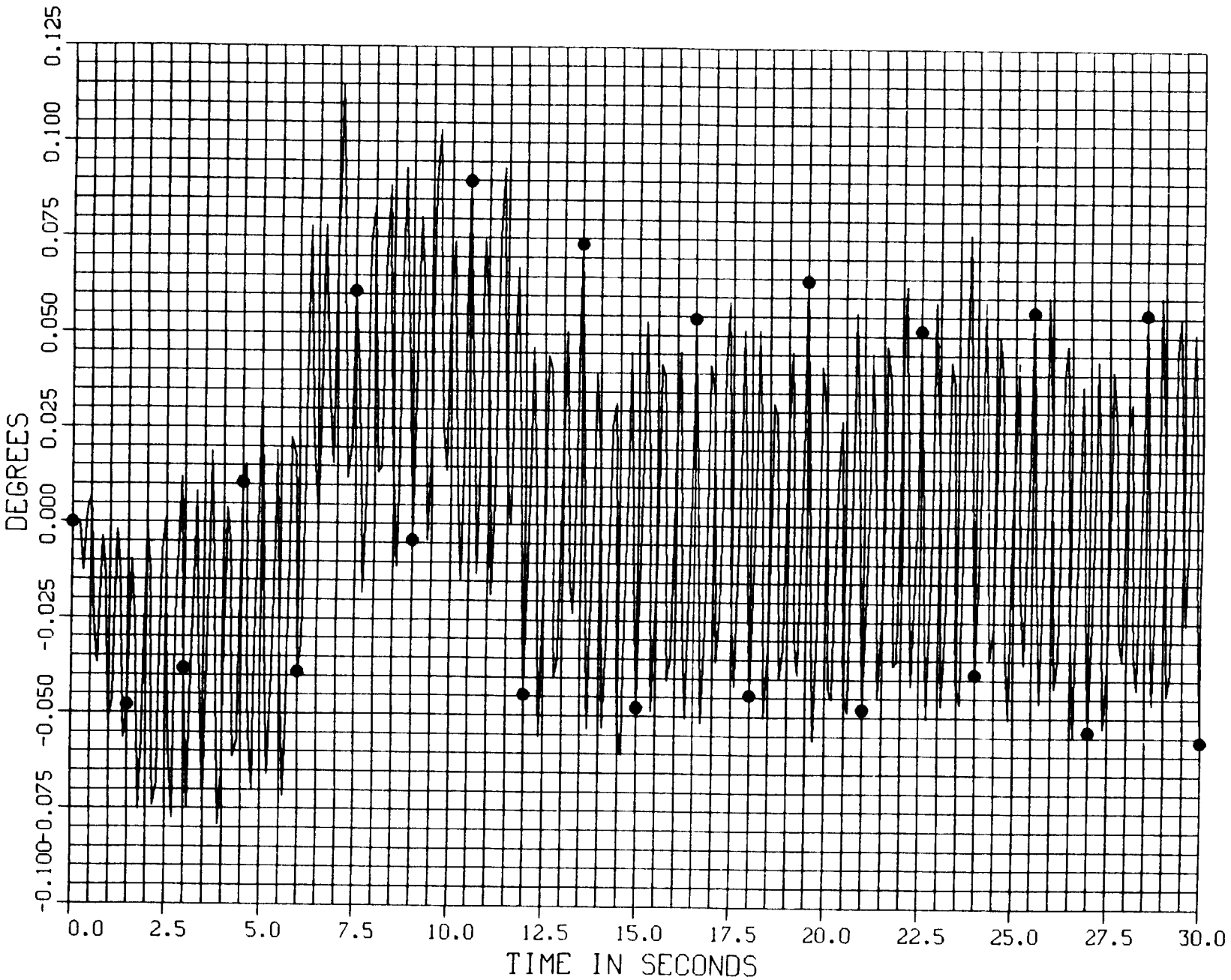

CONCLUSION

RULE THAT ONLY MODES FOR WHICH

max period/6 $>$ h (length of time delay)

CAN BE CONTROLLED APPEARS TO HAVE BEEN VALIDATED

AT LEAST FOR LQ REGULATOR of this calculation

NEED MORE ROBUST REGULATOR to do better

COMBINED PROBLEM OF SLEW MANEUVER CONTROL AND VIBRATION SUPPRESSION

Y. P. Kakad

Dept. of Electrical Engineering
University of North Carolina at Charlotte
Charlotte, NC 28223

4th Annual SCOLE Workshop

November 1987

COMBINED PROBLEM OF SLEW MANEUVER CONTROL AND VIBRATION SUPPRESSION

Y. P. Kakad

Dept. of Electrical Engineering
University of North Carolina at Charlotte
Charlotte, NC 28223

ABSTRACT

In this paper, the combined problem of slew maneuver control and vibration suppression of NASA Spacecraft Control Laboratory Experiment (SCOLE) is considered. The coupling between the rigid body modes and the flexible modes together with the effect of the control forces on the flexible antenna is discussed. The nonlinearities in the equations are studied in terms of slew maneuver angular velocities.

INTRODUCTION

In this paper, the analytics for the combined problem of slew maneuver and vibration suppression are developed. It is assumed that the slew maneuver is performed by applying moments on the rigid shuttle and the vibration suppression is achieved by means of forces on the flexible antenna and the reflector. The slew maneuver is considered to be an arbitrary maneuver about any given axis [16]. The effect of slew maneuver angular velocity on flexible modes is studied by examining the spectral norm of the matrix term associated with the coupling between the rigid-body modes and the flexible modes. Also, the kinematic nonlinearities are further analyzed in terms of the matrix spectral norm variation of the corresponding term with respect to slew maneuver angular velocity.

ANALYTICS

The slew maneuver is defined as

$\underline{\lambda}$ - Axis about which the slew maneuver is performed.

ξ - The slew Angle

$\underline{\omega}$ - The angular velocity of the orbiter in the inertial frame.

The four Euler parameters can be defined as

$$\begin{aligned} \epsilon_1 &= \lambda_1 \sin\frac{\xi}{2} \\ \epsilon_2 &= \lambda_2 \sin\frac{\xi}{2} \\ \epsilon_3 &= \lambda_3 \sin\frac{\xi}{2} \\ \epsilon_4 &= \cos\frac{\xi}{2} \end{aligned} \tag{1}$$

The four Euler parameters can be related to the angular velocity components of the rigid assembly as

$$\begin{bmatrix} \dot{\epsilon}_1 \\ \dot{\epsilon}_2 \\ \dot{\epsilon}_3 \\ \dot{\epsilon}_4 \end{bmatrix} = \begin{bmatrix} \epsilon_1 & \epsilon_4 & -\epsilon_3 & \epsilon_2 \\ \epsilon_2 & \epsilon_3 & \epsilon_4 & -\epsilon_1 \\ \epsilon_3 & -\epsilon_2 & \epsilon_1 & \epsilon_4 \\ \epsilon_4 & -\epsilon_1 & -\epsilon_2 & -\epsilon_3 \end{bmatrix} \begin{bmatrix} 0 \\ \omega_1 \\ \omega_2 \\ \omega_3 \end{bmatrix} \tag{2}$$

The slewing maneuver can be given in terms of the following equations [16]

$$I_o \dot{\underline{\omega}} + A_2 \ddot{\underline{q}} = \underline{G}(t) + \underline{N}_2(\omega) \tag{3}$$

$$A_2{}^T \dot{\underline{\omega}} + A_3 \ddot{\underline{q}} + B\dot{\underline{q}} + K\underline{q} = \underline{Q}(t) \tag{4}$$

where,

$\underline{G}(t)$ is the net moment applied about the mass center of the orbiter and is

given by the following equation (figs. 1 & 2)

$$\underline{G}(t) = \underline{G}_o(t) + (\underline{r} + \underline{a}) \times \underline{F}_2 \tag{5}$$

Also, $Q(t)$ represents the generalized force vector which is given by the following equation

$$Q(t) = \begin{vmatrix} \sum_{j=1}^{m} (Q_{jx_1}(t) + Q_{jy_1}(t)) + Q_{x_1} + Q_{y_1} + Q_{\psi_1} \\ \sum_{j=1}^{m} (Q_{jx_2}(t) + Q_{jy_2}(t)) + Q_{x_2} + Q_{y_2} + Q_{\psi_2} \\ \cdots \\ \cdots \\ \cdots \\ \sum_{j=1}^{m} (Q_{jx_i}(t) + Q_{jy_i}(t)) + Q_{xi} + Q_{yi} + Q_{\psi i} \\ \cdots \\ \cdots \end{vmatrix} \tag{6}$$

where, the generalized force components are given as

$$Q_{jx_i} = \int_0^L F_{jx}(z,t)\delta(z - z_j)\phi_{xi}(z)dz \tag{7}$$

$$Q_{jy_i} = \int_0^L F_{jy}(z,t)\delta(z - z_j)\phi_{yi}(z)dz \tag{8}$$

and

$$Q_{j\psi_i}(t) = 0 \tag{9}$$

Here, $F_{jx}(z,t)$ is the x component of the concentrated force applied at location j on the flexible antenna and F_{jy} is the y component of that force.

Also,

$$Q_{xi}(t) = F_{2x}(t)\phi_{xi}(L)$$

312

$$Q_{yi}(t) = F_{2y}(t)\phi_{yi}(L) \tag{10}$$

$$Q_{\psi i}(t) = M_{\psi}(t)\phi_{\psi i}(L)$$

Here, $\underline{F}_2$ is the force applied at the reflector C. G.

Thus,

$$M_{\psi}(t) = F_{2x} r_y + F_{2y} r_x + M_{2\psi} \tag{11}$$

The location of reflector C. G. is given by coordinates (r_x, r_y) and $M_{2\psi}$ represents the external moment applied at the reflector C. G. Also, the nonlinearities $\underline{N}_2$ can be expressed in terms of pure rigid body kinematic nonlinearity and the nonlinear coupling term between the rigid-body modes and the flexible modes.

$$\underline{N}_2 = A_4(\underline{\omega},\underline{\theta}) + A_5(\underline{\omega},\underline{\theta})\dot{\underline{q}} \tag{12}$$

(a) Slew Maneuver

If only a slew maneuver is to be considered, then $\underline{Q}(t) \equiv \underline{0}$ and $\underline{F}_2 \equiv \underline{0}$, and only moments are applied at the orbiter C. G. However, the angular velocity vector $\underline{\omega}$, is nonzero during the maneuver and the flexible modes will be excited. This effect of coupling between the rigid-body modes and flexible modes can be obtained by evaluating A_5 which depends on the angular velocity vector. In figure 3, using the matrix spectral norm as a measure, the coupling effect is studied as a function of slew angular velocity. The first ten flexible modes are considered for this analysis. The kinematic nonlinearity is also obtained in terms of matrix spectral norm as a function of $\underline{\omega}$. This analysis can be utilized in the linearization of the slew maneuver dynamical equations. An example of this is shown in figure 4 which is a single plane slew maneuver. In this case, it is almost a linear relationship in terms of a single angular velocity component.

(b) Slew Maneuver Control and Vibration Suppression

If it is desired to design control systems for the simultaneous task of slew maneuver control and vibration suppression, then equations (3)-(11) should be used. It can be seen that vibration control forces also affect the slew maneuver dynamics through control moment coupling terms.

Thus, these equations would suggest that in order to achieve control efficiency and to minimize the line of sight error in minimum time, it may be necessary to synthesize control systems for the combined problem of slew maneuver and vibration suppression.

REFERENCES

[1] L. W. Taylor, Jr. and A. V. Balakrishnan, "A Mathematical Problem and a Spacecraft Control Experiment (SCOLE) Used to Evaluate Control Laws for Flexible Spacecraft... NASA/IEEE Design Challenge," Proceedings of the Fourth VPI/AIAA Symposium on Dynamics and Control of Large Structures, pp 311-318, June 1983.

[2] A. S. Debs and M. Athans, "On the Optimal Angular Velocity Control of Asymmetrical Space Vehicles," IEEE Trans. Automat. Contr., pp 80-83, Feb. 1969.

[3] T. A. W. Dwyer, III, "The Control of Angular Momentum for Asymmetric Rigid Bodies," IEEE Trans. Automat. Contr., pp 686-688, June 1982.

[4] D. K. Robertson, "Three-dimensional Vibration Analysis of a Uniform Beam with Offset Inertial Masses at the Ends," NASA TM-86393, September 1985.

[5] T. R. Kane, P. W. Likins, and D. A. Levinson, Spacecraft Dynamics, New York: McGraw-Hill, 1983.

[6] J. Storch, S. Gates and D. O'Connor, "Three Dimensional Motion of a Flexible Beam with Rigid Tip Bodies," Charles Stark Draper Laboratory Report, Inter-lab Memorandum, October 1985.

[7] Y. P. Kakad, "Slew Maneuver Control of the Spacecraft Control Laboratory Experiment (SCOLE)," Proceedings of ACC Conference, pp 1039-1044 June 1986.

[8] Y. P. Kakad, "Dynamics and Control of Slew Maneuver of Large Flexible Spacecraft," Proceedings of AIAA Guidance, Navigation and Control Conference, pp 629-634, August 1986.

[9] B. Friedland, Control System Design - An Introduction to State-space Methods, New York: McGraw-Hill, 1986.

[10] H. Goldstein, Classical Mechanics, Reading: Addison-Wesley, Second Edition, 1981.

[11] M. Balas, "Feedback Control of Flexible Systems," IEEE Trans. Automat. Contr., pp 673-679, August 1978.

[12] A. E. Bryson, Jr. and Y. C. Ho, Applied Optimal Control - Optimization, Estimation, and Control, New York: John Wiley, revised printing, 1975.

[13] L. Meirovitch, Analytical Methods in Vibrations, New York: The Macmillan Company, 1967.

[14] E. S. Armstrong, "ORACLS - A System for Linear-Quadratic-Gaussian Control Law Design," NASA TP-1106, 1978.

[15] S. Joshi, "SCOLE Equations of Motion-A New Formulation," Proceedings of the 2nd Annual SCOLE Workshop, NASA TM-89048, pp. 14-25, December 1985.

[16] Y. P. Kakad, "Dynamics of Spacecraft Control Laboratory Experiment (SCOLE) Slew Maneuvers," NASA CR-4098, October 1987.

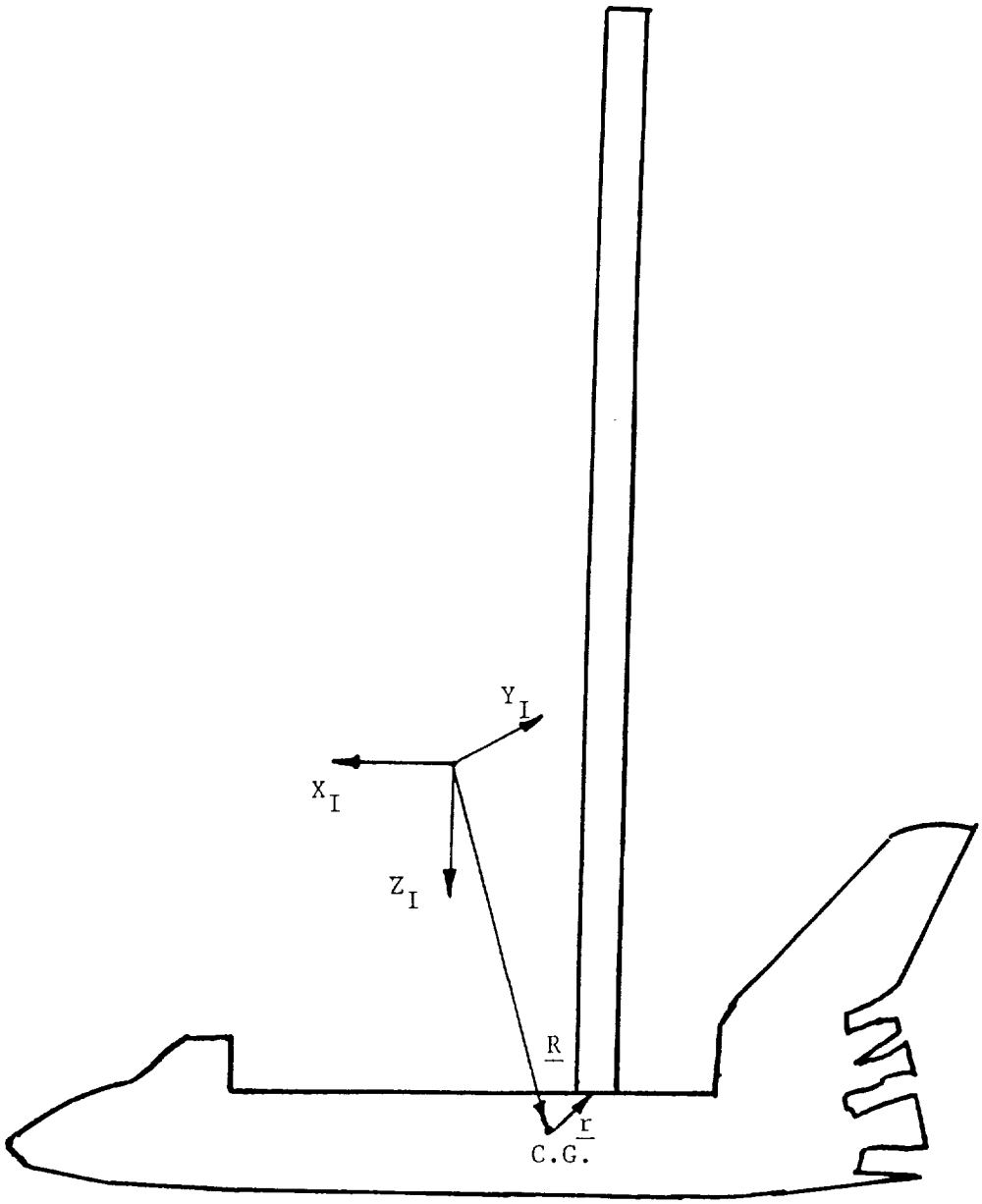

Figure 1- Position Vectors in Inertial Frame

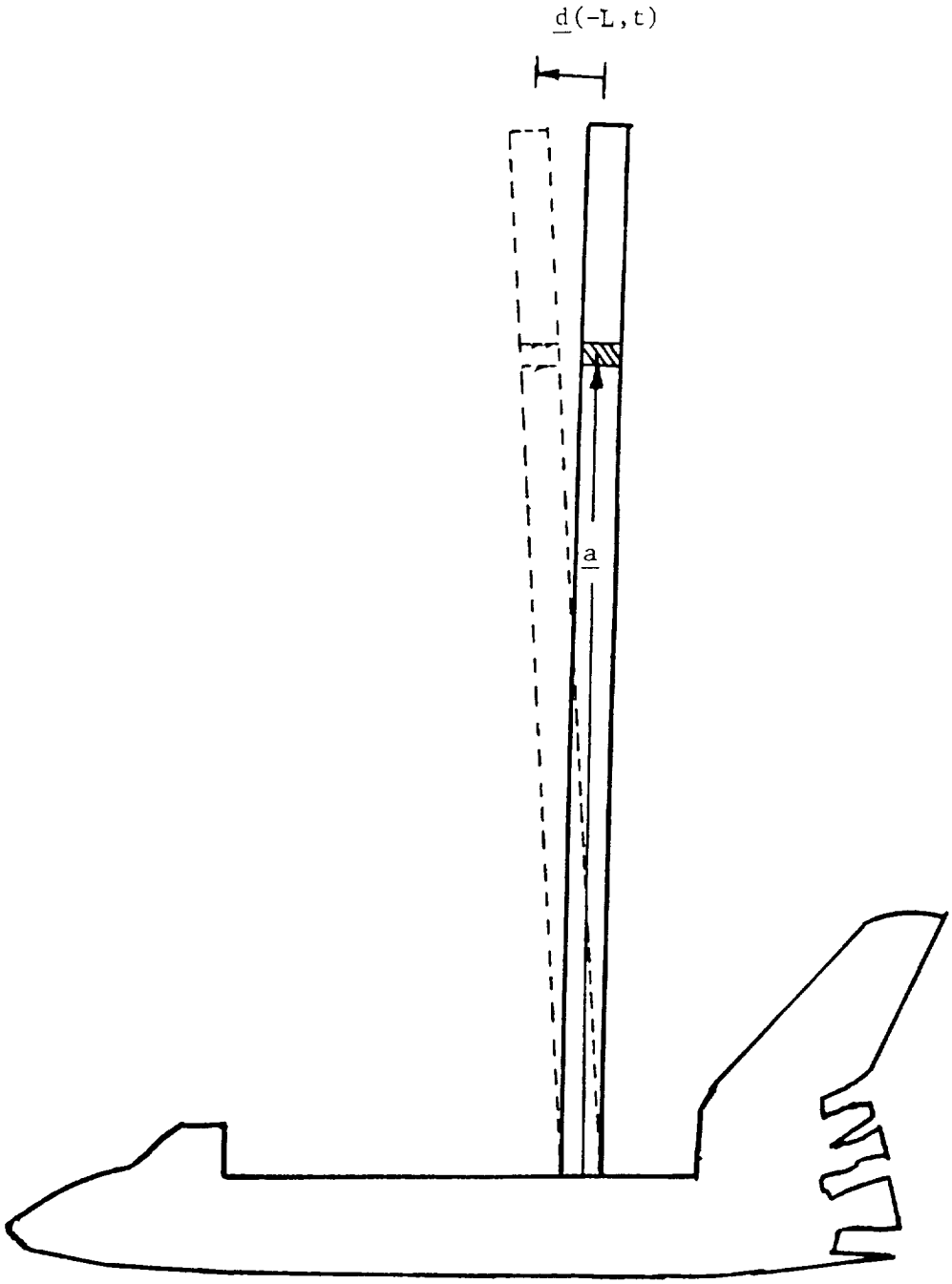

Figure 2- Vectors in Body-fixed Frame

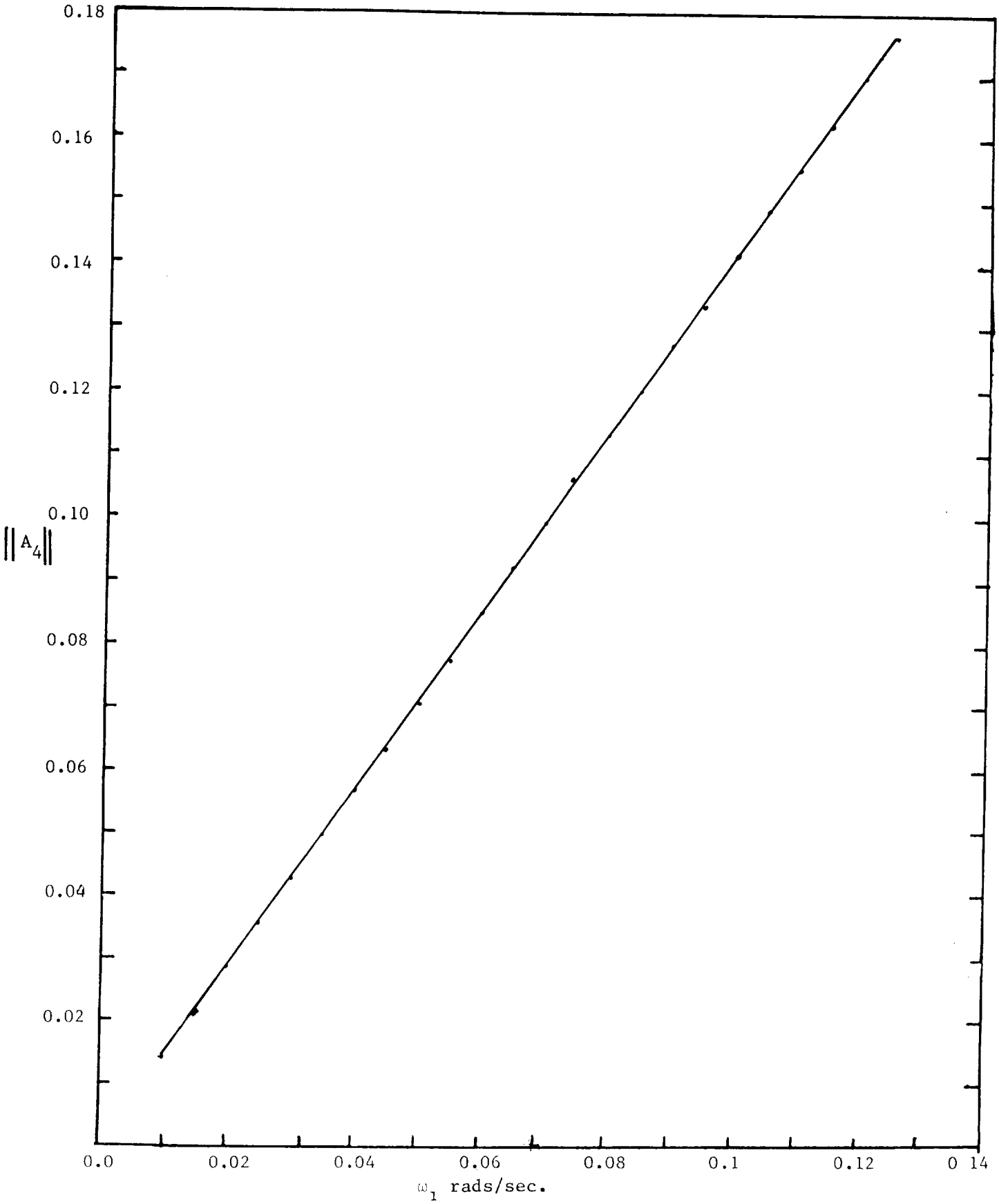

Figure 3- $\|A_4\|$ vs ω_1 ($\omega_2 = \omega_3 = 0$)

319

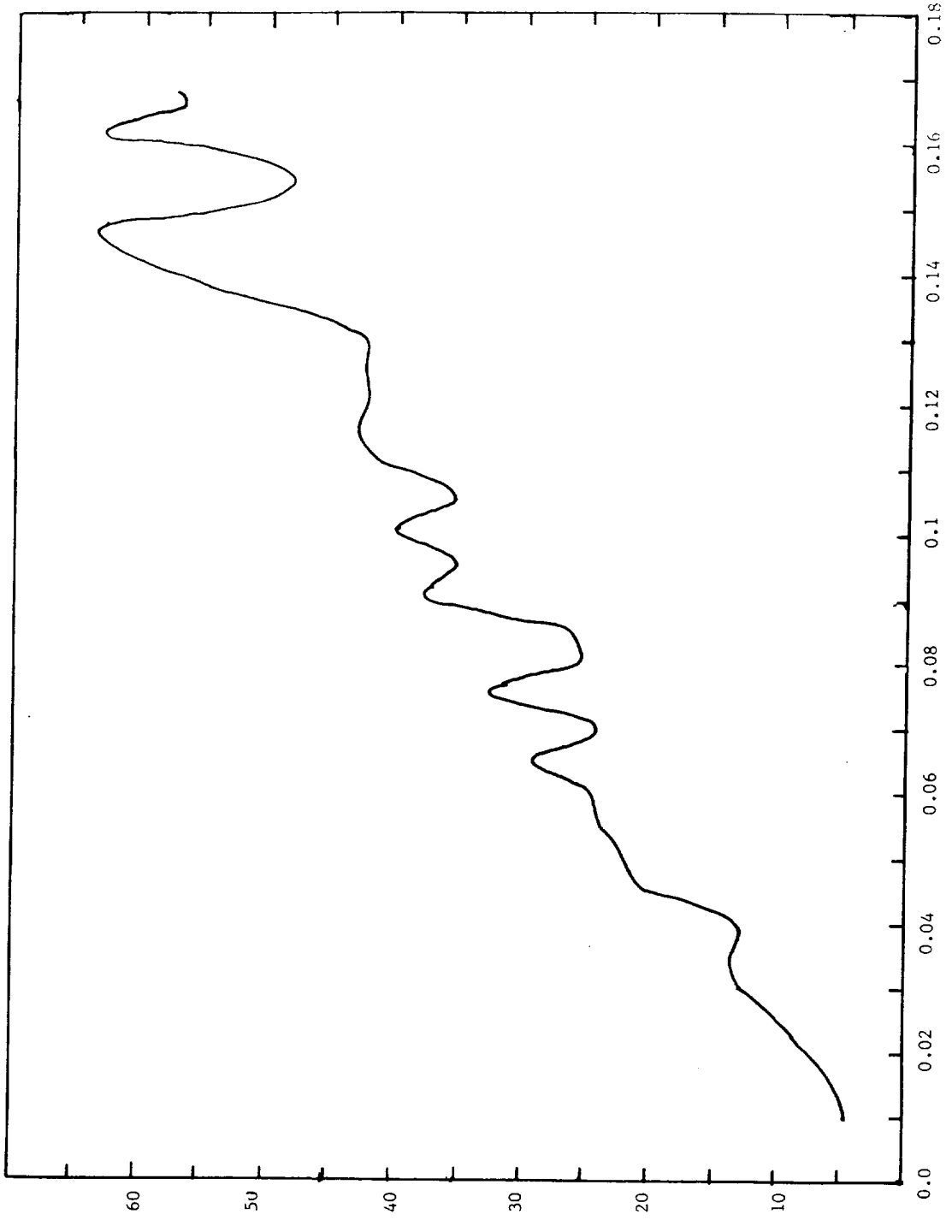

Figure 4 $\|A_5\|$ vs ω_1 ($\omega_2=\omega_3=0$)

320

N89-13474

ROBUST MODEL-BASED CONTROLLER SYNTHESIS FOR THE SCOLE CONFIGURATION

E. S. ARMSTRONG AND S. M. JOSHI
SPACECRAFT CONTROLS BRANCH
NASA LANGLEY RESEARCH CENTER
HAMPTON, VA 23665-5225

AND

E. J. STEWART
GEORGE WASHINGTON UNIVERSITY
HAMPTON, VA 23665

Robust Model-Based Controller Synthesis for the SCOLE Configuration

E.S. Armstrong S.M. Joshi E.J. Stewart*

NASA Langley Research Center
Hampton, VA 23665

ABSTRACT

The design of a robust compensator is considered for the SCOLE configuration using a frequency-response shaping technique based on the LQG/LTR algorithm. Results indicate that a tenth-order compensator can be used to meet stability-performance-robustness conditions for a 26th-order SCOLE model without destabilizing spillover effects. Since the SCOLE configuration is representative of many proposed spaceflight experiments, the results and design techniques employed potentially should be applicable to a wide range of large space structure control problems.

Introduction

Large space structures (LSS) have many properties that make them difficult to analyze and control [1]. They are mathematically modeled by computationally difficult partial differential equations or high-order, lumped, ordinary differential equations obtained through finite element methods. LSS have many low and closely spaced resonant frequencies, a number of which typically fall within the controller bandwidth. In LSS, vibrational issues must be treated as a first-order effect; it is this characteristic of the LSS control problem that most distinguishes it from spacecraft control problems of the past. Additionally, inherent damping is low and/or improperly modeled. Coupled with stringent operational requirements for orientation, shape control, and vibration suppression, these properties present an unconventional and unresolved control design problem to the system analyst.

A fundamental issue to be dealt with in any LSS control problem comes from the large amount of modeling error occurring in finite element models of such structures. In general, inaccuracy of modal data, such as elastic frequencies and mode shapes used to form coefficient matrices of the dynamic models, increases with increasing modal frequency. Hence, a frequency-dependent constraint is inherently imposed on the design process in that stabilization and performance requirements must be met without allowing the input control energy to "spill-over" and excite and destabilize the lightly damped, poorly modeled high-frequency dynamics.

At NASA's Langley Research Center, a LSS configuration known as the Spacecraft Control Laboratory Experiment (SCOLE) was conceived for the purpose of evaluating and comparing large space structure control and identification concepts [2]. The SCOLE configuration (shown schematically in Figure 1) consists of a 130-foot flexible beam anchored at one end to the cargo bay of the space shuttle with an antenna reflector connected to the opposite end. The center of mass of the reflector is offset from the attachment point. The SCOLE configuration is representative of many proposed space flight experiments and space-based antenna systems. Control inputs are available from torque actuators located on the orbiter and force actuators at the reflector center. Attitude sensors are located at the reflector center. A typical SCOLE control task is to slew or change the line-of-sight of the antenna rapidly and damp any induced structural vibrations to the degree required for the precise pointing of the antenna.

In this paper we consider a SCOLE large-angle slewing maneuver to have been completed and attack the problem of designing a model-based compensator to attenuate residual structural vibrational motion and antenna line-of-sight error. The SCOLE mathematical model is first discussed followed by descriptions of the design objectives and the compensator design approach. Finally, results from the application of the design methodology to the SCOLE problem are presented.

Mathematical Model

The basic distributed-parameter mathematical model of the SCOLE configuration is described in [2], while nonlinear and linear ordinary differential equation models are found in [3] and [4], respectively. A linear finite-element model consisting of three rigid rotational modes and the first ten structural elastic modes is used in this study. A state-space realization of the modal model has the

* George Washington University, Hampton, VA

form

$$\dot{x}_F = A_F x_F + B_F u \tag{1}$$

$$y_F = C_F x_F \tag{2}$$

where

$$A_F = \text{diag}(A_R, A_E) \tag{3}$$

$$A_R = \begin{bmatrix} 0 & I_3 \\ 0 & 0 \end{bmatrix}_{6\times6} \tag{4}$$

$$A_E = \text{diag}(A_E^1, A_E^2, \ldots, A_E^{10}) \tag{5}$$

and

$$A_E^i = \begin{bmatrix} 0 & 1 \\ -\omega_i^2 & -2\zeta_i\omega_i \end{bmatrix}_{2\times2} \tag{6}$$

for (i=1,...,10). Equation (4) describes the rigid body contribution and equations (5) and (6) describe the elastic contribution for ten vibrational modes of frequencies ω_i, (i = 1,..., 10). A uniform damping ratio of $\zeta_i = \zeta = 0.003$, (i = 1,..., 10), is assumed. The eigenvalues of A_E are given mathematically by

$$\lambda_i = -\zeta\omega_i \mp j\,\omega_i\sqrt{1-\zeta^2} \tag{7}$$

and are shown in Table I.

Five control inputs are generated using three torque actuators (one per X,Y,Z axis) on the orbiter and two force actuators (X and Y directions in Figure 1) at the reflector center. Three attitude sensors (one per axis) are located at the reflector center. Sensor and actuator dynamics were not included in this study. Rigid-body inertias, mode shape and slope data from the finite element analysis combine to define the control effectiveness matrix B_F and output response matrix C_F.

Analysis of (1) and (2) verifies that the system is completely controllable and observable. Attempts to reduce the number of control variables to the number of outputs retained controllability and observability but, in each three-control input combination, introduced lightly-damped, low-frequency transmission zeros [5] into the model. Since the presence of such transmission zeros has been demonstrated to reduce system performance in large space structure controller designs [6], the compensator was designed with the original five inputs and three outputs. However, in order to avoid numerical ill-conditioning brought about by the different physical characteristics of forces and torques, the inputs were scaled so that the frequency response of the largest ($\bar{\sigma}(j\omega)$) and smallest ($\underline{\sigma}(j\omega)$) singular values of the transfer matrix of (1) and (2), denoted by $G_F(j\omega)$, were nearly equal at low frequencies (as shown in Figure 2).

Design Objectives

The design objectives of this study are to produce a multivariable, model-based, feedback compensator operating on attitude sensor data which will generate force and torque inputs to stabilize the rigid body modes; enhance the stability of lightly damped, low-frequency modes without destroying the stability of higher-frequency modes; meet prescribed closed-loop performance (bandwidth) specifications; and possess some degree of stability robustness to unmodeled dynamics. Since a low-order controller is sought, it was decided to employ full-state controller design with a reduced-order plant model. The full-order model is reserved for evaluation purposes. Order reduction for the design plant was performed using modal truncation. Past studies ([6], [7]) have indicated that a 0.1 rad/sec closed-loop performance bandwidth is sufficient to maintain antenna pointing control, and a design model composed of the rigid body plus the first three elastic modes in Table I is adequate to achieve this bandwidth. Higher bandwidths will typically require the addition of extra elastic modes to the design model. Denoting the 12th-order design model transfer matrix by $G_p(s)$, for a unity-gain feedback compensator with transfer matrix $G_c(s)$, multivariable bandwidth will be defined as the frequency below which the smallest singular value of the closed-loop response matrix

$$G_{CL}(s) = G_p(s)G_c(s)[\ I + G_p(s)G_c(s)\ ]^{-1} \tag{8}$$

remains above unity for $s = j\omega$. In our case, we seek a compensator such that

$$\underline{\sigma}[G_{CL}(j\omega)] \geq 1.0 \text{ for } 0 \leq \omega \leq 0.1 \tag{9}$$

From the block diagonal structure of A_F in (1), the transfer matrix, $G_F(s)$, of the 26th-order system may now be written as

$$G_F(s) = G_p(s) + \Delta G(s) \tag{10}$$

where $\Delta G(s)$ represents the transfer matrix of the remaining 14th-order (residual) modal system. In this form, the dynamics represented by $\Delta G(s)$ can be interpreted as an "additive perturbation" to the $G_p(s)$ system and used as an approximate representation of unmodeled dynamics for use in stability robustness tests. Specifically, it is established in [8] that the unmodeled dynamics $\Delta G(s)$ will not destroy the closed-loop stability so long as

$$\bar{\sigma}(\ G_c(s)[\ I + G_p(s)G_c(s)\ ]^{-1}\ )\ \bar{\sigma}[\Delta G(s)] \leq 1 \tag{11}$$

for all $s = j\omega$, ω real. Condition (11) can be enforced in the compensator design stage to ensure that closed-loop stability will be preserved for at least that class of unmodeled dynamics whose spectral norm lies below $\bar{\sigma}[\Delta G(j\omega)]$.

The spillover effect on $\Delta G(s)$ due to the closed-loop compensation may be tested directly by applying a state-variable realization of $G_c(s)$ to the full 26th-order model given by (1) and (2) and examining the eigenvalues of the composite system.

A block diagram for the closed-loop configuration is shown in Figure 3. An approach for constructing $G_c(s)$ to stabilize $G_p(s)$ while satisfying (9) and (11) is presented in the next section.

Compensator Design Approach

The compensator design approach employed to meet the foregoing design objectives can be viewed as a variation of the well-known Linear-Quadratic-Gaussian/Loop-Transfer-Recovery (LQG/LTR) algorithm ([9], [10]). In the standard LQG/LTR approach, with the loop in Figure 3 broken at the output, a Kalman filter (G_{KF}) is designed to meet the complete set of stability-performance-robustness objectives. Thereafter, an optimal linear regulator is constructed such that the composite LQG compensator (G_c) loop gain behavior asymptotically approaches (recovers) that of G_{KF} in the sense that

$$G_p(j\omega)G_c(j\omega) \longrightarrow G_{KF}(j\omega)$$

pointwise in ω. Direct application of this LQG/LTR procedure to large space structures problems results in extremely conservative designs which cannot meet reasonable performance specifications [6]. However, the LQG/LTR structure still provides a viable approach for model-based controller synthesis when the standard procedure is modified in the following manner.

Step 1
Denote a state-variable realization of $G_p(s)$ by

$$\dot{x} = Ax + Bu \tag{12}$$

$$y = Cx \tag{13}$$

Select the design parameters L and μ in the Kalman filter algorithm

$$AQ + QA^T + LL^T - \frac{1}{\mu} QC^TCQ = 0 \tag{14}$$

$$H = \frac{1}{\mu} QC^T \tag{15}$$

such that

$$G_{KF}(s) = C(sI-A)^{-1}H \tag{16}$$

achieves a desired (target) loop gain for $G_p(s)G_c(s)$ over some low-frequency band containing the design bandwidth.

Step 2
By successively increasing $q > 0$ in equation (19) (to follow), design an optimal linear regulator which, when used in an LQG fashion with the Kalman filter from *Step 1*, asymptotically recovers the frequency response of the target loop gain over the low-frequency band. The resulting compensator is given by

$$G_c(s) = F(sI-\hat{A})^{-1}H \tag{17}$$

where

$$F = B^TP \tag{18}$$

$$A^TP + PA - PBB^TP + qC^TC = 0 \tag{19}$$

$$\hat{A} = A-BF-HC \tag{20}$$

Step 3
Attempt to adjust q in *Step 2* until the desired bandwidth condition (condition (9)) is met. Also check stability robustness by (11). If an excessively high q (indicated by violation of (11)) is required to achieve the required bandwidth, turn down the Kalman filter gain (by increasing μ in (14)) to "loosen" the target loop. In effect, this procedure reduces the target bandwidth until satisfaction of (11) is possible. The final design is accomplished by iteratively adjusting the linear regulator and Kalman filter design parameters until an appropriate compromise is made between bandwidth and stability robustness.

In large space structures applications, the inability (at *Step 1*) to meet loop gain magnitude over the desired bandwidth or (in *Step 3*) the production of too small a compromise bandwidth can often be overcome by the inclusion of additional flexible modes into the design model [6].

If, as in the SCOLE application to follow, an order-reduction study is performed on the resulting compensator, the complete set of stability-performance-robustness conditions needs to be re-evaluated with the reduced-order compensator.

SCOLE Application

Figure 4 shows the frequency response of the 12th-order (LQG) compensator, G_c, resulting from an application of the foregoing procedure to the 12th-order SCOLE design model, G_p. The figure indicates a well-behaved lead-lag structure with a 20 db/decade roll-off. Eigenvalues of the corresponding A-HC, A-BF, and $\hat{A}$ matrices are given in Table II. The frequency response of G_{CL} in equation (8) with the 26th-order evaluation model used in place of G_p is shown in Figure 5. Figure 5 demonstrates the satisfaction of the 0.1 rad/sec bandwidth requirement and a 60 db/decade roll-off. Eigenvalues of the composite system resulting from the LQG compensator applied to the evaluation model are given in the first column of Table III. The data indicate that the compensator was designed to concentrate on stabilizing the rigid body modes (first three entries of the A-HC block) without disturbing the stability of the three elastic modes (last three entries of the A-HC block) of the

design model. Table III also shows that there is insignificant spillover into ΔG. The stability robustness test (11) shown in Figure 6 shows more than 10 db robustness margin.

The possibility of a reduced-order compensator (ROC) satisfying the design conditions was also investigated. The methods of balanced realization [11], Hankel-norm reduction [12] and a method based on stable factorization [13] were employed. The ratio of largest to smallest Hankel singular values was 0.016 so little reduction based on nearly uncontrollable or unobservable compensator modes was expected. All of the methods gave similar results. In each order reduction method, only a 10th-order ROC would stabilize the design model. The stable factorization results were judged to be (slightly) better and will be discussed herein.

Table II shows the eigenvalues of the corresponding $\hat{A}$ matrix in the ROC, denoted by $\hat{A}_{ROC}$. Figure 7 shows a frequency response of the ROC. A comparison of Figures 4 and 7 shows that the only difference between the LQG and ROC frequency response plots is the removal of the dip in $\underline{\sigma}$ at the frequency of the third elastic mode. The importance of this characteristic can be seen from Figure 8 where the robustness condition (11) is evaluated using the ROC in place of G_c. Figure 8 indicates that an effect of the-order reduction is a reduction of stability margin at the frequency of the third elastic mode. A more positive effect from the reduced order compensation is seen in the second column of Table III where the eigenvalues of the ROC applied to the evaluation model are presented. The stability of the rigid-body modes from the LQG compensator is preserved with the auxiliary effect of adding stability to the first elastic mode. The net effect of the ROC is to enhance the stabilizing effect of the LQG compensator at the expense of a reduction of stability robustness margin.

Concluding Remarks

A loop-shaping procedure similar to that used in the LQG/LTR approach was used to design a model-based compensator for the SCOLE configuration, a generic large space structure configuration conceived for the purpose of evaluating and comparing control and identification approaches. Initially, the inputs of a full 26th-order SCOLE model were scaled to avoid numerical difficulties. A 12th-order controller design model was afterwards constructed from the full-order model using modal truncation. Applying a modification of the LQG/LTR technique to the design model produced a 12th-order model-based compensator satisfying stability-performance-robustness design conditions. Finally, an order-reduction technique based on stable factorization was used to produce a 10th-order compensator for controlling the full-order model without destabilizing spillover effects. It was noted that order reduction can have beneficial effects on closed-loop stability but may reduce stability robustness margins. Since the SCOLE configuration is representative of many proposed spaceflight experiments, the results and design techniques employed should potentially be applicable to a wide range of large space structure control problems.

References

[1] M. J. Balas, "Trends in Large Space Structure Control Theory: Fondest Hopes, Wildest Dreams," *IEEE Trans. Auto. Contr.*, Vol AC-27, No. 3, June 1982.

[2] L. W. Taylor and A. V. Balakrishnan, "A Mathematical Problem and a Spacecraft Control Laboratory Experiment (SCOLE) Used to Evaluate Control Laws for Flexible Spacecraft," First SCOLE Workshop, NASA Langley Research Center, Hampton, VA, December 4-7, 1984.

[3] Y. P. Kakad, "Dynamics of Spacecraft Control Laboratory Experiment (SCOLE) Slew Maneuvers," NASA CR 4098, October 1987.

[4] S. M. Joshi, "A Modal Model for SCOLE Structural Dynamics," First SCOLE Workshop, NASA Langley Research Center, Hampton, VA, December 4-7, 1984.

[5] A. Emami-Naeini and P. Van Dooren, "Computation of Zeros of Linear Multivariable Systems," *Automatica*, Vol. 18, No. 4, July 1982.

[6] N. Sundararajan, S. M. Joshi, and E. S. Armstrong, "Robust Controller Synthesis for a Large Flexible Space Antenna," *Journal of Guidance, Control, and Dynamics*, Vol. 10, No. 2, March-April 1987.

[7] S. M. Joshi, and E. S. Armstrong, "Design of Robust Line-of-Sight Pointing Control System for the SCOLE Configuration," Proc. 1987 American Control Conference, Minneapolis, MN, June 10-12, 1987.

[8] M. Vidyasagar, Control System Synthesis: A Factorization Approach, MIT Press, 1985.

[9] M. Athans, "A Tutorial on the LQG/LTR Method," Proc. 1986 American Control Conference," Seattle, WA, June 1986.

[10] G. Stein and M. Athans, "The LQG/LTR Procedure for Multivariable Feedback Control Design," *IEEE Trans Auto. Contr.*, Vol. AC-32, No. 2, February 1987.

[11] A. J. Laub, M. T. Heath, C. C. Paige, and R. C. Ward, "Computation of System Balancing Transformations and Other Applications of Simultaneous Diagonalization Algorithms," *IEEE Trans. Auto. Contr.*, Vol. AC-32, No. 2, February 1987.

[12] K. Glover, "All Optimal Hankel-norm Approximations of Linear Multivariable Systems and Their L^{∞}-error Bounds," *Int. J.Contr.*, Vol. 39, 1984.

[13] Yi Liu, and B, D. O. Anderson, "Controller Reduction Via Stable Factorization and Balancing," *Int. J. Contr.*, Vol. 44, 1986.

TABLE I
EIGENVALUES OF A_E

Mode	Eigenvalue*
1	(-0.00524, 1.747)
2	(-0.00591, 1.970)
3	(-0.0513, 5.108)
4	(-0.0224, 7.449)
5	(-0.0387, 12.903)
6	(-0.0898, 29.925)
7	(-0.104, 34.657)
8	(-0.232, 77.165)
9	(-0.243, 80.993)
10	(-0.446, 148.780)

TABLE II
EIGENVALUE* ANALYSIS OF COMPENSATORS

A-HC	A-BF	$\hat{A}$	$\hat{A}_{ROC}$
(-0.126, 0.126)	(-0.0563, 0.101)	(-0.420, 5.125)	(-0.776, 1.876)
(-0.126, 0.126)	(-0.0834, 0.0837)	(-1.038, 2.027)	
(-0.126, 0.126)	(-0.0959, 0.104)	(-0.203, 1.974)	(-0.204, 1.973)
(-0.00524, 1.747)	(-0.178, 1.976)	(-0.0489, 0.184)	(-0.0500, 0.185)
(-0.00591, 1.970)	(-0.905, 1.956)	(-0.197, 0.237)	(-0.197, 0.237)
(-0.0153, 5.108)	(-0.418, 5.130)	(-0.209, 0.210)	(-0.209, 0.210)

TABLE III
EIGENVALUES* OF FULL-ORDER SYSTEM FORCED BY LQG AND REDUCED-ORDER COMPENSATORS

	LQG	ROC
A-BF	(-0.0569, 0.101)	(-0.0550, 0.0998)
	(-0.0834, 0.0837)	(-0.0834, 0.0837)
	(-0.0971, 0.103)	(-0.0960, 0.103)
	(-0.179, 1.976)	(-0.181, 1.975)
	(-0.905, 1.975)	(-0.634, 1.823)
	(-0.418, 5.130)	
A-HC	(-0.122, 0.128)	(-0.122, 0.129)
	(-0.126, 0.126)	(-0.126, 0.126)
	(-0.126, 0.125)	(-0.128, 0.129)
	(-0.00524, 1.747)	(-0.152, 1.752)
	(-0.00591, 1.970)	(-0.00603, 1.970)
	(-0.0153, 5.108)	(-0.0137, 5.109)
ΔG	(-0.0243, 7.449)	(-0.0242, 7.449)
	(-0.0383, 12.903)	(-0.0383, 12.903)
	(-0.0898, 29.926)	(-0.0898, 29.259)
	(-0.104, 34.657)	(-0.104, 34.657)
	(-0.232, 77.165)	(-0.231, 77.165)
	(-0.243, 80.993)	(-0.243, 80.992)
	(-0.446, 148.780)	(-0.446, 148.780)

* Eigenvalues presented in (Real, + Imaginary) format.

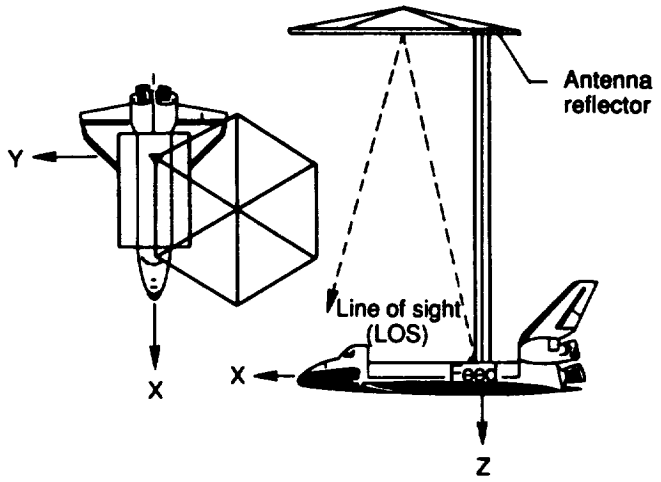

Figure 1. The SCOLE configuration

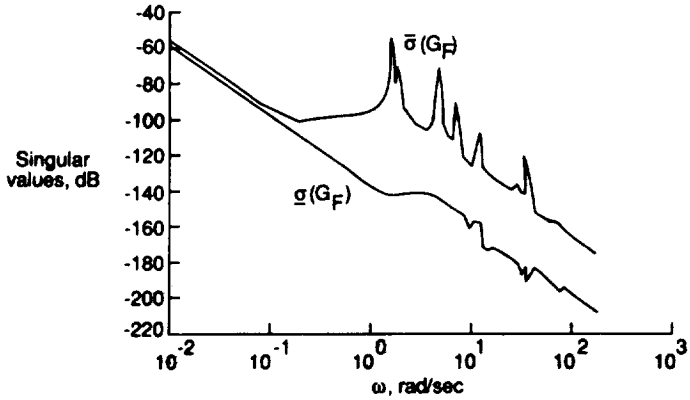

Figure 2. Frequency response of plant after scaling

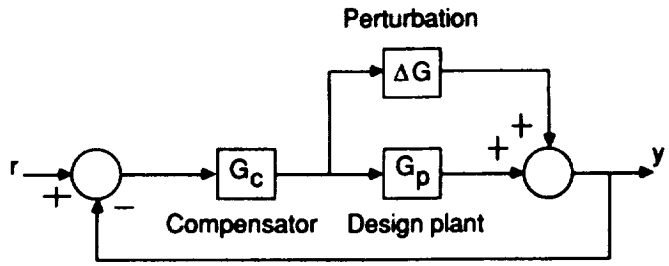

Figure 3. Closed-loop configuration

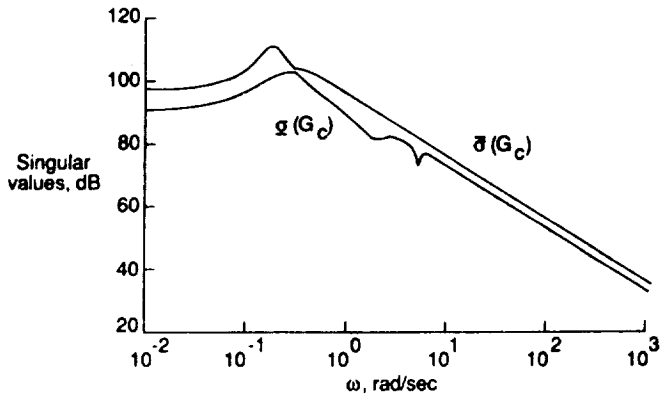

Figure 4. LQG compensator frequency response

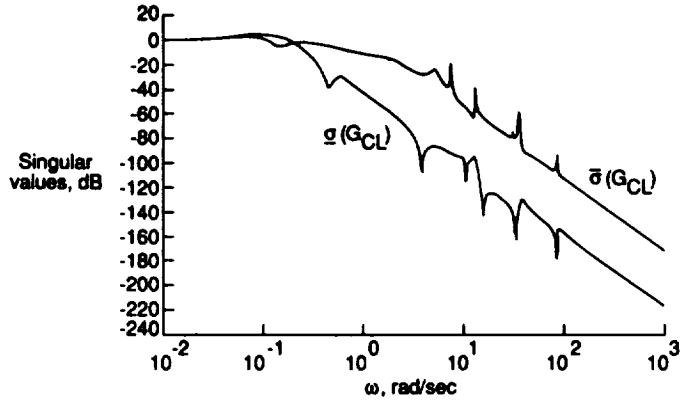

Figure 5. Closed-loop response of evaluation model controlled by LQG compensator

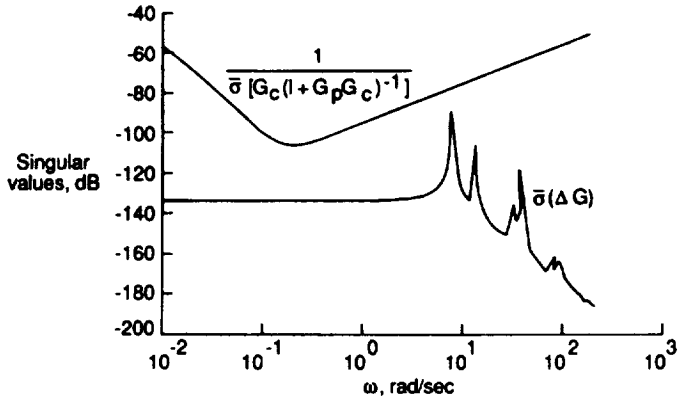

Figure 6. Stability robustness test with LQG compensator

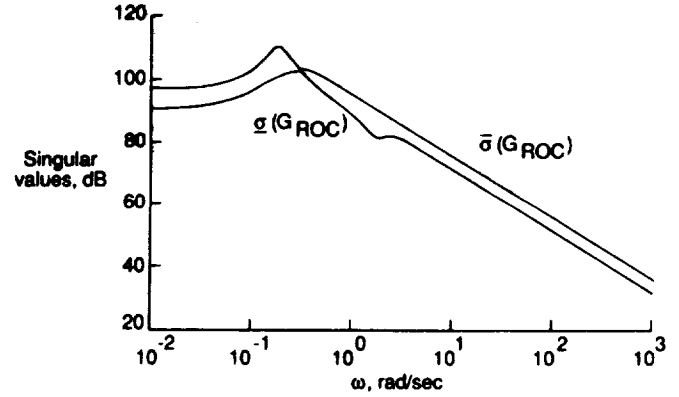

Figure 7. Frequency response of reduced-order compensator

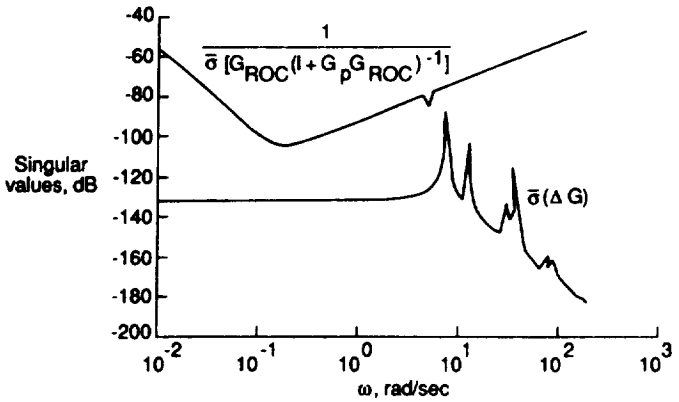

Figure 8. Stability robustness test with reduced-order compensator

ANALYTIC REDUNDANCY MANAGEMENT FOR SCOLE

Raymond C. Montgomery

Spacecraft Control Branch
NASA Langley Research Center
Hampton, VA 23665

Presented at the
4th Annual SCOLE Workshop
U. S. Air Force Academy
olorado Springs, CO

November 16, 1987

ANALYTIC REDUNDANCY MANAGEMENT FOR SCOLE

by

Raymond C. Montgomery
Spacecraft Control Branch
NASA Langley Research Center
Hampton, VA 23665

The objective of this work is to develop a practical sensor analytic redundancy management scheme for flexible spacecraft and to demonstrate it using the SCOLE experimental apparatus. The particular scheme to be used is taken from previous work on the Grid apparatus by Williams and Montgomery.

Reference:

Williams, J. P. and R. C. Montgomery: Failure Detection and Accommodation in Structural Dynamics Systems using Analytic Redundancy. 24th IEEE CDC, December 11-13, 1985.

OBJECTIVE OF WORK

DEVELOP & TEST A PRACTICAL SENSOR ARM SCHEME USING SCOLE

APPROACH

USE SCHEME PREVIOUSLY DEVELOPED FOR THE GRID BY WILLIAMS AND MONTGOMERY

OUTLINE

The presentation is organized as follows: First, the scheme used by Williams and Montgomery is summarized. The scheme is based on a LQG design which is next described. Experimental results taken from the SCOLE apparatus on the performance of the Kalman filter of the LQG are presented and finally plans for completion of the work are given.

OUTLINE

SUMMARIZE THE GRID SCHEME OF WILLIAMS AND MONTGOMERY

DESCRIPTION OF THE LQG DESIGN FOR THE SCHEME

RESULTS FROM THE SCOLE LAB EXPERIMENT

PLANS FOR COMPLETION OF THE WORK

The approach of Williams and Montgomery was to use a single active steady state Kalman filter which is designed for the estimated failure state in effect. Under the no-failure case the sensor residuals of this filter should be white with zero mean. The zero-mean character of the estimated residuals is monitored using Wald's sequential probability ratio test (SPRT). SPRT is a binary test to determine if a statistical variable is zero-mean or has a mean, m. As data samples are gathered a decision variable is monitored. It is initialized at zero and is sequentially modified by the data samples. If it crosses either of two decision thresholds a decision is made. One threshold corresponds to the zero-mean decision while the other is for the m-mean decision. A SPRT is run on each residual. If a decision of zero-mean is made the SPRT is reinitialized and run again. If a m-mean decision is made a failure is declared. In event of a declared failure the failure signature of the sensors in the residuals are examined to determine the failure state. A new LQG design for that failure state then replaces the current active design.

GRID ARM SCHEME – SUMMARY

USE SINGLE, ON-LINE, KALMAN FILTER

USE SPRT TO CHECK THE ZERO MEAN CHARACTER OF THE ESTIMATED MEASUREMENT ERROR

IF FAILURE IS DETECTED, ISOLATE USING FAILURE SIGNATURE IN THE ESTIMATED MEASUREMENT ERRORS

SCOLE ARM LQG DESIGN

The basis of the ARM to be used is the LQG. Therefore the first order of business is to develop a suitable LQG design wherein the modelling errors do not defeat the zero-mean character of the residuals. Most of the rest of the presentation concerns this design and its performance. For the design model we have used a 5-mode, modal model of SCOLE with the SCOLE platform fixed. Thus, there are no rigid body modes. Also the 5 modes selected are the five lowest frequency modes. Reaction jets are included in the filter but not in the regulator. The torque wheels on the other hand are used in both the filter and the regulator.

SCOLE ARM LQG DESIGN

DESIGN MODEL -- MODAL MODEL

FIXED SCOLE PLATFORM MODEL

NO RIDID BODY MODES

5 LOWEST FREQUENCY VIBRATION MODES

JETS INCLUDED IN FILTER, NOT IN REGULATOR

TORQUE WHEELS USED FOR THE REGULATOR

SCOLE CONFIGURATION

For the experiments repoorted herein and for the LQG design, the SCOLE platform rested on the ground and was considered fixed. We used the mid-mast and reflector accelerometers and the rate gyros on the mast tip. The actuators used were the reaction jets on the reflector and the torque wheeles at the mast tip.

SCOLE CONFIGURATION

SCOLE PLATFORM FIXED

SENSORS --

MID-MAST AND REFLECTOR ACCELEROMETERS

RATE GYROS ON MAST TIP

ACTUATORS --

JETS ON REFLECTOR

TORQUE WHEELS AT MAST TIP

SCALE MODEL AND TEST RESULTS

The next 10 slides are working charts organized in 5 pairs. They concern the 5 modes of the design model. The first chart of each pair contains the mode shape and frequency. This chart is followed by an experimental data record taken by manually exciting the structure at the natural frequency of the mode and taking free-decay data. The estimated mode amplitudes are indicated on the traces.

BRATIONAL MODE. FREQ (HZ) . 4426 X10 +00 ID= 1/2/1

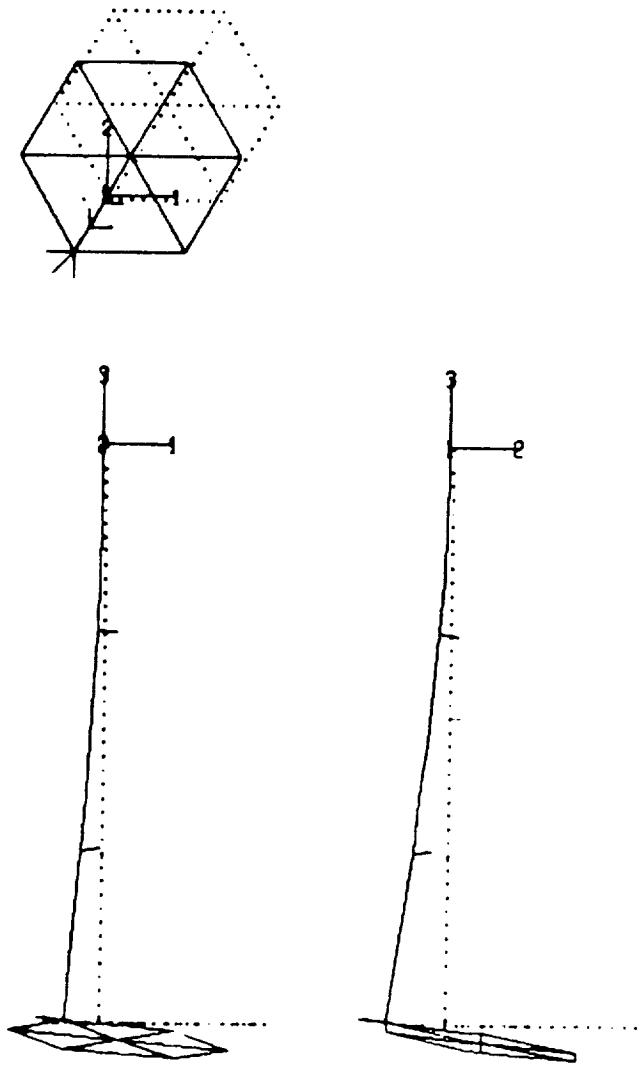

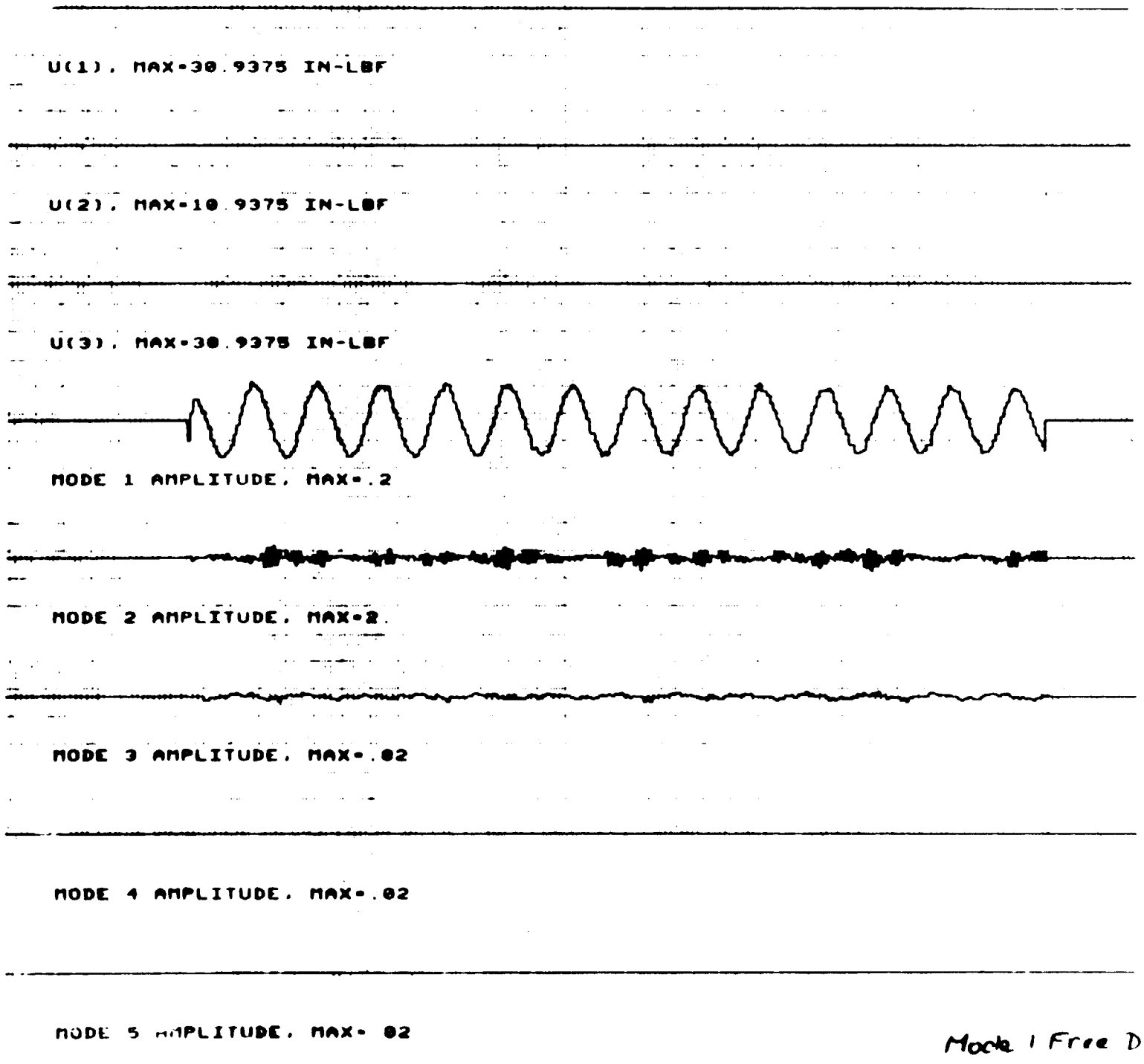

Mode 1.dat
Mode 1 Free Decay

IRATIONAL MODE. FREQ (HZ) .4466 X10 +00 ID= 1/2/2

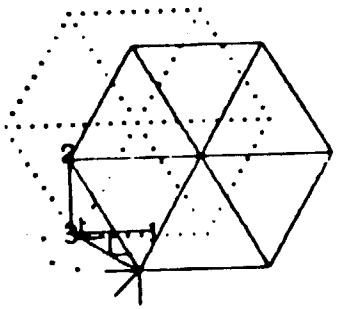

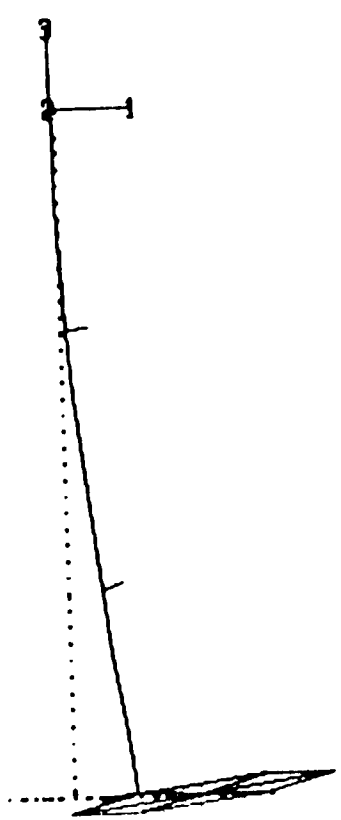

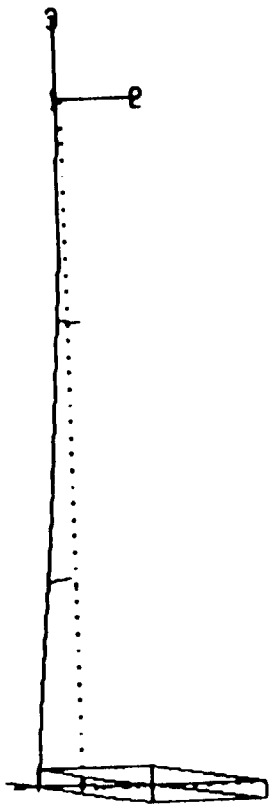

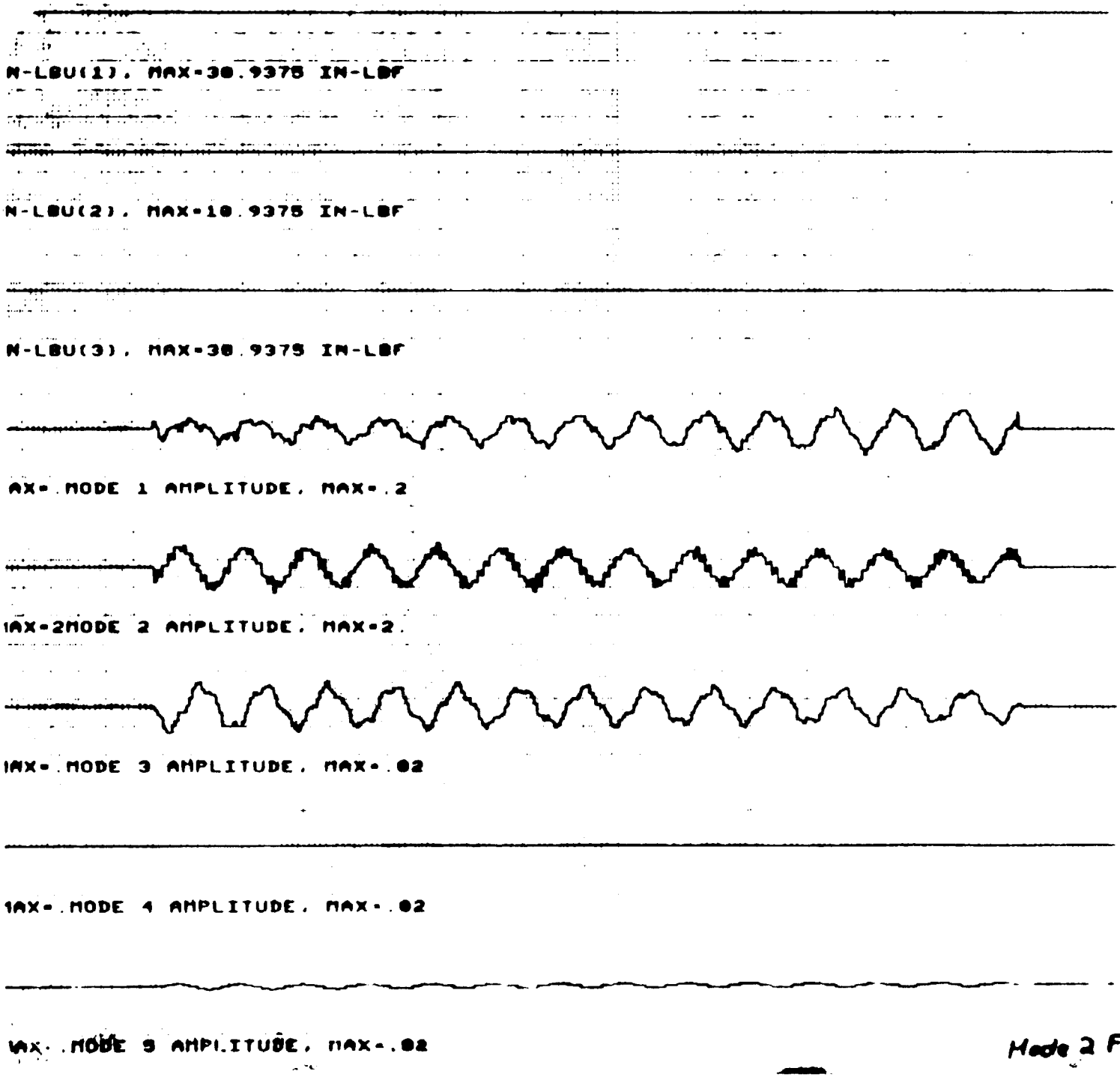

Mode 2 c

Mode 2 Free Decay

VIBRATIONAL MODE. FREQ (HZ) . 1504 X10 +01 ID= 1/2/3

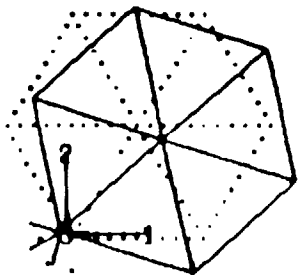

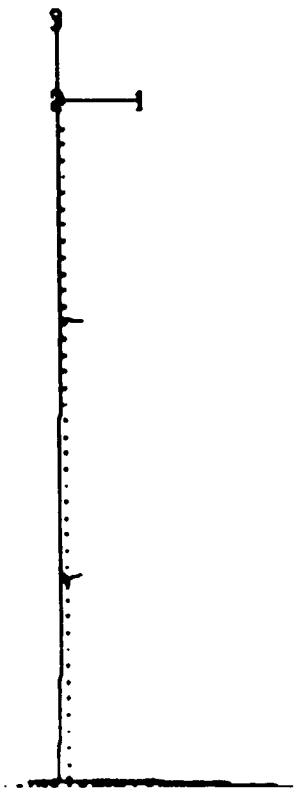

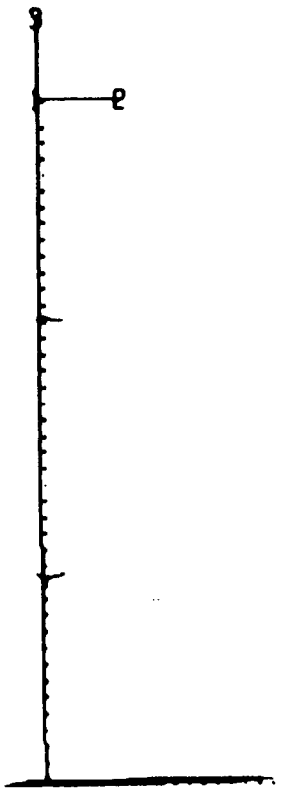

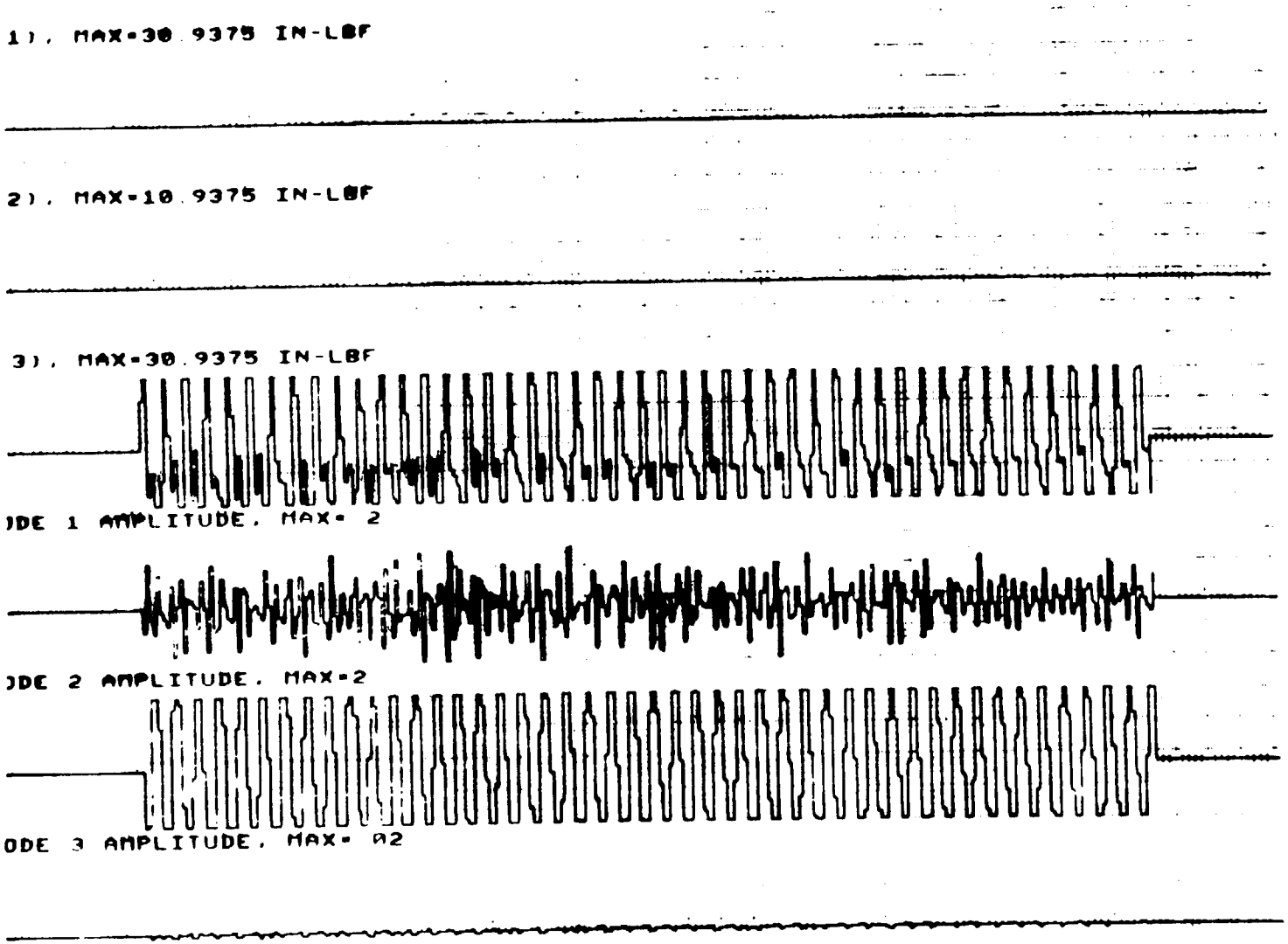

Mode 3.dat

Mode 3 free decay

ATIONAL MODE. FREQ (HZ) . 2913 X10 +01 ID= 1/2/4

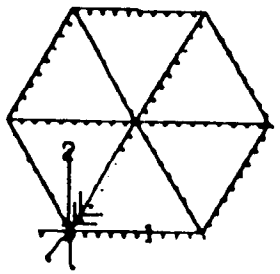

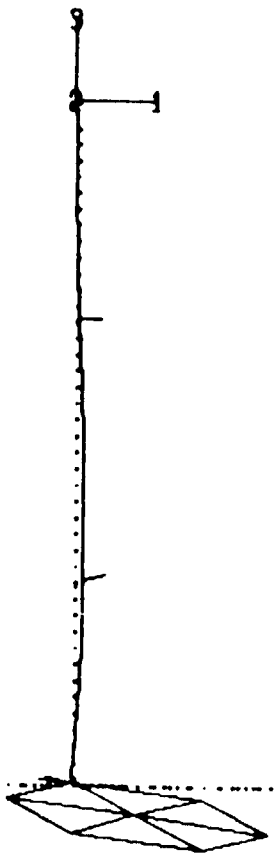

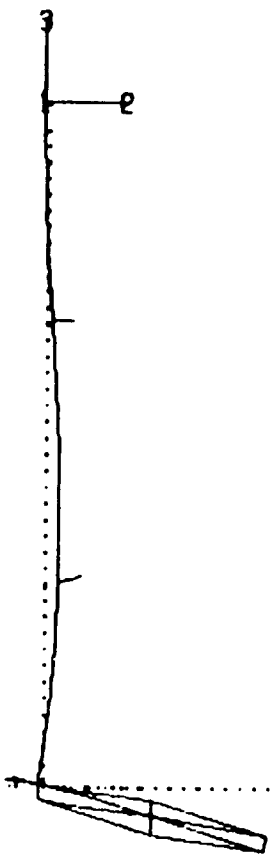

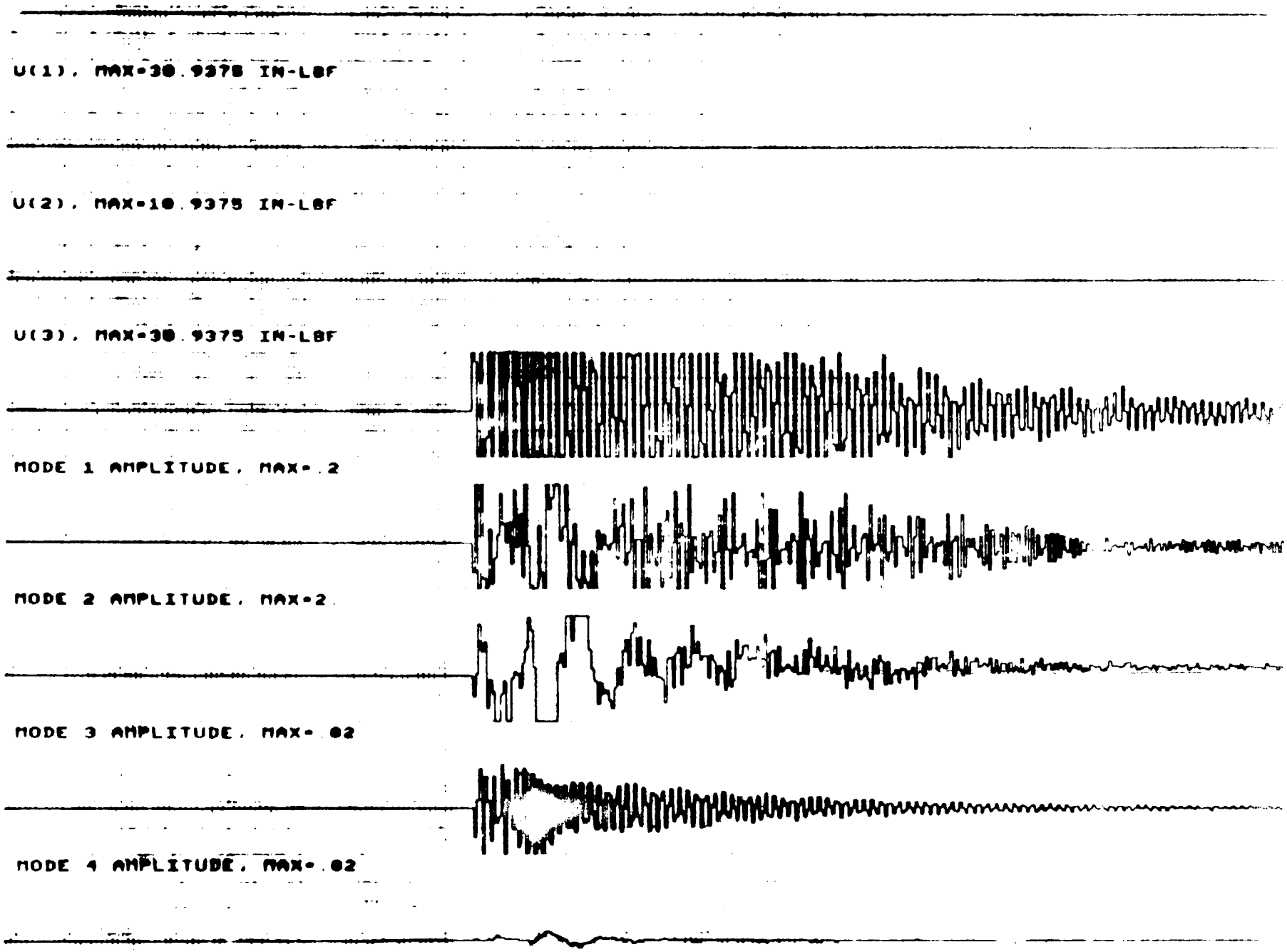
U(1), MAX=30.9378 IN-LBF
U(2), MAX=10.9375 IN-LBF
U(3), MAX=30.9375 IN-LBF
MODE 1 AMPLITUDE, MAX=.2
MODE 2 AMPLITUDE, MAX=2
MODE 3 AMPLITUDE, MAX=.02
MODE 4 AMPLITUDE, MAX=.02

VIBRATIONAL MODE. FREQ (HZ) .4345 X10 +01 ID= 1/2/5

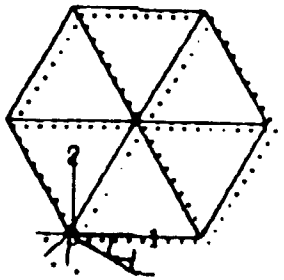

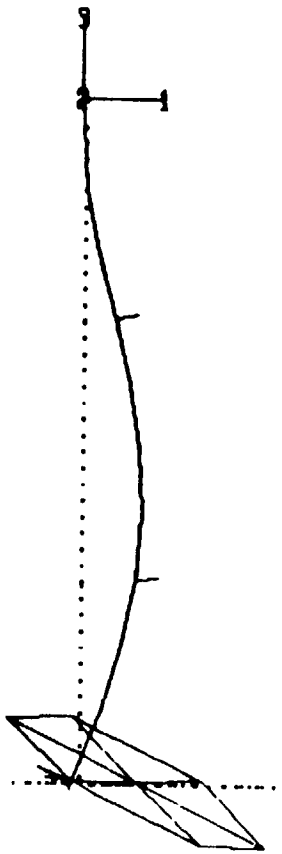

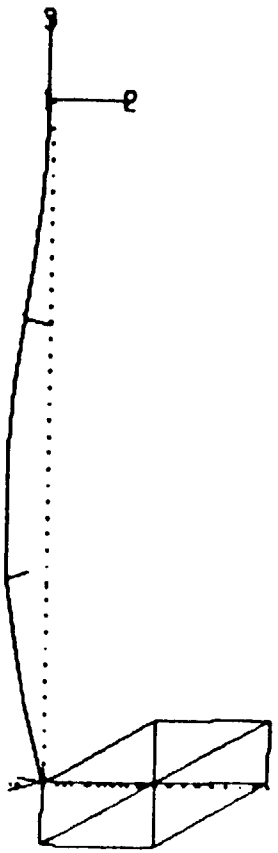

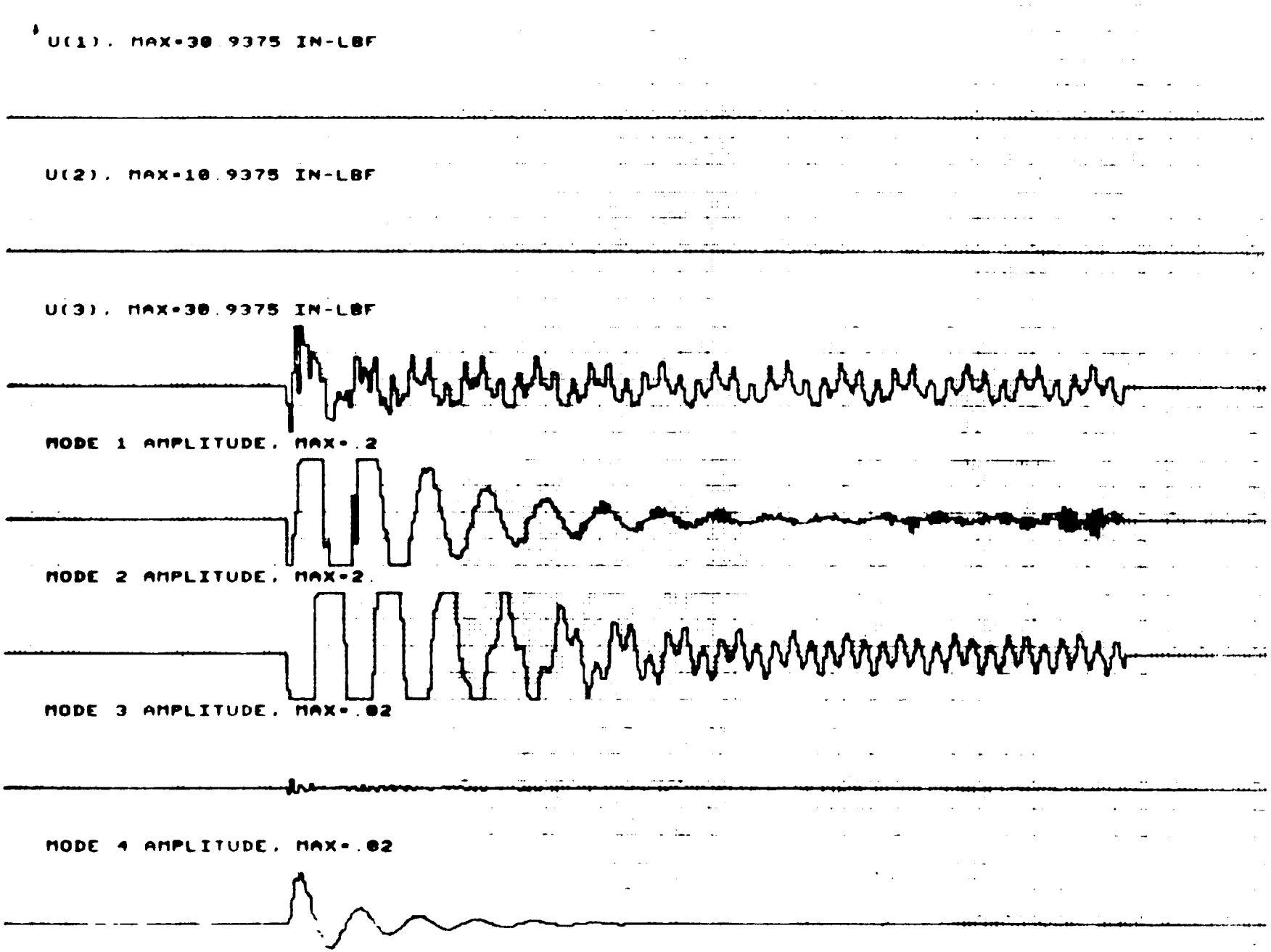

Mode 5 free decay

FUTURE PLANS

Tasks that remain to be accomplished are the complete validation of the Kalman filter and regulator for both free-decay and forced response. The SPRT must be tested on this nominal filter design and thresholds need to be set to avoid false alarms in light of the modelling errors inherent in the design. Possible sources of the modelling errors are excitation of modes not modelled and higher order and nonlinearities in the description of the sensors and actuators. The next step is to select several failure cases for the ARM and generate appropriate LQG designs for each of these. Then the ARM performance can be evaluated. Current plans call for this to be completed by mid June 1988. This schedule is ambitious and may slip because of NASA revectoring of resources.

FUTURE PLANS

VALIDATE NOMINAL KALMAN FILTER

TEST SPRT ON NOMINAL

DESIGN FOR NULL FAILURES OF SENSORS

VALIDATE FAILURE CASE DESIGNS

TEST OVERALL ARM FDI PERFORMANCE

TO BE COMPLETED BY BY MID JUNE '88

JUNE 1984

A MATHEMATICAL PROBLEM AND A SPACECRAFT CONTROL LABORATORY EXPERIMENT (SCOLE) USED TO EVALUATE CONTROL LAWS FOR FLEXIBLE SPACECRAFT... NASA/IEEE DESIGN CHALLENGE

by

Lawrence W. Taylor, Jr.
Spacecraft Control Branch
NASA Langley Research Center
Hampton, VA 23665

and

A. V. Balakrishnan
Chairman, IEEE Subcommittee on Large Space Structures, COLSS
System Sciences Department
University of California at Los Angeles
Los Angeles, CA

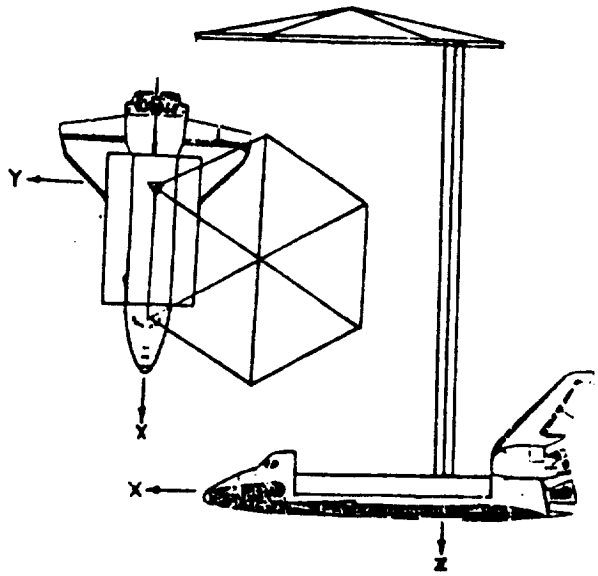

NASA IEEE

A MATHEMATICAL PROBLEM AND A SPACECRAFT CONTROL LABORATORY EXPERIMENT (SCOLE) USED TO EVALUATE CONTROL LAWS FOR FLEXIBLE SPACECRAFT... NASA/IEEE DESIGN CHALLENGE

by

Lawrence W. Taylor, Jr.
Spacecraft Control Branch
NASA Langley Research Center
Hampton, VA 23665

and

A. V. Balakrishnan
Chairman, IEEE Subcommittee on Large Space Structures, COLSS
System Sciences Department
University of California at Los Angeles
Los Angeles, CA

SUMMARY

The problem of controlling large, flexible space systems has been the subject of considerable research. Many approaches to control system synthesis have been evaluated using computer simulation. In several cases, ground experiments have also been used to validate system performance under more realistic conditions. There remains a need, however, to test additional control laws for flexible spacecraft and to directly compare competing design techniques. In this paper an NASA program is discussed which has been initiated to make direct comparisons of control laws for, first, a mathematical problem, then an experimental test article is being assembled under the cognizance of the Spacecraft Control Branch at the NASA Langley Research Center with the advice and counsel of the IEEE Subcommittee on Large Space Structures. The physical apparatus will consist of a softly supported dynamic model of an antenna attached to the Shuttle by a flexible beam. The control objective will include the task of directing the line-of-sight of the Shuttle/antenna configuration toward a fixed

target, under conditions of noisy data, limited control authority and random disturbances. The open competition started in the early part of 1984. Interested researchers are provided information intended to facilitate the analysis and control synthesis tasks. A workshop is planned for early December at the NASA Langley Research Center to discuss and compare results.

INTRODUCTION

Many future spacecraft will be large and consequently quite flexible. As the size of antennae is increased, the frequencies of the first flexible modes will decrease and overlap the pointing system bandwidth. It will no longer be possible to use low gain systems with simple notch filters to provide the required control performance. Multiple sensors and actuators, and sophisticated control laws will be necessary to ensure stability, reliability and the pointing accuracy required for large, flexible spacecraft.

Control of such spacecraft has been studied with regard given to modeling, order reduction, fault management, stability and dynamic system performance. Numerous example applications have been used to demonstrate specific approaches to pertinent control problems. Both computer simulations and laboratory experiment results have been offered as evidence of the validity of the approaches to control large, flexible spacecraft. Concerns remain, however, because of the chronic difficulties in controlling these lightly damped large-scale systems. Because of these concerns and because of the desire to offer a means of comparing technical approaches directly, an NASA/IEEE Design Challenge is being offered. An

experimental test article is being assembled under the cognizance of the Spacecraft Control Branch at the NASA Langley Research Center with the advice and counsel of the IEEE (COLSS) Subcommittee on Large Space Structures. This Spacecraft Control Laboratory Experiment (SCOLE) will serve as the focus of a design challenge for the purpose of comparing directly different approaches to control synthesis, modeling, order reduction, state estimation and system identification.

The configuration of the SCOLE will represent a large antenna attached to the Space Shuttle orbiter by a flexible beam. This configuration was chosen because of its similarity to proposed space flight experiments and proposed space-based antenna systems. This paper will discuss the "Design Challenge" in terms of both a mathematical problem and a physical experimental apparatus. The SCOLE program is not part of any flight program.

SYMBOLS

a	acceleration vector ft/sec^2
A	beam cross section area
c	observation matrix
d	noise contaminating direction cosine matrix measurements
e	line-of-sight error
E	modulus of elasticity
f	concentrated force expressions
F_4	force vector
g	concentrated moment expressions
GI	torsional rigidity
I	moment of inertia matrix for entire Shuttle/antenna configuration

I_1	moment of inertia matrix, Shuttle body
I_4	moment of inertia matrix, reflector body
I_ϕ	beam cross section moment of inertia, roll bending
I_Θ	beam cross section moment of inertia, pitch bending
I_Ψ	beam polar moment of inertia, yaw torsion
L	length of the reflector mast, beam
M_1	control moment applied to the Shuttle body
M_4	control moment applied to the reflector body
M_D	disturbance moment applied to the Shuttle body
m	mass of entire Shuttle/antenna configuration
m_1	mass of Shuttle body
m_4	mass of reflector body
P	mass density of beam
s	beam position variable
T_1	direction cosine matrix, Shuttle body $()_{earth} = T_1()_{Shuttle\ body}$
T_4	direction cosine matrix, reflector body $()_{earth} = T_4()_{reflector\ body}$
v_1	inertial velocity, Shuttle body
v_4	inertial velocity, reflector body
u_ϕ	lateral deflection of beam bending in y-z plane
u_Θ	lateral deflection of beam bending in x-z plane
u_Ψ	angular deflection of beam twisting about z axis
X,Y,Z	position variables
Δ	displacement of proof-mass actuator
δ	line-of-sight pointing requirement
ε	noise contaminating angular velocity measurements

θ, ϕ, Ψ pitch, roll, heading

ζ damping ratio

τ noise contaminating acceleration measurements

ω_1 angular velocity of Shuttle body

ω_4 angular velocity of reflector body

DISCUSSION

The objective of the NASA-IEEE Design Challenge concerning the control of flexible spacecraft is to promote direct comparison of different approaches to control, state estimation and systems identification. The design challenge has principal parts, the first using a mathematical model, and the second using laboratory experimental apparatus. The specific parts of the Spacecraft Control Laboratory Experiment (SCOLE) program will be discussed in detail.

Control Objectives

The primary control task is to rapidly slew or change the line-of-sight of an antenna attached to the space Shuttle orbiter, and to settle or damp the structural vibrations to the degree required for precise pointing of the antenna. The objective will be to minimize the time required to slew and settle, until the antenna line-of-sight remains within the angle δ. A secondary control task is to change direction during the "on-target" phase to prepare for the next slew maneuver. The objective is to change attitude and stabilize as quickly as possible, while keeping the line-of-sight error less than δ.

Math Model Dynamics

The initial phase of the design challenge will use a mathematical model of the Shuttle orbiter/antenna configuration. It is necessary to obtain a balance, of course, between complex formulations which might be more accurate and simplified formulations which ease the burden of analysis.

The dynamics are described by a distributed parameter beam equation with rigid bodies, each having mass and inertia at either end. One body represents Space Shuttle orbiter; the other body is the antenna reflector. The equations for the structural dynamics and Shuttle motion are formed by adding to the rigid-body equations of motion, beam-bending and torsion equations. The boundary conditions at the ends of the beam contain the forces and moments of the rigid Shuttle and reflector bodies. The nonlinear kinetmatics couples the otherwise uncoupled beam equations. Additional terms represent the action of two, 2-axis proof-mass actuators at locations on the beam chosen by the designer.

The rigid-body equations of motion for the Shuttle body are given by:

$$\dot{\omega}_1 = - I_1^{-1}(\tilde{\omega}_1 I_1 \omega_1 + M_1 + M_D + M_{B,1})$$

$$\dot{v} = \frac{F_{B,1}}{m_1}$$

Similarly, for the reflector body,

$$\dot{\omega}_4 = - I_4^{-1}(\tilde{\omega}_4 I_4 \omega_4 + M_4 + M_{B,4})$$

$$\dot{v}_4 = \frac{F_4 + F_{B,4}}{m_4}$$

The direction cosine matrices defining the attitudes of the Shuttle and reflector bodies are given by:

$$\dot{T}_1^T = - \tilde{\omega}_1 T_1^T$$

$$\dot{T}_4^T = - \tilde{\omega}_4 T_4^T$$

The direction cosine matrices defining the attitudes of the Shuttle and the reflector bodies are related to the beam end conditions.

$$T_4 = \begin{bmatrix} 1 & 0 & 0 \\ 0 & \cos\Delta\phi & -\sin\Delta\phi \\ 0 & \sin\Delta\phi & \cos\Delta\phi \end{bmatrix} \begin{bmatrix} \cos\Delta\Theta & 0 & \sin\Delta\Theta \\ 0 & 1 & 0 \\ -\sin\Delta\Theta & 0 & \cos\Delta\Theta \end{bmatrix} \begin{bmatrix} \cos\Delta\Psi & -\sin\Delta\Psi & 0 \\ \sin\Delta\Psi & \cos\Delta\Psi & 0 \\ 0 & 0 & 1 \end{bmatrix} T_1$$

where:

$$\Delta\Psi = u_\Psi \Big|_{s=L} - u_\Psi \Big|_{s=0}$$

$$\Delta\Theta = \frac{\partial u_\Theta}{\partial s} \Big|_{s=L} - \frac{\partial u_\Theta}{\partial s} \Big|_{s=0}$$

$$\Delta\phi = \frac{\partial u_\phi}{\partial s} \Big|_{s=L} - \frac{\partial u_\phi}{\partial s} \Big|_{s=0}$$

The equations of motion for the flexible beam-like truss connecting the reflector and Shuttle bodies consist of standard beam bending and torsion partial differential equations with energy dissapative terms which enable damped modes with constant characteristics for fixed, though dynamic, end conditions. The system of equations can be viewed as driven by changing end conditions and forces applied at the locations of the proof-mass actuators.

ROLL BEAM BENDING:

$$PA\frac{\partial^2 u_\phi}{\partial t^2} + 2\zeta_\phi\sqrt{PA\ EI_\phi}\frac{\partial^3 u_\phi}{\partial s^2\partial t} + EI_\phi\frac{\partial^4 u_\phi}{\partial s^4} = \sum_{n=1}^{4}\left[f_{\phi,n}\delta(s-s_n) + g_{\phi,n}\frac{\partial\delta}{\partial s}(s-s_n)\right]$$

PITCH BEAM BENDING:

$$PA\frac{\partial^2 u_\Theta}{\partial t^2} + 2\zeta_\Theta\sqrt{PA\ EI_\Theta}\frac{\partial^3 u_\Theta}{\partial s^2\partial t} + EI_\Theta\frac{\partial^4 u_\Theta}{\partial s^4} = \sum_{n=1}^{4}\left[f_{\Theta,n}\delta(s-s_n) + g_{\Theta,n}\frac{\partial\delta}{\partial s}(s-s_n)\right]$$

YAW BEAM TORSION:

$$PI_\Psi\frac{\partial^2 u_\Psi}{\partial t^2} + 2\zeta_\Psi I_\Psi\sqrt{GP}\frac{\partial^3 u_\Psi}{\partial s^2\partial t} - GI_\Psi\frac{\partial^2 u_\Psi}{\partial s^2} = \sum_{n=1}^{4} g_{\Psi,n}\delta(s - s_n)$$

where:

$$f_{\phi,1} = m_1\left.\frac{\partial^2 u_\phi}{\partial t^2}\right|_{s=0} \qquad \{\text{SHUTTLE BODY FORCE}\}$$

$$f_{\phi,2} = m_2\left.\frac{\partial^2 u_\phi}{\partial t^2}\right|_{s=s_2} + m_2\frac{\partial^2 \Delta_{\phi,2}}{\partial t^2} \qquad \{\text{PROOF-MASS ACTUATOR FORCE}\}$$

$$f_{\phi,3} = m_3 \left.\frac{\partial^2 u_\phi}{\partial t^2}\right|_{s=s_3} + m_3 \frac{\partial^2 \Delta_{\phi,2}}{\partial t^2} \qquad \{\text{PROOF-MASS ACTUATOR}\}$$

$$f_{\phi,4} = m_4 \left.\frac{\partial^2 u_\phi}{\partial t^2}\right|_{s=130} - I_{zz,4} \frac{\partial^2 u_\psi}{\partial t^2} /32.5 + F_y \qquad \{\text{REFLECTOR BODY FORCE}\}$$

$$f_{\Theta,1} = m_1 \left.\frac{\partial^2 u_\Theta}{\partial t^2}\right|_{s=s_1} \qquad \{\text{SHUTTLE BODY FORCE}\}$$

$$f_{\Theta,2} = m_2 \left.\frac{\partial^2 u_\Theta}{\partial t^2}\right|_{s=s_2} + m_2 \frac{\partial^2 \Delta_{\Theta,2}}{\partial t^2} \qquad \{\text{PROOF-MASS ACTUATOR FORCE}\}$$

$$f_{\Theta,3} = m_3 \left.\frac{\partial^2 u_\Theta}{\partial t^2}\right|_{s=s_3} + m_3 \frac{\partial^2 \Delta_{\Theta,2}}{\partial t^2} \qquad \{\text{PROOF-MASS ACTUATOR FORCE}\}$$

$$f_{\Theta,4} = m_4 \left.\frac{\partial^2 u_\Theta}{\partial t^2}\right|_{s=130} - I_{zz,4} \frac{\partial^2 u_\psi}{\partial t^2} /18.75 - F_x \qquad \{\text{REFLECTOR BODY FORCE}\}$$

$$\begin{pmatrix} g_{\phi,1} \\ g_{\Theta,1} \\ g_{\psi,1} \end{pmatrix} = I_1\dot{\omega}_1 + \omega_1 I_1 \omega_1 + M_1 + M_D \qquad \{\text{SHUTTLE BODY, MOMENTS}\}$$

$$\begin{pmatrix} g_{\phi,2} \\ g_{\Theta,2} \\ g_{\psi,2} \end{pmatrix} = 0 \qquad \{\text{PROOF-MASS ACTUATOR, MOMENT}\}$$

$$\begin{pmatrix} g_{\phi,3} \\ g_{\Theta,3} \\ g_{\psi,3} \end{pmatrix} = 0 \qquad \{\text{PROOF-MASS ACTUATOR, MOMENT}\}$$

$$\begin{pmatrix} g_{\phi,4} \\ g_{\Theta,4} \\ g_{\psi,4} \end{pmatrix} = I_4\dot{\omega}_4 + \omega_4 I_4 \omega_4 + M_4 + \tilde{R}_B F_{B,4} \qquad \{\text{REFLECTOR BODY, MOMENT}\}$$

The angular velocity of the reflector body is related to the Shuttle body by:

$$\omega_4 = \begin{pmatrix} \frac{\partial^2 u_\phi}{\partial s \partial t}\Big|_{s=L} \\ \frac{\partial^2 u_\Theta}{\partial s \partial t}\Big|_{s=L} \\ \frac{\partial u_\psi}{\partial t}\Big|_{s=L} \end{pmatrix} - \begin{pmatrix} \frac{\partial^2 u_\phi}{\partial s \partial t}\Big|_{s=0} \\ \frac{\partial^2 u_\Theta}{\partial s \partial t}\Big|_{s=0} \\ \frac{\partial u_\psi}{\partial t}\Big|_{s=0} \end{pmatrix} + \omega_1 \qquad \tilde{R}_B = \begin{bmatrix} 0 & 130 & 0 \\ -130 & 0 & 0 \\ 0 & 0 & 0 \end{bmatrix}$$

The line-of-sight error described in figure 2 is affected by both the pointing error of the Shuttle body and the misalignment of the reflector due to the deflection of the beam supporting the reflector. The line-of-sight is defined by a ray from the feed which is reflected at the center of the reflector. Its direction in the Shuttle body coordinates is given by:

$$R_{LOS} = \frac{-R_R + R_F + 2\left[R_A^T(R_R - R_F) \cdot R_A\right]}{\left|\left|R_R - R_F - 2\left[R_A^T R_R - R_F\right] \cdot R_A\right|\right|}$$

where:

R_F is the feed location (3.75, 0, 0)

R_R is the location of the center of the reflector (18.75, -32.5, -130)

R_A is a unit vector in the direction of the reflector axis in Shuttle body coordinates

The vector R_A can be related to the direction cosine attitude matrices for the Shuttle body, T_1, and the reflector body, T_4, by

$$R_A = \left[T_1^T T_4\right] \begin{pmatrix} 0 \\ 0 \\ 1 \end{pmatrix}$$

The relative alignment of the reflector to the Shuttle body is given by $T_1^T T_4$ which is a function of the structural deformations of the beam.

The line-of-sight error, e, is the angular difference between the target direction, given by the unit vector, D_T, and the line-of-sight direction in Earth axes, T_1R_{LOS}.

$$e = \text{ARCSIN} \left| D_T \times T_1 R_{LOS} \right| \quad \text{or} \quad \text{ARCSIN} \left| \tilde{D}_T T_1 R_{LOS} \right|$$

Computer programs are available which generate time histories of the rigid body and the mode shapes and frequencies for the body-beam-body configuration for "pitch" bending, "roll" bending and "yaw" twisting. Since the modes are based on solving explicitly the distributed parameter equations (without damping and without kinematic coupling) there is no limit to the number of modal characteristic sets that can be generated by the program. It will be the analyst's decision as to how many modes need to be considered.

Laboratory Experiment Description

The second part of the design challenge is to validate in the laboratory, the system performance of the more promising control system designs of the first part. The experimental apparatus will consist of a dynamic model of the Space Shuttle orbiter with a large antenna reflector attached by means of a flexible beam. The dynamic model will be extensively instrumented and will have attached force and moment generating devices for control and for disturbance generation. A single, flexible tether will be used to suspend the dynamic model, allowing complete angular freedom in yaw, and limited freedom in pitch and roll. An inverted position will be used to let the reflector mast to hang so that gravity effects on mast bending will be minimized. The dynamics of the laboratory model will of necessity be different from the mathematical model discussed earlier.

Design Challenge, Part One

For part one of the design challenge, the following mathematical problem is addressed. Given the dynamic equations of the Shuttle/antenna configuration, what control policy minimizes the time to slew to a target and to stabilize so that the line-of-sight (LOS) error is held, for a time, within a specified amount, δ. During the time that the LOS error is within δ, the attitude must change 90° to prepare for the next slew maneuver. This was previously referred to as the sescondary control task. The maximum moment and force generating capability will be limited. Advantage may be taken of selecting the most suitable initial alignment of the Shuttle/antenna about its assigned initial RF axis, line-of-sight. Random, broad band-pass disturbances will be applied to the configuration. Two proof-mass, force actuators may be positioned anywhere along the beam. The design guidelines are summarized below:

1. The initial line-of-sight error is 20 degrees.

$$e(o) = 20 \text{ degrees}$$

2. The initial target direction is straight down.

$$D_T = \begin{pmatrix} 0 \\ 0 \\ 1 \end{pmatrix}$$

3. The initial alignment about the line-of-sight is free to be chosen by the designer. Advantage may be taken of the low value of moment of inertia in roll. The Shuttle/antenna is at rest initially.

4. The objective is to point the line-of-sight of the antenna and stabilize to within 0.02 degree of the target as quickly as possible.

$$\delta = 0.02 \text{ degree}$$

5. Control moments can be applied at 100 Hz sampling rate to both the Shuttle and reflector bodies of 10,000 ft-lb for each axis. The commanded moment for each axis is limited to 10,000 ft-lb. The actual control moment's response to the commanded value is first-order with a time constant of 0.1 second.

   For the rolling moment applied to the Shuttle body:

$$-10^4 \leq M_{X,1,\text{command}} \leq 10^4$$

$$M_{X,1}(n+1) = e^{-0.1}\, M_{X,1}(n) + (1 - e^{-0.1})\, M_{X,1,\text{command}}(n)$$

   Equations for other axes and for the reflector body are similar.

6. Control forces can be applied at the center of the reflector in the X and Y directions only. The commanded force in a particular direction is limited to 800 lbs. The actual control force's response to the commanded value is first-order with a response time of 0.1 second.

   For the side for applied to the reflector body:

$$-800 \leq F_{Y,\text{command}} \leq 800$$

$$F_Y(n+1) = e^{-0.1}\, F_Y(n) + (1 - e^{-0.1})\, F_{Y,\text{command}}(n)$$

   Equations for X-axis are similar.

7. Control forces using two proof-mass actuators (each having both X and Y axes) can be applied at two points on the beam. The strokes are limited to ± 1 ft, and the masses weight 10 lbs each. The actual stroke follows a first-order response to limited commanded values.

For the X-axis of the proof-mass actuator at s_2:

$$-1 \leq \Delta_{X,2,\text{command}} \leq 1$$

$$\Delta_{X,2}(n+1) = e^{-0.1}\,\Delta_{X,2}(n) + (1 - e^{-0.1})\,\Delta_{X,2,\text{command}}(n)$$

Equations for other axes and locations are similar.

8. The inertial attitude direciton cosine matrix for the Shuttle body lags in time the actual values by 0.01 second and are made at a rate of 100 samples per second. Each element of the direction cosine measurement matarix is contaminated by additive, uncorrelated Gaussian noise having an rms value of 0.001. The noise has zero mean.

$$T_{s,\text{measured}}(n+1) = T_{s,\text{true}}(n) + \begin{bmatrix} d_{11}(n) & d_{12}(n) & d_{13}(n) \\ d_{21}(n) & d_{22}(n) & d_{23}(n) \\ d_{31}(n) & d_{32}(n) & d_{33}(n) \end{bmatrix}$$

where:

$$E\{d_{ij}(n)\} = 0$$

$$E\{d_{ij}(n)d_{kL}(n)\} = 0 \qquad \text{for } i \neq k \text{ or } j \neq L$$

$$E\{d_{ij}(n)d_{ij}(n+k)\} = 0 \qquad \text{for } k \neq 0$$

$$= [.001]^2 \qquad \text{for } k = 0$$

9. The angular velocity measurements for both the Shuttle and reflector bodies pass through a first-order filter with 0.05 sec time constant and lag in time the actual values by 0.01 second and are made at a rate of 100 samples per second. Each rate measurement is contaminated by additive, Gaussian, uncorrelated noise having an rms value of 0.02 degree per second. The noise has zero mean.

For example:

$$\omega_{1,X,\text{measured}}(n+1) = \omega_{1,X,\text{filtered}}(n) + \varepsilon_{1,X}(n)$$

$$E\{\varepsilon_{1,X}(n)\ \varepsilon_{1,X}(n+k)\} = 0 \qquad \text{for } k \neq 0$$

$$= (.02)^2 \qquad \text{for } k = 0$$

where

$$\dot{\omega}_{1,X,\text{filtered}} = -20\ \omega_{1,X,\text{filtered}} + 20\ \omega_{1,X,\text{true}}$$

10. Three-axis accelerometers are located on the Shuttle body at the base of the mast and on the reflector body at its center. Two-axes (X and Y) accelerometers are located at intervals of 10 feet along the mast. The acceleration measurements pass through a first-order filter with a 0.05 second time constant and lag in time the actual values by 0.01 second, and are made at a rate of 100 samples per second. Each measurement is contaminated by Gaussian additive, uncorrelated noise having an rms value of 0.05 ft/sec^2.

For example:

$$a_{1,X,\text{measured}}(n+1) = a_{1,X,\text{filtered}}(n) + \tau_{1,X}(n)$$

$$E\{\tau_{1,X}(n)\ \tau_{1,X}(n+k)\} = 0 \qquad \text{for } k \neq 0$$

$$= (.05)^2 \qquad \text{for } k = 0$$

where:

$$\dot{a}_{1,X,\text{filtered}} = -20\, a_{1,X,\text{filtered}} + 20\, \omega_{1,X,\text{true}}$$

11. Gaussian, uncorrelated step-like disturbances are applied 100 times per second to the Shuttle body in the form of 3-axes moments, having rms values of 100 ft-lbs. These disturbances have zero mean.

    For example:

$$E\{M_{D,X}(n)\ M_{D,X}(n+k)\} = 0 \qquad \text{for } k \neq 0$$

$$= (100)^2 \qquad \text{for } k = 0$$

In summary, the designer's task for part one is to: (1) derive a control law for slewing and stabilization, coded in FORTRAN; (2) select an initial attitude in preparation for slewing 20 degrees; and (3) select two positions for the 2-axes proof-mass actuators. An official system performance assessment computer program will be used to establish the time required to slew and stabilize the Shuttle/antenna configuration.

Design Challenge, Part Two

As in part one, the task is to minimize the time to slew and stabilize a Shuttle/antenna configuration. The difference is that in part two of the design challenge, a physical laboratory model will be used instead of the dynamic equations of part one. The constraints on total moment and force generation capability will apply to part two, as for part one. Again, the analyst may select the initial alignment about the assigned initial RF line-of-sight. Disturbances will be injected into the Shuttle/antenna model. The designer's task will be similar to that for part one.

CONCLUDING REMARKS

A Design Challenge, in two parts, has been offered for the purpose of comparing directly different approach to controlling a flexible Shuttle/antenna configuration. The first part of the design challenge uses only mathematical equations of the vehicle dynamics; the second part uses a physical laboratory model of the same configuration. The Spacecraft Control Laboratory Experiment (SCOLE) program is being conducted under the cognizance of the Spacecraft Control Branch at the NASA Langley Research Center. The NASA/IEEE Design Challenge has the advice and counsel of the IEEE-COLSS Subcommittee on Large Space Structures. Workshops will be held to enable investigators to compare results of their research.

MASS CHARACTERISTICS

	CG LOCATION, FT X	Y	Z	WEIGHT, LB	I_{XX} SLG-FT^2	I_{YY} SLG-FT^2	I_{ZZ} SLG-FT^2	I_{XY} SLG-FT^2	I_{XZ} SLG-FT^2	I_{YZ} SLG-FT^2
SHUTTLE	0	0	0	205,000	905,443	6,789,100	7,086,601	0	145,393	0
MAST, CG	0	0	-65.	400	17,495	17,495	0	0	0	0
REFLECTOR, CG	18.75	-32.5	-130.	400	4,969	4,969	9,938	0	0	0
REFLECTOR, ATTACHMENT POINT					18,000	9,336	27,407	-7,570	0	0
TOTAL	.036	-.063	-.379	205,800	1,132,508	7,007,447	7,113,962	-7,555	115,202	52,293

The moment of inertia becomes:

$$I = \begin{bmatrix} I_{xx} & -I_{xy} & -I_{xz} \\ -I_{xy} & I_{yy} & -I_{yz} \\ -I_{xz} & -I_{yz} & I_{zz} \end{bmatrix} = \begin{bmatrix} 1,132,508 & 7,555 & -115,202 \\ 7,555 & 7,007,447 & -52,293 \\ -115,202 & -52,293 & 7,113,962 \end{bmatrix}$$

$$I_1 = \begin{bmatrix} 905,443 & 0 & -145,393 \\ 0 & 6,789,100 & 0 \\ -145,393 & 0 & 7,086,601 \end{bmatrix}$$

$$I_4 = \begin{bmatrix} 4,969 & 0 & 0 \\ 0 & 4,969 & 0 \\ 0 & 0 & 9,938 \end{bmatrix}$$

$m = 6391.30$ slugs

$m_1 = 6366.46$ slugs

$m_2 = 0.3108$ slugs

$m_3 = 0.3108$ slugs

$m_4 = 12.42$ slugs

$PA = 0.09556$ slugs/ft

$EI_\phi = 4.0 \times 10^7$ lb-ft^2

$\zeta_\phi = .003$

$PA = 0.09556$ slugs/ft

$EI_\theta = 4.0 \times 10^7$ lb-ft^2

$\zeta_\theta = .003$

$PI_\psi = 0.9089$ slug-ft

$GI_\psi = 4.0 \times 10^7$ lb-ft^2

$\zeta_\psi = .003$

Figure 1. Drawing of the Shuttle/Antenna Configuration.

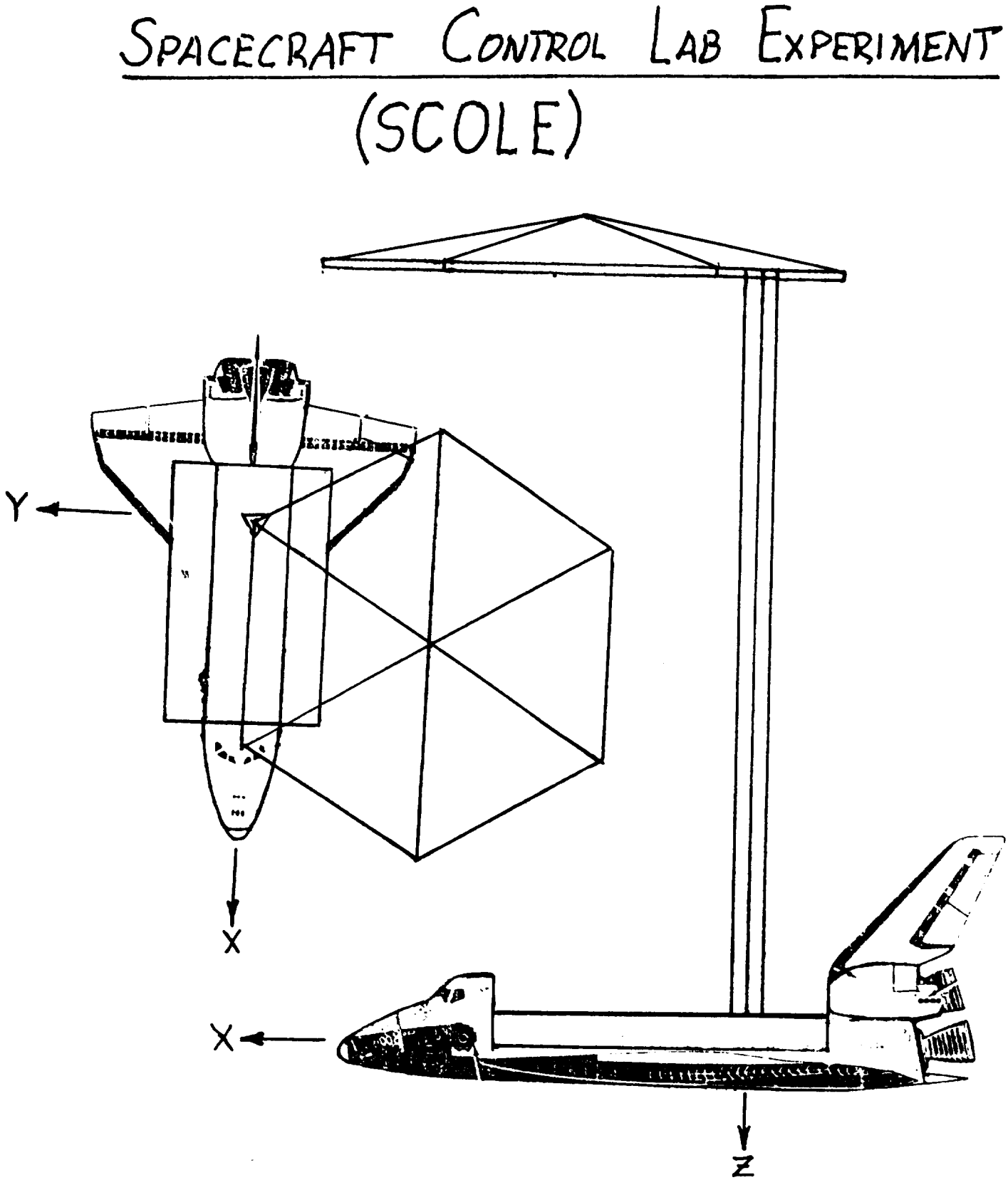

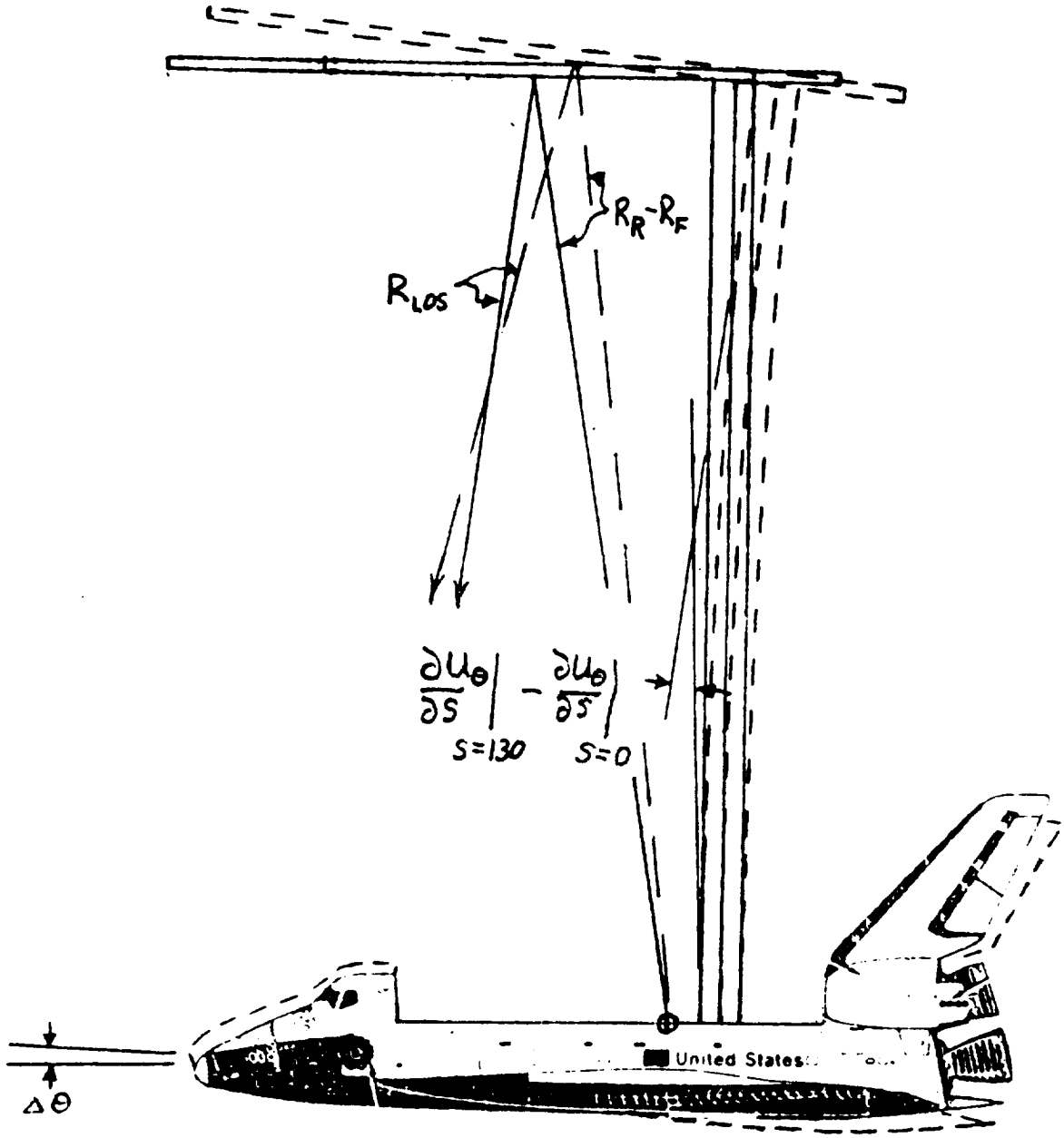

Figure 2.- Schematic of the effect of bending on the line-of-sight pointing error.

Figure 3. SPACECRAFT CONTROL LABORATORY* EXPERIMENT (SCOLE)

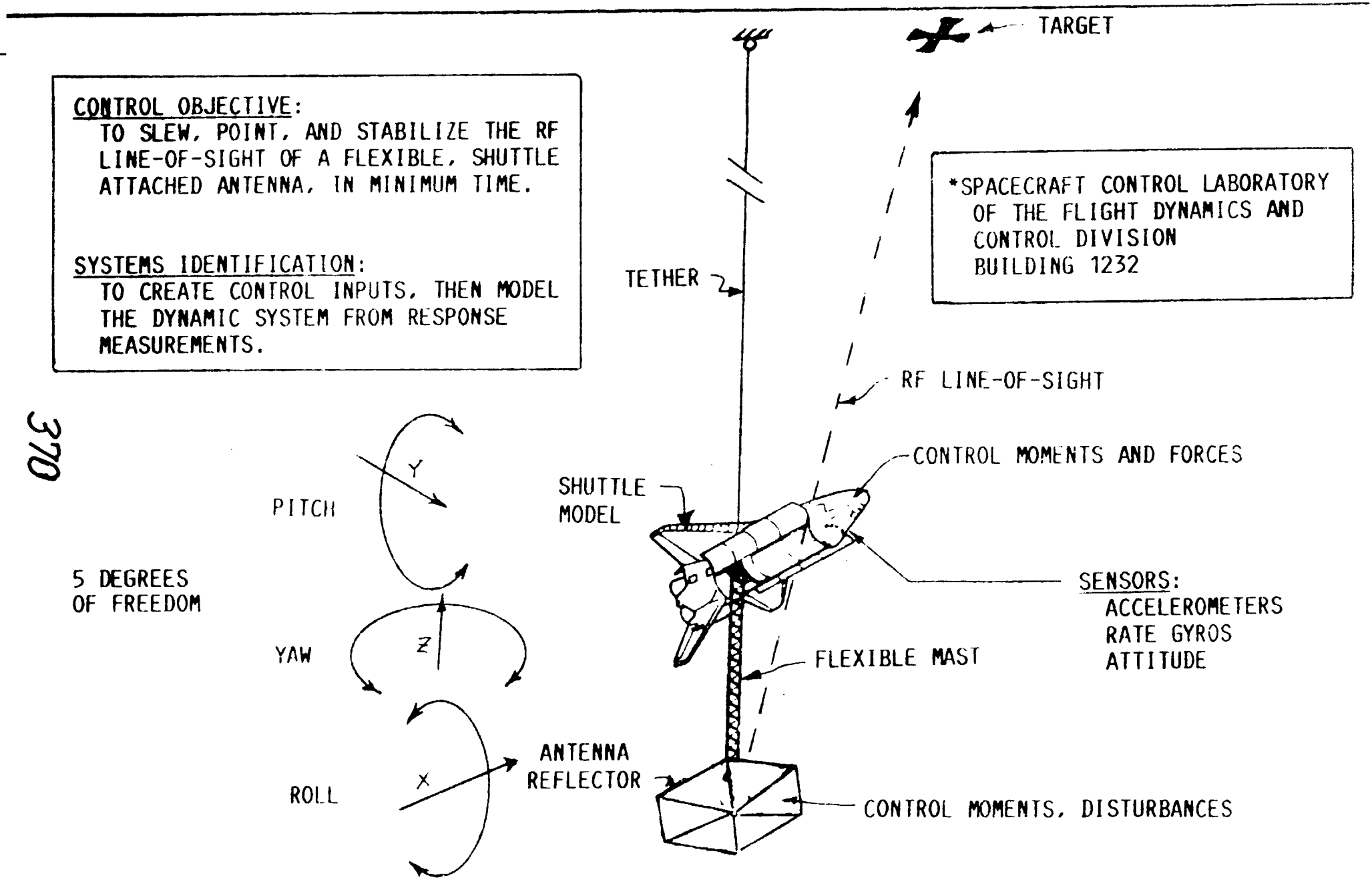

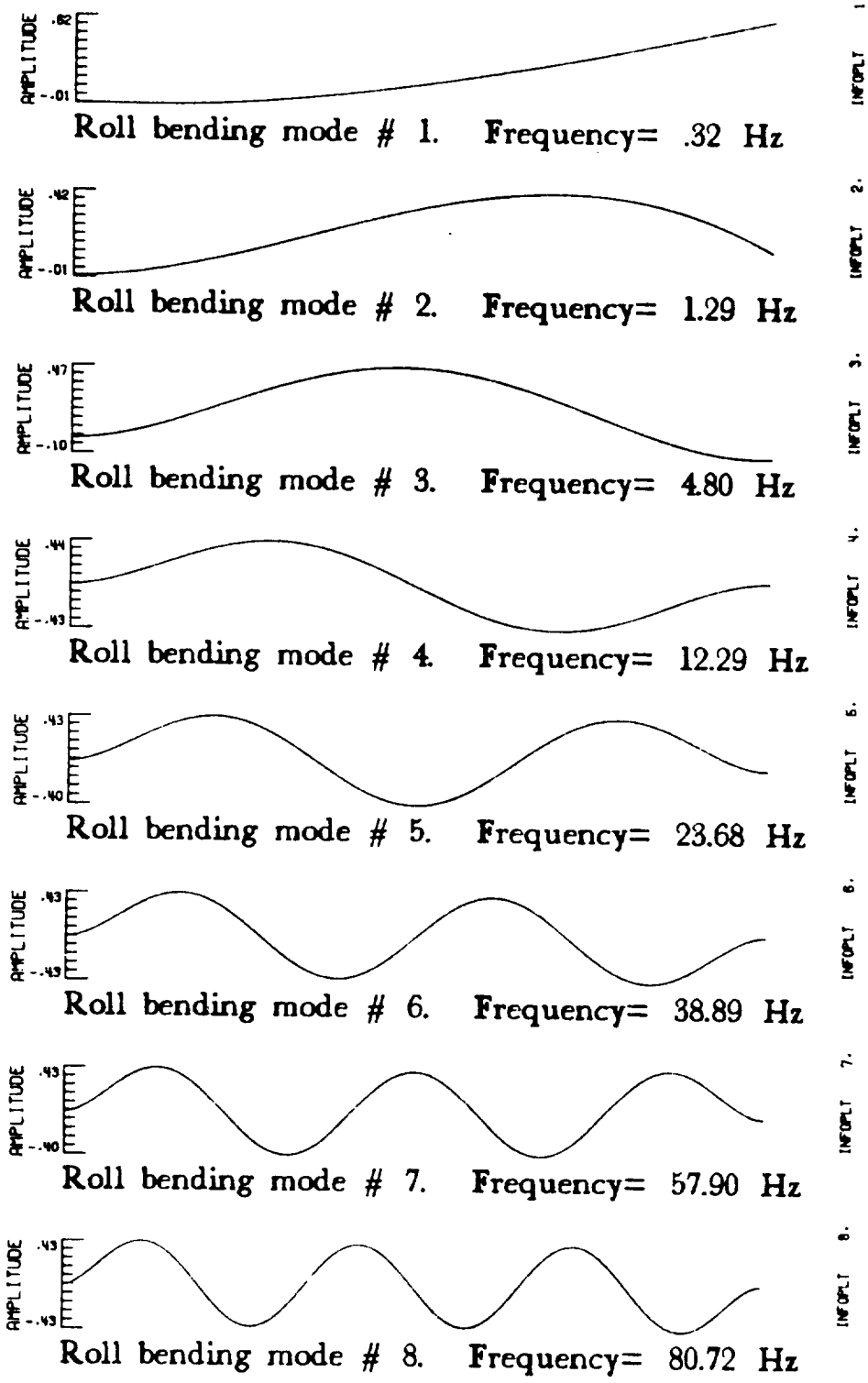

Figure 4a.- Plots of normalized roll bending mode shapes for SCOLE configuration.

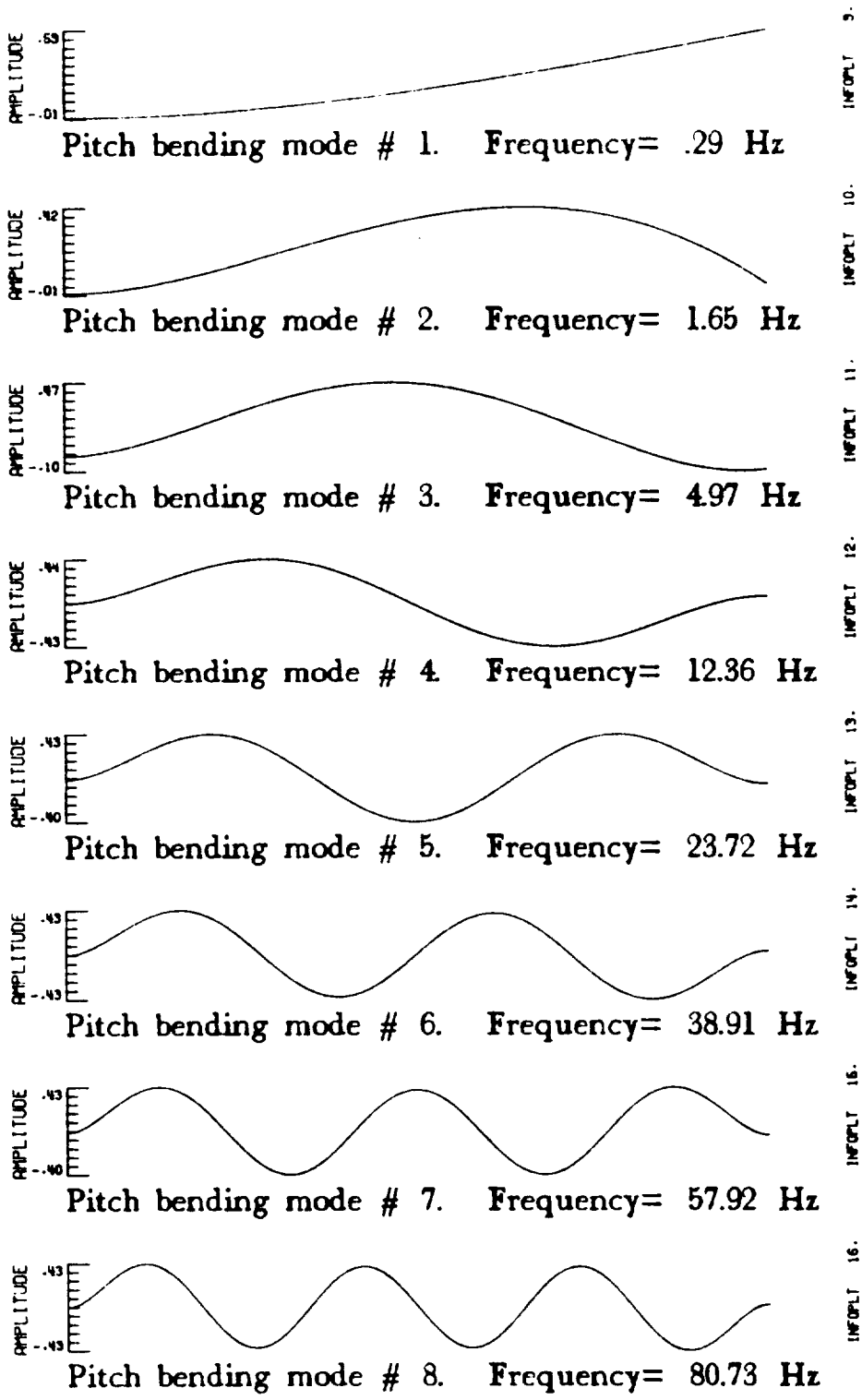

Figure 4b.- Plots of normalized pitch bending mode shapes for SCOLE configuration.

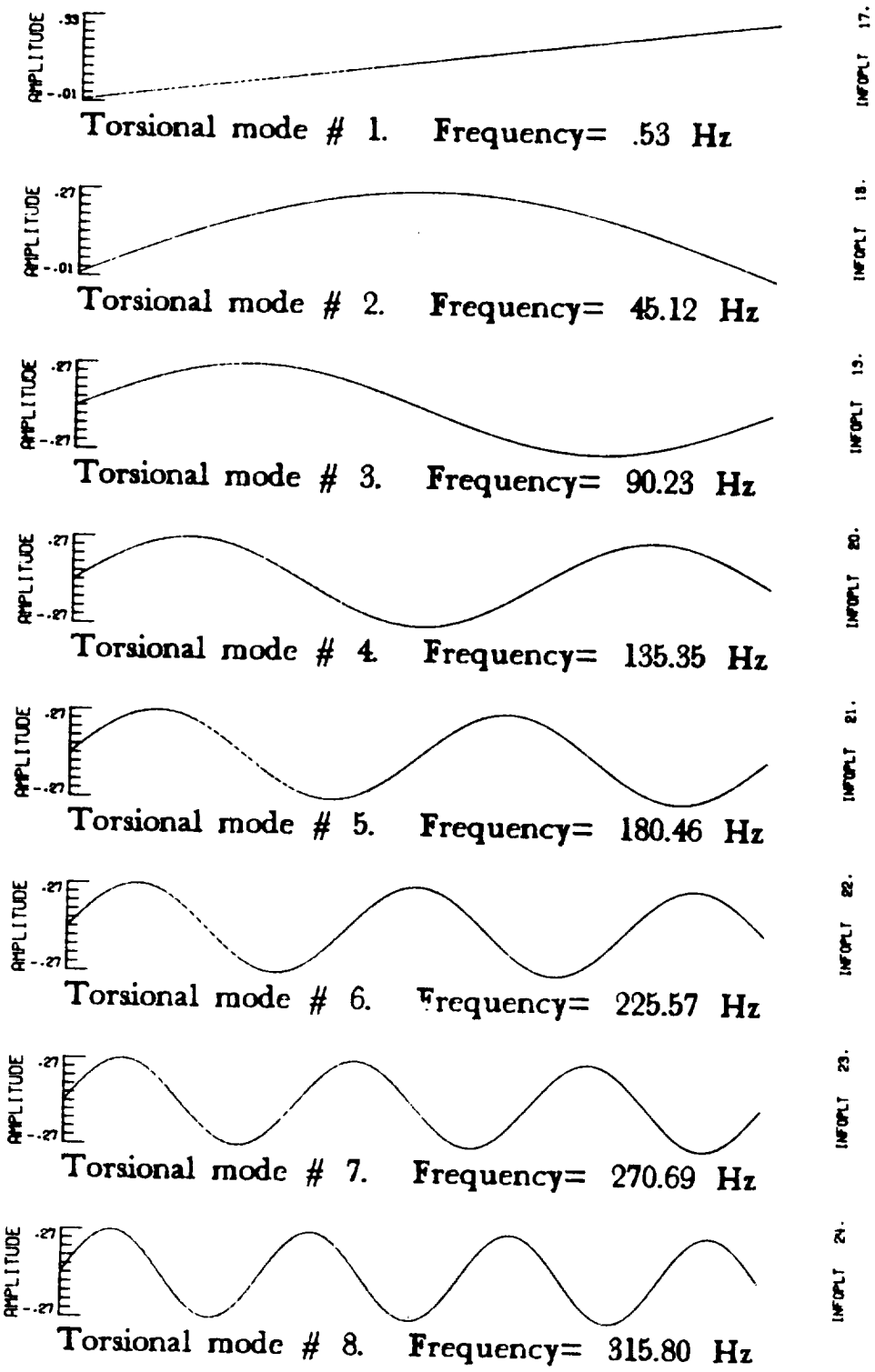

Figure 4c.- Plots of normalized torsional mode shapes for SCOLE configuration.

Summary of Selected Papers

b y

Lawrence W. Taylor
NASA Langley Research Center

CONTROL DESIGN CHALLENGES of LARGE SPACE SYSTEMS and SPACECRAFT CONTROL LABORATORY EXPERIMENT (SCOLE)

Gene Lin of Control Research Corporation

Examines the Resulting Excitation due to Bang-Bang Slewing

Effect of Excitation on Line-of-Sight Error

Concept of Modal Dashpots

Examines the Resulting Excitation Employing Modal Dashpot Design

Examines Linear Velocity Feedback Force Control (Also Angular)

Computer Simulation

Needs to be Applied to SCOLE Experimental Apparatus

INITIAL TEST RESULTS on STATE ESTIMATION on the SCOLE MAST

Dean Sparks of NASA Langley Research Center

Modal State Estimation Tested on SCOLE (Fixed Shuttle Body)

Kalman Filter used for State Estimation

Six Linear Accelerometers and 3-Axis Rate Gyro

Large Discrepencies Between Linear Finite Element Model and Experiment

Sinusoidal Input Forcing Function

Gravity Effects Very Pronounced

A Large Number of Modes Required for Accurate Static Deflection

Nonlinear Kinematics Can Be Significant

The DYNAMICS and CONTROL of the IN-ORBIT SCOLE CONFIGURATION

MINIMUM TIME ATTITUDE SLEWING MANEUVERS of a RIGID SPACECRAFT

STABILITY ANALYSIS of LARGE SPACE STRUCTURE CONTROL SYSTEMS with DELAYED INPUT

Peter Bainum, A.S.S.R. Reddy, Cheick M. Diarra and Feiyue Li of Howard University

Examines the Changes in Modal Characteristic due to Orbital Motion

Linear Elasticity Assumed

Retain Nonrotating Mode Shapes

Examines Stability for Rigid Case with Increasing Complexity

Derives Control Law using Linear, Flexible (4 Modes) SCOLE

Computer Simulations

Need to Introduce Disturbances, Noise

Need to Apply to Experimental Apparatus

C-5

CONTROL DESIGN APPROCHES for LaRC EXPERIMENTS

Steve Yurkovich and Umit Ozguner of Ohio State University

LQG, MEOP

Computer Simulations

Model Reference Adaptive Control

Employ Hyperstability and Positivity Concepts

Combine with Parameter Identification

Computer Simulations

Noise and Parameter Uncertainity Models Not Necessarily Realistic

Need to Apply to Experimental Apparatus

SOME NONLINEAR DAMPING MODELS in FLEXIBLE STRUCTURES

A. V. Balakrishnan of UCLA

Nonlinear Damping Term ie $|x|^a|dx/dt|^b dx/dt$

Uses Krylov and Bogoliubov Approximation

"Solves" Equations for SCOLE Bending and Torsion

Examines Multivariable Case

Draws Analogy with Nonlinear, Boundary Feedback Control

Useful Results for Modeling Nonlinear Damping

Useful for Systems Identification

Experimental Evidence Supports Findings

Need Approximations for Modal Model

SOME NONLINEAR DAMPING MODELS in FLEXIBLE STRUCTURES

A. V. Balakrishnan of UCLA

Nonlinear Damping Term ie $|x|^a dx/dt|^b dx/dt$

Uses Krylov and Bogoliubov Approximation

"Solves" Equations for SCOLE Bending and Torsion

Examines Multivariable Case

Draws Analogy with Nonlinear, Boundary Feedback Control

Useful Results for Modeling Nonlinear Damping

Useful for Systems Identification

Experimental Evidence Supports Findings

Need Approximations for Modal Model

INFINITE-DIMENSIONAL APPROACH to SYSTEMS IDENTIFICATION

of SPACE CONTROL LABORATORY EXPERIMENT (SCOLE)

S. A. Hossain and K. Y. Lee of Penn State University

Retains Physical Parameters ie Coefficients in P.D.E.s

Truncation problem avoided

Weighted Least Squares

Computer Simulations for a Few Different Examples

Convergent after Several Iterations

Additive Noise Used is Not Particularly Realistic

Good to tie-in to Physical Parameters

OPTIMIZATION-BASED DESIGN of CONTROL SYSTEMS for FLEXIBLE STRUCTURES

E. Polak, T. Baker, T-L. Wuu and Y-P. Harn of University of California at Berkeley

Approach is to Use "Nonsmooth Optimization Algorithms"

Design Closed-Loop Finite Dimensional Compensators for Flexible Structures

Does Not Require Modal Decomposition, Avoiding Spillover Problem

Applicable to Mixed Ordinary and P.D.E. Systems

Classical Design Objectives

Applied to Flexible Beam with Tip Mass

Computer Simulation

Need to Test with Disturbances, Noise

PLACING DYNAMIC SENSORS and ACTUATORS on FLEXIBLE SPACE STRUCTURES

Gregory Norris and Robert Skelton of Purdue University

Input/Output Cost Analysis Decomposes the Quadratic Cost into Contributions from Each Stochastic Input and Weighted Output.

Closed Loop is Considered

Past Treatment Required Perfect Sensors and Actuators

Now Consider Dynamics of Sensors and Actuators

Applied to SCOLE

Important to Consider Closed Loop and Dynamics of Elements

Order Reduction is an Important Problem

COMBINED PROBLEM of SLEW MANEUVER CONTROL and VIBRATION SUPPRESSION

Y. P. Kakad of University of North Carolina at Charlotte

Derives the Nonlinear Equations of Motion Suitable for Slewing and Vibration Control

Analyzes the Kinematic Nonlinearities in terms of the Matrix Spectral Norm

Analyzes Arbitrary Slew Maneuver

It May be Necessary to Synthesize Control Systems for the Combined Problem

---

Interesting Approach

Determining "Optimal" Control Might be Difficult

EFFECT of ACTUATOR DYNAMICS on CONTROL of BEAM FLEXURE DURING NONLINEAR SLEW of SCOLE MODEL

Shalom (Mike) Fisher of Naval Research Laboratory

Simulation Includes Limited Proof-Mass Deflection and Time Delay

Examines Line-of-Sight Errors due to Slewing and Settling

NASTRAN Finite Element Model (12 Vibrational Modes)

Nonlinear DISCOS Simulation of 20' Slew

LQR Design

Force Limit

Computer Simulation

Ready for Experimental Apparatus

COMPUTATIONAL EXPERIMENTS in the OPTIMAL SLEWING of FLEXIBLE STRUCTURES

T. E. Baker and E. Polak

Considers the "Swinging Flexible Arm Problem"

45 Degree Rotation

Torque Limit

Minimizes Total Energy Required for Time Limit

Same with Upper Bound on Potential (Elastic) Energy

Computer Simulation

Need to Consider Disturbances, Noise

PARAMETER IDENTIFICATION USING MODAL DATA

L. Meirovitch and M. A. Norris of V.P.I.

Uses Indirect Method ie Modal "Data" not Sensor Data

Rayleigh-Ritz method

Iterative, Sensitivity Analysis

SCOLE Laboratory Experiment Application

4 Degree-of-Freedom Model

Estimated EI, I(Antenna)

Work at early stage.

Important coupling not yet included.

NONLINEARITIES in SPACECRAFT STRUCTURAL DYNAMICS

Lawrence W. Taylor and Kelly Latimer of NASA Langley Research Center

Many Modes are Needed for Accurate Static and Dynamic Characteristics

Large Amplitude Deflection Effects are Examined

Lumped Mass and Assymptotic Approximations are Evaluated

A 3-Dimensional Beam Equation is Derived for Large Deflections

Linear and Nonlinear Damping Models are Examined

Distributed Parameter Models are Seen To Reduce the Number of Parameters

---

The Dynamic Model of the SCOLE Experimental Apparatus Needs to be Improved

Effort is Needed in Solving the 3-Dimensional Beam Equation

The Nonlinear Damping Seen in the SCOLE is Probably Due to Aerodynamics

ANALYTICAL REDUNDANCY MANAGEMENT for SCOLE

Ray Montgomery of NASA Langley Research Center

Examines Problem of Control Performance when Elements are Failed

Uses Expected Quadratic Performance Index

Combinatorial Problem forces Cut and Try

Important Consideration for Some Applications with Long Life/MTBF

NASA
National Aeronautics and Space Administration

Report Documentation Page

1. Report No.	2. Government Accession No.	3. Recipient's Catalog No.
NASA TM-101503		

4. Title and Subtitle	5. Report Date
Proceedings of the 4th Annual SCOLE Workshop	October 1988
	6. Performing Organization Code

7. Author(s)	8. Performing Organization Report No.
Lawrence W. Taylor, Jr. (Compiler)	
	10. Work Unit No.
	506-46-11-01

9. Performing Organization Name and Address	11. Contract or Grant No.
NASA Langley Research Center Hampton, VA 23665	
	13. Type of Report and Period Covered
12. Sponsoring Agency Name and Address	Technical Memorandum
National Aeronautics and Space Administration Washington, DC 20546	14. Sponsoring Agency Code

15. Supplementary Notes

16. Abstract

This publication is a collection of papers presented at the Fourth Annual Spacecraft Control Laboratory Experiment (SCOLE) Workshop held at the USAF Academy, Colorado Springs, Colorado, November 16, 1987. The papers address the modeling, systems identification, and control synthesis for the Spacecraft Control Laboratory Experiment (SCOLE) configuration.

17. Key Words (Suggested by Author(s))	18. Distribution Statement
Large Flexible Spacecraft Control, Structural Dynamics	Unclassified-Unlimited Subject Category-18

19. Security Classif. (of this report)	20. Security Classif. (of this page)	21. No. of pages	22. Price
Unclassified	Unclassified	395	A17